

Structural, Physical and Biological Studies of Transition Metal Schiff Base Complexes

Submitted in fulfilment of the requirements for the degree of

Master of Science

By

Justine C. de Ponte

BSc (Hons) (UKZN)

2013

School of Chemistry & Physics,
College of Agriculture, Engineering, and Science,
University of KwaZulu-Natal, Pietermaritzburg

Declaration

I declare that:

- (1) The research reported in this dissertation/thesis, except where otherwise indicated, is my original research.
- (2) This dissertation/thesis has not been submitted for any degree or examination at any other university.
- (3) This dissertation/thesis does not contain other persons' data, pictures, graphs or other information, unless specifically acknowledged as being sourced from other persons.
- (4) This dissertation/thesis does not contain other persons' writing, unless specifically acknowledged as being sourced from other researchers. Where other written sources have been quoted, then:
 - a) Their words have been re-written but the general information attributed to them has been referenced;
 - b) Where their exact words have been used, their writing has been placed inside quotation marks, and referenced.
- (5) Where I have reproduced a publication of which I am author, co-author or editor, I have indicated in detail which part of the publication was actually written by myself alone and have fully referenced such publications.
- (6) This dissertation/thesis does not contain text, graphics or tables copied and pasted from the Internet, unless specifically acknowledged, and the source being detailed in the dissertation/thesis and in the References sections.

SIGNED:

DATE:

Justine de Ponte

We hereby certify that this statement is correct to the best of our knowledge.

SIGNED:

DATE:

Professor O. Q. Munro (Supervisor)

SIGNED:

DATE:

Dr M. P. Akerman (Co-Supervisor)

Acknowledgements

Firstly I would like to acknowledge both my supervisors, Professor Munro and Dr Akerman, for their help and guidance throughout the project.

I would also like to thank Professor Field for his assistance in the refinement of crystal structures and UV-vis guidance.

To Mr Craig Grimmer who always had a plan B when things looked dismal and his hours of help with NMR analysis.

Thanks especially go to Colin Wilson for being my mother duck. Thank you for your constant interest in what I was doing and guidance in every little problem I may have come to him with, experimental or technological.

A special thanks for my family and boyfriend, Shaun Hollander. You were always there to support me in anyway necessary. Thank you for helping me through this adventure.

List of Abbreviations and Symbols

| | |
|------------------|--|
| CNS | Central nervous system |
| CSD | Cambridge structural database |
| DFT | Density functional theory |
| DMF | Dimethyl formamide |
| DMSO | Dimethylsulfoxide |
| DNA | Deoxyribose nucleic acid |
| ES ⁺ | Electrospray |
| HOMO | Highest occupied molecular orbital |
| IC ₅₀ | Half maximal inhibitory concentration |
| IR | Infrared |
| IUC1 | International Union of Crystallography |
| LUMO | Lowest occupied molecular orbital |
| MLCT | Metal to ligand charge transfer |
| NMR | Nuclear magnetic resonance |
| ORTEP | Oak Ridge thermal ellipsoid plot program |
| PAMAM | Polyamidoamine |
| RMSD | Root mean square deviation |
| Salen | Salicylaldehyde & Ethylenediamine ligand |
| TD-SCF | Time dependant self-consistent field |
| TOF | Time of flight |
| UV | Ultraviolet |
| Vis | Visible |

Abstract

The aims of this work were first to synthesize and fully characterize compounds that may function as bleomycin analogues and, second, to test their anticancer activity *in vitro*. Three novel tetradentate O,N,N,O Schiff base ligands, H_3L^1 , H_2L^3 and H_2L^3 were synthesized by condensation of three different 1,3-diaminoalkane bridging units with two equivalents of (2,4-dihydroxy-phenyl)-(phenyl)methanone. These ligands contain two neutral imine nitrogen donors and two anionic phenolate oxygen donors for the coordination of metal ions. The choice of ligand was guided by the fact that Cu(II) bleomycin analogues with ligands employing O,N,N,O donor atom sets are able to cleave double-stranded DNA via oxygen radical formation. Using these ligands, six novel metal complexes of copper(II), nickel(II) and zinc(II) were synthesized and fully characterised. Two novel ligand crystal structures and six novel metal complex crystal structures are reported in this work.

The X-ray structures of the two structurally characterized nickel(II) complexes $[Ni(L^2)]$ and $[Ni(L^3)]$ adopted the same nominally square planar coordination geometry, with the metal ion bound by the pairs of imine nitrogen and ortho-phenolic oxygen atoms of the ligand's tetradentate donor atom set. The Ni–N and Ni–O distances averaged 1.892(3) Å and 1.845(2) Å, respectively. However, when reacted with Cu(II) and Zn(II), the ligands favored the formation of multinuclear complexes as a result of metal ion bridging by ionized oxygen donor atoms (either the phenolic oxygen atoms or an alkoxide oxygen atom of the 2-hydroxy substituted alkane bridge in the case of H_3L^1) of the polyfunctional ligands. For the di- and trinuclear copper(II) complexes, the mean Cu–N and Cu–O distances averaged 1.953(3) Å and 2.082(3) Å, respectively. For the dinuclear zinc(II) complex, the mean Zn–N and Zn–O distances averaged 2.074(3) Å and 2.042(3) Å, respectively.

Electron spin resonance (ESR) measurements on the paramagnetic trinuclear copper(II) complexes confirmed that the trinuclear solid state structures remain intact in fluid solution (DMF) and that two of the three copper(II) ions are antiferromagnetically coupled, leaving the third as an $S = 1/2$ center with a hyperfine coupling constant to the $I = 3/2$ Cu nucleus of 14.80 G. Super-hyperfine coupling (15.13 G) to two N atoms was also evident, consistent

with one of the terminal copper(II) centers (O,N,N,O donor atom set) being the site of the unpaired spin density in the molecule.

Density functional theory (DFT) simulations were used to determine the electronic structures of the diamagnetic mononuclear nickel(II) complexes. The simulations reproduced the structures of $[\text{Ni}(\text{L}^2)]$ and $[\text{Ni}(\text{L}^3)]$ accurately with similarity coefficients for the two complexes of 0.982 and 0.990, respectively. The simulated electronic spectra (TD-DFT) of the nickel(II) complexes showed reasonably good agreement with the experimental spectra and were useful for the assignment of the low-lying MLCT state (near 400 nm) for the complexes as well as the higher-lying π - π^* transitions between 300–350 nm.

All of the metal complexes and one ligand were sent to MINTEK¹ (Project AuTEK) for anti-cancer screening. The copper(II) complexes (bleomycin analogues capable of generating hydroxyl radicals in vivo) showed significant cytotoxicity against the human cancer cell lines A549, DU145, HT-29, and U21. The trinuclear complexes were the most cytotoxic with mean IC_{50} values of 6(2) and 7(1) μM for $[\text{Cu}_3(\text{L}^2)_2\text{Cl}_2(\text{DMF})_2]$ and $[\text{Cu}_3(\text{L}^3)_2(\text{H}_2\text{O})_2]\text{Cl}_2$, respectively. The nickel(II) complexes $[\text{Ni}(\text{L}^2)]$ and $[\text{Ni}(\text{L}^3)]$ were comparatively inactive with mean IC_{50} values of >50 and 35(16) μM , respectively, consistent with the fact that they do not readily generate reactive oxygen species in a cellular environment.

¹ 200 Malibongwe Drive, Strijdom Park, Randburg

Contents

| | |
|---|-------|
| Acknowledgments | III |
| List of Abbreviations and Symbols | IV |
| Abstract | V |
| List of Figures | X |
| List of Tables | XVIII |
| Chapter 1 Introduction | 1 |
| 1.1 Preface | 1 |
| 1.2 Chemistry of Copper | 3 |
| 1.3 Chemistry of Nickel | 4 |
| 1.4 Chemistry of Zinc | 5 |
| 1.5 Applications of Metal Schiff Base Complexes | 6 |
| 1.6 Metal Based Anti-Microbial and Anti-Cancer Agents | 9 |
| 1.7 Bleomycin and Its Analogues | 12 |
| 1.8 Project Objectives | 20 |
| Chapter 2 Experimental | 22 |
| 2.1 Instrumentation and Chemicals | 22 |
| 2.2 Ligand Synthesis | 23 |
| 2.2.1 Synthesis of 4, 4'-{2-hydroxypropane-1,3-diylidene-bis[nitrilo (phenylmethanediyl)]}dibenzene-1,3-diol, H ₃ L ¹ | 23 |
| 2.2.2 Synthesis of 4,4'-{2,2-dimethylpropane-1,3-diylidene-bis[nitrilo (phenylmethanediyl)]}dibenzene-1,3-diol, H ₂ L ² | 24 |
| 2.2.3 Synthesis of 4,4'-{propane-1,3-diylidene-bis[nitrilo (phenylmethanediyl)]}dibenzene-1,3-diol, H ₂ L ³ | 25 |
| 2.3 Metal Chelate Synthesis | 26 |
| 2.3.1 Synthesis of [Cu ₂ (L ¹)(OAc)(DMF)], where L ¹ = 6,6'-((1E,1'E)-((2- oxidopropane-1,3-diyl)bis(azanylylidene))bis(phenylmethanylylidene)) bis(3- hydroxyphenolate), OAc = acetate and DMF = dimethylformamide | 26 |
| 2.3.2 Synthesis of [(L ²)(Cl)(DMF)Cu•Cu•Cu(L ²)(Cl)(DMF)], where L ² = 6,6'- ((1E,1'E)-((2,2-dimethylpropane-1,3-diyl)bis(azanylylidene))bis(phenyl methanylylidene))bis(3-hydroxyphenolate), [Cu ₃ (L ²) ₂ Cl ₂ (DMF) ₂] | 27 |
| 2.3.3 Synthesis of [Ni(L ²)], where L ² = 6,6'-((1E,1'E)-((2,2-dimethyl propane-1,3- diyl)bis(azanylylidene))bis(phenyl methanylylidene))bis(3-hydroxyphenolate) | 28 |
| 2.3.4 Synthesis of [(L ³)(H ₂ O)Cu•Cu•Cu(L ³)(H ₂ O)]Cl ₂ where L ³ = 6,6'-((1E,1'E)- (propane-1,3-diylbis(azanylylidene))bis(phenylmethanylylidene)) bis(3- | 29 |

| | |
|--|----|
| hydroxyphenolate), $[\text{Cu}_3(\text{L}^3)_2(\text{H}_2\text{O})_2]\text{Cl}_2$ | |
| 2.3.5 Synthesis of $[\text{Ni}(\text{L}^3)]$, where $\text{L}^3 = 6,6'-((1\text{E},1'\text{E})\text{-}(\text{propane-1,3-diylbis}(\text{azanylylidene}))\text{bis}(\text{phenylmethanylylidene}))\text{bis}(3\text{-hydroxyphenolate})$ | 30 |
| 2.3.6 Synthesis of $[\text{Zn}_2(\text{L}^3)_2]$ where $\text{L}^3 = 6,6'-((1\text{E},1'\text{E})\text{-}(\text{propane-1,3-diylbis}(\text{azanylylidene}))\text{bis}(\text{phenylmethanylylidene}))\text{bis}(3\text{-hydroxyphenolate})$ | 31 |
| Chapter 3 Synthesis | 32 |
| 3.1 Imines and Schiff bases | 32 |
| 3.2 Metal Complexation | 35 |
| Chapter 4 Spectroscopy | 37 |
| 4.1 NMR Spectroscopy | 37 |
| 4.2 UV-vis Spectroscopy | 40 |
| 4.3 Infrared Spectroscopy | 50 |
| 4.4 Electron Spin Resonance | 54 |
| 4.5 Conclusions | 68 |
| Chapter 5 X-ray Crystallography | 69 |
| 5.1 Introduction | 69 |
| 5.2 Objectives | 73 |
| 5.3 Experimental Methods | 73 |
| 5.3.1 General Crystallographic Procedures | 73 |
| 5.4 Experimental Data for Ligands | 74 |
| 5.4.2 X-ray Structure of H_3L^1 | 74 |
| 5.4.3 X-ray Structure of H_2L^2 | 74 |
| 5.5 Experimental Data for Metal Complexes | 75 |
| 5.5.1 X-ray Structure of $[\text{Cu}_2(\text{L}^1)(\text{OAc})(\text{DMF})]$ | 75 |
| 5.5.2 X-ray Structure of $[\text{Cu}_3(\text{L}^2)_2\text{Cl}_2(\text{DMF})_2]$ | 76 |
| 5.5.3 X-ray Structure of $[\text{Ni}(\text{L}^2)]$ | 76 |
| 5.5.4 X-ray Structure of $[\text{Cu}_3(\text{L}^3)_2(\text{H}_2\text{O})_2]\text{Cl}_2$ | 77 |
| 5.5.5 X-ray Structure of $[\text{Ni}(\text{L}^3)]$ | 77 |
| 5.5.6 X-ray Structure of $[\text{Zn}_2(\text{L}^3)_2]$ | 78 |
| 5.6 Results and Discussion | 78 |
| 5.6.1 Analysis of the X-ray structure of H_3L^1 | 78 |
| 5.6.2 Analysis of the X-ray structure of H_2L^2 | 82 |
| 5.6.3 Analysis of the X-ray structure of $[\text{Cu}_2(\text{L}^1)(\text{OAc})(\text{DMF})].\text{DMF}$ | 86 |
| 5.6.4 Analysis of the X-ray structure of $[\text{Cu}_3(\text{L}^2)_2\text{Cl}_2(\text{DMF})_2].5\text{H}_2\text{O}.\text{DMF}$ | 90 |

| | |
|---|-----|
| 5.6.5 Analysis of the X-ray structure of [Ni(L ²)].4H ₂ O.DMF | 94 |
| 5.6.6 Analysis of the X-ray structure of [Cu ₃ (L ³) ₂ (H ₂ O) ₂]Cl ₂ | 97 |
| 5.6.7 Analysis of the X-ray structure of [Ni(L ³)].H ₂ O | 102 |
| 5.6.8 Analysis of the X-ray structure of [Zn ₂ (L ³) ₂].5DMF | 105 |
| 5.7 Concluding Remarks | 109 |
| Chapter 6 Computational Chemistry | 110 |
| 6.1 Introduction | 110 |
| 6.2 Experimental | 116 |
| 6.3 DFT Calculations of Metal Chelates | 116 |
| 6.3.1 Geometry Optimisations | 116 |
| 6.3.2 Electronic Transition Calculations | 119 |
| 6.3.3 Infrared Calculations | 129 |
| 6.4 Conclusions | 133 |
| Chapter 7 Biological Studies | 134 |
| 7.1 Introduction | 134 |
| 7.2 Experimental | 137 |
| 7.3 Results and Discussion | 138 |
| 7.4 Conclusions | 145 |
| Chapter 8 Future work | 146 |
| 8.1 Future Compounds | 146 |
| Chapter 9 Conclusions | 153 |
| Chapter 10 References | 155 |
| Appendix A: NMR Spectra | 163 |
| Appendix B: UV-vis Spectra | 167 |
| Appendix C: Infrared Spectra | 169 |
| Appendix D: Crystallographic data | 173 |
| Appendix E: DVD of Electronic Data | |

List of Figures

| Figure | Title | Page |
|--------|--|------|
| 1.1 | Structure of (5-amino-5-methyl-3,7-diazanonanedioate)copper(II). | 1 |
| 1.2 | Ligands proposed for synthesis and chelation to Cu(II), Ni(II) and Zn(II). | 2 |
| 1.3 | Copper metal in its raw state. | 3 |
| 1.4 | Metallic nickel in its raw state. | 4 |
| 1.5 | Metallic zinc in its raw state. | 5 |
| 1.6 | Structure of (N,N'-bis(4-methoxysalicylidene)ethane-1,2-diamine)copper(II), a potential sensor for organic solvents. | 6 |
| 1.7 | Structure of the copper(II) Schiff base duplicated from Roy et al. A catalyst for the oxidation of organic compounds. | 7 |
| 1.8 | Structure of the ligand ethylenebis(salicylideneminate). | 8 |
| 1.9 | Structures of DNA polymerase targeting anti-cancer drugs. The highlighted areas indicate where the enzyme will bind. | 10 |
| 1.10 | Stacking of the nickel(II) salphen complexes, showing an interplanar spacing of 3.567 Å. | 12 |
| 1.11 | Structure of bleomycin from Streptomyces verticillus and its components. | 13 |
| 1.12 | Activation of bleomycin (BLM) in the presence of oxygen and iron. | 14 |
| 1.13 | Cleavage by bleomycin (BLM) in low oxygen concentrations. | 15 |
| 1.14 | DNA cleavage by bleomycin (BLM) in high oxygen concentrations. | 16 |
| 1.15 | Structures of hemin-intercalators studied by Hashimoto et al. with the highlighted DNA recognition portion. | 17 |
| 1.16 | Structures of (5-amino-5-methyl-3,7-diazanonanedioate)copper(II) (a) and ((2S,8R)-5-amino-2,8-dibenzyl-5-methyl-3,7-diazanonanedioate)copper(II) (b). Both complexes are capable of inducing double-stranded DNA cleavage. | 18 |
| 1.17 | Monitoring hydroxyl radical production by rhodamine B decay in | 19 |

| | | |
|-----|--|----|
| | phosphate buffer. The reaction conditions for each are as follows: | |
| | ● aerobic activation with both H ₂ O ₂ and sodium ascorbate, ▲ aerobic activation with only sodium ascorbate, ● anaerobic activation with both H ₂ O ₂ and sodium ascorbate ▲ anaerobic activation with only sodium ascorbate, + quenching of ascorbate activation by ethanol. Reproduced from reference 42. | |
| | Diagrams depicting the numbering schemes used for the | |
| 2.1 | assignment of the NMR spectra of H ₃ L ¹ ; A = ¹ H NMR and B = ¹³ C NMR. | 23 |
| | Diagrams depicting the numbering schemes used for the | |
| 2.2 | assignment of the NMR spectra of H ₂ L ² , A = ¹ H NMR and B = ¹³ C NMR. | 24 |
| | Diagrams depicting the numbering schemes used for the | |
| 2.3 | assignment of the NMR spectra of H ₂ L ³ , A = ¹ H NMR and B = ¹³ C NMR. | 25 |
| 2.4 | Structure of [Cu ₂ (L ¹)(OAc)(DMF)]. | 26 |
| 2.5 | Structure of [Cu ₃ (L ²) ₂ Cl ₂ (DMF) ₂]. | 27 |
| | Diagrams depicting the numbering schemes used for the | |
| 2.6 | assignment of the NMR spectra of [Ni(L ²)], A = ¹ H NMR and B = ¹³ C NMR. | 28 |
| 2.7 | Structure of [Cu ₃ (L ³) ₂ (H ₂ O) ₂]Cl ₂ . | 29 |
| | Diagrams depicting the numbering schemes used for the | |
| 2.8 | assignment of the NMR spectra of [Ni(L ³)], A = ¹ H NMR and B = ¹³ C NMR. | 30 |
| 2.9 | Structure of [Zn ₂ (L ³) ₂]. | 31 |
| 3.1 | Imine formation via a Stieglitz rearrangement. | 32 |
| 3.2 | Imine formation via a Schmidt reaction. | 33 |
| 3.3 | Imine formation via a Hoesch reaction. | 33 |
| 3.4 | Condensation reaction of a carbonyl and a primary amine. | 34 |
| 3.5 | General reaction scheme for the synthesis of the ligands in this work. | 34 |
| 3.6 | Reaction scheme employed in the chelation of ligands. | 36 |
| 4.1 | ¹ H NMR spectrum of H ₂ L ² in DMSO-d ₆ . | 37 |

| | | |
|------|---|----|
| 4.2 | ^1H NMR spectrum of $[\text{Ni}(\text{L}^2)]$ in DMSO- d_6 . | 38 |
| 4.3 | ^1H NMR spectrum of $[\text{Zn}_2(\text{L}^3)_2]$ in DMSO- d_6 . | 39 |
| 4.4 | UV-vis spectrum of H_2L^3 in DMF at 298 K. | 41 |
| 4.5 | UV-vis spectrum of H_2L^2 in DMF at 298 K. | 42 |
| 4.6 | UV-vis spectrum of $[\text{Zn}_2(\text{L}^3)_2]$ in DMF at 298 K. | 43 |
| 4.7 | UV-vis spectrum of $[\text{Cu}_3(\text{L}^3)_2(\text{H}_2\text{O})_2]\text{Cl}_2$ in DMF at 298 K. | 44 |
| 4.8 | UV-vis spectrum of $[\text{Ni}(\text{L}^3)]$ in DMF at 298 K. | 44 |
| 4.9 | Copper(II) complexes with derivatives of salen and tetrahydrosalen. Redrawn from Ref. 56. | 46 |
| 4.10 | Copper(II) complexes with tetradentate imine-phenol type ligands. Redrawn from Ref. 15. | 47 |
| 4.11 | Nickel(II) chelates as synthesised by Jamshid et al. (A, B) and Garg et al. (C-E). Redrawn from Ref. 59. | 48 |
| 4.12 | Infrared spectrum of H_2L^2 with assigned bands. | 51 |
| 4.13 | Infrared spectrum of $[\text{Cu}_3(\text{L}^2)_2\text{Cl}_2(\text{DMF})_2]$ with assigned bands. | 51 |
| 4.14 | Energy levels of an electron in a magnetic field redrawn from ref 63. | 55 |
| 4.15 | Spectra of a typical isotropic g-tensor. | 56 |
| 4.16 | Spectra of a typical tetragonal g-tensor. | 56 |
| 4.17 | Spectra of a typical rhombic g-tensor. | 57 |
| 4.18 | Copper(II) Schiff-bases as synthesised by Losada et al. | 57 |
| 4.19 | Copper(II) salen complex with bulky groups synthesised by Dyers Jr. et al. | 58 |
| 4.20 | Two S-methylisothiosemicarbazide salen-type copper(II) complexes synthesised by Arion et al. | 60 |
| 4.21 | Structures of $[\text{Cu}(\text{mnpama})]$ and $[\text{Cu}(\text{ampama})]$ as synthesised by Balla et al. where R is the chosen amino acid. | 60 |
| 4.22 | Solid state ESR spectrum of $[\text{Cu}_3(\text{L}^2)_2\text{Cl}_2(\text{DMF})_2]$ at 298 K. | 61 |
| 4.23 | X-ray structure of $[\text{Cu}_3(\text{L}^2)_2\text{Cl}_2(\text{DMF})_2]$ illustrating the two independent trinuclear complexes of the asymmetric unit and highlighting the arrangement between adjacent Cu(II) ions that might facilitate antiferromagnetic spin-coupling. | 62 |
| 4.24 | Solid state ESR spectrum of $[\text{Cu}_3(\text{L}^3)_2(\text{H}_2\text{O})_2]\text{Cl}_2$ at 298 K. | 63 |

| | | |
|--------|--|----|
| 4.25 | ESR spectrum of $[\text{Cu}_3(\text{L}^2)_2\text{Cl}_2(\text{DMF})_2]$ in DMF at 298 K. | 64 |
| 4.26 | ESR Spectrum of $[\text{Cu}_3(\text{L}^2)_2\text{Cl}_2(\text{DMF})_2]$ in DMF at 298 K with labelled superhyperfine coupling. | 65 |
| 4.27 | ESR spectrum of $[\text{Cu}_3(\text{L}^3)_2(\text{H}_2\text{O})_2]\text{Cl}_2$ in DMF at 298 K. | 66 |
| 4.28 | ESR Spectrum of $[\text{Cu}_3(\text{L}^3)_2(\text{H}_2\text{O})_2]\text{Cl}_2$ in DMF at 298 K with labelled superhyperfine coupling. | 67 |
| 5.1.1 | Diagram of a single molecule of 2,2'-(Propane-1,3-diylbis(nitrilo (phenylmethylidene)))diphenol. Redrawn from the CSD coordinates of KUVLIX. | 70 |
| 5.1.2 | Diagram of a single molecule of diperchlorato-bis(m2-2,2'-(1,3-propanediylbis(nitriloethylidyne))bisphenolato)-tri-copper(II). Redrawn from the CSD coordinates of AQETEV. | 71 |
| 5.1.3 | Diagram of a single molecule of (N,N'-bis((1-(2-oxyphenyl) ethyl)imino)propane)-nickel(II) methanol solvate. Redrawn from the CSD coordinates of LOFXIO. | 72 |
| 5.6.1 | Partially labelled thermal ellipsoid plot of H_3L^1 . Thermal ellipsoids are drawn at 50% probability, only the major component of the disordered CHOH group is shown for clarity, hydrogen atoms have been omitted for clarity and the DMF solvent molecule was draw with isotropic thermal parameters. | 79 |
| 5.6.2 | Intramolecular hydrogen bonding in H_3L^1 . | 79 |
| 5.6.3 | Hydrogen bonding in the lattice of H_3L^1 . | 80 |
| 5.6.4 | Stacking of H_3L^1 molecules in the crystal lattice. | 81 |
| 5.6.5 | Short contacts present in the crystal lattice of H_3L^1 . | 81 |
| 5.6.6 | Partially labelled thermal ellipsoid plot of H_2L^2 . Thermal ellipsoids are drawn at 50% probability, hydrogen atoms have been omitted for clarity. | 83 |
| 5.6.7 | Intramolecular hydrogen bonding of H_2L^2 . | 83 |
| 5.6.8 | Hydrogen bonding between H_2L^2 molecules. | 84 |
| 5.6.9 | Stacking of H_2L^2 molecules in the lattice due to hydrogen bonding. | 85 |
| 5.6.10 | Partially labelled thermal ellipsoid plot of $[\text{Cu}_2(\text{L}^1)(\text{OAc})(\text{DMF})]$. Thermal ellipsoids are drawn at 50% probability, hydrogen atoms have been omitted for clarity. | 86 |

| | | |
|--------|--|-----|
| 5.6.11 | Packing in the unit cell of $[\text{Cu}_2(\text{L}^1)(\text{OAc})(\text{DMF})]$ as viewed along the a-axis. | 87 |
| 5.6.12 | Hydrogen bonding present between complexes and solvent in $[\text{Cu}_2(\text{L}^1)(\text{OAc})(\text{DMF})]$. | 88 |
| 5.6.13 | Partially labelled thermal ellipsoid plot of $[\text{Cu}_3(\text{L}^2)_2\text{Cl}_2(\text{DMF})_2]$. Thermal ellipsoids are drawn at 50% probability, hydrogen atoms have been omitted for clarity. | 91 |
| 5.6.14 | Packing in the unit cell of $[\text{Cu}_3(\text{L}^2)_2\text{Cl}_2(\text{DMF})_2]$ as viewed along the a-axis. | 92 |
| 5.6.15 | Partially labelled thermal ellipsoid plot of $[\text{Ni}(\text{L}^2)]$. Thermal ellipsoids are drawn at 50% probability, hydrogen atoms have been omitted for clarity. | 94 |
| 5.6.16 | Packing in the unit cell of $[\text{Ni}(\text{L}^2)]$ as viewed down the b-axis. | 95 |
| 5.6.17 | Short contacts present in $[\text{Ni}(\text{L}^2)]$ molecules. | 96 |
| 5.6.18 | Partially labelled thermal ellipsoid plot of $[\text{Cu}_3(\text{L}^3)_2(\text{H}_2\text{O})_2]\text{Cl}_2$. Thermal ellipsoids are drawn at 50% probability, hydrogen atoms have been omitted for clarity. | 98 |
| 5.6.19 | Packing in the unit cell of $[\text{Cu}_3(\text{L}^3)_2(\text{H}_2\text{O})_2]\text{Cl}_2$ viewed along the a-axis. | 99 |
| 5.6.20 | Hydrogen bonding in the lattice of $[\text{Cu}_3(\text{L}^3)_2(\text{H}_2\text{O})_2]\text{Cl}_2$. | 99 |
| 5.6.21 | Short contacts and hydrogen bonds in the lattice of $[\text{Cu}_3(\text{L}^3)_2(\text{H}_2\text{O})_2]\text{Cl}_2$. | 100 |
| 5.6.22 | Partially labelled thermal ellipsoid plot of $[\text{Ni}(\text{L}^3)]$. Thermal ellipsoids are drawn at 50% probability, hydrogen atoms have been omitted for clarity. | 102 |
| 5.6.23 | Packing in the unit cell of $[\text{Ni}(\text{L}^3)]$ viewed along the b-axis. | 103 |
| 5.6.24 | Hydrogen bonding in the crystal lattice of $[\text{Ni}(\text{L}^3)]$. | 103 |
| 5.6.25 | Short contacts present in the crystal lattice of $[\text{Ni}(\text{L}^3)]$. | 104 |
| 5.6.26 | Partially labelled thermal ellipsoid plot of $[\text{Zn}_2(\text{L}^3)_2]$. Thermal ellipsoids are drawn at 50% probability, hydrogen atoms have been omitted for clarity. | 106 |
| 5.6.27 | Short contacts present in the crystal lattice of $[\text{Zn}_2(\text{L}^3)_2]$. | 107 |
| 6.1 | Structure and isomers of $[\text{NiL}_{33}(\text{MeOH})]^{2+}$ as determined by | 112 |

| | | |
|------|---|-----|
| | Salehzadeh et al. Adapted from Salehzadeh et al. | |
| 6.2 | Structures of the nickel(II) chelates studied by Trujillo et al. Diagram adapted from Trujillo et al. | 113 |
| 6.3 | 16-membered mixed-donor nickel(II) chelates synthesised by Chandra et al. | 114 |
| 6.4 | Structures of the nickel(II) chelates of salen and phosphasalen ligands. | 115 |
| 6.5 | Overlay of the X-ray structure (orange) and DFT-optimised structure (blue) of $[\text{Ni}(\text{L}^3)]$, overlay similarity = 0.990. | 117 |
| 6.6 | Overlay of the X-ray structure of molecule A (orange) and DFT optimised structure (blue) of $[\text{Ni}(\text{L}^2)]$, overlay similarity index = 0.982. | 118 |
| 6.7 | Overlay of the calculated and experimental UV-visible spectra of $[\text{Ni}(\text{L}^3)]$. | 120 |
| 6.8 | Cartesian axes of $[\text{Ni}(\text{L}^3)]$. | 122 |
| 6.9 | Frontier molecular orbitals of $[\text{Ni}(\text{L}^3)]$ involved in the UV-visible electronic transitions of the metal complex. | 123 |
| 6.10 | Overlay of the calculated and experimental UV-visible spectra for $[\text{Ni}(\text{L}^2)]$. | 124 |
| 6.11 | Cartesian axes of $[\text{Ni}(\text{L}^2)]$. | 126 |
| 6.12 | Frontier molecular orbitals of $[\text{Ni}(\text{L}^2)]$ involved in the UV-visible electronic transitions of the metal complex. | 127 |
| 6.13 | Comparative Ni(II) 3d orbital energy level diagram. | 128 |
| 6.14 | Overlay of the calculated and experimental frequency data for $[\text{Ni}(\text{L}^3)]$. | 130 |
| 6.15 | Overlay of the calculated and experimental frequency data for $[\text{Ni}(\text{L}^2)]$. | 131 |
| 6.16 | Plot of experimental frequency versus calculated frequency for the imine C=N stretching vibrations of both nickel(II) chelates. | 132 |
| 7.1 | Structure of $[\text{Cu}(\text{N}^1\text{-}(2\text{-acetylpyridine})\text{pyridine-2-carboxamidrazone})\text{Cl}_2]$. | 135 |
| 7.2 | Structures of copper(II) complexes of 2,4-diiodo-6-((pyridine-2-ylmethyl amino)methyl)phenol redrawn from Hindo et al. | 135 |

| | | |
|-----|--|-----|
| 7.3 | Modified indolo[3,2-c]quinolines redrawn from Primik et al. | 136 |
| 7.4 | Comparison of the $-\log IC_{50}$ values for all compounds averaged across the cell lines. | 139 |
| 7.5 | Structures of some commercially available chemotherapeutic agents. | 141 |
| 7.6 | Comparison of $-\log IC_{50}$ values of $[Cu_3(L^2)_2Cl_2(DMF)_2]$, cisplatin, 5-fluorouracil, etoposide and bleomycin. | 143 |
| 7.7 | Comparison of $[Cu_3(L^2)_2Cl_2(DMF)_2]$ and literature copper(II) chelates. | 144 |
| 8.1 | Proposed structure for hydroxyl group position rotations to the ortho and para positions. | 146 |
| 8.2 | Proposed synthesis of the ortho and para dimethoxybenzophenones. | 147 |
| 8.3 | Proposed structure highlighting the inclusion of an imidazole functional group to the compounds synthesised in this project. | 148 |
| 8.4 | Protection of amine groups with t-Boc. | 148 |
| 8.5 | Synthetic route for addition of an imidazole group. | 149 |
| 8.6 | Biotinylation agent and product for biotin tagging. | 150 |
| 8.7 | Conjugation of biotin to a PAMAM dendrimer. | 151 |
| 8.8 | Methylated mononuclear copper(II) compound. | 152 |
| A.1 | 1H NMR spectrum of H_3L^1 in DMSO- d_6 . | 163 |
| A.2 | 1H NMR spectrum of H_2L^3 in DMSO- d_6 . | 163 |
| A.3 | 1H NMR spectrum of $[Ni(L^3)]$ in DMSO- d_6 . | 164 |
| A.4 | ^{13}C NMR spectrum of H_3L^1 in DMSO- d_6 . | 164 |
| A.5 | ^{13}C NMR spectrum of H_2L^2 in DMSO- d_6 . | 165 |
| A.6 | ^{13}C NMR spectrum of H_2L^3 in DMSO- d_6 . | 165 |
| A.7 | ^{13}C NMR spectrum of $[Ni(L^2)]$ in DMSO- d_6 . | 166 |
| A.8 | ^{13}C NMR spectrum of $[Ni(L^3)]$ in DMSO- d_6 . | 166 |
| B.1 | UV-vis spectrum of H_3L_1 in DMF at 298 K. | 167 |
| B.2 | UV-vis spectrum of $[Cu_2(L^1)(OAc)(DMF)]$ in DMF at 298 K. | 167 |
| B.3 | UV-vis spectrum of $[Cu_3(L^2)_2Cl_2(DMF)_2]$ in DMF at 298 K. | 168 |
| B.4 | UV-vis spectrum of $[Ni(L^2)]$ in DMF at 298 K. | 168 |
| C.1 | Infrared spectrum of H_3L^1 . | 169 |

| | | |
|-----|---|-----|
| C.2 | Infrared spectrum of $[\text{Cu}_2(\text{L}^1)(\text{OAc})(\text{DMF})]$. | 169 |
| C.3 | Infrared spectrum of $[\text{Ni}(\text{L}^2)]$. | 170 |
| C.4 | Infrared spectrum of H_2L^3 . | 170 |
| C.5 | Infrared spectrum of $[\text{Cu}_3(\text{L}^3)_2(\text{H}_2\text{O})_2]\text{Cl}_2$. | 171 |
| C.6 | Infrared spectrum of $[\text{Ni}(\text{L}^3)]$. | 171 |
| C.7 | Infrared spectrum of $[\text{Zn}_2(\text{L}^3)_2]$. | 172 |

List of Tables

| Table | Title | Page |
|-------|--|------|
| 1.1 | Response of nitric oxide to the different polymeric films studied by Mao et al. | 8 |
| 4.1 | Comparison of the chemical shifts of H_2L^2 and $[Ni(L^2)]$. | 39 |
| 4.2 | Comparison of UV-visible transitions for all ligands and complexes. | 45 |
| 4.3 | UV-visible absorption data for copper(II) chelates. | 48 |
| 4.4 | UV-visible absorption data for nickel(II) chelates. | 49 |
| 4.5 | Observed frequencies (cm^{-1}) for the absorption bands in the solid IR spectra of ligands and complexes synthesised in this work. | 52 |
| 4.6 | Frequencies of copper(II) chelates in this work and literature. | 53 |
| 4.7 | Frequencies of nickel(II) chelates characterised in this work and related structures from the literature. | 54 |
| 4.8 | ESR data for copper(II) complexes studied by Losada et al. | 58 |
| 4.9 | ESR data for the salen type copper(II) complexes synthesised by Klement et al. | 59 |
| 4.10 | ESR data of amino acid derived copper complexes synthesised by Balla et al. | 61 |
| 5.1.1 | Average coordination bond lengths and angles for AQETEV. | 71 |
| 5.1.2 | Coordination bond lengths and angles for LOFXIO. | 72 |
| 5.6.1 | Intramolecular hydrogen bond and short contact lengths (\AA) and angles ($^\circ$) for H_3L^1 . | 80 |
| 5.6.2 | Intermolecular hydrogen bond and short contact lengths (\AA) and angles ($^\circ$) for H_3L^1 . | 82 |
| 5.6.3 | Intramolecular hydrogen bond lengths (\AA) and angles ($^\circ$) for H_2L^2 . | 84 |
| 5.6.4 | Intermolecular short contacts and hydrogen bond lengths | 86 |

| | | |
|--------|---|-----|
| | (Å) and angles (°) for H_2L^2 . | |
| 5.6.5 | Hydrogen bond and short contact lengths (Å) and angles (°) for $[Cu_2(L^1)(OAc)(DMF)]$. | 89 |
| 5.6.6 | Table of coordination bond lengths for $[Cu_2(L^1)(OAc)(DMF)]$. | 89 |
| 5.6.7 | Table of coordination bond angles in $[Cu_2(L^1)(OAc)(DMF)]$. | 90 |
| 5.6.8 | Short contact lengths (Å) and angles (°) for $[Cu_3(L^2)_2Cl_2(DMF)_2]$. | 92 |
| 5.6.9 | Table of average coordination bond lengths in $[Cu_3(L^2)_2Cl_2(DMF)_2]$. | 93 |
| 5.6.10 | Table of average coordination bond angles in $[Cu_3(L^2)_2Cl_2(DMF)_2]$. | 93 |
| 5.6.11 | Short contact lengths (Å) and angles (°) for $[Ni(L^2)]$. | 96 |
| 5.6.12 | Table of average coordination bond lengths in $[Ni(L^2)]$. | 97 |
| 5.6.13 | Table of average coordination bond angles for $[Ni(L^2)]$. | 97 |
| 5.6.14 | Hydrogen bonds and short contact lengths (Å) and angles (°) for $[Cu_3(L^3)_2(H_2O)_2]Cl_2$. | 100 |
| 5.6.15 | Table of coordination bond lengths in $[Cu_3(L^3)_2(H_2O)_2]Cl_2$. | 101 |
| 5.6.16 | Table of coordination bond angles in $[Cu_3(L^3)_2(H_2O)_2]Cl_2$. | 101 |
| 5.6.17 | Hydrogen bond and short contact lengths (Å) and angles (°) for $[Ni(L^3)]$. | 104 |
| 5.6.18 | Table of coordination bond lengths and bond angles in $[Ni(L^3)]$. | 105 |
| 5.6.19 | Short contact lengths (Å) and angles (°) for $[Zn_2(L^3)_2]$. | 107 |
| 5.6.20 | Table of coordination bond lengths in $[Zn_2(L^3)_2]$. | 107 |
| 5.6.21 | Table of coordination bond angles for $[Zn_2(L^3)_2]$. | 108 |
| 5.6.22 | Table of coordination bond lengths and bond angles between zinc(II) ions in the dinuclear structure $[Zn_2(L^3)_2]$. | 108 |
| 6.1 | Calculated and experimental bond lengths (Å) of $[NiL_{33}(MeOH)]^{2+}$. | 112 |
| 6.2 | Experimental and calculated bond lengths (Å) in nickel(II) chelates reported by Trujillo et al. | 113 |

| | | |
|-----|--|-----|
| 6.3 | Calculated and experimental bond lengths (Å) and bond angles (°) of the nickel(II) chelates of salen and phosphasalen ligands. | 115 |
| 6.4 | Comparison of selected bond lengths (Å) and angles (°) of the calculated and experimental structure of [Ni(L ³)]. | 117 |
| 6.5 | Comparison of selected bond lengths (Å) and angles (°) of the calculated and experimental structure of [Ni(L ²)]. | 119 |
| 6.6 | Experimental and calculated electronic transitions for [Ni(L ³)]. | 121 |
| 6.7 | Experimental and calculated electronic transitions for [Ni(L ²)]. | 125 |
| 6.8 | NBO 3d atomic orbital energies and electron populations of [Ni(L ²)] and [Ni(L ³)]. | 129 |
| 6.9 | Experimental and calculated vibrational frequencies of the nickel(II) chelates. | 133 |
| 7.1 | IC ₅₀ values of the modified indolo[3,2-c]quinolines copper(II) chelates. | 137 |
| 7.2 | Tabulation of the half maximal inhibitory concentrations. | 138 |
| D.1 | Crystal data and structure refinement for H ₃ L ¹ . | 173 |
| D.2 | Crystal data and structure refinement for H ₂ L ² . | 174 |
| D.3 | Crystal data and structure refinement for [Cu ₂ (L ¹)(OAc)(DMF)]. | 175 |
| D.4 | Crystal data and structure refinement for [Cu ₃ (L ²) ₂ Cl ₂ (DMF) ₂]. | 176 |
| D.5 | Crystal data and structure refinement for [Ni(L ²)]. | 177 |
| D.6 | Crystal data and structure refinement for [Cu ₃ (L ³) ₂ (H ₂ O) ₂]Cl ₂ . | 178 |
| D.7 | Crystal data and structure refinement for [Ni(L ³)]. | 179 |
| D.8 | Crystal data and structure refinement for [Zn ₂ (L ³) ₂]. | 180 |

1. Introduction

1.1 Preface

Cancer is a global health problem as it does not discriminate who it affects, is deadly if left untreated, and thus commands a regimen of treatment methods from health care professionals. Some tumour cells have an innate resistance to the drugs used to treat them and so secondary cancers can become resistant after primary treatment. This project focuses on reproducing bleomycin activity with regard to DNA cleavage *via* radical production. Various analogues of a known copper compound, (5-amino-5-methyl-3,7-diazanonanedioate) copper(II), have been synthesised in this project by imine formation. This complex was studied by Pamatong *et al.* and is shown below in **Figure 1.1**.

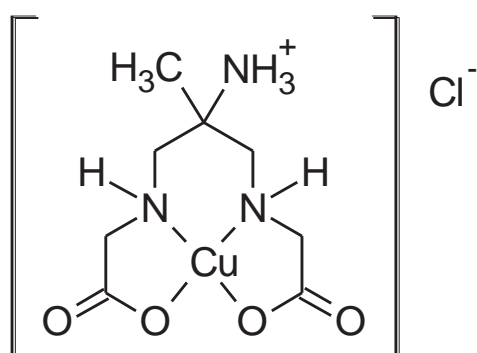


Figure 1.1: Structure of (5-amino-5-methyl-3,7-diazanonanedioate) copper(II).^[1]

In the present work, structural analogues of the ligand in **Figure 1.1** will be chelated to copper(II), nickel(II) and zinc(II). The complexes therefore have the same N₂O₂ tetradentate coordination sphere as (5-amino-5-methyl-3,7-diazanonanedioate) copper(II). These chelates would be aimed towards uses in cancer treatment and would therefore be screened as such. Illustrated below in **Figure 1.2** are the ligands to be synthesised. The ligands consist of 2,4-dihydroxybenzophenone linked by a synthetically variable di(azomethine) bridge.

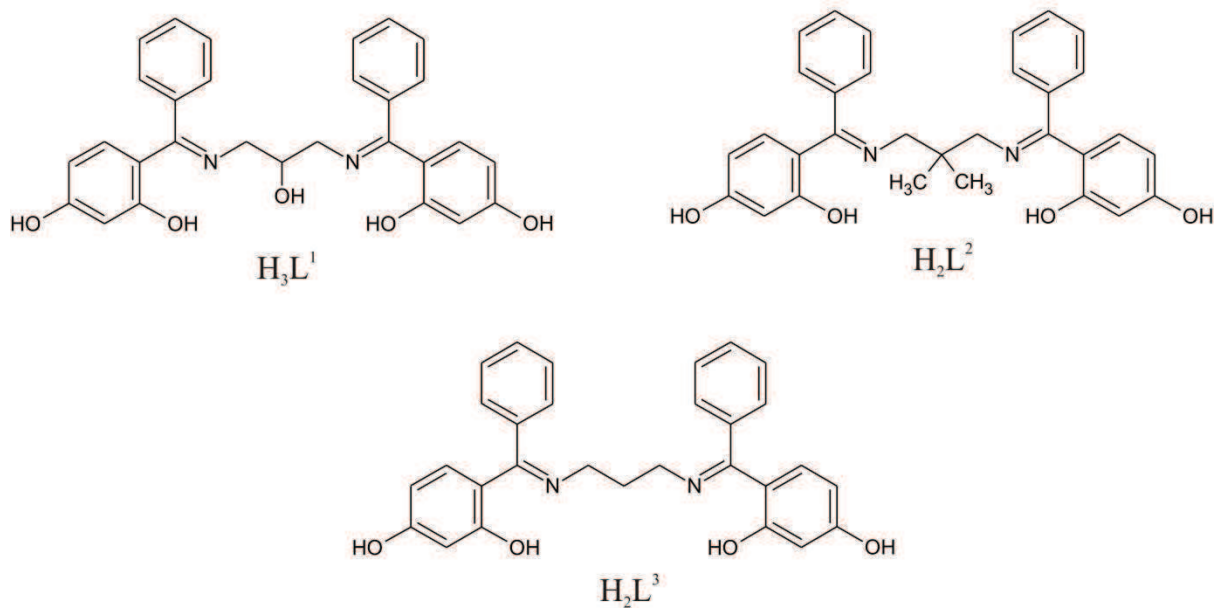


Figure 1.2: Ligands proposed for synthesis and chelation to Cu(II), Ni(II) and Zn(II).

1.2 Chemistry of Copper



Figure 1.3: Copper metal in its raw state.^[2]

The date of copper's discovery is not clearly known, but its extraction from its commonly found ores was already well developed by 3400 B.C. by the early Egyptians.^[3] Copper (**Figure 1.3**) has many ores of which an example is *malachite* ($\text{CuCO}_3 \cdot \text{Cu}(\text{OH})_2$) that has a brilliant green colour and was used as a pigment by the Renaissance artists in the fabrics of paintings.^[3] Copper has an atomic number of 29, atomic mass of 65.55 g mol^{-1} , it has a melting point of $1083 \text{ }^\circ\text{C}$ ^[3-5] and it boils at $2310 \text{ }^\circ\text{C}$ ^[3]. The copper atom has one electron in its $4s$ shell, outside its filled $3d$ shell giving an electronic configuration of $[\text{Ar}] 3d^{10} 4s^1$. Copper's most common oxidation states are (I) and (II).^[4] Copper(I) adopts square planar or tetrahedral geometries more commonly; whereas copper(II) will favour a distorted octahedral geometry with two longer *trans* bonds.^[4] These distortions can be attributed to the d^9 configuration of copper(II).^[4] Copper(II) is classified as an intermediate acid^[6] meaning it will favour coordination by intermediate bases, such as NO_2^- . Copper is classified as a noble metal and can sometimes be found in its pure state which has a fine rose-pink sheen, however once molten the colour is green.^[3, 5] The pure metal is soft, malleable and ductile with a very high electrical and heat conductivity.^[3, 5] This coupled with its reasonable cost allows for its wide use in electrics.^[5] Copper is miscible with gold and other metals and is used in alloys, such as its most commonly known mixture with zinc; brass.^[4] In biology, copper is used in the oxygen transport molecule haemocyanin in molluscs and arthropods^[6] as well as in the terminal oxidase enzyme system in the mitochondrial respiratory chain of all living cells.

1.3 Chemistry of Nickel



Figure 1.4: Metallic nickel in its raw state.^[7]

Nickel (**Figure 1.4**) was first isolated accidentally in 1751 by Axel Fredrik Cronstedt who believed it to be copper. Nickel has an atomic number 28, atomic mass of 58.69 g mol^{-1} , it has a melting point of $1455 \text{ }^\circ\text{C}$ and boils at $2732 \text{ }^\circ\text{C}$.^[5] The nickel atom has two electrons in its $4s$ shell making its electronic configuration $[\text{Ar}] 3d^8 4s^2$. Nickel's most common oxidation state is nickel(II); however less common are the nickel(III) and nickel(IV) states. Nickel(II) has a wide variety of geometries, namely octahedral, trigonal bipyramidal, square pyramidal, tetrahedral and, most commonly, square planar.^[4] In the planar d^8 configuration one of the d orbitals ($d_{x^2-y^2}$) will be uniquely high in energy making the eight electrons occupy the four lower d orbitals leaving the one highest in energy vacant.^[4] Nickel(II) is also an intermediate acid^[6] meaning it will favour coordination by intermediate bases, such as SO_3^{2-} . Nickel ores that are found naturally all consist of metal mixtures.^[5] It is less magnetic than iron and loses its magnetism at $340 \text{ }^\circ\text{C}$.^[5] Nickel is used in many alloys, one of the more important being stainless steel. Due to its corrosion resistance it is often applied in a thin layer *via* electroplating as a protective barrier, for example in the automotive industry bumpers may be nickel plated.^[4-5] It is also used as a catalyst in a Raney nickel hydrogenation reaction using hydrogen to reduce organic compounds.^[5] Nickel is used by several enzymes and a cofactor in biology.^[8] For example, nickel(II) is incorporated in Factor F430 which is a cofactor of methyl coenzyme M reductase.^[9] This Factor is involved in the last step of methanogenesis.^[9] However, nickel(II) can be very toxic in living systems if taken in high doses.^[10-11] Unlike copper(II), nickel(II) does not produce hydroxyl radicals, capable of cleaving DNA. Comparison of the copper(II) and nickel(II) compounds could therefore aid elucidation of the mode of action of the potential chemotherapeutic agents.

1.4 Chemistry of Zinc



Figure 1.5: Metallic zinc in its raw state.

Zinc (**Figure 1.5**) was first isolated in 1746 by Marggraf upon heating its oxide with carbon, which acts as a reducing agent.^[3] It has an atomic number of 30, atomic mass of 65.41 g mol^{-1} , it melts at $419 \text{ }^\circ\text{C}$ ^[3, 5] and boils at $907 \text{ }^\circ\text{C}$ ^[3]. The zinc atom has the electronic configuration of $[\text{Ar}] 3d^{10} 4s^2$. The most common oxidation state is zinc(II). Like copper(II) and nickel(II), zinc(II) is an intermediate Lewis acid^[6] meaning it will favour coordination by intermediate bases, such as SCN^- . Since copper(II), nickel(II) and zinc(II) are all Lewis acids of comparable strength with similar ionic radii (0.072 nm, 0.069 nm, 0.074 nm, respectively), it should be possible to chelate all three to the same ligands. Zinc complexes tend to be four to six coordinate species and the main geometry is tetrahedral.^[3, 6] Zinc ores are quite plentiful; the ore that supplies the most zinc is called *sphalerite* and is a sulphide. Zinc is easily extracted from its ores.^[3-5] It is a white metal that, if polished, has a lustre that is tarnished and dulled by air exposure.^[3-5] Zinc metal is relatively hard and very brittle, especially at $200 \text{ }^\circ\text{C}$ where it can be ground to powder.^[5] The main use of zinc is in the making of alloys, the most commonly known being brass, and in galvanising steel.^[5] Zinc acts as a very strong reducing agent and when combined with hydrochloric acid is commonly used by chemists as a reducing system.^[3] In biological systems the Zn^{2+} ion is commonly utilised due to its slightly softer accepting nature in comparison to Mg^{2+} , which means it is a stronger Lewis acid for biological molecules.^[6] As zinc will not readily undergo redox reactions it simplifies its chemistry in these biological systems.^[6] Furthermore, its labile nature with respect to chelating and releasing ligands is a desirable feature in biology and in synthetic chemistry.^[6] Zinc occurs in two important enzymes; carbonic anhydrase, that functions in the hydration-dehydration cycle of carbon dioxide and carboxypeptidases that catalytically hydrolyse peptide bonds in proteins.^[6]

1.5 Applications of Metal Schiff Base Complexes

Schiff bases are used as ligands for a wide variety of metal ions as the complexes they form can perform a variety of functions, ranging from nitric oxide sensors^[12] to pharmaceuticals^[13]. The ligands themselves can be used for photochromic and thermochromic purposes in the solid state.^[14] A few Schiff base metal complexes have been selected for a brief overview of the wide application of these complexes.

Yao *et al.*^[15] synthesised and characterised four copper(II) Schiff base complexes in an attempt to study their solvatochromism. They found that only one complex, [*N,N'*-bis(4-methoxy salicylidene)-1,2-diaminoethane]copper(II), displayed colour isomerism. It produced three coloured solids; brown from methanol in the presence of water, blue from methanol with water absent and green from ethanol and DMSO. They reported a range of violet to blue colouring of the solutions of the green solid when dissolved in different solvents. Yao *et al.*^[15] stated that as the σ donor capacity of the solvent increased the solvent would coordinate to the metal centre *via* substitution of a water molecule, and this would in turn change the energy of the transitions leading to the solvatochromic effect. The structure is shown below in **Figure 1.6**.

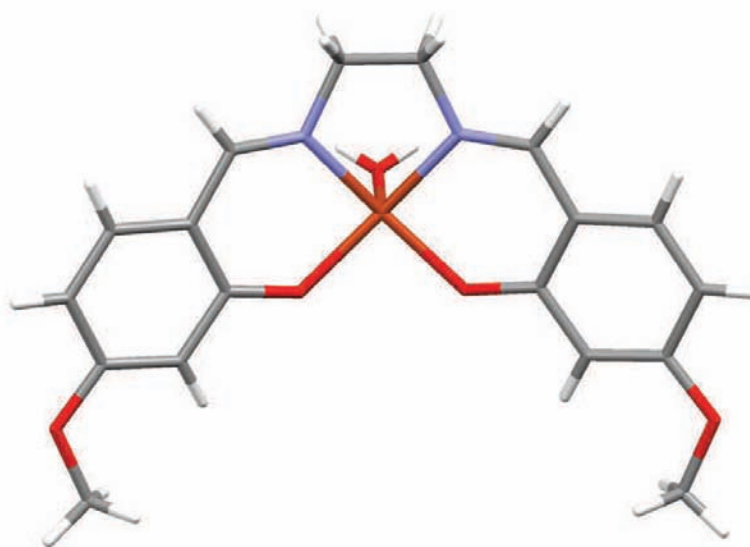


Figure 1.6: Structure of (*N,N'*-bis(4-methoxysalicylidene)ethane-1,2-diamine)copper(II), a potential sensor for organic solvents.^[15]

Research into the oxidation of hydrocarbons, such as toluene and cyclohexane by means of a metal complex catalyst is of some importance as the products of these reactions are of industrial significance.^[16] Cyclohexanol, for example, is the oxidised product of cyclohexane and is used in the manufacture of adipic acid, which is one of the materials used for pesticides and rubber chemicals, among many other things.^[16] Roy *et al.*^[16] successfully synthesised and studied tetranuclear copper(II) Schiff base complexes (**Figure 1.7**) for use as catalysts in these types of oxidation reactions. They found that in a slightly acidic medium under ambient conditions with hydrogen peroxide as the oxidant, cyclohexane and toluene were oxidised to cyclohexanol and cyclohexanone, and benzyl alcohol and benzaldehyde, respectively. They also reported that by varying the proportions of nitric acid and oxidant with respect to the catalyst and reaction times, one can optimize the yield of these reactions with respect to both reaction products; alcohol and aldehyde or ketone. It was suggested that the nitric acid would accommodate the pentacoordinated copper centre in the catalyst by protonation of the ligand, which allows for increased unsaturation of the copper atom.^[16]

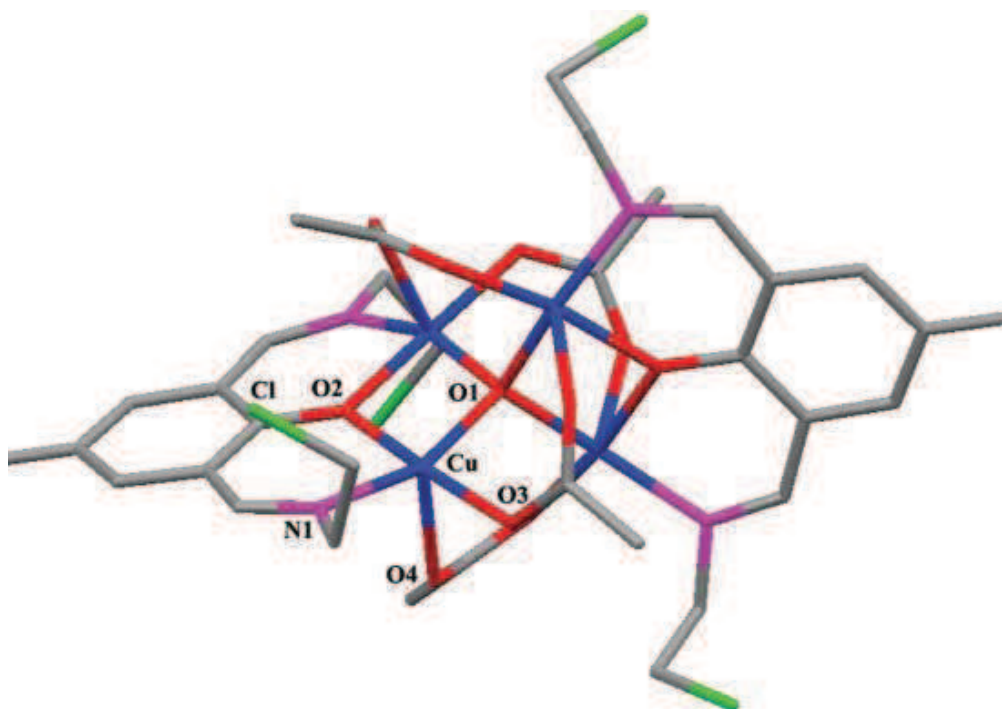


Figure 1.7: Structure of the copper(II) Schiff base duplicated from Roy *et al.*^[16] A catalyst for the oxidation of organic compounds.

Nitric oxide is a compound of interest as it is a signal molecule (endothelial-derived relaxing factor which promotes smooth muscle relaxation) for animals and in order to study its biological uses there is a need for selective and sensitive measurement of it. ^[12] Most of the specific molecular materials used in surface-modified electrodes are metal complexes. Mao *et al.* ^[12] developed metal complexes of salen, (ethylenebis(salicylideneimine)) using iron, cobalt, copper and manganese, which they then constructed into an electropolymerized film in order to study its application in electrochemical nitric oxide sensors. The structure of salen is shown in **Figure 1.8**.

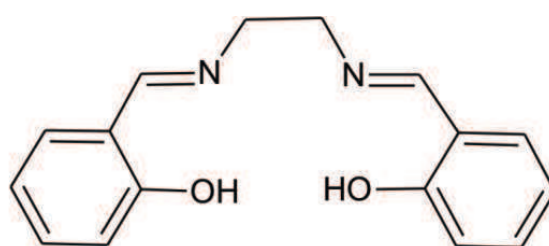


Figure 1.8: Structure of the ligand ethylenebis(salicylideneimine).

In previous studies with the same aim, nickel(II) was used as the metal for complexation by salen, porphyrin and phthalocyanine ligands. ^[12] Mao *et al.* ^[12] found that these complexes produced similar results, which suggested that the metal centre was not the key factor in producing the electrochemical catalytic activity. It was suggested that the nitric oxide oxidation was possibly due to electron conjugation.

Table 1.1: Response of nitric oxide to the different polymeric films studied by Mao *et al.* ^[12]

| Film used | Linear range of detection | Detection limit (nM) |
|-----------|---------------------------|----------------------|
| Co(salen) | 19.8 nm – 2.80 μ M | 12 |
| Fe(salen) | 19.6 nm – 1.13 μ M | 10 |
| Cu(salen) | 23.4 nm – 2.10 μ M | 19.8 |
| Mn(salen) | 39.6 nm – 1.50 μ M | 20 |

1.6 Metal-Based Anti-Microbial and Anti-Cancer Agents

Some of the earliest documentations of copper chemistry show its use as an anti-microbial agent.^[17] Between 2600 and 2200 B.C. copper was used in the sterilisation of drinking water and chest wounds. Then around 1500 B.C. it was documented that copper compounds were being prescribed to treat ailments such as burn wounds, itching and neck growths.^[17] In 1867 the first publication of copper's role in the immune system was published when copper workers were found to be immune to the cholera outbreaks in Paris.^[17] Then in 1895 Kobert published inorganic copper preparations that were proven to be effective in the treatment of eczema, tubercular infections, lupus, and syphilis.^[17] In Germany in 1912, facial epitheliomas were successfully treated using a combination of copper chloride and lecithin.^[17] In 1913 at the University of Liverpool and in 1930 in France, injections of colloidal copper were proven to help treat solid tumours. Bayer synthesised an organic copper complex used for the treatment of tuberculosis which led to copper treatments of tuberculosis persisting into the 1940s.^[17] The anti-microbial effects of copper have been incorporated into everyday surfaces in an attempt to decrease the spread of microbes, especially in hospitals and clinics. Copper alloys have thus been used to make things such as doorknobs and tray tables.

Cancer is defined as abnormal cell growth.^[18-19] The proliferation can lead to masses of tissue, which are then called malignant tumours.^[19] There are three main pathways to treating people with cancer; chemotherapy, radiation therapy and surgery. Radiation therapy involves utilising radiation from radioactive substances to target these fast dividing cells causing destruction of the tissue or tumour. This technique is based on the fact that these fast dividing cells are more susceptible to radiation damage than healthy cells.^[19] Alternatively, chemotherapy can be used to treat cancer. Chemotherapy is the treatment of cancer using drugs, (sometimes alone but more commonly in combinations) that target cancer cells. These drugs either stop cancer cell division or slow it down.^[19] Chemotherapy is sometimes used in conjunction with radiation therapy.

Anti-cancer drugs are generally designed to target rapidly proliferating cells.^[20] This includes cancer cells, but also non-cancerous but rapidly dividing cells, such as hair follicles. This lack of specificity leads to the unpleasant side-effects of chemotherapy. This is shown, for

example, by the targeting of DNA polymerase by the drugs Vernolepin and Helenalin.^[18, 20] DNA polymerase is an enzyme that cells use to replicate their DNA in order to proliferate. The drug's mode of action is *via* an irreversible conjugate addition of the α - β -unsaturated carbonyls in the drugs (**Figure 1.9**) and the thiol present on the enzyme itself. This abnormality in the enzyme means it loses functionality and the DNA cannot replicate.

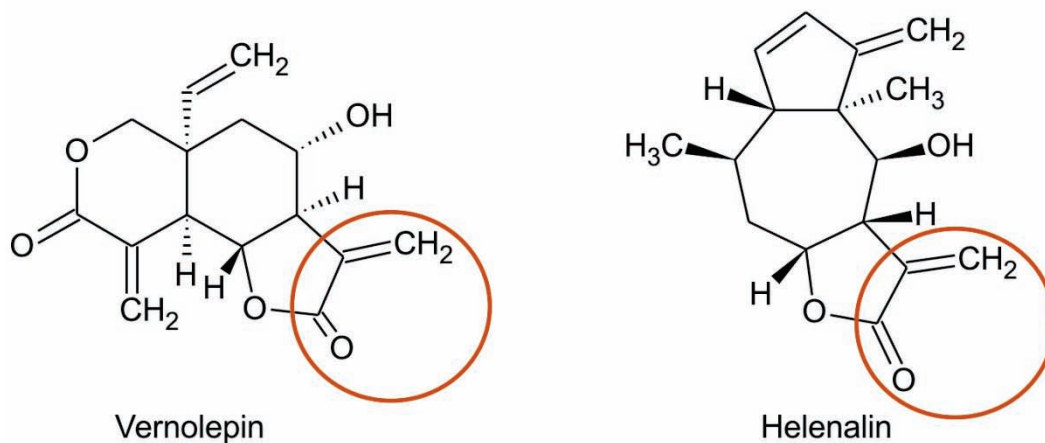


Figure 1.9: Structures of DNA polymerase targeting anti-cancer drugs. The highlighted areas indicate where the enzyme will bind.

Cisplatin is one of the most well known and widely used metal-based anti-cancer drugs, due to its high success. It was first FDA approved for clinical use in 1978.^[21] It works by binding DNA through its bases, preferentially through guanine.^[22] This forms an intermediate of $[\text{PtCl}(\text{guanine-DNA})(\text{NH}_3)_2]^+$, meaning another chlorine atom can be displaced by another guanine to form a crosslink. The crosslink prevents mitosis from occurring and will trigger DNA to attempt a repair. The repair will prove unsuccessful, which leads the cell to initiate apoptosis; programmed cell death. The main problem with this drug is that if the cancer returned it would be cisplatin-resistant. Cisplatin does, however, have its side-effects, namely kidney damage, nerve damage, nausea and vomiting, electrolyte imbalances, and loss of hearing.

Sugars are of the utmost importance in many biological activities, for example, signal transduction and as targets of bacterial or viral infection of cells.^[23] This is why efforts have

been made to understand and imitate these processes.^[23] Striegler and Gichinga^[23] synthesised a sugar discriminating, binuclear Schiff base copper(II) complex. They suggested that the ligand itself was the determining factor for the sugar recognition as it would determine the complex's geometry. They therefore synthesised one asymmetrical and two symmetrical complexes in order to study the effects of changing the ligand structure. In so doing they proved that although structurally similar and with identical sugar binding sites, the slightest structural changes had large effects on the complex's interactions with the sugar.

It has been found that certain guanine-rich DNA sequences are potential targets for chemotherapeutics in cancerous cells. These guanine-rich sequences utilise hydrogen bonding to form tetrads (four in-plane guanine bases hydrogen-bonded), which in turn lead to quadruplex DNA structures (stacks of tetrads).^[24-31] These guanine-rich structures can be stabilised by electrostatic interactions with alkali metal cations.^[24-25] Using a complex to stabilise these quadruplex structures, specifically in human telomeric DNA (DNA consisting of TTAGGG sequence repeats that end in guanine-rich single-strand overhangs) leads to inhibition of an enzyme called telomerase which is responsible for preventing shortening of telomeric DNA.^[24-31] This enzyme is over-expressed by cancer cells and therefore is an essential factor in immortalising cancer cells.^[24-31] In research done by Arola-Arnal *et al.*^[24] a series of salen and salphen complexes of nickel(II), copper(II), zinc(II) and vanadium(IV) were synthesised and their interactions with human telomeric DNA was studied.

Arola-Arnal *et al.*^[24] used their studies to elucidate important features in metal chelates for interaction with quadruplex DNA to enable further research to be done to create potential anti-cancer agents. It was found that the planar complexes of nickel(II) and copper(II) were efficient stabilisers of the quadruplex structures. They also discovered that when the metal atom was bound to the ligand it reduced electron density in the rings which allows for better π - π stacking interactions (**Figure 1.10**). The zinc(II) complex lacked interaction due to its non-planar region and pentacoordination.

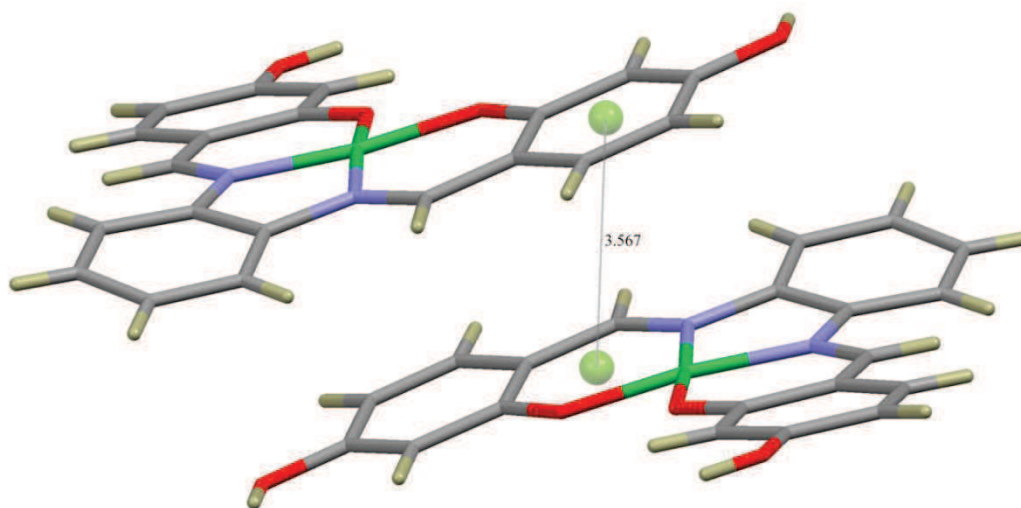


Figure 1.10: Stacking of the nickel(II) salen complexes, showing an centroid-to-centroid spacing of 3.567 Å.^[24]

These select examples show the wide application of Schiff base ligands when coordinated to copper(II), nickel(II), zinc (II) and other metals.

The above examples also show that although there are effective chemotherapeutics available, they all have their disadvantages. It is thus critical that there is constant research into the development of new, more effective drugs.

1.7 Bleomycin and Its Analogues

Bleomycin is of interest as its mode of action is reproducible using smaller and easier to produce compounds. The compounds synthesised in this project were based on a well known bleomycin analogue^[1] (**Figure 1.1**), to mimic the mode of action and thus find application in cancer treatment.

Bleomycin was first isolated in 1966 by Umezawa *et al.*^[32] from *Streptomyces verticillus*. It was deemed a glycopeptide anti-biotic that had anti-cancer properties.^[33] It has since been used in combination with drugs, such as cisplatin, for the treatment of mostly testicular

cancer, but also for types of lymphomas. [32, 34] Hashimoto *et al.* [35] have proposed that there are three components to bleomycin; the DNA recognition component (the bis(thiazole) moiety), the binding site which activates the bleomycin by chelating a metal and finally, a sugar component. The structure of bleomycin and its components are illustrated in **Figure 1.11**.

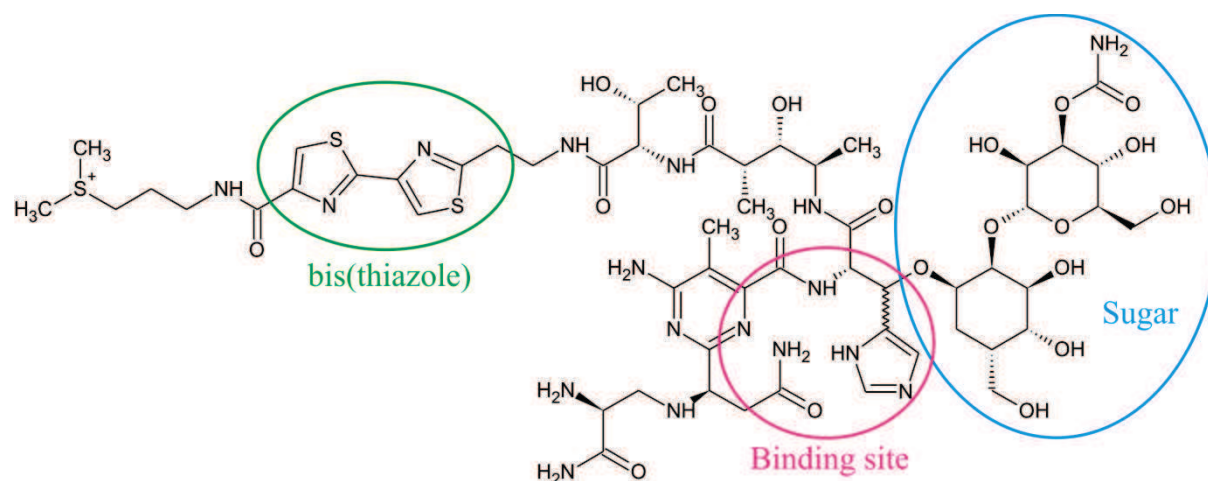


Figure 1.11: Structure of bleomycin from *Streptomyces verticillus* and its components.

Bleomycin is not an active species on its own. It requires chelation of a reduced transition metal ion in order to be activated and this is only achieved in the presence of oxygen and a reductant of some sort. [32, 34-35] Once activated, bleomycin can bind DNA in two alternative ways; *via* intercalation or by binding the minor groove. [36] The bleomycin structure chelates metal ions and the complex cleaves DNA by producing reactive oxygen species such as superoxide and hydroxide free radicals. [37] It is believed to function as an anti-cancer treatment that works by inducing both double- and single- stranded DNA breaks [35]. Furthermore, the metal centres are thought to play a very important role in the activation of the phosphate group present in the backbone of the DNA molecule in order for it to be attacked by the nucleophilic radicals, created by activation of a water molecule *via* the metal centre. [38] Bleomycin can degrade species in two ways; *via* a radical pathway or through formation of hydroxyl radicals. [32]

A proposed cleavage mechanism is suggested by Chen and Stubbe.^[32] It suggests that in the presence of oxygen and a suitable reductant, bleomycin will chelate iron(II) to form an Fe(II)-O₂-Bleomycin species. (Bleomycin first forms an Fe(II)-bleomycin complex which will activate the oxygen).^[39] The iron is oxidised from Fe(II) to Fe(III), whilst the oxygen in the compound undergoes a reduction, yielding a negatively charged bleomycin-Fe(III) species.^[35] Further reaction occurs to afford the activated bleomycin-Fe(III)-OOH species. This compound can then either; cleave the protein, damage lipids, cleave DNA/RNA or degrade back to its original inactive form. The overall reaction mechanism is shown below in **Figure 1.12**.

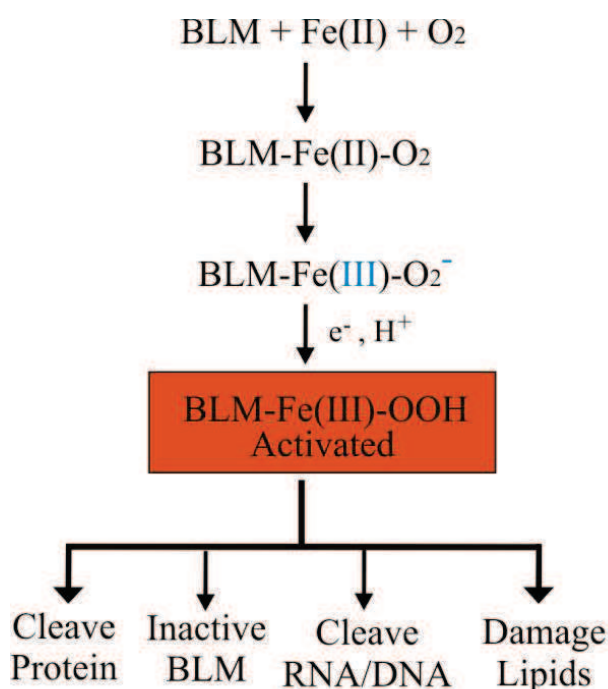


Figure 1.12: Activation of bleomycin (BLM) in the presence of oxygen and iron.

During DNA cleavage, the activated compound will remove the 4'-hydrogen from the deoxyribose of a pyrimidine^[40] that is 3' to a guanine thus forming a 4'-radical intermediate. Bleomycin recognises guanosine-cytosine rich fragments in DNA for its cleavage action by intercalating its bis(thiazole) component.^[33] Two pathways are possible for the 4'-radical, depending on oxygen concentration. At lower concentrations of oxygen, the radical can be oxidised to a carbocation which will then form an oxidised, abasic site by the addition of two

equivalents of water. The abasic site refers to the loss of a nucleotide base. This also removes the pyrimidine from its deoxyribose segment attached to the DNA backbone. This is illustrated in **Figure 1.13**.

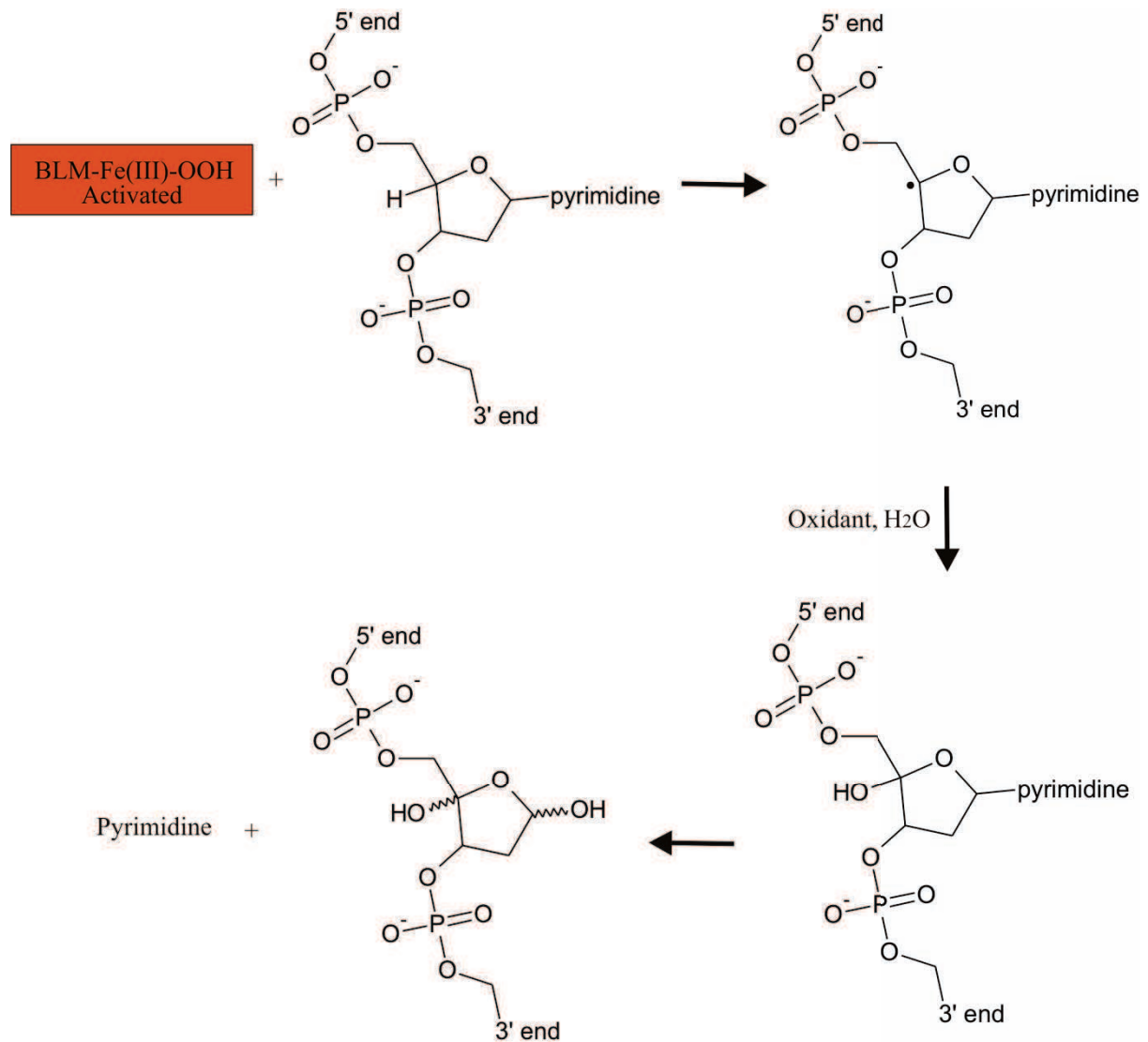


Figure 1.13: Cleavage by bleomycin (BLM) in low oxygen concentrations.

Alternatively, in the presence of higher oxygen concentrations, the radical could be converted to a peroxy radical in a reaction involving oxygen. This peroxy radical is then reduced to a hydroperoxide, which reacts further to ultimately afford cleaved DNA in the form of three end products; a pyrimidine propenal, the 5'- phosphate end of DNA and the 3'-

phosphoglycolate end of DNA.^[41] They also propose that a single bleomycin molecule is responsible for double stranded DNA cleavage. This is illustrated in **Figure 1.14**.

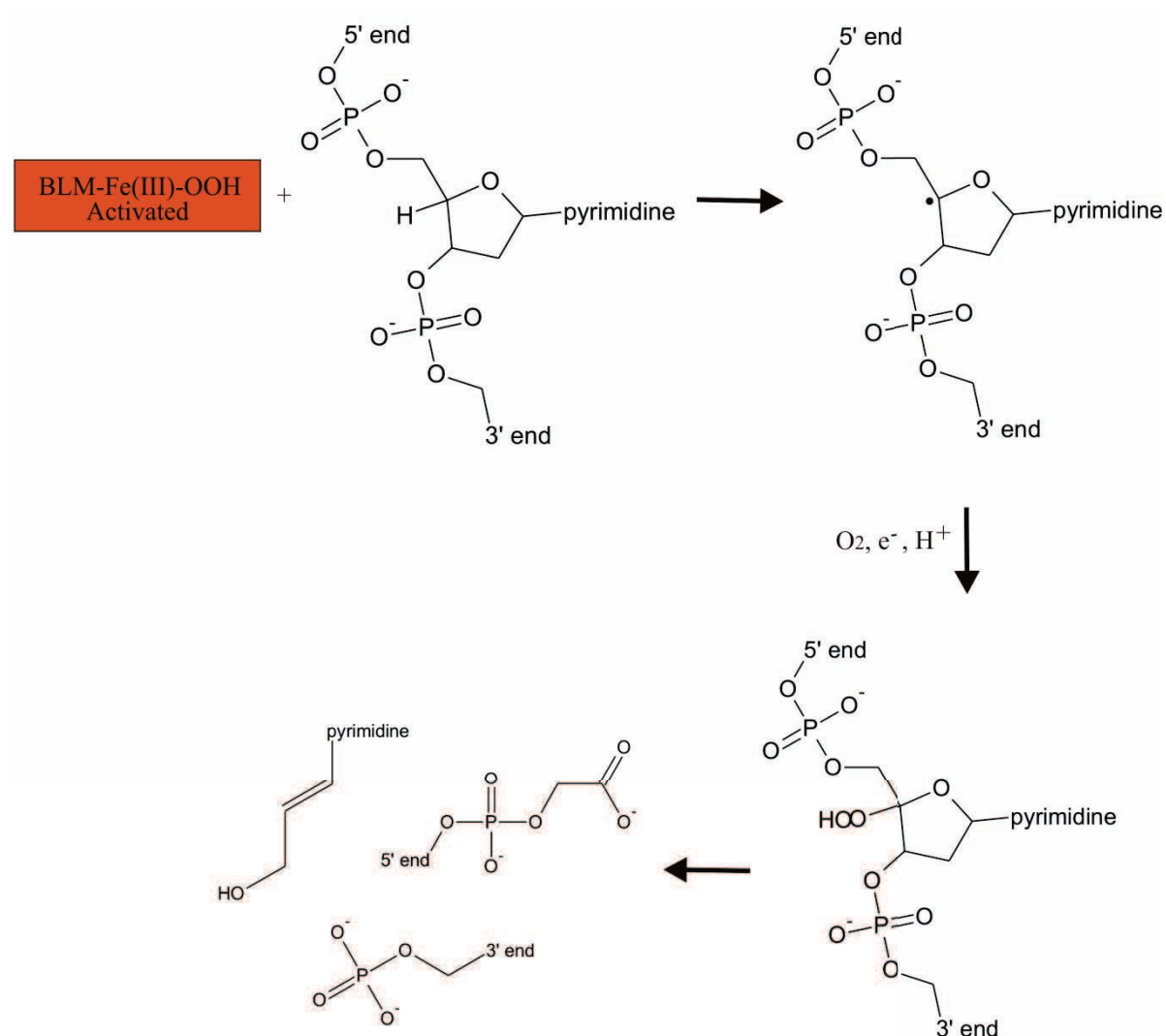


Figure 1.14: DNA cleavage by bleomycin (BLM) in high oxygen concentrations.

In 1986 Hashimoto *et al.*^[35] synthesised novel hemin-intercalators that cleaved DNA using bleomycin as their model. The design of their ligands incorporated a DNA-recognition and intercalation portion and a hemin group. Hemin is considered to be an oxygen activating molecule, which would follow the above mechanism for bleomycin induced DNA cleavage. These hemin-ligands were chelated to iron(II) for the purposes of their studies. They found two of their complexes were strong DNA cleavers, the structures are shown in **Figure 1.15**.

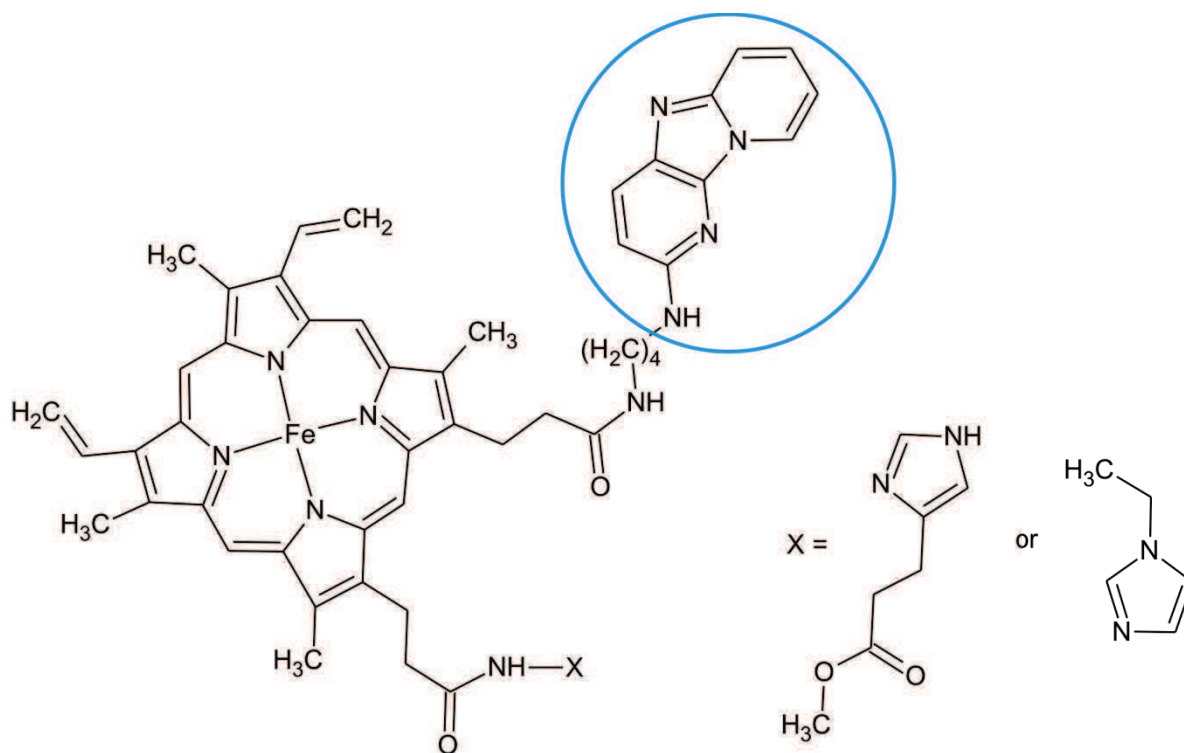


Figure 1.15: Structures of hemin-intercalators studied by Hashimoto *et al.*^[35] with the highlighted DNA recognition portion.

The intercalator portion of the compound is 2-amino-6-methyldipyrido[1,2-*a*:3',2'-*d*]imidazole and was found to be of utmost importance in DNA recognition and intercalation in order to allow for effective DNA-cleavage. This moiety is suitable for DNA intercalation as it is planar and aromatic. It is thus able to intercalate between the planar aromatic base pairs of DNA. The intercalated moiety is stabilised by favourable π - π interactions with the aromatic base pairs. The other factor for strong DNA-cleavage was found to be any functional group in the hemin molecule that acts as an intramolecular ligand for iron(II). The DNA cleavage studies performed by Hashimoto *et al.*^[35] revealed that their hemin-intercalators were cleaving DNA in a pattern almost identical to that of bleomycin. The cleavage by these hemin-intercalators was performed preferentially at guanine-cytosine and guanine-thymine sequences which afforded a 5'-phosphoryl group and three groups on the 3'-end; one being a hydroxyl group. Some of the hemin-intercalators studied by Hashimoto *et al.*^[35] were found to have anti-tumour activity similar to that of bleomycin.

Pamatong *et al.*^[1] reported a bleomycin analogue of copper which was shown to produce hydroxyl radicals and induce DNA cleavage. Their research was directed towards creating a complex that could perform non-random, double-stranded DNA cleavage as this is known to induce cell apoptosis as it is much harder for the cell to repair than a single strand DNA break. They designed their complexes with two priorities in mind, a metal centre that can be reactivated and DNA recognition segments. These features allow the complex to carry out its function; nick the DNA, bind at the nicked site, activate oxygen and finally, induce strand scission in order to yield linear DNA fragments.^[1] The two complexes synthesised in their study are shown below in **Figure 1.16**.

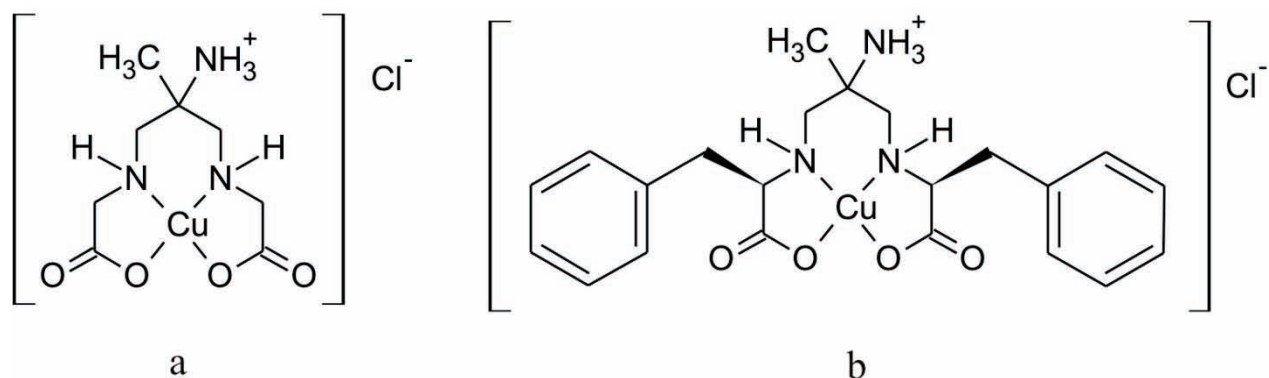


Figure 1.16: Structures of (5-amino-5-methyl-3,7-diazanonanedioate)copper(II) (a) and ((2*S*,8*R*)-5-amino-2,8-dibenzyl-5-methyl-3,7-diazanonanedioate)copper(II) (b). Both complexes are capable of inducing double-stranded DNA cleavage.

The amino acids glycine and phenylalanine were used in the synthesis of the ligands for their hydrophobic nature as this creates the possibility for hydrophobic interactions with DNA bases. The ammonium group allows for favourable electrostatic interaction with the negatively charged phosphate backbone of the DNA helix. This interaction also allows for the amino acid segments to be positioned into the hydrophobic interior of the DNA itself. In their studies of these complexes, Pamatong *et al.* found that both complexes cleave DNA.^[1] However, they found that the phenylalanine complex cleaves DNA more efficiently than the glycine complex. They attribute this difference in activity to the phenylalanine side chain, proposing that the charge and aromaticity allows for improved DNA binding, which leads to more efficient cleavage. Their studies also went so far as to prove that hydroxyl radicals were

the active species in DNA cleavage by studying the effects of the compounds in the presence of hydroxyl radical quenchers.

In further studies done by Pamatong *et al.*,^[42] copper(II) was chosen as the metal centre due to its redox activity and its well known ability to generate activated oxygen species which lead to cleavage of DNA through hydrolysis of its phosphodiester. In this study it was again shown that the bleomycin analogues, shown above in **Figure 1.16**, cleave DNA by the production of hydroxyl radicals and not through any other activated oxygen species or metal-oxo intermediates. Their results are shown in **Figure 1.17**.

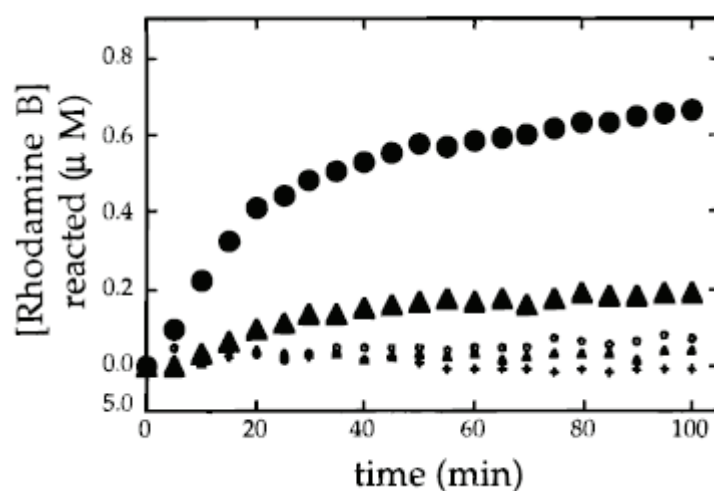


Figure 1.17: Monitoring hydroxyl radical production by rhodamine B decay in phosphate buffer. The reaction conditions for each are as follows: ● aerobic activation with both H₂O₂ and sodium ascorbate, ▲ aerobic activation with only sodium ascorbate, • anaerobic activation with both H₂O₂ and sodium ascorbate ▲ anaerobic activation with only sodium ascorbate, + quenching of ascorbate activation by ethanol. Reproduced from reference^[42].

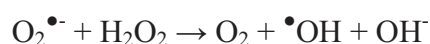
Figure 1.17 shows three different hydroxyl radical quenchers were used along with the synthesised chelates and no reaction took place. This was done to show that the active oxidant in the reaction was indeed the hydroxyl radicals produced.

The study focused on the mechanism of radical production, which was shown to favour the Haber-Weiss reaction rather than that of the Fenton or Fenton-like copper peroxo mechanisms. In his last paper in 1934, Professor Fritz Haber conceptualised that utilising both hydrogen peroxide and superoxide, a highly reactive hydroxyl radical could be produced.^[43-44] Once it was discovered that free radicals were produced in biological systems, the reaction was seen as a pathway to produce more toxic radicals from less reactive species.^[44] The Haber-Weiss reaction is, however, thermodynamically unfavourable and therefore requires a catalyst. In the original paper it was shown that a metal catalyst can be used in two separate reactions which afford the overall Haber-Weiss reaction.^[44] The Fenton reaction is the reaction of hydrogen peroxide with a metal-catalyst resulting in the formation of a hydroxyl radical.^[43] Pamatong *et al.* used superoxide dismutase to remove the O_2^- from the reaction which leaves **only** the reducing agent and hydrogen peroxide. This is key to the Fenton reaction and lead to no products being formed.^[42] These reactions are shown below:

Fenton reaction:



Haber-Weiss Reaction



These examples show the biological significance of copper(II) and suggest that it is likely to be an effective metal for use as chemotherapeutic agents in this project.

1.8 Project Objectives

The literature survey has shown there is room for expansion in the library of bleomycin analogues for use as anti-cancer agents. Analogues are created in order to simplify manufacturing and to create smaller molecules that allow for the same or better activity. The ligands for this project were therefore based on a known bleomycin analogue^[1], (5-amino-5-

methyl-3,7-diazanonanedioate)copper(II). The compounds comprise a tetradentate ligand consisting of two nitrogen and two oxygen donors with a square planar geometry at the metal centre. Coordination of the ligands with concomitant deprotonation of the hydroxyl groups affords a dianionic, N_2O_2 tetradentate ligand. A phenyl ring was included as a substituent in the design of the ligands as copper complexes with phenyl ring substituents have been observed to have a higher chemotherapeutic activity and more specific, or non-random, DNA cleavage activity,^[1]. This is possibly due to enhanced binding to the DNA strands. Following full characterisation of the novel ligands, chelation to copper(II) will create novel complexes that should act as hydroxyl radical producing, bleomycin analogues. Nickel(II) and zinc(II) will also be chelated in an attempt to vary the activity of the compounds because these metals are commonly grouped together in such studies. Since nickel(II) and zinc(II) do not produce hydroxyl radicals in solution, enhanced activity of the copper chelates, relative to nickel(II) and zinc(II) would suggest that hydroxyl radical generation is the likely mode of action.

The following specific objectives have been identified for the project:

- To produce novel ligands, structurally similar to known bleomycin analogues.
- To form novel metal complexes of Cu(II), Ni(II) and Zn(II) using these ligands.
- To fully characterise all ligands and metal complexes using NMR, IR, EPR/ESR and UV/visible spectroscopy as well as single crystal X-ray crystallography.
- Perform computational modelling on the metal complexes.
- To screen the novel compounds for biological activity against various human cancer lines.

2. Experimental

2.1 Instrumentation and Chemicals

All solvents used were reagent grade and acquired from Merck. All reagents were purchased from Sigma-Aldrich and used as received, except zinc acetate which was purchased from SAARCHEM. No special conditions were used in any of the reactions.

^1H and ^{13}C NMR spectra were recorded on either a Bruker Avance III 500 or Bruker Avance III 400 spectrometer at frequencies of 500 MHz/400 MHz (^1H) and 125 MHz/100 MHz (^{13}C) using either a 5 mm BBOZ probe or a 5 mm TBIZ probe. All proton and carbon chemical shifts are quoted relative to the relevant solvent signal (*e.g.* DMSO- d_6 : ^1H , 2.50 ppm, ^{13}C , 39.5 ppm). Proton-proton coupling constants are reported in Hertz. All experiments were conducted at 30 °C unless specified otherwise.

Liquid-chromatography-mass-spectrometry was carried out using a Waters Micromass LCT Premier TOF Mass Spectrometer using the ES+ ionisation mode. Infrared spectra were collected using solids on a Bruker Alpha-P spectrometer with an Attenuated Total Reflection Platinum Diamond 1 reflectance accessory.

UV-visible spectra were collected from 1000 nm to 200 nm using a Shimadzu UV-1800 Spectrophotometer using DMF as the solvent in 1.0 cm pathlength quartz cuvettes.

2.2 Ligand Synthesis

2.2.1 Synthesis of 4, 4'-{2-hydroxypropane-1,3-diylidene-bis[nitrilo(phenylmethanediyl)]}dibenzene-1,3-diol, H₃L¹

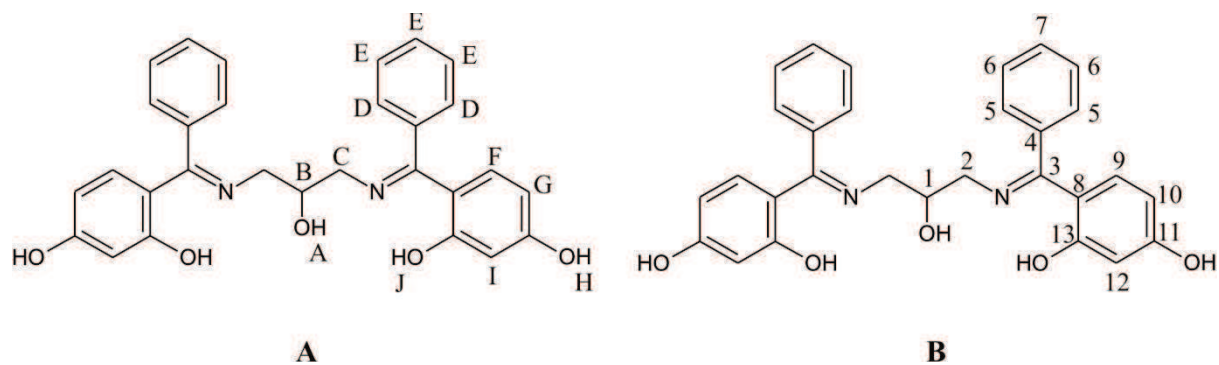


Figure 2.1: Diagrams depicting the numbering schemes used for the assignment of the NMR spectra of H₃L¹; A = ¹H NMR and B = ¹³C NMR.

To 2,4-dihydroxybenzophenone (5.790 g, 27.03 mmol) in methanol (40 mL) was added 1,3-diamino-2-hydroxypropane (1.310 g, 14.53 mmol) in methanol (10 mL) with magnetic stirring which afforded an orange solution. This solution was heated to reflux for 24 hours, during which time the product precipitated as a bright yellow powder. This was isolated by filtration, washed with methanol and allowed to air dry. Yield: 71 % (4.603 g, 9.540 mmol). A portion of the powder was recrystallised in a test tube by slow diffusion of diethyl ether into a solution of the ligand in dimethylformamide (DMF). The crystals formed were cubic in shape and yellow in colour.

¹H NMR (ppm) (DMSO-*d*₆): δ 3.19-3.28 (m, 5 H, B & C), 3.88 (br s, 1 H, A), 6.06 (dd, *J* = 2.4 Hz, *J* = 8.8 Hz, 2 H, G), 6.17 (d, *J* = 2.4 Hz, 2 H, I), 6.45 (d, *J* = 8.8 Hz, 2 H, F), 7.17-7.19 (m, 4 H, D), 7.48-7.50 (m, 6 H, E), 9.42 (br s, 2 H, H), 15.83 (s, 2 H, J).
¹³C NMR (ppm) (DMSO-*d*₆): δ 54.0 (t, 2), 69.7 (d, 1), 103.2 (d, 12), 105.9 (d, 10), 111.9 (s, 8), 127.2 (d, 5), 128.6 (d, 6), 128.9 (d, 7), 132.6 (d, 9), 133.2 (s, 4), 161.7 (s, 11), 166.8 (s, 13), 173.7 (s, 3). HRMS (TOF) C₂₉H₂₆N₂O₅: calculated 482.5271, found *m/z* 483.1923 [M+1]. UV-vis (DMF) [λ_{\max} , nm (ϵ , M⁻¹ cm⁻¹)]: 389 (2.99 × 10³), 312 (2.07 × 10⁴), 281

(2.54×10^4). IR (cm^{-1}): 3440 [w br, $\nu(\text{O-H})$], 3251 [w br, $\nu(\text{O-H})$], 1567 [m, $\nu(\text{C=N})$], 1540 [m, $\nu(\text{C=N})$], 1226 [s, $\nu(\text{C-O})$].

2.2.2 Synthesis of 4,4'-{2,2-dimethylpropane-1,3-diylidene-bis[nitrilo(phenylmethanediyl)]}dibenzene-1,3-diol, H_2L^2

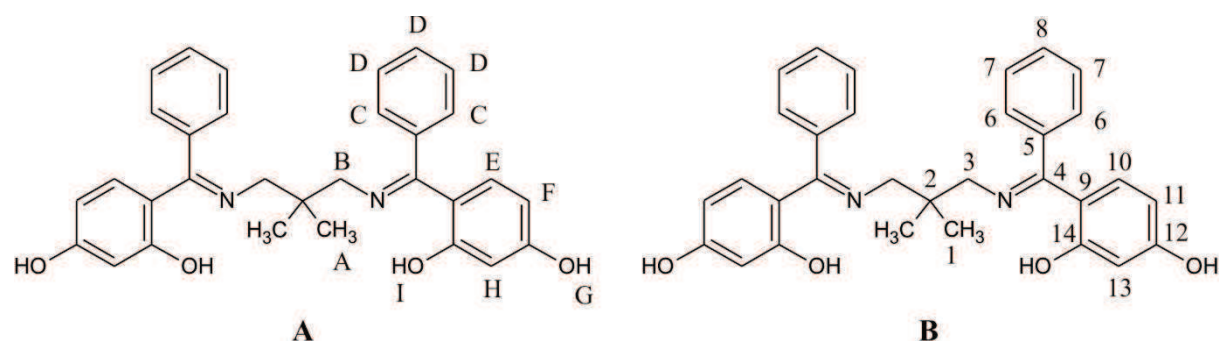


Figure 2.2: Diagrams depicting the numbering schemes used for the assignment of the NMR spectra of H_2L^2 , A = ^1H NMR and B = ^{13}C NMR.

To a solution of 2,4-dihydroxybenzophenone (5.874 g, 27.42 mmol) in methanol (40 mL) was added 1,3-diamino-2,2-dimethylpropane (1.518 g, 14.86 mmol) in methanol (10 mL) with magnetic stirring resulting in no change in colour (the solution remained yellow). This solution was heated to reflux for 24 hours yielding the product as a pale yellow powder. This was filtered and washed with methanol and allowed to air dry. Yield: 81% (5.320 g, 11.08 mmol). A portion of the powder was recrystallised by slow diffusion of diethyl ether into a saturated solution of the ligand in DMF. The crystals formed were cubic in shape and yellow in colour.

^1H NMR (ppm) ($\text{DMSO}-d_6$): δ 0.92 (s, 6 H, A), 3.04 (s, 4 H, B), 6.08 (dd, $J = 8.8$ Hz, $J = 2.4$ Hz, 2 H, F), 6.21 (d, $J = 2.4$ Hz, 2 H, H), 6.45 (d, $J = 8.8$ Hz, 2 H, E), 7.11-7.12 (m, 4 H, C), 7.45-7.48 (m, 6 H, D), 9.72 (br s, 2 H, G), 15.94 (s, 2 H, I). ^{13}C NMR (ppm) ($\text{DMSO}-d_6$): δ 23.8 (q, 1), 35.7 (s, 2), 58.5 (t, 3), 103.1 (d, 13), 106.1 (d, 11), 111.9 (s, 9), 127.0 (d, 6), 128.6 (d, 7), 128.9 (d, 8), 132.5 (d, 10), 133.2 (s, 5), 161.7 (s, 12), 166.3 (s, 14),

173.6 (s, 4). HRMS (TOF) $C_{31}H_{30}N_2O_4$: calculated 494.5809, found m/z 495.2289 [M+1]. UV-vis (DMF) [λ_{max} , nm (ϵ , $M^{-1} cm^{-1}$)]: 393 (2.40×10^3), 313 (2.01×10^4), 281 (2.57×10^4). IR (cm^{-1}): 3637 [w br, $\nu(O-H)$], 1583 [m, $\nu(C=N)$], 1242 [s, $\nu(C-O)$].

2.2.3 Synthesis of 4,4'-{propane-1,3-diylidene-bis[nitrilo(phenylmethanediyl)]} dibenzene-1,3-diol, H_2L^3

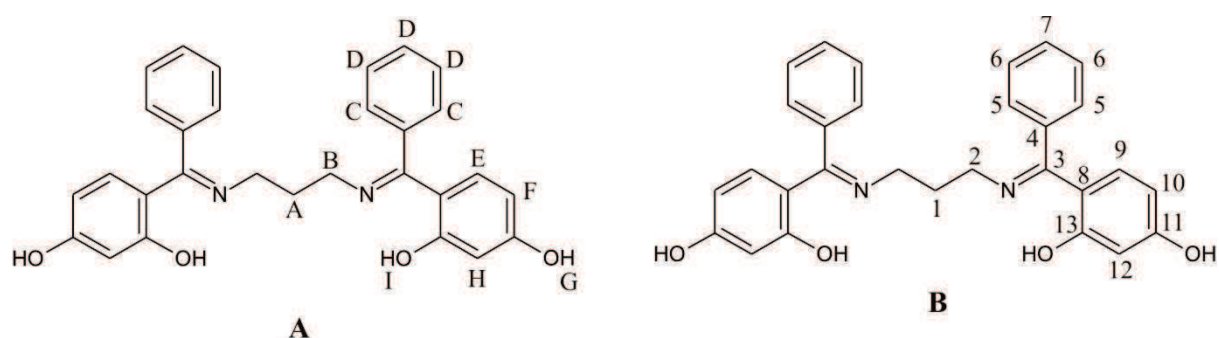


Figure 2.3: Diagrams depicting the numbering schemes used for the assignment of the NMR spectra of H_2L^3 , A = 1H NMR and B = ^{13}C NMR.

To a solution of 2,4-dihydroxybenzophenone (5.950 g, 27.78 mmol) in methanol (40 mL) was added 1,3-diaminopropane (1.396 g, 18.83 mmol) in methanol (10 mL) with magnetic stirring which afforded a yellow solution. This solution was heated to reflux for 24 hours yielding the product as a yellow powder. This was then filtered and washed with methanol and allowed to air dry. Yield: 85% (5.538 g, 11.87 mmol).

1H NMR (ppm) ($DMSO-d_6$): δ 1.84 (q, $J = 6.9$ Hz, 2 H, A), 3.22 (m, 4 H, B), 3.50 (br s, 2 H, G), 6.06 (dd, $J = 2.4$ Hz, $J = 8.8$ Hz, 2 H, F), 6.17 (d, $J = 2.4$ Hz, 2 H, H), 6.44 (d, $J = 8.7$ Hz, 2 H, E), 7.19 (m, 4 H, C), 7.47-7.57 (m, 6 H, D), 15.85 (br s, 2 H, I). ^{13}C NMR (ppm) ($DMSO-d_6$): δ 31.4 (t, 1), 47.3 (t, 2), 103.2 (d, 12), 106.1 (d, 10), 111.7 (s, 8), 127.0 (d, 5), 128.65 (d, 6), 128.9 (d, 7), 132.5 (d, 9), 133.1 (s, 4), 161.9 (s, 11), 166.6 (s, 13), 173.4 (s, 3). HRMS (TOF) $C_{29}H_{26}N_2O_4$: calculated 466.52774, found m/z 467.1965 [M+1]. UV-vis

(DMF) [λ_{\max} , nm (ϵ , $M^{-1} \text{ cm}^{-1}$): 390 (2.99×10^3), 312 (2.09×10^4), 281 (2.56×10^4).
IR (cm^{-1}): 3056 [w br, $\nu(\text{O-H})$], 1571 [s, $\nu(\text{C=N})$], 1241 [s, $\nu(\text{C-O})$], 1190 [m, $\nu(\text{C-O})$].

2.3 Metal Chelate Synthesis

2.3.1 Synthesis of $[\text{Cu}_2(\text{L}^1)(\text{OAc})(\text{DMF})]$, where $\text{L}^1 = 6,6'-((1E,1'E)-((2\text{-oxidopropane-1,3-diyl})\text{bis}(\text{azanylylidene}))\text{bis}(\text{phenylmethanylylidene}))\text{bis}(\text{3-hydroxyphenolate})$, OAc = acetate and DMF = dimethylformamide

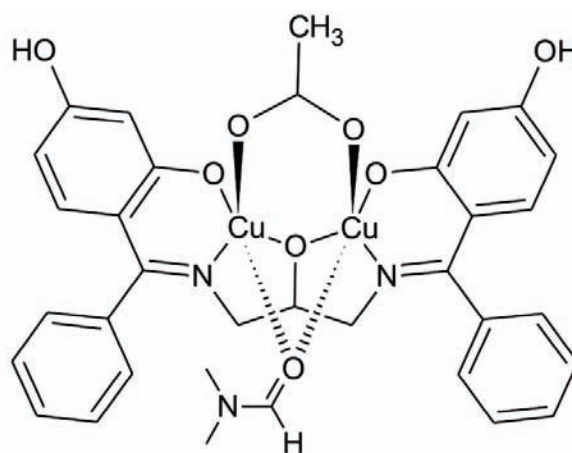


Figure 2.4: Structure of $[\text{Cu}_2(\text{L}^1)(\text{OAc})(\text{DMF})]$.

To H_3L^1 (0.208 g, 0.4310 mmol) in methanol (10 mL), ethanol (5 mL) and DMF (10 mL) was added copper acetate monohydrate (0.173 g, 0.867 mmol) turning the solution a dark emerald green. This was refluxed further for 2 hours. This yielded the product as a green precipitate. Yield: 84% (0.238 g, 0.357 mmol). A portion of the powder was recrystallised by slow diffusion of diethyl ether into a portion of the reaction mixture. This gave diamond-shaped emerald green crystals.

HRMS (TOF) $\text{C}_{31}\text{H}_{27}\text{N}_2\text{Cu}_2\text{O}_7$: calculated 666.6478, found m/z 687.0232 [M-1+23 sodium adduct]. UV-vis (DMF) [λ_{\max} , nm (ϵ , $M^{-1} \text{ cm}^{-1}$): 360 (1.93×10^4), 293 (3.41×10^4).

IR (cm⁻¹): 3196 [w br, ν(O-H)], 3355 [w br, ν(O-H)], 1649 [s, ν(C=N)], 1210 [m, ν(C-O)], 1238 [s, ν(C-O)].

2.3.2 Synthesis of [(L²)(Cl)(DMF)Cu•Cu•Cu(L²)(Cl)(DMF)], where L² = 6,6'-((1*E*,1'*E*)-(2,2-dimethylpropane-1,3-diyl)bis(azanylylidene))bis(phenylmethanylylidene))bis(3-hydroxyphenolate), [Cu₃(L²)₂Cl₂(DMF)₂]

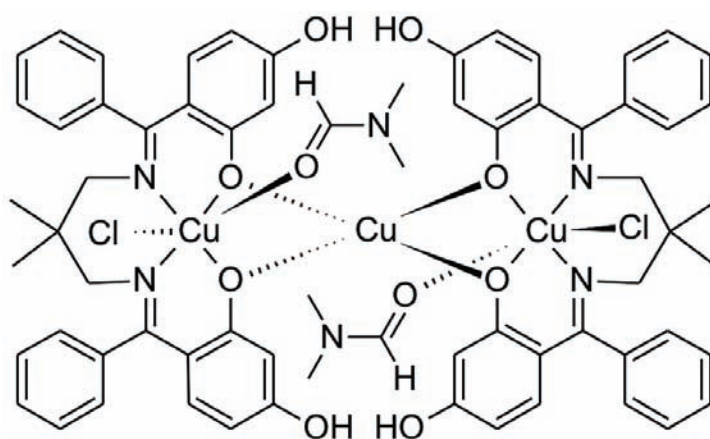


Figure 2.5: Structure of [Cu₃(L²)₂Cl₂(DMF)₂].

To a stirred solution of H₂L² (0.204 g, 0.412 mmol) in metanol (10 mL), ethanol (5 mL) and DMF (5 mL) was added a solution of copper chloride dihydrate (0.111 g, 0.651 mmol). The solution was heated to reflux yielding a bright red-brown solution. The product formed as a brown precipitate. This was filtered and washed with cold THF. Yield: 39% (0.226 g, 0.1623 mmol). Recrystallisation was achieved by slow evaporation of the reaction mixture. The crystals formed were red and rectangular.

HRMS (TOF) C₃₁H₂₈N₂CuO₄: calculated 556.1110, found *m/z* 556.1429 [Cu(L²)+1] dissociation of the bridging copper occurs. UV-vis (DMF) [λ_{max}, nm (ε, M⁻¹ cm⁻¹): 598 (4.49 × 10²) 362 (3.05 × 10⁴), 295 (7.36 × 10⁴). IR (cm⁻¹): 3055 [w br, ν(O-H)], 3345 [w br,

$\nu(\text{O-H})$], 3588 [w br, $\nu(\text{O-H})$], 1660 [s, $\nu(\text{C=N})$], 1198 [s, $\nu(\text{C-O})$], 1216 [s, $\nu(\text{C-O})$], 1246 [s, $\nu(\text{C-O})$].

2.3.3 Synthesis of $[\text{Ni}(\text{L}^2)]$, where $\text{L}^2 = 6,6'-((1E,1'E)-((2,2\text{-dimethyl propane-1,3-diyl})\text{bis}(\text{azanylylidene}))\text{bis}(\text{phenyl methanylylidene}))\text{bis}(3\text{-hydroxyphenolate})$

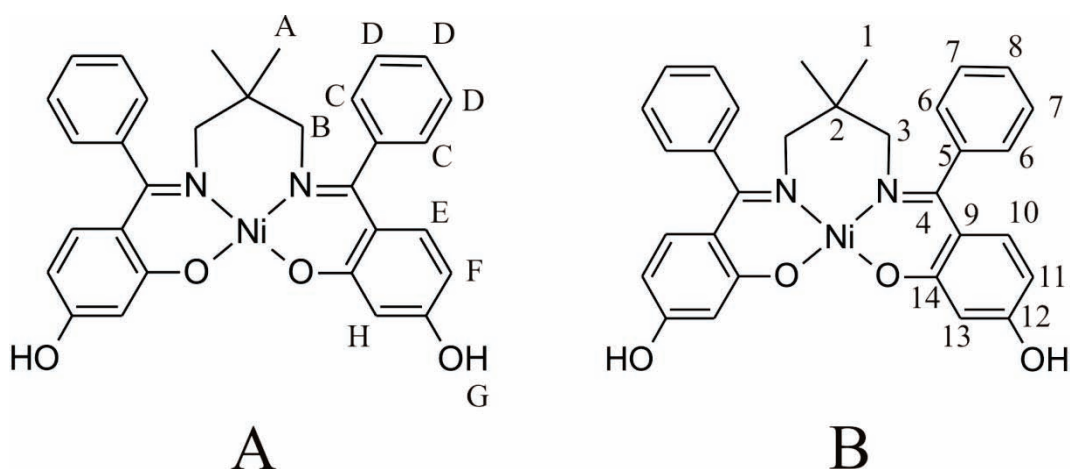


Figure 2.6: Diagrams depicting the numbering schemes used for the assignment of the NMR spectra of $[\text{Ni}(\text{L}^2)]$, A = ^1H NMR and B = ^{13}C NMR.

To a refluxing solution of H_2L^2 (0.225 g, 0.4549 mmol) in methanol (10 mL), an ethanol (5 mL) and DMF (10 mL) mixture containing nickel chloride hexahydrate (0.118 g, 0.4964 mmol) was added; this resulted in a clear yellow solution with some precipitate present. Reflux was maintained for two hours, which led to the solution turning brown. This gave the product in solution. Crystals were formed by slow evaporation of the reaction mixture. The crystals that formed were red and needle-like. Yield: 50% (0.128 g, 0.232 mmol).

^1H NMR (ppm) ($\text{DMSO-}d_6$): δ 0.72 (s, 6 H, A), 3.35 (br s, 4 H, B), 5.78 (dd, 2H, $J = 9.0$ Hz, $J = 2.2$ Hz, 2 H, F), 6.04 (d, $J = 2.2$ Hz, 2 H, H), 6.20 (d, $J = 8.9$ Hz, 2 H, E), 7.09-7.11 (m, 4 H, C), 7.40-7.48 (m 6 H, D), 9.65 (br s, 2 H, G). ^{13}C NMR (ppm)

(DMSO-*d*₆): δ 25.7 (q, 1), 33.8 (s, 2), 61.1 (t, 3), 104.9 (d, 11), 106.2 (d, 13), 117.6 (s, 9), 127.4 (d, 6), 128.3 (d, 7), 128.5 (d, 8), 133.9 (d, 10), 137.8 (s, 5), 161.9 (s, 14), 165.7 (s, 12), 171.2 (s, 4). HRMS (TOF) C₃₁H₂₈N₂NiO₄: calculated 551.2584 found *m/z* 573.1290 [M+23 sodium adduct]. UV-vis (DMF) [λ_{max} , nm (ϵ , M⁻¹ cm⁻¹): 404 (1.07 × 10⁴), 349 (1.31 × 10⁴). IR (cm⁻¹): 3575 [w br, ν (O-H)], 3631 [w br, ν (O-H)], 1616 [m, ν (C=N)], 1561 [m, ν (C=N)], 1220 [m, ν (C-O)], 1190 [m, ν (C-O)], 1164 [s, ν (C-O)].

2.3.4 Synthesis of [(L³)(H₂O)Cu•Cu•Cu(L³)(H₂O)]Cl₂ where L³ = 6,6'-((1*E*,1'*E*)-(propane-1,3-diylbis(azanylylidene))bis(phenylmethanylylidene))bis(3-hydroxyphenolate), [Cu₃(L³)₂(H₂O)₂]Cl₂

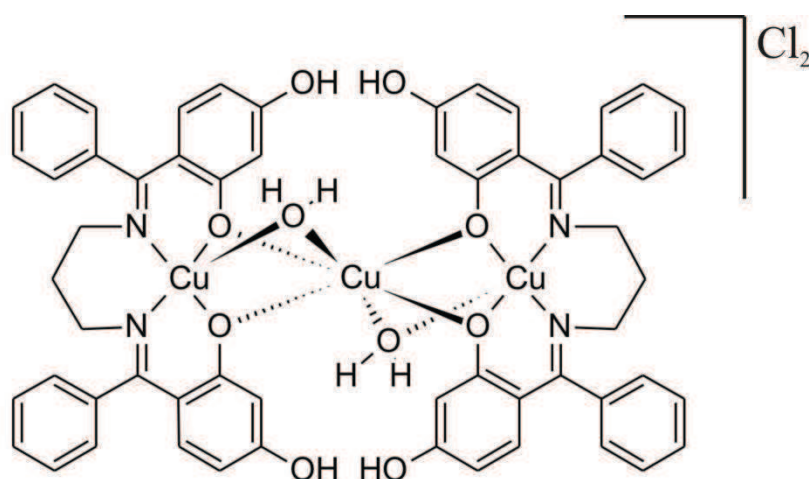


Figure 2.7: Structure of [Cu₃(L³)₂(H₂O)₂]Cl₂.

To a stirred solution of H₂L³ (0.226 g, 0.484 mmol) in methanol (10 mL), ethanol (5 mL) and DMF (5 mL) was added a solution of copper chloride dihydrate (0.109 g, 0.640 mmol). This turned the solution a dark red-brown colour. The solution was stirred and allowed to slowly evaporate, which afforded the product as a brown powder. Yield: 21% (0.115 g, 0.0995 mmol). Recrystallisation was achieved by slow evaporation of the reaction mixture. The crystals formed were red and rectangular.

HRMS (TOF) $C_{29}H_{24}N_2CuO_4$: calculated 528.0584, found m/z 550.0935 [$Cu(L^3)+23$; sodium adduct] dissociation of the copper bridge occurs. UV-vis (DMF) [λ_{max} , nm (ϵ , $M^{-1} cm^{-1}$): 596 (5.83×10^2) 358 (2.43×10^4), 295 (5.68×10^4). IR (cm^{-1}): 3417 [w, $\nu(O-H)$], 3267 [m, $\nu(O-H)$], 3143 [m, $\nu(O-H)$], 1599 [m, $\nu(C=N)$], 1251 [m, $\nu(C-O)$], 1222 [s, $\nu(C-O)$], 1191 [s, $\nu(C-O)$].

2.3.5 Synthesis of $[Ni(L^3)]$, where $L^3 = 6,6'-((1E,1'E)-(propane-1,3-diylbis(azanylylidene))bis(phenylmethanylylidene))bis(3-hydroxyphenolate)$

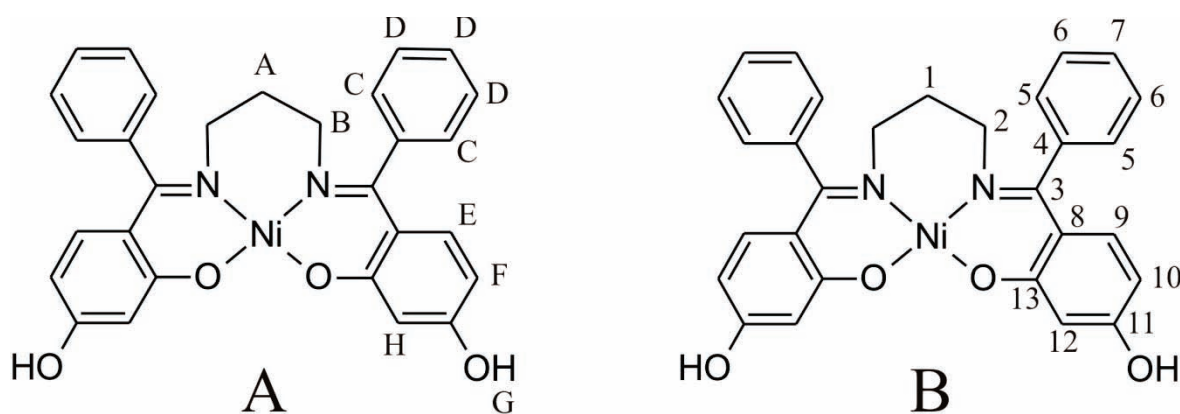


Figure 2.8: Diagrams depicting the numbering schemes used for the assignment of the NMR spectra of $[Ni(L^3)]$, A = 1H NMR and B = ^{13}C NMR.

To a refluxing solution of H_2L^3 (0.217 g, 0.4651 mmol) in methanol (10 mL), ethanol (5 mL) and DMF (10 mL) was added nickel chloride hexahydrate (0.167 g, 0.7025 mmol); the solution turned clear brown. Reflux was maintained for 2 hours. This produced the product in solution. Crystals were obtained by slow evaporation of the reaction mixture. The crystals formed were brown and cubic. Yield: 75% (0.169 g, 0.3230 mmol).

1H NMR (ppm) ($DMSO-d_6$): δ 1.34 (m, 2 H, A), 3.31 (signal obscured by water, B), 5.82 (dd, $J = 9.0$ Hz, $J = 2.4$ Hz, 2 H, F), 6.09 (d, $J = 2.4$ Hz, 2 H, H), 6.13 (d, $J = 8.9$ Hz, 2 H, E), 7.08-7.10 (m, 4 H, C), 7.43-7.47 (m, 6 H, d), 9.97 (br s, 2 H, G). ^{13}C NMR (ppm)

(DMSO-*d*₆): δ 26.8 (1), 48.2 (2), 104.3 (12), 104.7 (10), 117.3 (8), 127.1 (5), 128.5 (6), 129.0 (7), 134.0 (9), 136.0 (4), 161.9 (11), 166.1 (13), 171.0 (3). HRMS (TOF) C₂₉H₂₄N₂NiO₄: calculated 523.2053, *m/z* 522.1093 [M⁺]. UV-vis (DMF) [λ_{max} , nm (ϵ , M⁻¹ cm⁻¹): 407 (6.29 × 10³), 348 (8.67 × 10³) 313 (1.45 × 10⁴). IR (cm⁻¹): 3621 [w, ν (O-H)], 1605 [s, ν (C=N)], 1580 [s, ν (C=N)], 1234 [s, ν (C-O)], 1177 [m, ν (C-O)], 1166 [m, ν (C-O)].

2.3.6 Synthesis of [Zn₂(L³)₂] where L³ = 6,6'-((1*E*,1'*E*)-(propane-1,3-diylbis(azanylylidene))bis(phenylmethanylylidene))bis(3-hydroxyphenolate)

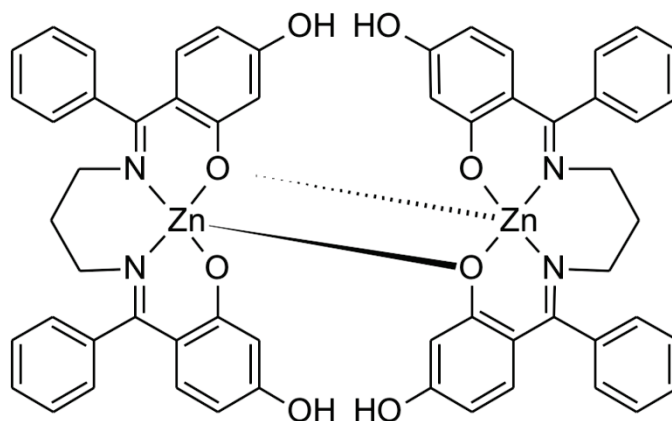


Figure 2.9: Structure of [Zn₂(L³)₂].

To a refluxing solution of H₂L³ (0.205 g, 0.439 mmol) in methanol (10 mL), ethanol (5 mL) and DMF (10 mL) was added zinc acetate dihydrate (0.100 g, 0.456 mmol). The solution was then a clear yellow colour which contained the product. The reaction mixture was then placed in a vapour diffusion chamber with diethyl ether for recrystallisation which yielded yellow cubic crystals.

NMR was unassigned, refer to Chapter 4 (Section 4.1). UV-vis (DMF) [λ_{max} , nm (ϵ , M⁻¹ cm⁻¹): 349 (1.50 × 10⁴), 285 (2.53 × 10⁴). IR (cm⁻¹): 3054 [w, ν (O-H)], 1658 [w, ν (C=N)], 1531 [s, ν (C=N)], 1239 [s, ν (C-O)], 1183 [m, ν (C-O)].

3. Synthesis

3.1 Imines and Schiff bases

An imine is simply a compound that has a nitrogen-carbon double bond. If the imine was synthesised using a carbonyl and primary amine with an aryl group present it is referred to as a Schiff base. The key defining factor is that a Schiff base will not contain hydrogen bonded to the imine nitrogen atom.^[18]

There are many ways to synthesise an imine. A Stieglitz rearrangement^[45] is one of the common methods. It is the rearrangement of an alkyl group from the carbon to the nitrogen in trityl N-haloamines using either a base or phosphorous pentachloride.^[46] This rearrangement is shown below in **Figure 3.1**.

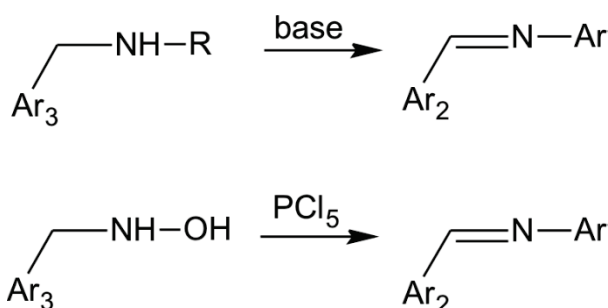


Figure 3.1: Imine formation via a Stieglitz rearrangement.

The Schmidt reaction utilises an alcohol or an alkene with hydrazoic acid to form an alkyl azide. During the reaction the alkyl azide will undergo a Curtius rearrangement to form an imine. The Curtius rearrangement functions using pyrolysis; the method of using elevated temperatures to alter organic compounds without oxygen participation.^[46] The reaction for the alkene is illustrated in **Figure 3.2**.

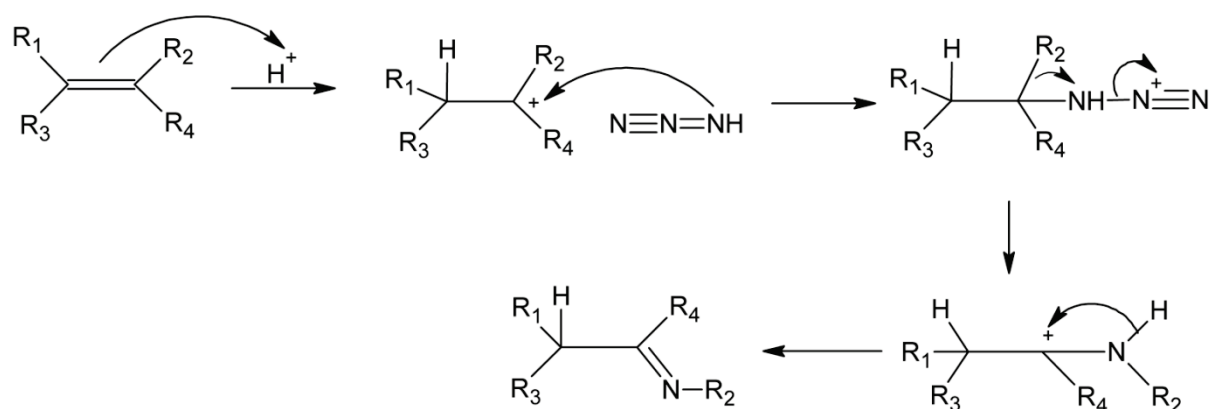


Figure 3.2: Imine formation via a Schmidt reaction.

The Hoesch reaction involves a phenol and nitrile with zinc chloride and hydrochloric acid at low temperatures to form an imine as an intermediate.^[20] The reaction mechanism is shown below in **Figure 3.3**.

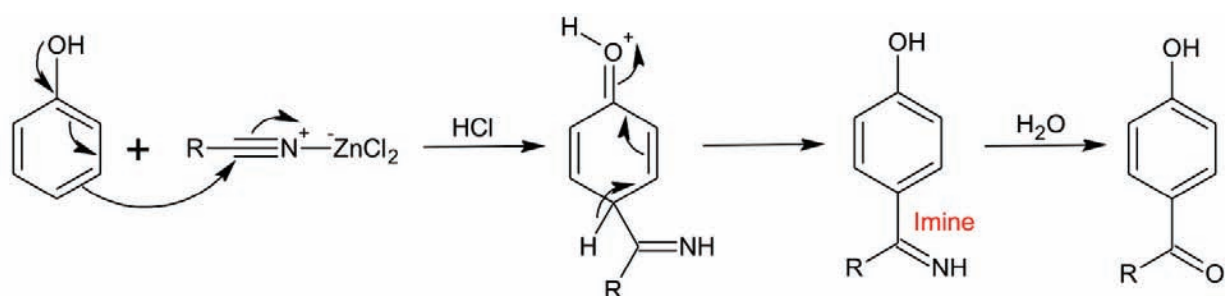


Figure 3.3: Imine formation via a Hoesch reaction.

The most commonly used reaction to form an imine is that of a simple condensation reaction. This is the addition of a primary amine to an aldehyde or ketone to form a hemiaminal as an unstable intermediate. This intermediate has a hydroxyl attached to the same carbon as the amine and thus can undergo dehydration to yield the desired imine.^[46] The stepwise mechanism is illustrated in **Figure 3.4**. The aforementioned condensation reaction is the most widely used due to the high yield and simplicity.

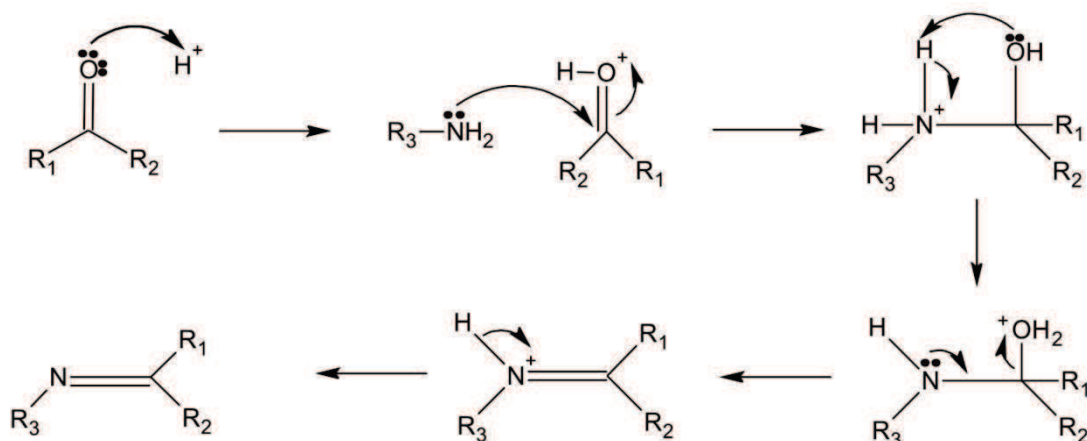


Figure 3.4: Condensation reaction of a carbonyl and a primary amine.

Imines or Schiff bases are well known compounds and are widely used as ligands as they are easy to synthesise and have flexibility in their applications. They are also ideal as they can chelate a variety of metals.^[13, 47-49] These metals include, but are not limited to: Cu(II), Mo(IV), Ni(II), Pd(II) and Zn(II).^[13]

The condensation of a primary amine and ketone was the method employed in the synthesis of the ligands used in this project. The overall reaction is shown in **Figure 3.5**. Although removal of the water from the reaction mixture can help to drive the reaction forward, and is a technique often employed in Schiff base synthesis, it was found to be unnecessary in this synthesis.

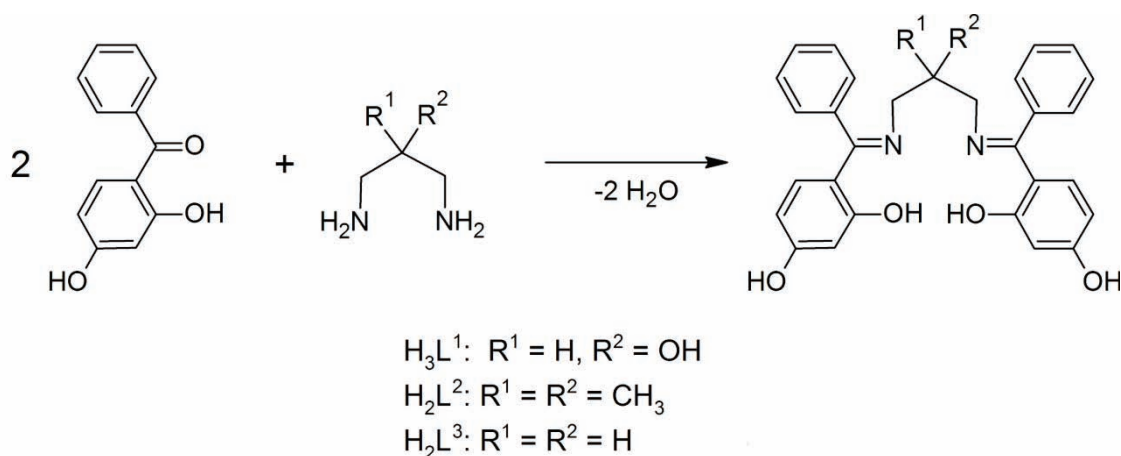


Figure 3.5: General reaction scheme for the synthesis of the ligands in this work.

In this project, four novel ligands were synthesised. The ligands are all Schiff base salen-type compounds. The ligands were synthesised using a 1:2 mol ratio of the selected diamine and 1,3-diamino-2-hydroxypropane in a methanol and refluxed for twenty-four hours. Relatively high yields were obtained from this reaction mechanism; H_3L^1 : 71%, H_2L^2 : 81% and H_2L^3 : 85%. The product was then crystallised by slow diffusion in DMF and diethyl ether.

3.2 Metal Complexation

There are many starting materials that could be utilised in the synthesis of the metal complexes. The most commonly used salts for copper being copper(II) chloride, copper(II) nitrate, copper(II) sulphate and copper(II) acetate. Copper(II) acetate was used in order to produce a dinuclear complex as the acetate ions would allow for bridging between the two copper centres. When this same reaction was attempted with copper nitrate, no chelation was detected. For synthesis of the mononuclear complexes, both copper(II) nitrate and copper(II) chloride were utilised.

With regard to the nickel starting materials, the most commonly used salts for nickel are nickel(II) chloride, nickel(II) acetate, nickel(II) nitrate and nickel(II) sulphate. Although nickel(II) acetate was used in the same reaction as the above copper(II) acetate reaction in an attempt to form a similar dinuclear complex, the reaction was unsuccessful. Again, both nickel(II) chloride and nickel(II) nitrate were used to form the mononuclear complexes. The reactions with nitrate salts took longer and therefore nickel(II) chloride was favoured in the subsequent reactions.

The chelation process was a simple two hour reflux of the ligand and metal salt. The chelation was achieved with concomitant deprotonation of the ligands yielding $N_2 O_2$ tetradentate, dianionic ligands. The complexes are therefore neutral. The overall reaction scheme is shown below in **Figure 3.6**.

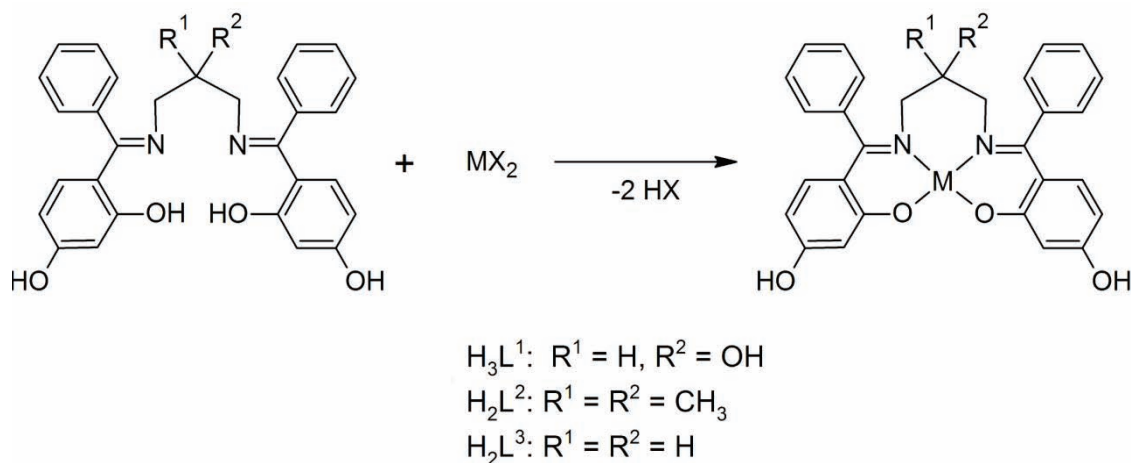


Figure 3.6: Reaction scheme employed in the chelation of metal ions by the ligands.

In this project, six novel metal chelates were synthesised utilising the three ligands synthesised. The metal chelates were synthesised using a 1:1 mol ratio of the ligand and chosen metal salt in a mixture of methanol, ethanol and DMF and refluxed for two hours. However, it was expected that for H_2L^1 a ratio of 2:1 for metal salt and ligand would be required due to the extra hydroxyl group. Relatively good yields were obtained from this reaction mechanism; $[Cu_2(L^1)(OAc)(DMF)]: 84\%$, $[Cu_3(L^2)_2Cl_2(DMF)_2]: 39\%$, $[Ni(L^2)]: 50\%$, $[Cu_3(L^3)_2(H_2O)_2]Cl_2: 21\%$ and $[Ni(L^3)]: 75\%$. Crystallisation occurred via evaporation of the reaction mixture. The combination of hard nitrogen and oxygen atoms makes the ligands ideal for coordination to small, hard metal ions such as copper(II), nickel(II) and zinc(II).

4. Spectroscopy

4.1 NMR Spectroscopy

Nuclear magnetic resonance (NMR) spectroscopy is one of the most widely used characterisation methods in synthetic chemistry. It exploits the magnetic properties of certain isotopes. In ^1H NMR spectroscopy, each proton in a specific magnetic environment will resonate at a specific frequency as it is shielded or deshielded by its neighbouring atoms. NMR spectroscopy was used to characterise the ligands and the nickel(II) complexes synthesised in this work. The ^1H and ^{13}C NMR spectra of the ligands and metal chelates are expected to differ as the metal ion will either shield or deshield the ^1H and ^{13}C nuclei. If the metal shields the nuclei an upfield shift will be observed, whereas if the metal deshields the nuclei a downfield shift will be observed.^[50] All NMR spectroscopy experiments were conducted in $\text{DMSO-}d_6$ for consistency. The solvent signals and impurities have been marked on the NMR spectra to simplify assignment. The DMF assigned peaks originate from the reaction mixture used to synthesise the compounds. The ^1H NMR spectra of ligand H_2L^2 and its nickel(II) complex are shown in **Figures 4.1** and **Figure 4.2**, as exemplary spectra.

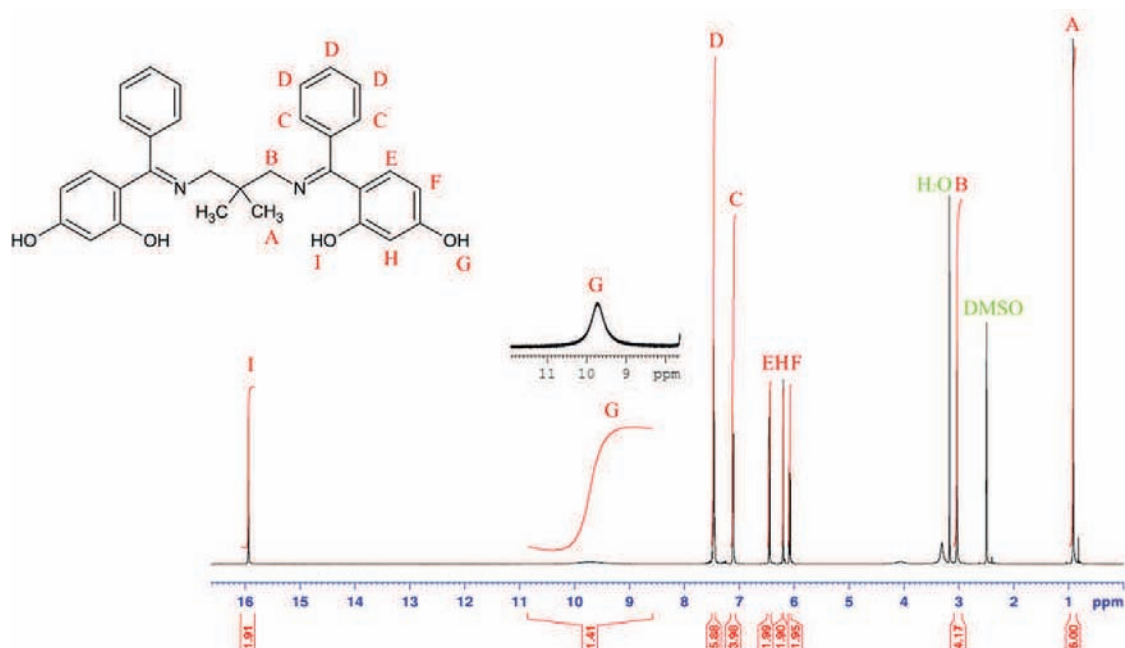


Figure 4.1: ^1H NMR spectrum of H_2L^2 in $\text{DMSO-}d_6$.

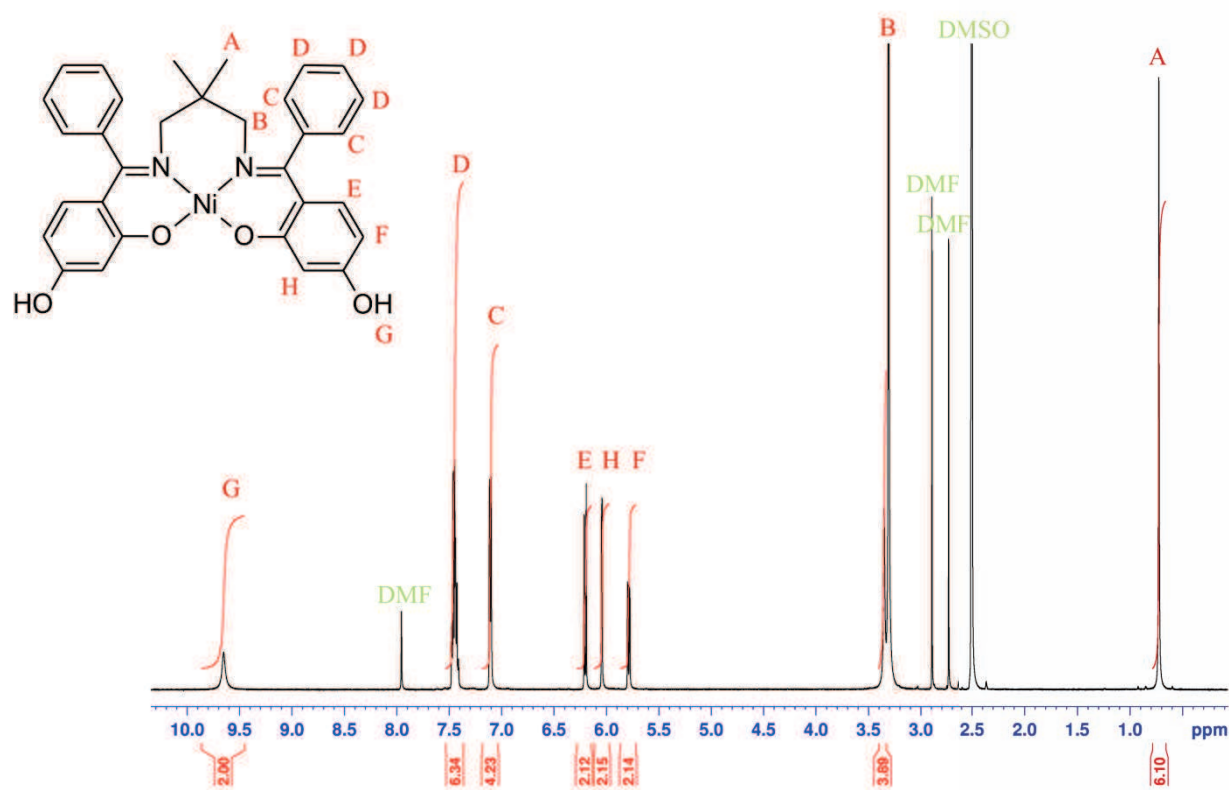


Figure 4.2: ^1H NMR spectrum of $[\text{Ni}(\text{L}^2)]$ in $\text{DMSO-}d_6$.

In the ligand, the protons of the methyl groups on the bridgehead carbon atom resonate the most upfield and *ortho* hydroxyl protons resonate the most downfield. The aromatic protons are in the range of 6-8 ppm. In **Figure 4.1**, the two different types of hydroxyl groups give two separate signals with signal **G** being much broader than signal **I**. This suggests that the protons **G** are subject to chemical exchange with other hydroxyl protons and that the protons **I** are hydrogen bonded in solution; the chemical shift of ~16 ppm for the latter is consistent with strong hydrogen bonding in solution. When comparing the two NMR spectra a key feature is that the signal at 15.94 ppm has disappeared due to the loss of these hydroxyl protons upon chelation of the metal. This is also noticeable in the ^1H NMR spectra of H_2L^3 and $[\text{Ni}(\text{L}^3)]$. With the exception of the methylene (**B**) protons, the protons of the ligand experienced a slight upfield shift upon coordination of the ligand to nickel(II). This shows that the nickel(II) ion is acting in a shielding manner. A comparison of the chemical shifts and assignments for H_2L^2 and $[\text{Ni}(\text{L}^2)]$ is shown in **Table 4.1**. All additional NMR spectra are available in **Appendix A**.

Table 4.1: Comparison of the chemical shifts of H_2L^2 and $[Ni(L^2)]$.

| Proton | Chemical Shift (ppm) | |
|--------|----------------------|-------------|
| | H_2L^2 | $[Ni(L^2)]$ |
| A | 0.92 | 0.72 |
| B | 3.04 | 3.35 |
| C | 6.08 | 5.78 |
| D | 6.21 | 6.04 |
| E | 6.45 | 6.20 |
| F | 7.11-7.12 | 7.09-7.11 |
| G | 7.45-7.48 | 7.40-7.48 |
| H | 9.72 | 9.65 |
| I | 15.94 | - |

The 1H NMR of the zinc complex showed only broad unresolved signals (**Figure 4.3**). This is attributed to the quadrupole moment of the zinc atom, $Q = 0.15 \times 10^{-28} \text{ m}^2 \text{ A}$, preventing acquisition of high-resolution spectra. There may also be a dynamic monomer \leftrightarrow dimer equilibrium that leads to a more complex spectrum and thus creating the broadening. For these reasons, no further NMR spectroscopic characterisation was attempted for the zinc complex.

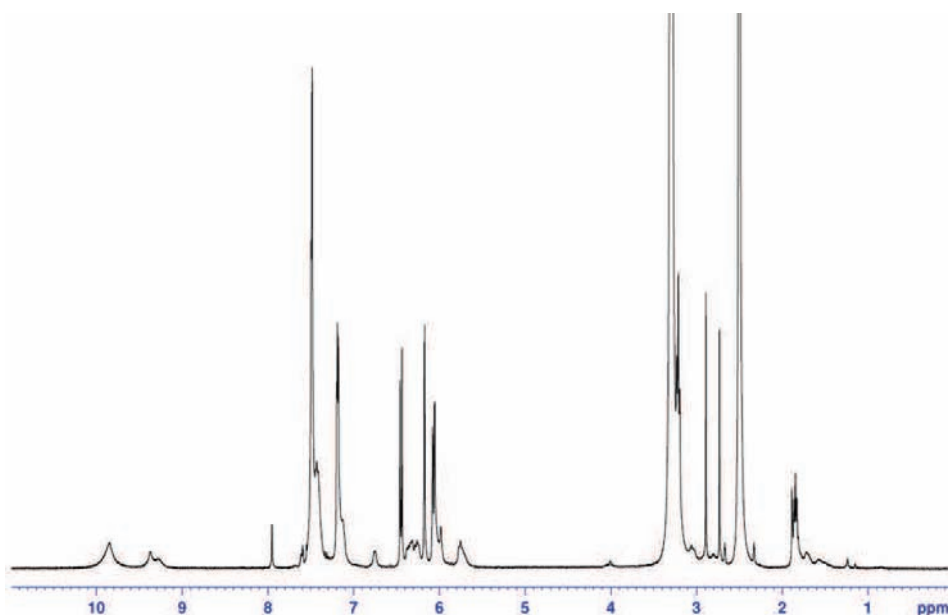


Figure 4.3: 1H NMR spectrum of $[Zn_2(L^3)_2]$ in $DMSO-d_6$.

As the copper(II) ion is paramagnetic in nature, the copper(II) complexes of the ligands were not studied through NMR spectroscopy. They were, however, studied by electron spin resonance (ESR) or electron paramagnetic resonance (EPR) spectroscopy as discussed in **Section 4.4**.

4.2 UV-vis Spectroscopy

Electronic energy level transitions are observed in the ultraviolet and visible regions of the electromagnetic spectrum i.e. transition frequencies in the range 10^4 to 10^6 cm^{-1} are observed.^[50] The most important electronic transition for molecules in general is from the highest occupied molecular orbital (HOMO) to the lowest unoccupied molecular orbital (LUMO). This HOMO-LUMO transition is a π - π^* transition for conjugated organic molecules (like the Schiff base ligands studied in this work) and usually gives rise to very intense absorption bands.^[50] However, other transitions are possible for Schiff base ligands in view of the lone pairs on the imine nitrogen atoms. These are n - π^* transitions, which involve an electron being transferred from the non-bonding (n) lone pair orbital on the nitrogen atom to the π^* orbitals of the ligand. These transitions are generally weaker than the π - π^* transitions, and are further distinguished by usually appearing at somewhat lower energies.^[51] Once the ligand is bonded to the metal through coordination of the lone pair on the heteroatom, additional bands are possible due to the transfer of an electron from a metal-based orbital (usually a d orbital) to the LUMO of the ligand i.e. the π^* orbital. These d - π^* transitions give rise to metal-to-ligand charge transfer (MLCT) bands that are lower in energy and generally relatively weak.^[6] We finally note that d - d bands associated purely with the metal are sometimes observed in the absorption spectra of Schiff base ligand complexes: this is due to “intensity stealing” brought about by the mixing of ligand π -orbitals with metal d -orbitals.^[6, 51-54]

We show in **Figure 4.4** the absorption spectrum measured in DMF for the Schiff base ligand which has a propylene spacer between the two imine nitrogen atoms (previously labelled H_2L^3). Three bands are observed: a weak band at 390 nm and two more intense bands at 312 and 281 nm. The weak low energy band is assigned to a n - π^* transition: as discussed above this involves the excitation of a lone pair electron in a non-bonding orbital (n) on the imine

nitrogen atom to the higher energy π^* orbital on the ligand. The intense bands are assigned to intraligand $\pi\text{-}\pi^*$ transitions associated with the conjugated framework of the ligand.

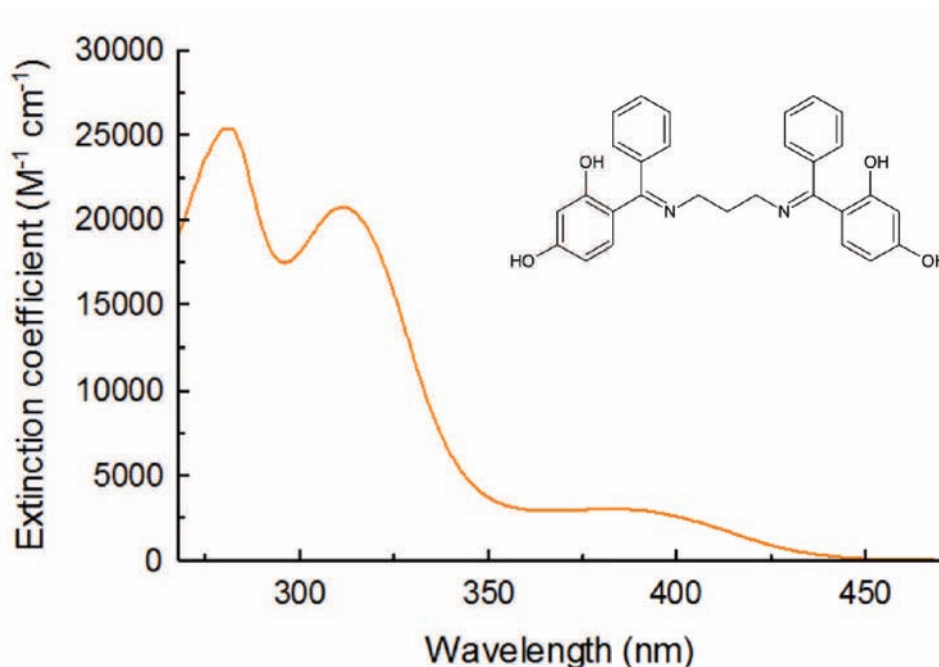


Figure 4.4: UV-vis spectrum of H_2L^3 in DMF at 298 K.

For comparison purposes we also show in **Figure 4.5** the absorption spectrum measured in DMF for the Schiff base ligand which has a dimethyl substituted propylene spacer between the two imine nitrogen atoms (previously labelled H_2L^2). As expected, essentially the same set of bands is observed as for the parent unsubstituted ligand, and so the same assignments apply: the two high energy intense bands in **Figure 4.5** are assigned to $\pi\text{-}\pi^*$ transitions and the weak low energy band at 393 nm is assigned to a $\text{n-}\pi^*$ transition.

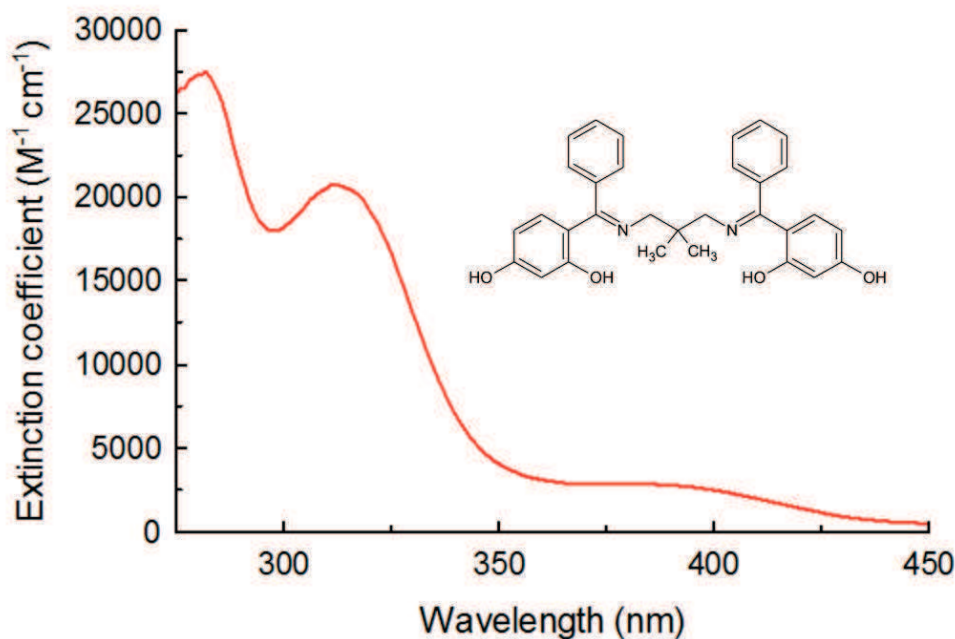


Figure 4.5: UV-vis spectrum of H_2L^2 in DMF at 298 K.

We now examine the absorption spectra measured in DMF for complexes of the above two ligands: that for the di-zinc complex (previously labelled $[Zn_2(L^3)_2]$) is shown in **Figure 4.6**. Only two intense high energy bands at 285 and 349 nm are observed. We assign these to intraligand $\pi-\pi^*$ transitions, and note that they are red-shifted as compared to the $\pi-\pi^*$ bands recorded at 281 and 313 nm for the ligand itself. This is due to the influence of the metal on the spacing of the π orbitals of the ligand, in particular due to back donation of electron density from the electron-rich metal centre to the π^* orbitals of the ligand. Also note that the $n-\pi^*$ transition recorded at 390 nm for the ligand has disappeared – as expected, as the nitrogen atom lone pair is now involved in bonding to the zinc and is not available for excitation to the π^* orbital of the ligand. Finally, note that there is no expectation of a MLCT band, as the d^{10} configuration of zinc(II) is one of enhanced stability; as a result absorption spectra of zinc(II) complexes of π -acceptor ligands generally only display intraligand bands.^[55]

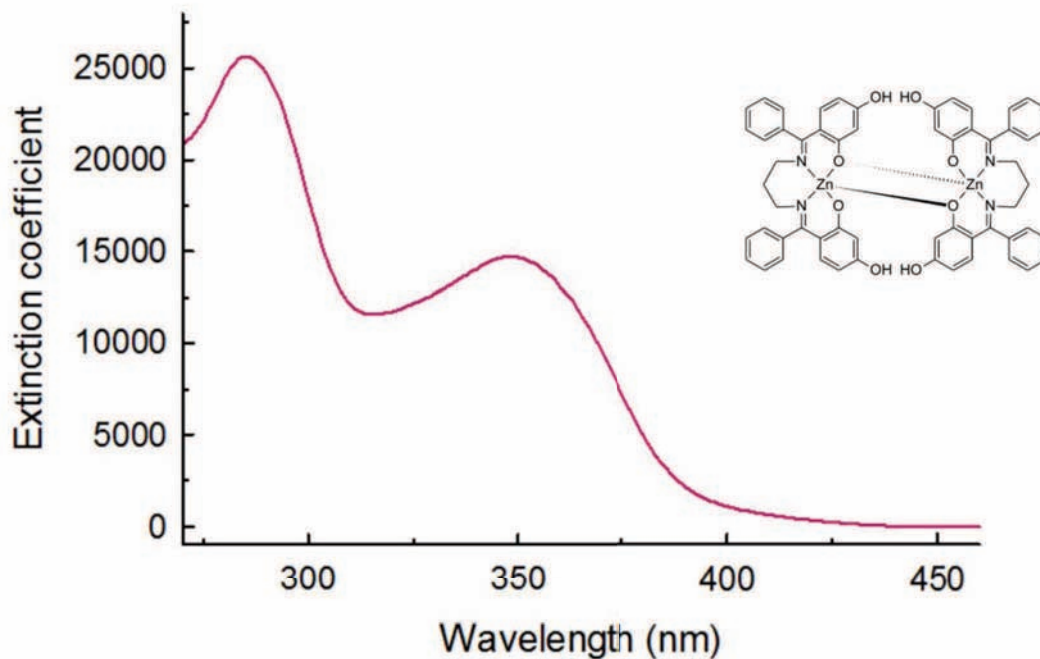


Figure 4.6: UV-vis spectrum of $[\text{Zn}_2(\text{L}^3)_2]$ in DMF at 298 K.

We now turn to the absorption spectrum measured in DMF for the trinuclear copper(II) (i.e. d^9) complex (previously labelled $[\text{Cu}_3(\text{L}^3)_2(\text{H}_2\text{O})_2]\text{Cl}_2$) shown in **Figure 4.7**. Note the insert to the figure which shows the presence of a weak band at 596 nm that is not observed in the spectrum measured for the zinc complex. This band is assigned to a d-d transition and, indeed, fits with the d-d transitions in the 570-580 nm range for the copper(II) complexes reported by Klement *et al.*^[56] These d-d transitions generally have extinction coefficients below $100 \text{ M}^{-1} \text{ cm}^{-1}$. However, the transition can borrow intensity from nearby $\pi\text{-}\pi^*$ bands the extinction coefficient can increase as is the case here. The two intense high energy bands at 295 and 358 nm are assigned to $\pi\text{-}\pi^*$ transitions and, as for the zinc complex, are red shifted as compared to the $\pi\text{-}\pi^*$ bands recorded for the ligand itself – see **Figure 4.4**.

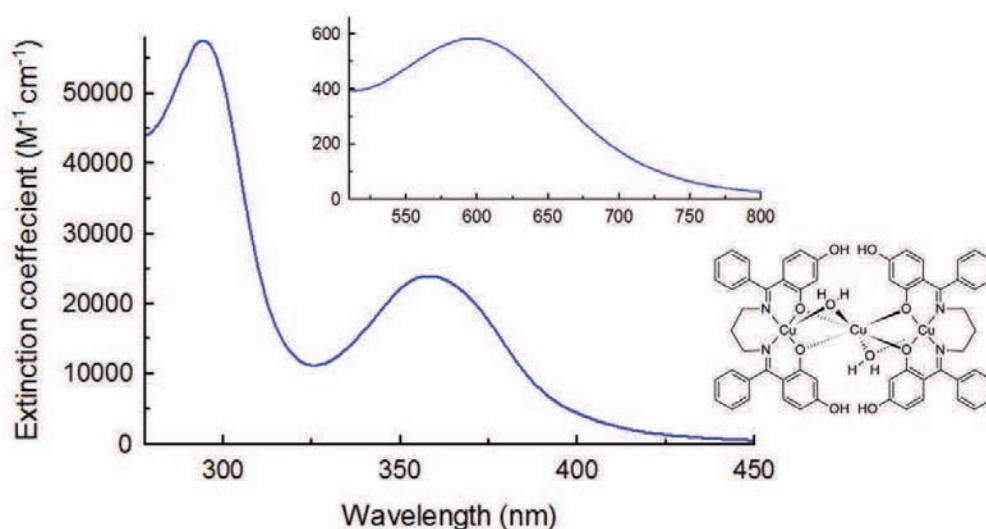


Figure 4.7: UV-vis spectrum of $[\text{Cu}_3(\text{L}^3)_2(\text{H}_2\text{O})_2]\text{Cl}_2$ in DMF at 298 K.

The absorption spectrum measured in DMF for the mononuclear Ni(II) complex (previously labelled $[\text{Ni}(\text{L}^3)]$) is shown in **Figure 4.8**. This spectrum is also distinguished from the spectrum recorded for the zinc complex by the presence of a MLCT band which, in this case, appears at 407 nm – there are also intraligand $\pi-\pi^*$ absorption bands at 348 nm and 313 nm. As already noted, MLCT transitions occur when the transition metal atom has an incomplete d-subshell and the ligand has an empty π^* orbital, as is the case for this d^8 nickel(II) complex – it is then possible for an electron to transfer from the metal centre to an empty orbital on the ligand.

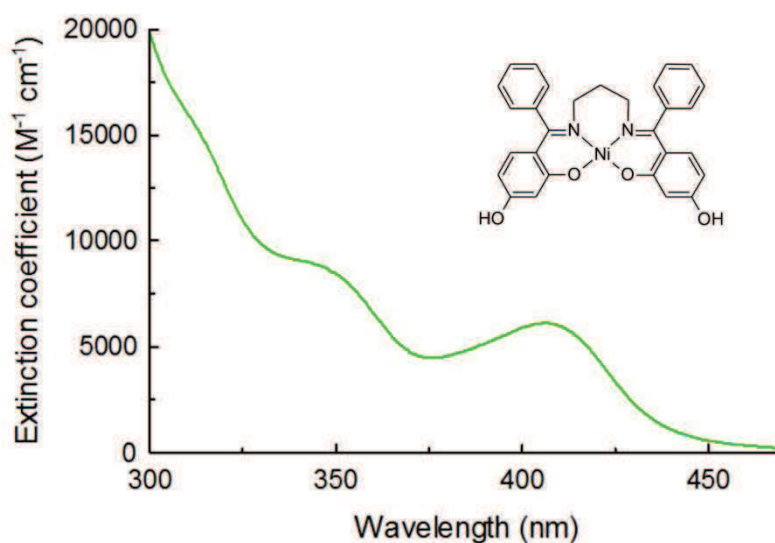


Figure 4.8: UV-vis spectrum of $[\text{Ni}(\text{L}^3)]$ in DMF at 298 K.

Table 4.2 provides a list of the absorption wavelengths and band assignments for all three ligands and the six complexes which have been studied. All the assignments follow from the discussions above. As expected there is little variation in the spectra recorded for the ligands as these are dominated by intraligand π - π^* absorptions that are essentially unaffected by changes in the alkyl bis(imine) linkages. More interesting are the differences in the absorption spectra measured for zinc, copper and nickel complexes that depend on the presence or absence of MLCT bands. This, in turn, depends on the electronic configuration of the metal. Of most interest is the absorption spectrum of the nickel(II) complex with its relatively strong MLCT absorption band. Irradiation into this band could well lead to strong emission by the complex as has been observed for other d^8 metal complexes with aromatic ligands.^[57] This will be the subject of further investigations.

Table 4.2: Comparison of UV-visible transitions for all ligands and complexes.

| | Wavelengths (nm) and extinction coefficients ($M^{-1} \text{ cm}^{-1}$) | | | |
|--|---|----------------------------|----------------------------|----------------------------|
| | $(\pi$ - $\pi^*)$ | n - π^* | MLCT | d-d |
| H_3L^1 | 281 (2.54×10^4) | 389 (2.99×10^3) | - | - |
| | 312 (2.07×10^4) | | | |
| H_2L^2 | 281 (2.57×10^4) | 393 (2.40×10^3) | - | - |
| | 313 (2.01×10^4) | | | |
| H_2L^3 | 281 (2.56×10^4) | 390 (2.99×10^3) | - | - |
| | 312 (2.09×10^4) | | | |
| [Cu ₂ (L ¹)(OAc)(DMF)] | 293 (3.41×10^4) | - | - | - |
| | 360 (1.93×10^4) | | | |
| [Cu ₃ (L ²) ₂ Cl ₂ (DMF) ₂] | 295 (7.36×10^4) | - | - | 598 (4.49×10^2) |
| | 362 (3.05×10^4) | | | |
| [Ni(L ²)] | 349 (1.31×10^4) | - | 404 (1.07×10^4) | - |
| [Cu ₃ (L ³) ₂ (H ₂ O) ₂]Cl ₂ | 295 (5.68×10^4) | - | - | 596 (5.83×10^2) |
| | 358 (2.43×10^4) | | | |
| [Ni(L ³)] | 313 (1.45×10^4) | - | 407 (6.29×10^3) | - |
| | 348 (8.67×10^3) | | | |
| [Zn ₂ (L ³) ₂] | 285 (2.53×10^4) | - | - | - |
| | 349 (1.50×10^4) | | | |

All additional spectra are available in **Appendix B**.

For further discussion some literature examples of copper(II) and nickel(II) salen complexes have been compared to the copper(II) and nickel(II) chelates of this work. A range of copper(II) complexes with derivatives of salen and tetrahydrosalen were synthesised by Klement *et al.*^[56] and studied using UV-vis spectroscopy. These complexes are shown in **Figure 4.9**. A separate range of copper(II) complexes with tetradentate imine-phenols type ligands were synthesised and characterised using UV-vis spectroscopy by Yao *et al.*^[15] and are shown in **Figure 4.10**.

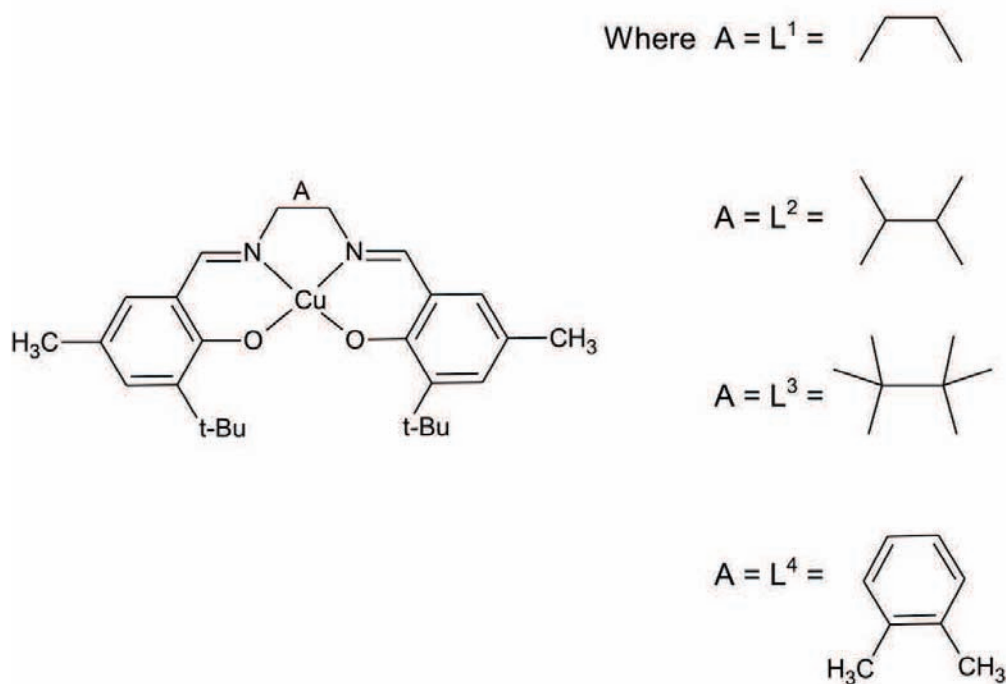


Figure 4.9: Copper(II) complexes with derivatives of salen and tetrahydrosalen. Redrawn from Ref. ^[56].

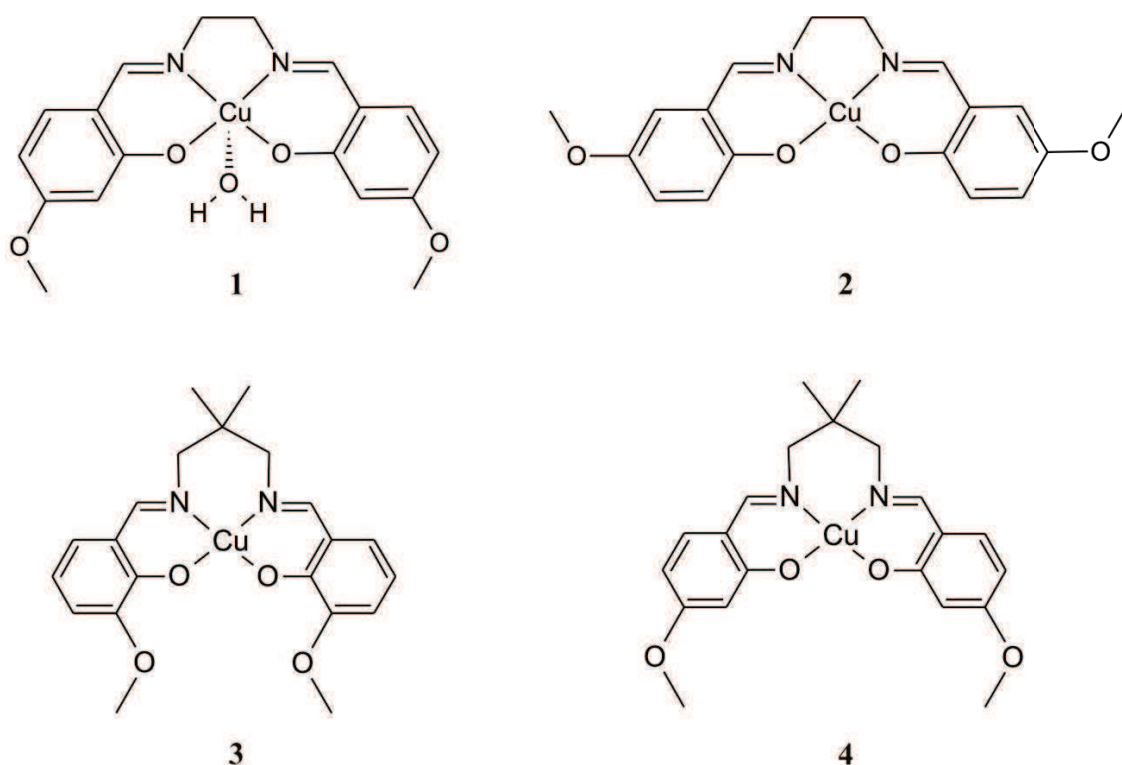


Figure 4.10: Copper(II) complexes with tetradentate imine-phenol type ligands. Redrawn from Ref. [15].

Complexes CuL^1 to CuL^4 were studied in acetone, whereas, complexes 1-4 were studied in methanol. All transition wavelengths and extinction coefficients for the literature chelates and copper(II) chelates of this work are shown in **Table 4.3**. The intense bands in the 380 nm region for the CuL series of chelates were assigned as metal-to-ligand charge transfer bands. The weak bands in the region of 570 nm were assigned to d-d transitions. For complexes 1-4 the intense bands at 216-270 nm and 350-390 nm have been assigned as π - π^* transitions in the benzene ring and as charge transfer n - π^* transitions, respectively. Finally, the weak bands in the 560-570 nm range were assigned to d-d transitions. The band maxima are in favourable agreement to those found in the literature, however, the intensity of the bands of the copper(II) chelates studied in this work is almost ten times higher than those of the literature compounds. This may be due to the increased electron density on the ligand in comparison to that of a salen ligand.

Table 4.3: UV-visible absorption data for copper(II) chelates.

| Complex | Absorption maxima: λ_{\max} (nm), (ϵ_{\max} ($M^{-1} \text{ cm}^{-1}$)) | | | | |
|--|---|--------------|--------------|--------------|-----------|
| CuL^{1a} | - | - | 380 (10 700) | - | 572 (580) |
| CuL^{2a} | - | - | 380 (12 000) | - | 570 (650) |
| CuL^{3a} | - | - | 380 (14 000) | - | 570 (600) |
| CuL^{4a} | - | - | 405 (13 700) | 444 (19 500) | 580 (540) |
| 1^b | 218 (8 799) | 270 (11 324) | 356 (9 888) | - | 570 (328) |
| 2^b | 218 (6 482) | 266 (7 035) | 386 (5 628) | - | 560 (200) |
| 3^b | 216 (5 412) | 268 (5 347) | 386 (4 999) | - | 566 (332) |
| 4^b | 215 (5 638) | 268 (6 422) | 382 (5 118) | - | 560 (268) |
| [Cu₃(L³)₂(H₂O)₂]Cl₂ | - | 295 (56 786) | 358 (24 314) | - | 596 (583) |
| [Cu₃(L²)₂Cl₂(DMF)₂] | - | 295 (73 566) | 362 (30 483) | - | 598 (449) |
| [Cu₂(L¹)(OAc)(DMF)] | - | 293 (34 060) | 360 (19 268) | - | - |

^a Ref. [56], ^b Ref. [15].

The following nickel(II) chelates of salen complexes were studied by Jamshid *et al.*^[58] and Garg *et al.*^[59] These compounds are shown in **Figure 4.11**.

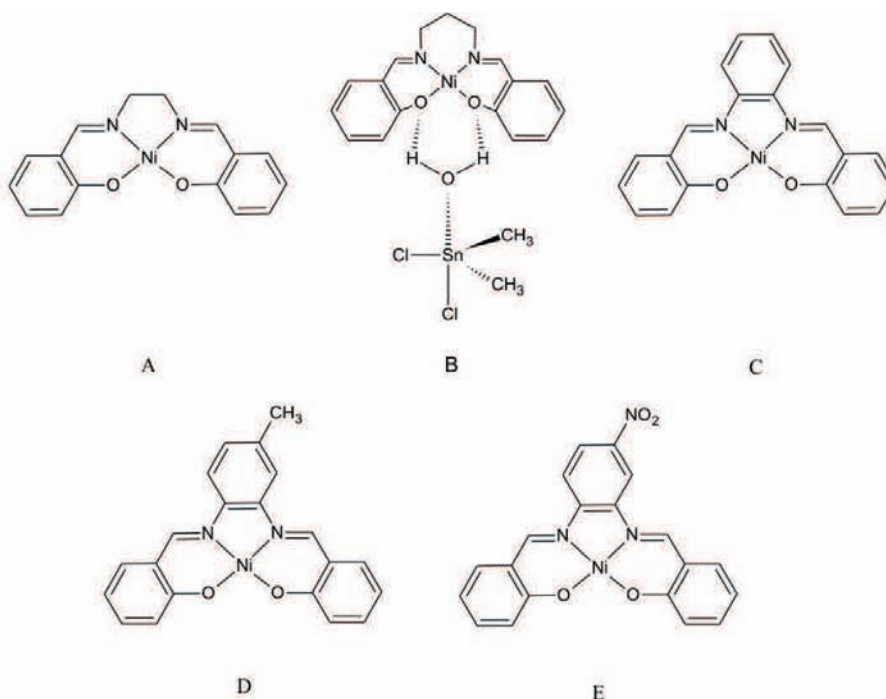


Figure 4.11: Nickel(II) chelates as synthesised by Jamshid *et al.*^[58] (A, B) and Garg *et al.*^[59] (C-E). Redrawn from Ref. [59].

Jamshid *et al.*^[58] determined the spectrum of A and B in chloroform, whereas, Garg *et al.*^[59] used DMSO for complexes C-E. The visible transitions for the literature nickel(II) chelates are shown in **Table 4.4** along with the nickel(II) chelates in this work. No extinction coefficients were given in the referenced papers. The band in B at <300 nm in complex B is assigned as $\pi-\pi^*$ band which is overlapped with chloroform bands. The band at 330 nm in complex B is assigned as $\pi-\pi^*$ transition. A point of interest in the data is to note how the MLCT band has changed from complex A to complex B due to the addition of the dimethyltin(IV) dichloride; 412 nm to 338 nm respectively. The tabulated bands for complexes C-E have all been assigned as charge transfer bands. However, Garg *et al.*^[59] noted that the complexes with aliphatic imines were noted to have weaker bands in the 530-600 nm range which were assigned as unresolved d-d transitions and these bands were not visible in aromatic imine bridges due to the high-intensity charge transfer transitions masking them. The complexes studied in this work show a similarity in band wavelength and assignment with slightly lower wavelength maxima for each band. This may be due to solvent differences and, as can be seen from complex B, axial ligand binding.

Table 4.4: UV-visible absorption data for nickel(II) chelates.

| Complex | Absorption maxima: λ_{\max} (nm) | | | |
|-----------------------|--|-----|-----|-----|
| A ^a | - | 330 | 412 | - |
| B ^a | <300 | 338 | - | - |
| C ^b | - | 380 | 450 | 479 |
| D ^b | 354 | 386 | 450 | 481 |
| E ^b | 300 | 386 | 422 | 486 |
| [Ni(L ²)] | - | 349 | 404 | - |
| [Ni(L ³)] | 313 | 348 | 407 | - |

^a Ref. ^[58], ^b Ref. ^[59].

A simple Zn(salen) complex was studied by Pagadala *et al.*^[60] in DMSO. The Zn(salen) complex gave two bands at 261 nm and 366 nm. The band at 261 nm was assigned by Pagadala *et al.*^[60] as a $\pi-\pi^*$ transition and the band at 366 nm was assigned as a ligand to metal charge transfer. However, Zheng and Chen^[61] point out that the assignments are

complex and possibly less like LMCT. The zinc(II) chelate synthesised here exhibited band maxima at 285 nm and 349 nm, which were both assigned as π - π^* transitions.

4.3 Infrared Spectroscopy

Sir William Herschel used sunlight passing through a prism to divide light into its spectral colours. He then used several mercury thermometers with blackened reservoirs to study the thermal distribution for each colour. He found that this was not a new type of radiation but instead obeyed the laws of optics like visible light and so named this range *infrared*.^[62] Infrared spectroscopy is the study of vibrational transitions. It is used by analytical chemists in the same way as NMR and UV-vis spectroscopy or mass spectrometry.^[62] Every substance has a unique IR spectrum which could be likened to the fingerprint of a person. Vibrational energy levels do not have large energy gaps between them and so the transitions will be seen in the lower infrared region. The absorption bands are due to vibrations of nuclei in molecules. Each band in an infrared spectrum is due to absorption of photons by transitions between vibrational levels in the ground state of the compound being studied.^[50] Due to the number of infrared bands observed in the spectra of these complexes, only the most characteristic peaks have been assigned and discussed.

The most characteristic band of a Schiff base type ligand is the product of its defining feature, the imine group. This band is generally found in the region of 1615-1630 cm^{-1} .^[62] The next characteristic band for the compounds prepared in this work is that of the phenolic-OH groups present in the region of 3125-3705 cm^{-1} .^[62] Also identified are the C-O bands which cover the region of 1180-1260 cm^{-1} .^[62] Assigned spectra for H_2L^2 and $[\text{Cu}_3(\text{L}^2)_2\text{Cl}_2(\text{DMF})_2]$ are shown in **Figures 4.12** and **4.13**, respectively and the assigned bands are shown in **Table 4.5** for all the ligands and metal chelates synthesised in this work.

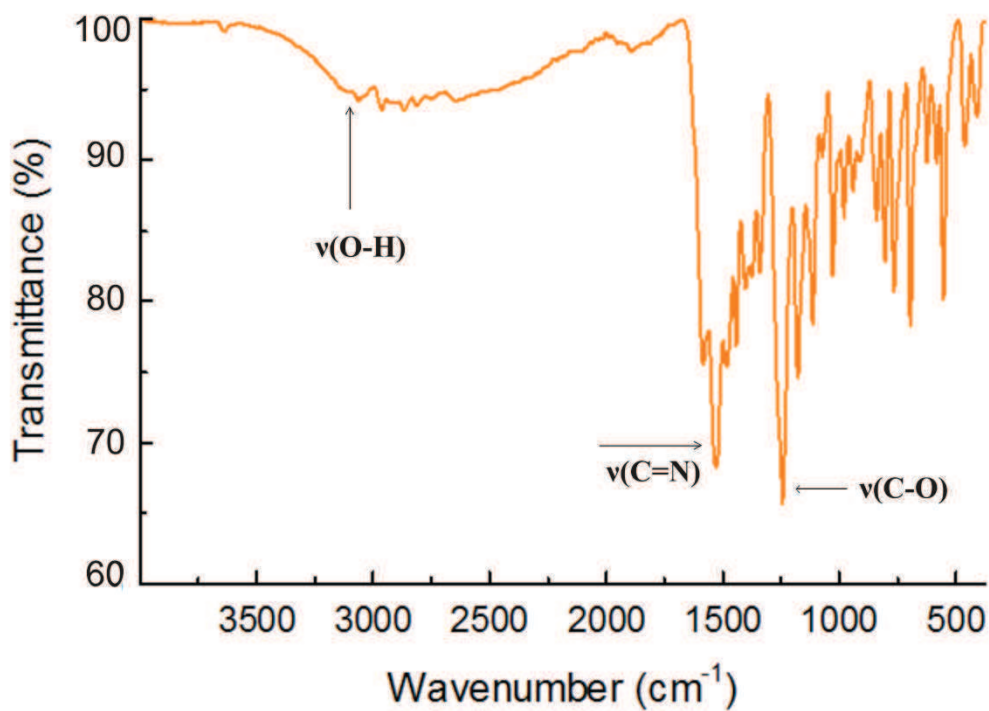


Figure 4.12: Infrared spectrum of H_2L^2 with assigned bands.

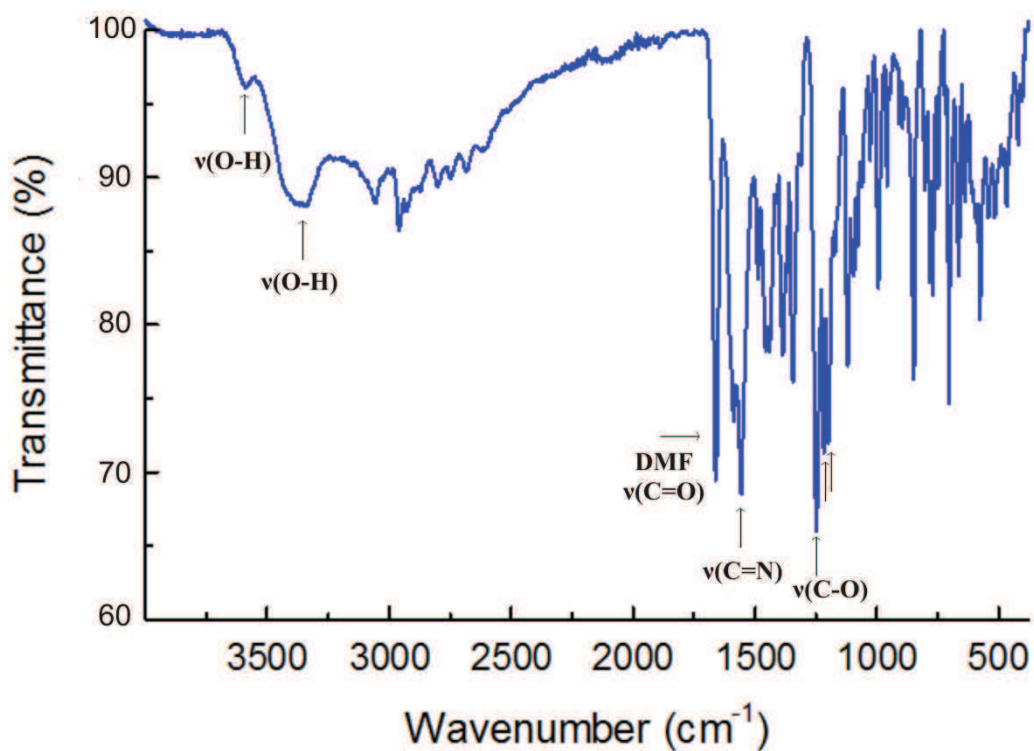


Figure 4.13: Infrared spectrum of $[Cu_3(L^2)_2Cl_2(DMF)_2]$ with assigned bands.

As can be seen from **Figure 4.12** and **Figure 4.13**, the O-H region of the metal complex becomes more intense than the ligand. This trend is seen in all the ligands and their associated metal complexes and is attributed to the large number of water molecules present in their crystal lattices, as shown by single-crystal X-ray diffraction. A notable feature in the spectra of the compounds is that the ligands show a single band for the C-O stretch whereas there are more bands in the metal complexes after chelation. Another feature is that of an increase in the frequency of the C=N vibration in some compounds when chelation occurs. This is typical of ligands coordinated to metal ions through the imine nitrogen atom as discussed below in the comparison done of some literature examples. The spectra of each compound are available in **Appendix C**.

Table 4.5: Observed frequencies (cm⁻¹) for the absorption bands in the solid IR spectra of ligands and complexes synthesised in this work.

| Compound | $\nu(\text{O-H})$ | $\nu(\text{C=N})$ | $\nu(\text{C-O})$ |
|--|-------------------|-------------------|-------------------|
| H ₃ L ¹ | 3251 (br w) | 1540 (m) | 1226 (s) |
| | 3440 (br w) | 1567 (m) | |
| H ₂ L ² | 3637 (br w) | 1528 (m) | 1242 (s) |
| H ₂ L ³ | 3056 (br w) | 1571 (s) | 1241 (s) |
| | | | 1190 (m) |
| [Cu ₂ (L ¹)(OAc)(DMF)] | 3196 (br w) | 1528 (s) | 1210 (m) |
| | 3355 (br w) | | 1238 (s) |
| [Cu ₃ (L ²) ₂ Cl ₂ (DMF) ₂] | 3055 (br w) | | 1198 (s) |
| | 3345 (br w) | 1556 (s) | 1216 (s) |
| [Ni(L ²)] | 3588 (br w) | | 1246 (s) |
| | 3575 (br w) | 1561 (m) | 1164 (s) |
| [Cu ₃ (L ³) ₂ (H ₂ O) ₂]Cl ₂ | 3631 (br w) | 1616 (m) | 1190 (m) |
| | | | 1220 (m) |
| [Ni(L ³)] | 3143 (m) | | 1191 (s) |
| | 3267 (m) | 1599 (m) | 1222 (s) |
| [Zn ₂ (L ³) ₂] | 3417 (w) | | 1251 (m) |
| | | | 1166 (m) |
| [Ni(L ³)] | 3621 (w) | 1580 (s) | 1177 (m) |
| | | 1605 (s) | 1234 (s) |
| [Zn ₂ (L ³) ₂] | | | 1183 (m) |
| | 3054 (w) | 1531 (s) | 1239 (s) |

Abbreviations: w, weak; m, medium; s, strong; br, broad.

There were also C=O bands present in the 1600 cm⁻¹ region of the spectra of H₃L¹, H₂L³, [Cu₂(L¹)(OAc)(DMF)], [Cu₃(L²)₂Cl₂(DMF)₂], and, [Zn₂(L³)₂] due to the presence of DMF solvate molecules. The nickel(II) compounds, however, had no DMF present in the X-ray structures.

The copper(II) chelates shown in **Figure 4.9** and **Figure 4.10** will again be used as a literature comparison for the copper(II) chelates in this work. As the chelates being studied are of the salen type system the comparison between the literature IR work done by both Klement *et al.*^[56] and Yao *et al.*^[15] will be focused only on the assignment of the ν(C=N) bands. The assignments of these bands are shown in **Table 4.6**. As can be seen from the assignments in **Table 4.6** the copper(II) chelates compare very favourably to the literature compounds.

Table 4.6: Frequencies of copper(II) chelates in this work and literature.

| Chelate | ν(C=N) (cm ⁻¹) |
|--|----------------------------|
| [Cu ₂ (L ¹)(OAc)(DMF)] | 1528 |
| [Cu ₃ (L ²) ₂ Cl ₂ (DMF) ₂] | 1556 |
| [Cu ₃ (L ³) ₂ (H ₂ O) ₂]Cl ₂ | 1599 |
| CuL ^{1a} | 1620 |
| CuL ^{2a} | 1630 |
| CuL ^{4a} | 1615 |
| 1 ^b | 1640 |
| 2 ^b | 1632 |
| 3 ^b | 1618 |
| 4 ^b | 1636 |

^a Ref. ^[56], Figure 4.9; ^b Ref. ^[15], Figure 4.10.

The nickel(II) chelates used for comparison are those shown in **Figure 4.11** synthesised by Jamshid *et al.*^[58] The frequencies of the ν(C=N) bands of the literature nickel(II) chelates and the nickel(II) chelates of this work are shown in **Table 4.7**. A notable feature here is the

appearance of two bands in the chelates synthesised in this work in comparison to that of the literature chelates. The bands at higher frequencies seem to correlate favourably with those in the literature; the appearance of two bands for the C=N groups of the present complexes is consistent with the presence of the expected symmetric and antisymmetric modes for the functional group pair.

Table 4.7: Frequencies of nickel(II) chelates characterised in this work and related structures from the literature.

| Chelate | $\nu(\text{C}=\text{N})$ (cm^{-1}) |
|------------------|---|
| A ^a | 1624 |
| B ^a | 1659 |
| NiL ² | 1561, 1616 |
| NiL ³ | 1580, 1605 |

^a Ref. [58], Figure 4.11.

[Zn₂(L³)₂] gave a $\nu(\text{C}=\text{N})$ band at 1531 cm^{-1} which is a favourable comparison with the literature compound Zn(salen) complex as studied by Pagadala *et al.*^[60] which gave a $\nu(\text{C}=\text{N})$ band at 1633 cm^{-1} .

4.4 Electron Spin Resonance

Electron Spin Resonance (ESR) is a method of studying paramagnetic solids and solutions. A paramagnetic compound is a compound that has a permanent magnetic dipole and so the ESR spectrum depends upon the magnetic properties of the complex being studied. A continuous wave is formed as the magnetic field is swept. At the centre of the spectrum is the g-factor, which is one of the factors used to characterise the complex present. Nuclei with spin I not equal to zero create line splitting which give further information on metal centre geometry.^[63] Hyperfine coupling in ESR is the equivalent to spin-spin coupling in NMR.^[64] Hyperfine coupling is when the electron magnetic moment couples to the magnetic moment of the closest nucleus, typically that of the atom housing the unpaired spin.^[64] Super-hyperfine

coupling is when an electron couples to the nucleus of another atom.^[64] This method was used to study the copper complexes, $[\text{Cu}_3(\text{L}^2)_2\text{Cl}_2(\text{DMF})_2]$ and $[\text{Cu}_3(\text{L}^3)_2(\text{H}_2\text{O})_2]\text{Cl}_2$ as both are paramagnetic. Both solution and solid studies were done on both compounds.

The energy of a magnetic dipole (E_m) in a magnetic field (B) which is directed along z is calculated by^[63]:

$$E_m = -\boldsymbol{\mu} \cdot \mathbf{B} = \mu_B \cdot B \cdot m_l, \mu_B = e\hbar/4\pi m_e = \text{Bohr magneton}$$

This means the energy will split into $(2l + 1)$ levels. In a hydrogen atom the ground state has no orbital angular momentum ($l = 0$) but it does however have a spin angular momentum of its electron which therefore gives rise to its magnetic dipole. The energy is therefore calculated as^[63]:

$$E_m = g \mu_B B m_s, m_s = \pm 1/2$$

Where g for a hydrogen atom is 2.00228^[63] and so the energy is split into two Zeeman levels as shown in **Figure 4.14**.

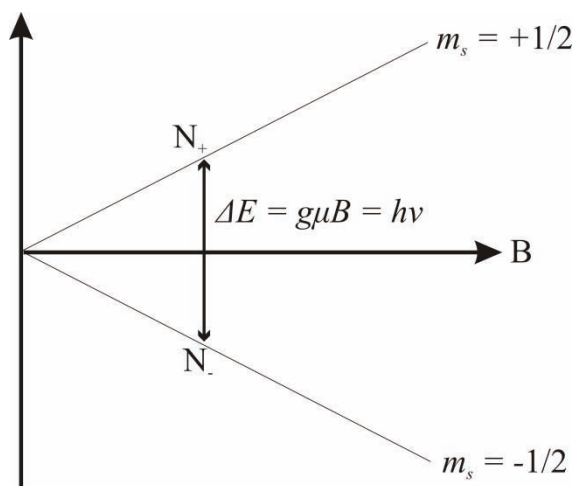


Figure 4.14: Energy levels of an electron in a magnetic field redrawn from ref ^[63].

There are three typical spectra that can be obtained through ESR. The first is where $g_x = g_y = g_z$. This gives the isotropic g -tensor. Shown in **Figure 4.15** is the shape of an isotropic g -tensor spectrum.

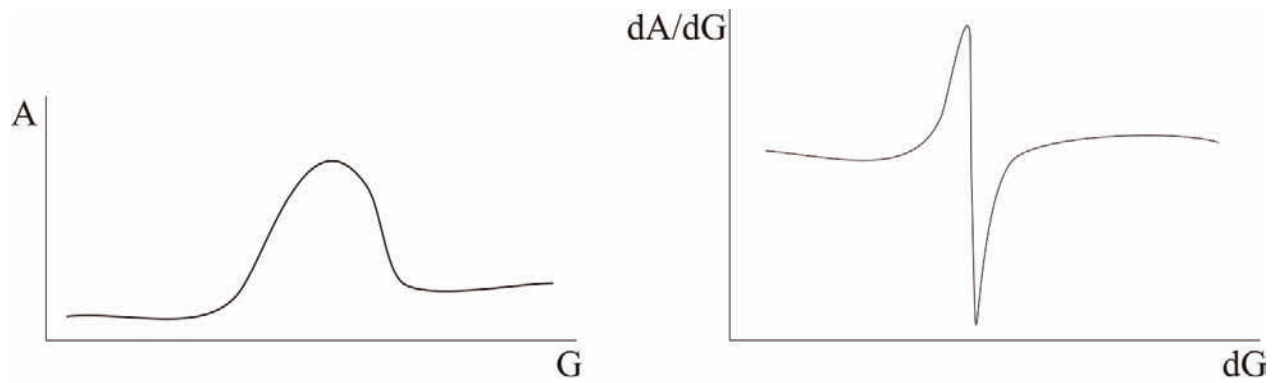


Figure 4.15: Spectra of a typical isotropic g -tensor.

Another typical spectrum would be a tetragonal g -tensor. This is where $g_x = g_y \neq g_z$. The shape of this spectrum is illustrated in **Figure 4.16**.

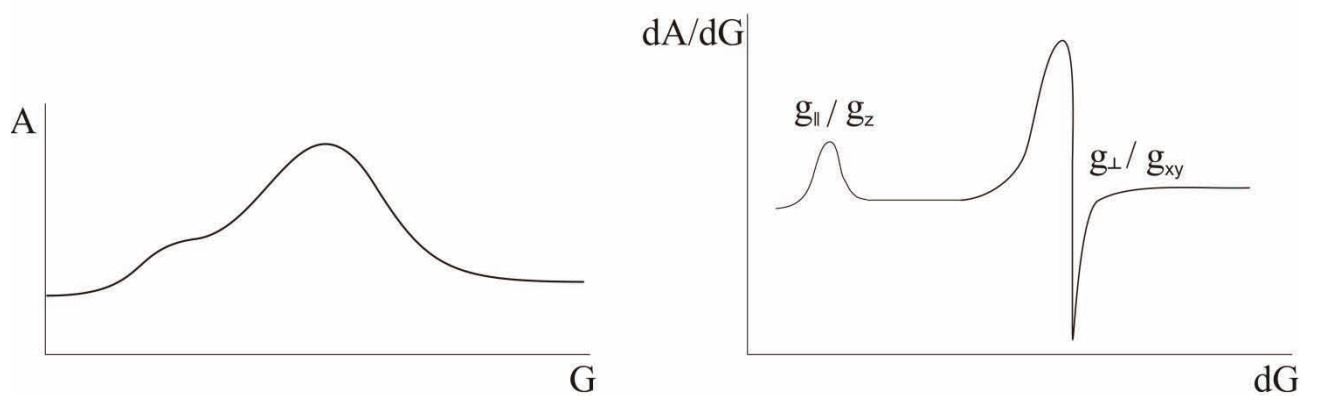


Figure 4.16: Spectra of a typical tetragonal g -tensor.

The last of the three typical spectra is where $g_x \neq g_y \neq g_z$. This is a rhombic g -tensor and the shape of the spectrum is illustrated in **Figure 4.17**.

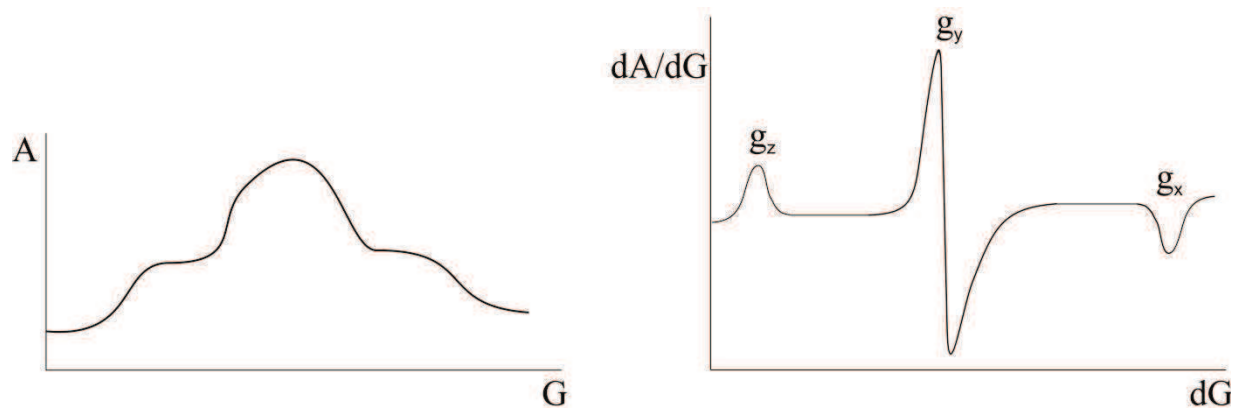


Figure 4.17: Spectra of a typical rhombic g -tensor.

Working from this a few similar copper(II) chelates were researched and will be discussed briefly so as to give some background as to what may be expected in the copper(II) chelates of this work.

An ESR study was done on three copper(II) Schiff-base complexes by Losada *et al.*^[65] The complexes are synthesised by chelation of one copper(II) ion to two ligands. The copper(II) chelates are shown in **Figure 4.18**. They found that in a frozen solution of chloroform the complexes had axial spectra. Axial spectra have a tetragonal g -tensor, meaning that the tensor components $g_x = g_y$.

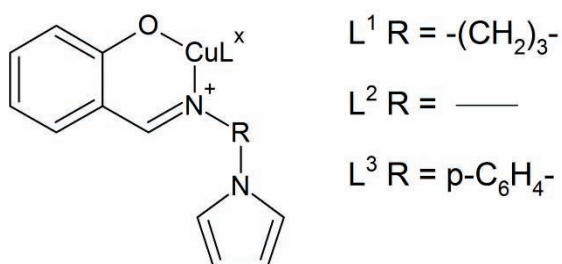


Figure 4.18: Copper(II) Schiff-bases as synthesised by Losada *et al.*^[65]

Losada *et al.*^[65] found that all the complexes synthesised displayed the order $g_{\parallel} > g_{\perp}$ and $A_{\parallel} > A_{\perp}$. They state that often the ratio of $g_{\parallel} / A_{\parallel}$ can be used as an index of tetrahedral

distortions. The value of this ratio for the complexes studied by Losada *et al.*^[65] was 125 - 135 cm which is indicative of complexes without any tetrahedral distortions of the CuN₂O₂ plane. It was also found that the data for A decreased slightly due to the electron-withdrawing effect of substituents on the ligands which meant that the spin density of the unpaired electron on the copper(II) ion was lowered slightly. The data for these complexes is shown in **Table 4.8**.

Table 4.8: ESR data for copper(II) complexes studied by Losada *et al.*^[65]

| | g_{\parallel} | g_{\perp} | g_{iso} | $A_{\parallel} \times 10^4$ (cm ⁻¹) | $A_{\perp} \times 10^4$ (cm ⁻¹) | A_{iso} | $g_{\parallel} / A_{\parallel}$ (cm) |
|--------------------------------------|-----------------|-------------|-----------|--|--|-----------|--------------------------------------|
| Cu(L¹)₂ | 2.239 | 2.031 | 2.100 | 175 | 24 | 72 | 127 |
| Cu(L²)₂ | 2.241 | 2.046 | 2.111 | 171 | 21 | 71 | 130 |
| Cu(L³)₂ | 2.246 | 2.052 | 2.181 | 166 | 19 | 68 | 134 |

Another copper(II) complex (**Figure 4.19**) studied by Dyers Jr. *et al.*^[66] which gave 11 discernible hyperfine lines both at room temperature and at low temperature in THF. These lines were attributed to two ¹⁴N and two imine ¹H nuclei present. The spectra of the complex showed no sensitivity to alternative solvents which indicates that the solvents do not bind axially to the copper(II) ion. A_{\parallel} and A_{\perp} were found to be 197.25 Gs (184 x 10⁻⁴ cm⁻¹) and 36.50 Gs (34.1 x 10⁻⁴ cm⁻¹), and g_{\parallel} and g_{\perp} were determined as 2.2091 and 2.0470, respectively. This data was found to be consistent with the square-planar structure Dyers Jr. *et al.*^[66] determined *via* X-ray crystallography.

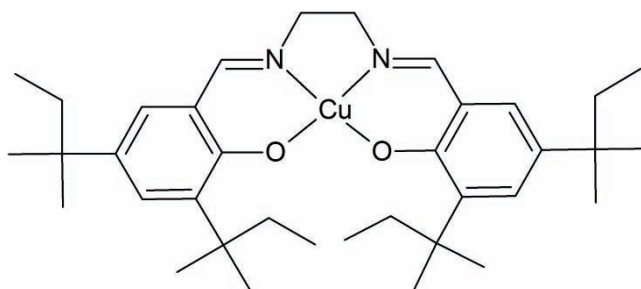


Figure 4.19: Copper(II) salen complex with bulky groups synthesised by Dyers Jr. *et al.*^[66]

In the study done by Klement *et al.*^[56] discussed in **Sections 4.2** and **4.3**, the ESR spectra of the copper(II) complexes (**Figure 4.9**) were recorded at both room temperature and at 77 K in a toluene-acetone solution (20% v/v acetone). The spectra of these compounds in toluene showed weak signals of the dimeric species due to aggregation, whereas, the more intense signals were attributed to monomeric species. Upon addition of the acetone no signals due to the dimeric species were observed. The ESR spectra of the copper(II) complexes in toluene-acetone solutions exhibit axial symmetry with hyperfine and super-hyperfine coupling. Klement *et al.*^[56] observed an interaction of the unpaired electron spin with the copper(II) nuclear spin ($I = 3/2$), two equivalent nitrogen donor nuclei ($I = 1$), and with two hydrogens attached to the carbon adjacent to the imine nitrogen ($I = 1/2$). Klement *et al.*^[56] reported a $g_{\parallel} / A_{\parallel}$ ratio of approximately 105 cm for these complexes which is in agreement with the square-planar copper(II) geometry confirmed by the X-ray structure obtained. All the data for the complexes synthesised by Klement *et al.*^[56] is illustrated in **Table 4.9**.

Table 4.9: ESR data for the salen type copper(II) complexes synthesised by Klement *et al.*^[56]

| | g_{iso} | g_{\parallel} | g_{\perp} | A_{iso} (MHz) | A_{\parallel} (MHz) | A_{\perp} (MHz) |
|------------------------|-----------|-----------------|-------------|-----------------|-----------------------|-------------------|
| CuL¹ | 2.094 | 2.194 | 2.041 | 253 | 621 | 87 |
| CuL² | 2.094 | 2.194 | 2.041 | 253 | 621 | 94 |
| CuL³ | 2.094 | 2.191 | 2.040 | 270 | 627 | 80 |
| CuL⁴ | 2.096 | 2.198 | 2.041 | 260 | 625 | 87 |

Two S-methylisothiosemicarbazide salen-type copper(II) complexes (**Figure 4.20**) were synthesised by Arion *et al.*^[67] These complexes were studied *via* ESR in a solution of CH₂Cl₂/DMF at both the X-band (~9 GHz, 80K) and at the Q-band (35 GHz, 2 K) and determined to be essentially axial. The complexes were found to display similar spin Hamiltonian parameters to other copper(II) complexes that have the coordination sphere of N₂O₂. The data for Cu^{II}L is as follows: g_{\perp} is ~ 2.055, g_{\parallel} is ~ 2.226 which is within the range of 2.20-2.25 and A_{\parallel} is ~ 640 MHz which is within the range of 600 – 660 MHz as was determined by Peisach and Blumberg.^[68]

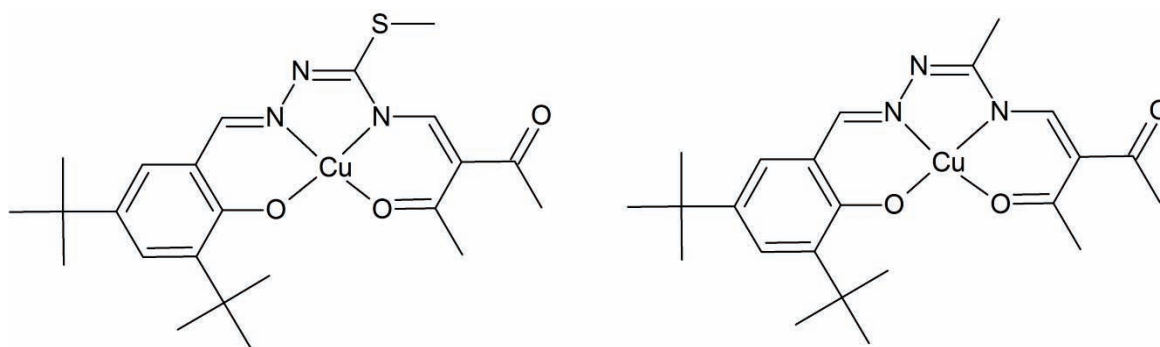


Figure 4.20: Two S-methylisothiosemicarbazide salen-type copper(II) complexes synthesised by Arion *et al.*^[67]

The copper(II) complexes that formed part of the design of the complexes in this work were also studied using EPR. Balla *et al.*^[69] synthesised two copper(II) amino acid based complexes that were designed as hydroxyl radical producers. These complexes are shown in **Figure 4.21**.

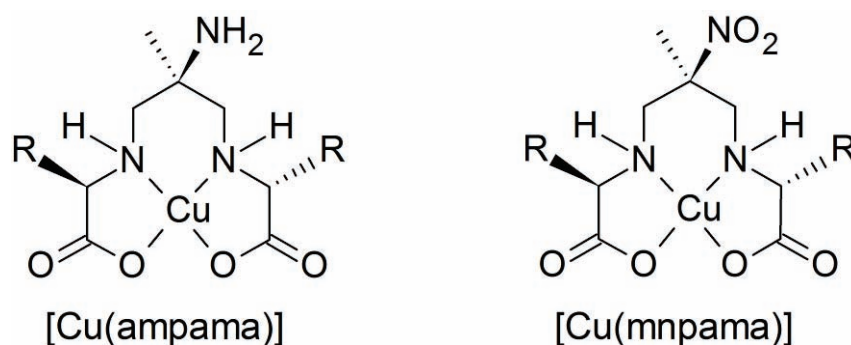


Figure 4.21: Structures of [Cu(mnpama)] and [Cu(ampama)] as synthesised by Balla *et al.*^[69] where R is the chosen amino acid.

The ESR spectra of complexes [Cu(ampama)] and [Cu(mnpama)] were measured in a solution of dimethylformamide and water (1:2) at 298 K and 77 K. Balla *et al.*^[69] reported that all these complexes involving α -amino acids have similar spectra. They display a spectrum typical for square planar geometry with N_2O_2 coordination sphere and weakly bound axial ligands. The ESR data as given by Balla *et al.*^[69] is summarised in **Table 4.10**.

Table 4.10: ESR data of amino acid derived copper complexes synthesised by Balla *et al.*^[69]

| | g_{\parallel} | g_{\perp} | $A_{\parallel} / 10^{-4} \text{ cm}^{-1}$ | $A_{\perp} / 10^{-4} \text{ cm}^{-1}$ |
|----------------------------------|-----------------|-------------|---|---------------------------------------|
| [Cu((S,S)-mnpala)] | 2.24 | 2.06 | 194 | 22 |
| [Cu((S,S)-Hampala)] ⁺ | 2.24 | 2.06 | 192 | 27 |
| [Cu((R,S)-mnpala)] | 2.24 | 2.05 | 201 | 21 |
| [Cu((R,S)-Hampala)] ⁺ | 2.25 | 2.07 | 191 | 22 |
| [Cu((S,S)-mnppe)] | 2.24 | 2.06 | 192 | 20 |
| [Cu((S,S)-Hamppe)] ⁺ | 2.24 | 2.06 | 189 | 18 |
| [Cu((R,S)-mnppe)] | 2.23 | 2.05 | 196 | 19 |
| [Cu((S,S)-mnpval)] | 2.23 | 2.05 | 196 | 18 |
| [Cu((R,S)-mnpval)] | 2.23 | 2.05 | 202 | 20 |
| [Cu((R,S)-mnpneu)] | 2.25 | 2.06 | 189 | 22 |
| [Cu((R,S)-mnpneu)] | 2.22 | 2.05 | 201 | 18 |
| [Cu(mnp- β -ala)] | 2.29 | 2.07 | 174 | 23 |
| [Cu((R,S)-mnpaba)] | 2.27 | 2.08 | 178 | 24 |

The solid state ESR spectrum of $[\text{Cu}_3(\text{L}^2)_2\text{Cl}_2(\text{DMF})_2]$ (**Figure 4.22**) was measured using crushed crystals at room temperature (298 K).

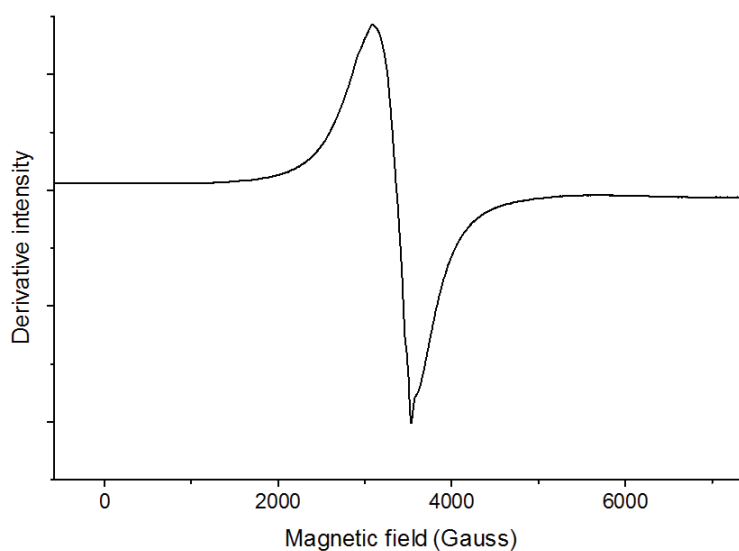


Figure 4.22: Solid state ESR spectrum of $[\text{Cu}_3(\text{L}^2)_2\text{Cl}_2(\text{DMF})_2]$ at 298 K.

This spectrum is consistent with two of the three Cu(II) ions being antiferromagnetically coupled, leaving the third $S = \frac{1}{2}$ ion unchanged and thus responsible for the ESR spectrum **Figure 4.22** does not show characteristic signalling that would be indicative of a magnetically coupled copper system.^[70] The spectrum is consistent with the X-ray crystal structure of this complex. This spectrum is the typical shape for an isotropic g-tensor, where $g_x = g_y = g_z$. An interesting feature of this complex is the fact that it is trinuclear and is still a paramagnetic compound. This may indicate that two of the unpaired electrons centred on adjacent Cu(II) ions are antiferromagnetically coupled, leaving the third Cu(II) centre EPR-active and thus responsible for the spectrum. Alternatively, the ESR spectrum reflects the sum of the contributions from the three independent paramagnetic Cu(II) centres. The possible pairing of the electrons in the $d_{x^2-y^2}$ orbitals of adjacent Cu(II) centres would have to be between the two centres closer together, Cu1 with Cu2 not Cu1 with Cu3 or Cu3 with Cu4 not Cu3 with Cu3. This coupling would then leave the terminal Cu(II) ion carrying the unpaired spin that would generate the ESR spectrum. The structure of $[\text{Cu}_3(\text{L}^2)_2\text{Cl}_2(\text{DMF})_2]$ is shown in **Figure 4.23** to illustrate which nuclei would couple antiferromagnetically.

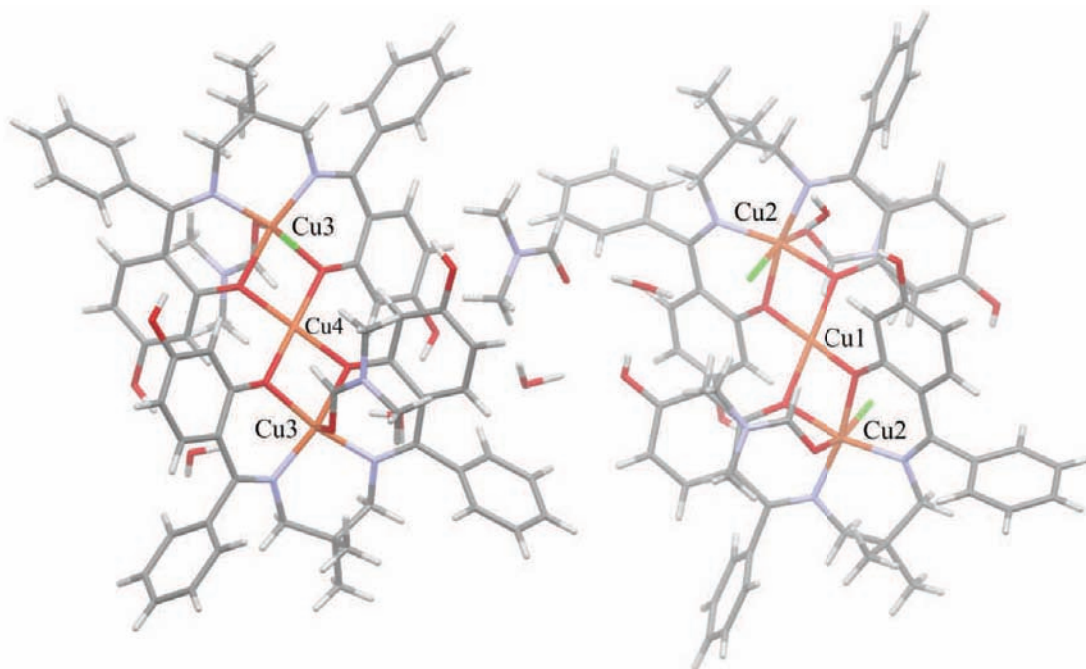


Figure 4.23: X-ray structure of $[\text{Cu}_3(\text{L}^2)_2\text{Cl}_2(\text{DMF})_2]$ illustrating the two independent trinuclear complexes of the asymmetric unit and highlighting the arrangement between adjacent Cu(II) ions that might facilitate antiferromagnetic spin-coupling.

The solid state ESR spectrum for $[\text{Cu}_3(\text{L}^3)_2(\text{H}_2\text{O})_2]\text{Cl}_2$ (**Figure 4.24**) was obtained using a clean fine powder at room temperature (298 K).

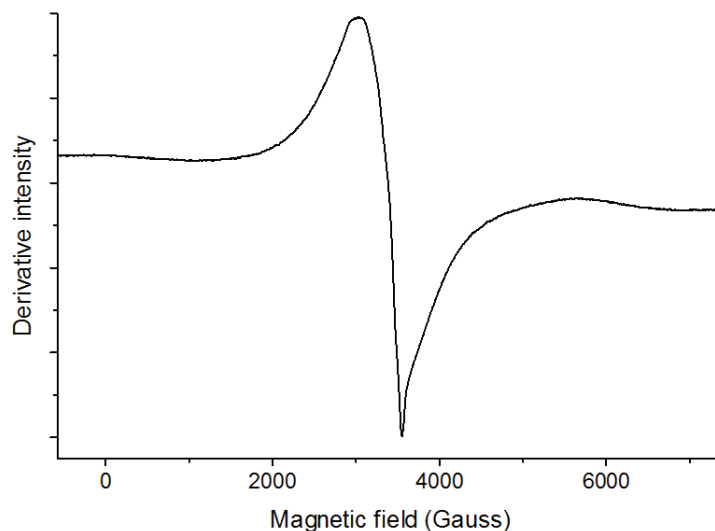


Figure 4.24: Solid state ESR spectrum of $[\text{Cu}_3(\text{L}^3)_2(\text{H}_2\text{O})_2]\text{Cl}_2$ at 298 K.

This unusual spectral shape seems to be indicative of a trinuclear system. The spectrum in **Figure 4.24** is almost identical to that of $[\text{Cu}_3(\text{L}^2)_2\text{Cl}_2(\text{DMF})_2]$ in the solid state. This is due to the complex also being a trinuclear copper complex thus allowing for two of the Cu(II) ions exhibiting antiferromagnetic coupling leaving a third terminal Cu(II) ion unpaired to create the ESR spectrum.

Figure 4.25 shows the solution ESR spectrum for $[\text{Cu}_3(\text{L}^2)_2\text{Cl}_2(\text{DMF})_2]$ recorded in dimethylformamide (DMF) at room temperature. The expected spectrum from a mononuclear Cu(II) complex with an isotropic g -tensor would be a quartet pattern (1: 3: 3:1 intensity ratio) due to the unpaired spin coupling with $I = 3/2$ nucleus. This is inconsistent with the spectrum of $[\text{Cu}_3(\text{L}^2)_2\text{Cl}_2(\text{DMF})_2]$. In the case of a mononuclear Cu(II) complex with a tetragonal g -tensor, the xy tensor component accounts for the most intense absorption or derivative feature at high magnetic field. This intense feature is, furthermore, split into three progressively weaker lines at lower field due to the unpaired electron coupling with the $I = 3/2$ nucleus of the Cu(II) ion. The spectrum in **Figure 4.25** as a whole reflects this type of

pattern; the weakest lines at the lowest field, however, are overlapped and thus an imperfect 4-line pattern is observed. In short, $[\text{Cu}_3(\text{L}^2)_2\text{Cl}_2(\text{DMF})_2]$ gives a tetragonal type ESR spectrum ($g_z > g_{xy}$) in fluid solution at room temperature with g_z essentially unresolved and visibly absent from the spectrum. Interestingly, the main spectral feature close to 3500 G exhibits three sharp peaks in both the positive and negative maxima of the derivative spectrum. This is consistent with super-hyperfine coupling to two $I = 1$ nuclei such as ^{14}N to give 5 lines. Clearly the unpaired electron on a terminal Cu(II) centre shows long-range super-hyperfine coupling to 2 N atoms.

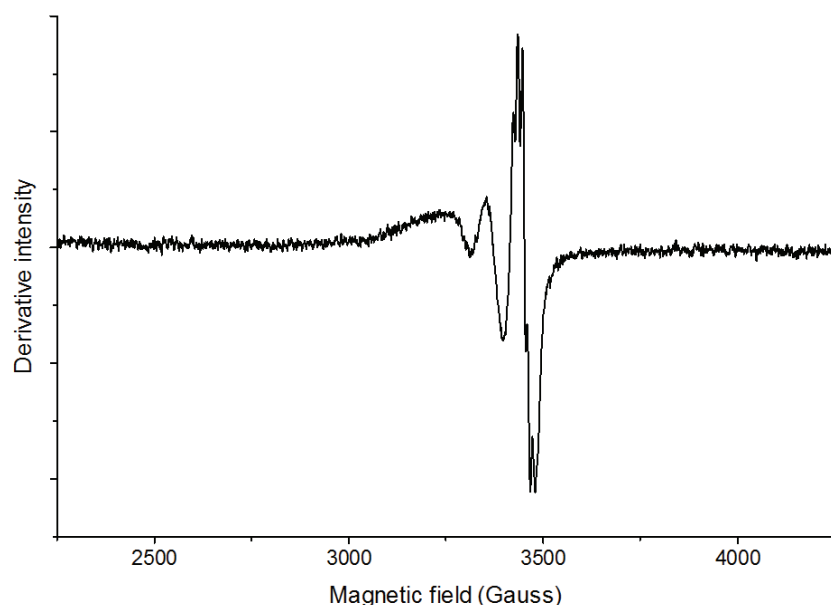


Figure 4.25: ESR spectrum of $[\text{Cu}_3(\text{L}^2)_2\text{Cl}_2(\text{DMF})_2]$ in DMF at 298 K.

The hyperfine coupling shows four peaks overall as was to be expected. The first two peaks are broad and so overlap which results in what is seen in **Figure 4.25** as the initial broad band. The four line pattern seen is due to the electron in each Cu(II) ion spin coupling with the $I = 3/2$ nucleus. The peak-to-peak separation gives the hyperfine coupling constant, 76 G ($710 \times 10^{-4} \text{ cm}^{-1}$). Note that the hyperfine coupling is seen for g_{xy} only as g_z is very weak.

$$\text{Multiplicity} = 2nI + 1 = 2(1)(3/2) + 1 = 4$$

Shown in **Figure 4.26** is the spectrum of $[\text{Cu}_3(\text{L}^2)_2\text{Cl}_2(\text{DMF})_2]$ in DMF with the super-hyperfine splitting labelled. The super-hyperfine coupling is to another nucleus beyond copper. This is visible as three sharp peaks on the high-field line in the spectrum (on both the positive and negative derivative). This is due to the electron coupling to a single $I = 1$ ^{14}N nucleus in the molecule. The two nitrogen atoms are spectroscopically equivalent and the radical is localised on one end of the trinuclear structure as the middle Cu(II) ion is antiferromagnetically coupled with the other end's Cu(II) ion. The super-hyperfine coupling constant was measured as 11 G ($10.3 \times 10^{-4} \text{ cm}^{-1}$).

$$\text{Multiplicity} = 2nI + 1 = 2(2)(1) + 1 = 5$$

The spectrum is consistent with the structures determined as it shows that the unpaired spin is delocalised on the chelating ligand and there is unpaired spin density in the imine bond region.

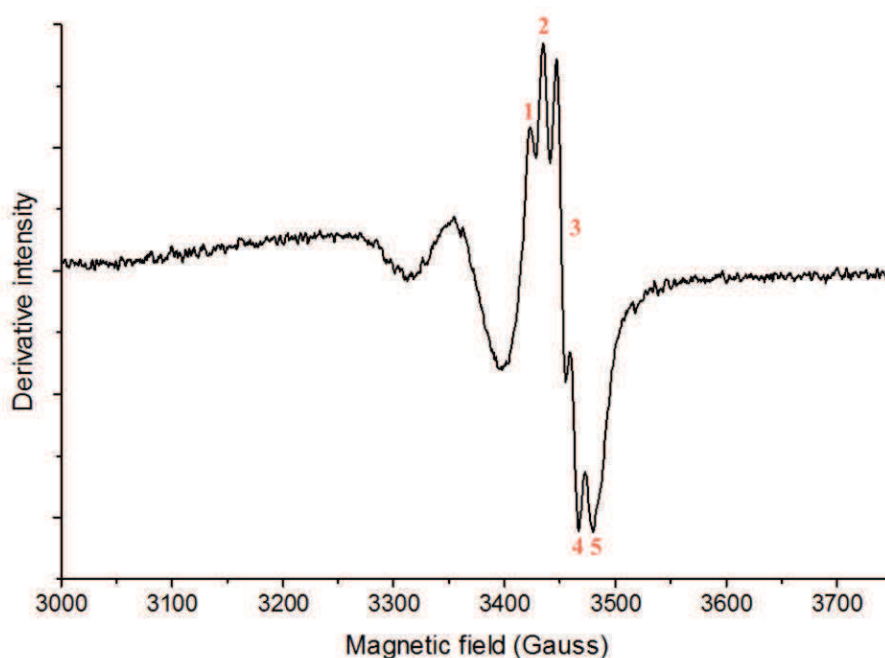


Figure 4.26: ESR Spectrum of $[\text{Cu}_3(\text{L}^2)_2\text{Cl}_2(\text{DMF})_2]$ in DMF at 298 K with peaks labelled to highlight the super-hyperfine coupling.

Shown in **Figure 4.27** is the solution ESR spectrum of $[\text{Cu}_3(\text{L}^3)_2(\text{H}_2\text{O})_2]\text{Cl}_2$ in DMF at room temperature (298 K). The spectrum is almost identical to that of $[\text{Cu}_3(\text{L}^2)_2\text{Cl}_2(\text{DMF})_2]$ which is to be expected due to the similarity in X-ray structure of the two compounds.

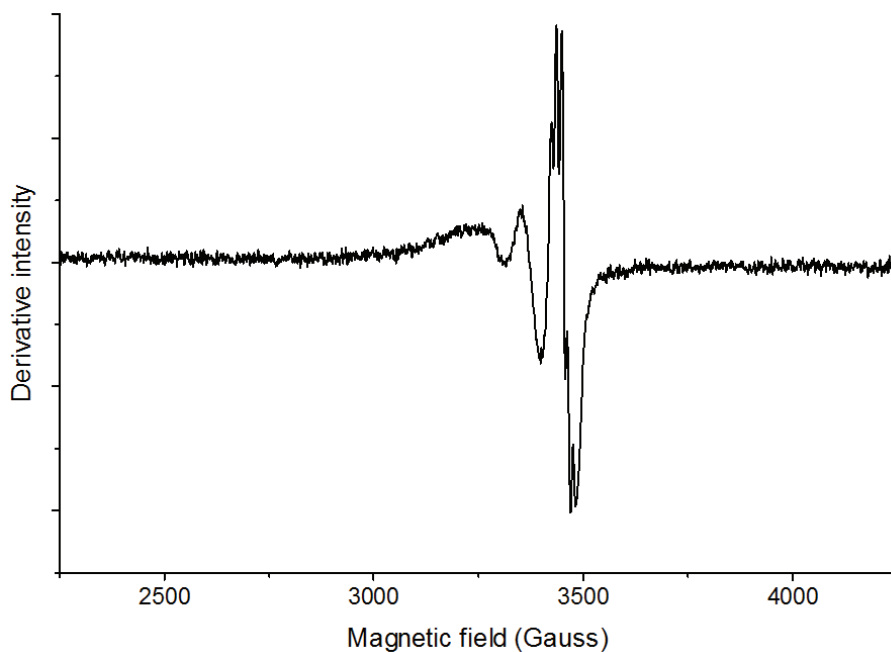


Figure 4.27: ESR spectrum of $[\text{Cu}_3(\text{L}^3)_2(\text{H}_2\text{O})_2]\text{Cl}_2$ in DMF at 298 K.

The ESR spectrum reflects typical hyperfine coupling to the $I = 3/2$ copper nucleus for a tetragonal g -tensor with incomplete resolution of the low-field lines due to line broadening. The most intense signal of the pattern at approximately 3300 G exhibits splitting into several lines consistent with super-hyperfine coupling to two $I = 1$ N atoms. The fact that the spectrum of $[\text{Cu}_3(\text{L}^3)_2(\text{H}_2\text{O})_2]\text{Cl}_2$ is very similar to that of $[\text{Cu}_3(\text{L}^2)_2\text{Cl}_2(\text{DMF})_2]$ supports the idea that two of the three Cu(II) centres in the latter complex are antiferromagnetically coupled, leaving the third Cu(II) centre responsible for the ESR spectral pattern of **Figure 4.27**.

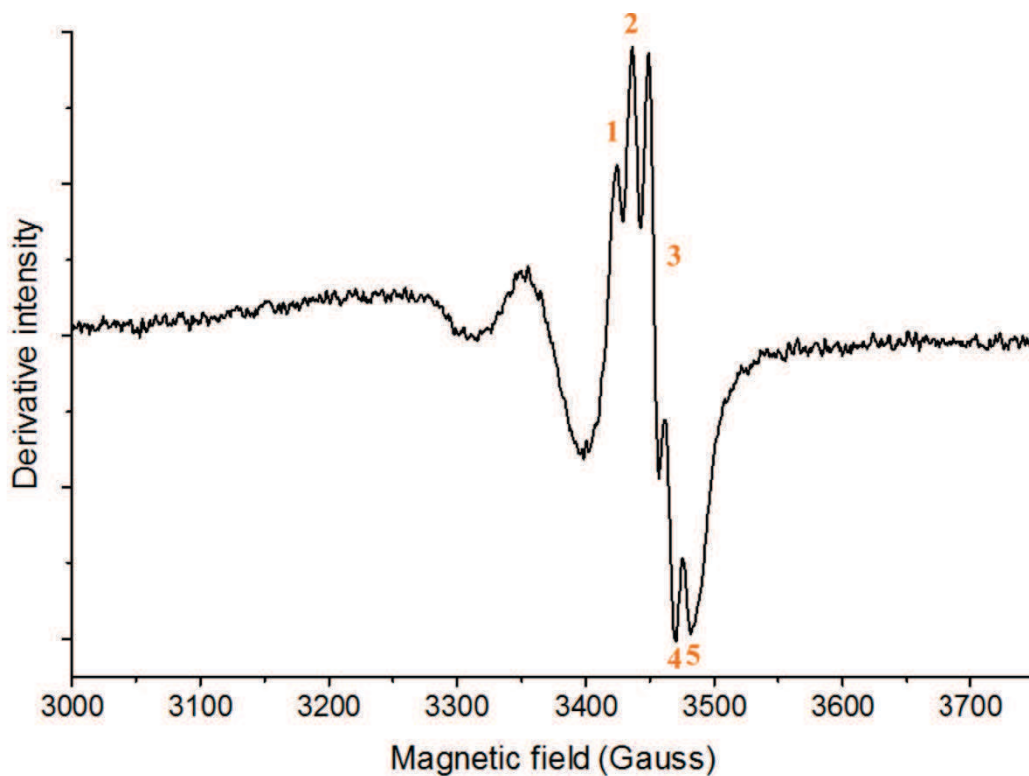


Figure 4.28: ESR Spectrum of $[\text{Cu}_3(\text{L}^3)_2(\text{H}_2\text{O})_2]\text{Cl}_2$ in DMF at 298 K with peaks labelled to highlight the super-hyperfine coupling.

Shown in **Figure 4.28** is the spectrum of $[\text{Cu}_3(\text{L}^3)_2(\text{H}_2\text{O})_2]\text{Cl}_2$ in DMF with the super-hyperfine splitting labelled. The peak-to-peak separation gives the hyperfine coupling constant, 77 G ($719 \times 10^{-4} \text{ cm}^{-1}$). As was the case for $[\text{Cu}_3(\text{L}^2)_2\text{Cl}_2(\text{DMF})_2]$, the hyperfine coupling is seen for g_{xy} only as g_z is very weak. The super-hyperfine coupling constant measured for this compound was 13 G ($12.2 \times 10^{-4} \text{ cm}^{-1}$).

The hyperfine coupling constants for $[\text{Cu}_3(\text{L}^2)_2\text{Cl}_2(\text{DMF})_2]$ and $[\text{Cu}_3(\text{L}^3)_2(\text{H}_2\text{O})_2]\text{Cl}_2$, compared favourably to the A_{iso} values as reported by Losada *et al.*^[65]

4.5 Conclusions

The NMR spectra of the ligands show two broad bands indicating the two hydroxyl groups present. Once the metal has chelated to the ligand, only the more upfield broad band is found in the spectra. This is indicative of the metal chelating to the two *ortho* hydroxyls and therefore the loss of the most downfield broad band. The UV-vis spectra show little variation in the ligand spectra as would be expected. The metal complexes show variations in the presence or absence of MLCT bands or d-d transitions. The infrared spectra of the ligands showed only one band for the C-O stretch as compared to multiple bands in the metal complexes. The nickel complexes showed two bands for the $\nu(\text{C}=\text{N})$ mode at different frequencies which is consistent with the presence of symmetric and asymmetric modes for this functional group. The complexes of this work compared favorably with those of a similar nature in the literature. The ESR data confirmed that the trinuclear solid state structure is maintained in solution. Two of the three copper(II) ions couple antiferromagnetically, leaving the third as an $S = \frac{1}{2}$ centre with hyperfine coupling constant to the $I = \frac{3}{2}$ Cu nucleus of *ca.* 76 G. In a DMF solution, super-hyperfine coupling (*ca.* 12 G) was found to occur to two nitrogen atoms which is consistent with the donor atom set of the terminal copper(II) centres being the site of the unpaired spin density.

5. X-ray Crystallography

5.1 Introduction

Schiff bases have been synthesised and chelated to various metals all around the world. Both the ligands and their complexes have shown a variety of uses ranging from anion sensors^[12], antimicrobial agents^[13], photo- and thermochromism^[14] to displaying solvatochromism^[15]. A review by Kumar *et al.*^[13] reported that chromium azomethine and a Schiff base cobalt complex were used as dyes for items such as leathers, food packages and wools. As was mentioned in Chapter 1 a copper(II) complex, [*N,N'*-bis(4-methoxy-salicylidene)-1,2-diaminoethane]copper(II) (**Figure 1.6**), was synthesised by Yao *et al.*^[15] and due to the σ donor capacity of the solvent increasing the solvent would coordinate to the metal centre *via* substitution of a water molecule, and this would in turn change the energy of the transitions leading to the solvatochromic effect. A zinc(II) Schiff base complex that was studied by Yu *et al.*^[71] was found to exhibit bright pure blue emission. Yu *et al.*^[71] examined the complex through absorption, emission and thermal analysis and found the complex to be suitable for use as an organic light-emitting diode. These are used in full-colour, flat panel displays and the blue emission is quite coveted.

The Cambridge Structural Database^[72] (CSD) was used to find crystal structures related to those synthesised in this work. Neither the ligands synthesised, nor their metal chelates are reported in the CSD^[72]. Three literature structures were chosen for discussion due to their similarity to the compounds crystallised in this project.

KUVLIX^[73] (**Figure 5.1.1**) is a dibenzophenone derivative with an *ortho* hydroxyl group. It crystallised in the monoclinic space group $P 2_1/c$ with $Z = 4$. The only hydrogen bonding present in the crystal is intramolecular hydrogen bonding between the imine nitrogen atom and the *ortho* phenolic hydrogen atoms.

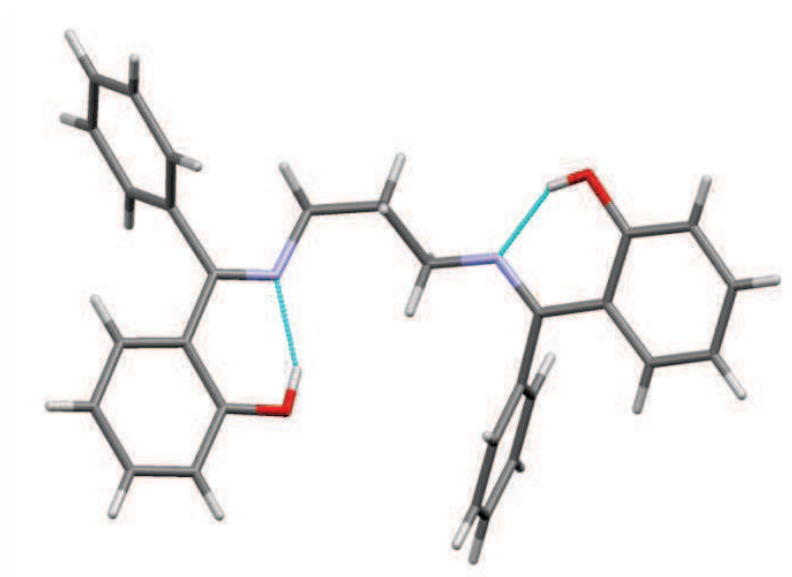


Figure 5.1.1: Diagram of a single molecule of 2,2'-(propane-1,3-diylbis(nitrilo(phenylmethylidene))) diphenol. Redrawn from the CSD^[72] coordinates of KUVLIX^[73].

A copper chelate of similar ligand structure, AQETEV (**Figure 5.1.2**), was crystallised by Datta *et al.*^[74] It crystallised in the monoclinic space group $P 2_1/n$ with $Z = 2$. The compound is a trinuclear complex of copper(II). The *ortho* phenolic oxygens are bridging two copper(II) ions. The charge is then neutralised by the copper(II) ions bound within each ligand and the axially-bound perchlorate ions. There was no hydrogen bonding present in the lattice and very few short contacts existed. This structure is quite significant in that it is trinuclear and the copper(II) chelates studied in this work also adopted a trinuclear structure.

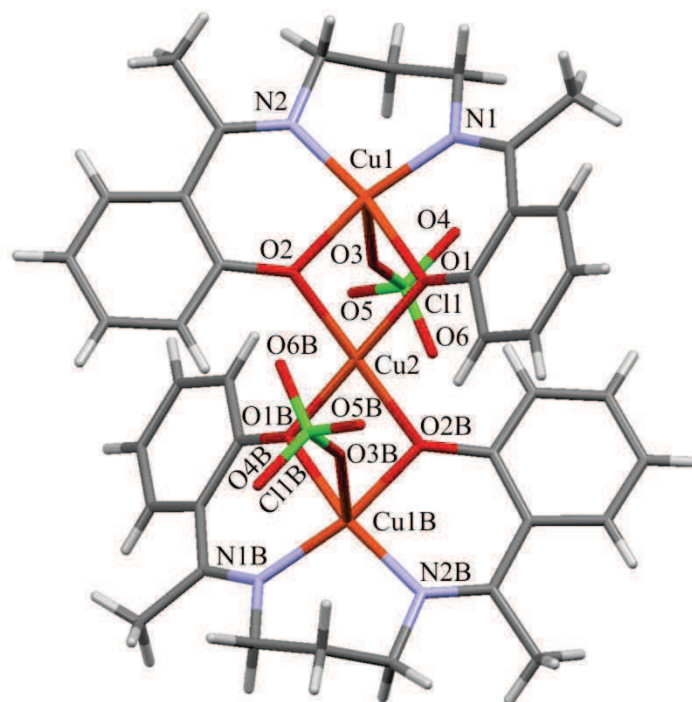


Figure 5.1.2: Diagram of a single molecule of diperchlorato-bis(m2-2,2'-(1,3-propane diylbis(nitriloethylidyne))bisphenolato)-tri-copper(II). Redrawn from the CSD^[72] coordinates of AQETEV^[74].

Table 5.1.1: Average coordination bond lengths and angles for AQETEV^[74].

| Bond Lengths (Å) | | Bond Angles (°) | |
|------------------|----------|-----------------|-----------|
| Cu1-N | 1.961(4) | N1-Cu1-N2 | 101.18(1) |
| Cu1-O | 1.929(3) | N1-Cu1-O1 | 88.79(1) |
| Cu1-Os | 2.617(6) | N2-Cu1-O2 | 91.64(1) |
| Cu2-O | 1.954(3) | O1-Cu1-O2 | 78.15(1) |
| | | N1-Cu1-O3 | 103.90(2) |
| | | N2-Cu1-O3 | 98.60(2) |
| | | O1-Cu1-O3 | 81.86(2) |
| | | O2-Cu1-O3 | 79.21(2) |
| | | O1-Cu2-O2 | 76.95(1) |
| | | O-Cu2-OB av | 103.05(1) |

A nickel(II) complex of a related ligand was reported by Ray *et al.*^[75] It crystallised in the monoclinic space group $P 2_1/c$ with $Z = 4$. The nickel(II) ion is in the expected square planar coordination geometry for a tetradentate dianionic ligand. The nickel(II) balances the ligand's charge giving a neutral molecule overall. The structure is solvated by methanol. An interesting structural feature in this compound is the presence of a bifurcated hydrogen bond between the phenolic oxygens and the alcoholic hydrogen present in the methanol molecule. Of further interest is the fact that the same ligand with nickel(II) favours the formation of mononuclear complexes opposed to the bridged trinuclear structure observed with copper(II).

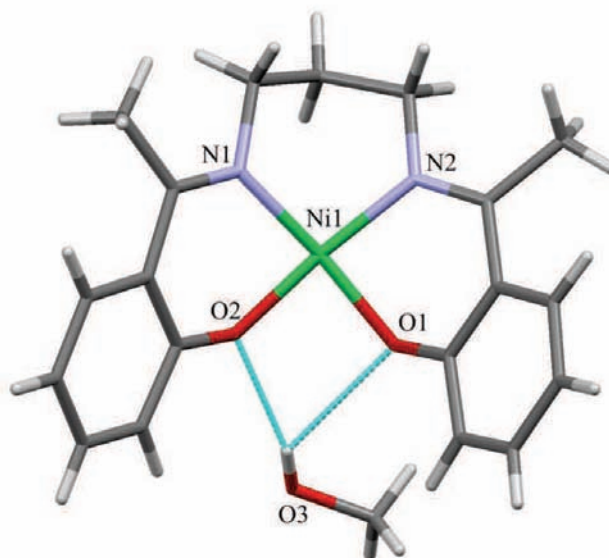


Figure 5.1.3: Diagram of a single molecule of (N,N'-bis((1-(2-oxyphenyl)ethyl)imino)propane)-nickel(II) methanol solvate. Redrawn from the CSD^[72] coordinates of LOFXIO^[75].

Table 5.1.2: Coordination bond lengths and angles for LOFXIO^[75]

| Bond Lengths (Å) | | Bond Angles (°) | |
|------------------|----------|-----------------|----------|
| N1-Ni1 | 1.883(2) | N1-Ni1-N2 | 94.58(8) |
| N2-Ni1 | 1.901(2) | N1-Ni1-O2 | 90.79(7) |
| O1-Ni1 | 1.855(2) | N2-Ni1-O1 | 89.43(8) |
| O2-Ni1 | 1.828(1) | O1-Ni1-O2 | 85.48(7) |

As can be seen from the above examples the coordination of the ligand to a metal ion can vary quite drastically. This is made clearly visible by the differences in structure between the nickel(II) and copper(II) complexes. The nickel complex is found to be mononuclear, whilst the copper(II) complex trinuclear and this could be attributed to the differences in ionic radii. As nickel(II) ion has a smaller ionic radius (0.069 nm vs 0.072 nm), it is possibly unable to form trinuclear bridged structures like those observed for copper(II) ion.

5.2 Objectives

The crystal structure of each of the two ligands and six metal chelates that were successfully crystallised will be determined and reported along with an analysis of the relevant bond lengths and angles. Any features of interest will be highlighted and discussed.

5.3 Experimental Methods

5.3.1 General Crystallographic Procedures

X-Ray diffraction data were collected on an Oxford Diffraction Xcalibur2 CCD 4-circle diffractometer equipped with an Oxford Instruments Cryojet. The data were collected at room temperature unless otherwise stated, with Mo K α ($\lambda = 0.71073 \text{ \AA}$) radiation at a crystal-to-detector distance of 50 mm using omega scans at $\theta = 29.389^\circ$, with varying exposure times taken at 2.01 kW X-ray power with 0.75° frame widths. The data were reduced with the program CrysAlis RED^[76] using outlier rejection, scan speed scaling, as well as standard Lorentz and polarization correction factors. A multi-scan absorption correction was applied to the data^[77]. Unless otherwise stated, direct methods (SHELXS-97, WinGX32)^[78-79] were used to solve the structures. All non-H atoms were located in the E-map and refined anisotropically with SHELXL-97.^[80] All hydrogen atoms in each of the structures resolved were included as idealized contributors in the least squares process with standard SHELXL-97^[80] parameters.

For some crystals, X-ray diffraction data were recorded on a Brüker APEX-II Duo CCD diffractometer equipped with an Oxford Instruments Cryojet and Incoatec IuS microsources (Mo and Cu) with Quazar multilayer optics. The data were collected at room temperature unless otherwise stated, using Mo K α ($\lambda = 0.71073 \text{ \AA}$) radiation and ϕ - ω scans. Data collection and reduction were performed by the program SAINT^[81]. Empirical (multi-scan) absorption corrections were applied using SADABS. The structure was solved by direct methods using direct methods (SHELXS-97, WinGX32)^[78-79] and further refined by full-matrix least-squares on F2 using SHELXL-97.^[80] The H atoms were located by difference Fourier synthesis; those attached to carbon atoms were refined in idealized positions using the standard riding model employed in SHELXL-97.^[80]

5.4 Experimental Data for Ligands

5.4.1 X-ray Structure of H₃L¹

Yellow cubic crystal (0.30 \times 0.40 \times 0.40 mm). C₃₂H₃₃N₃O₆, fw = 555.61 amu, $a = 12.631(5) \text{ \AA}$, $b = 15.619(5) \text{ \AA}$, $c = 14.201(5) \text{ \AA}$, $\alpha = 90^\circ$, $\beta = 92.792(5)^\circ$, $\gamma = 90^\circ$, $V = 2798.3(17) \text{ \AA}^3$. Monoclinic, $P 2_1/n$, $Z = 4$, $D_c = 1.319 \text{ g cm}^{-3}$, $\mu = 0.092 \text{ mm}^{-1}$, $T = 296(2) \text{ K}$, $R_1 (wR_2) = 0.0703 (0.2000)$ for 3340 unique data with $I > 2\sigma(I)$, $R_1 (wR_2) = 0.1247 (0.2301)$ for all 6298 data ($R_{\text{int}} = 0.0487$).

The asymmetric unit of H₃L¹ contained a single ligand molecule and one DMF molecule with $Z = 4$. The final value of R_1 was 0.0703 and wR_2 was 0.2000. A semi-empirical multi-scan^[82] absorption correction was applied to the data. The maximum and minimum electron densities on the final difference Fourier map were 0.911 and $-0.956 \text{ e \AA}^{-3}$, respectively. All data relating to the X-ray structures (atomic coordinates, structure refinement details and the IUCR CheckCIF^[83] report) are available in **Appendix D**.

5.4.2 X-ray Structure of H₂L²

Colourless block crystal (0.12 \times 0.15 \times 0.35 mm). C₃₁H₃₀N₂O₄, fw = 494.57 amu, $a = 9.014(2) \text{ \AA}$, $b = 21.434(4) \text{ \AA}$, $c = 13.680(2) \text{ \AA}$, $\alpha = 90^\circ$, $\beta = 103.228(10)^\circ$, $\gamma = 90^\circ$,

$V = 2572.93(8) \text{ \AA}^3$. Monoclinic, $P 2_1/c$, $Z = 4$, $D_c = 1.277 \text{ g cm}^{-3}$, $\mu = 0.085 \text{ mm}^{-1}$, $T = 100(2) \text{ K}$, $R_1 (wR_2) = 0.0466 (0.1091)$ for 4875 unique data with $I > 2\sigma(I)$, $R_1 (wR_2) = 0.0637 (0.1160)$ for all 6342 data ($R_{\text{int}} = 0.0483$).

The asymmetric unit of H_2L^2 contained a single molecule with $Z = 4$. The final value of R_1 was 0.0466 and wR_2 was 0.1160. A semi-empirical multi-scan^[82] absorption correction was applied to the data. The maximum and minimum electron densities on the final difference Fourier map were 0.277 and $-0.237 \text{ e \AA}^{-3}$, respectively. All data relating to the X-ray structures (atomic coordinates, structure refinement details and the IUCR CheckCIF^[83] report) are available in **Appendix D**.

5.5 Experimental Data for Metal Complexes

5.5.1 X-ray Structure of $[\text{Cu}_2(\text{L}^1)(\text{OAc})(\text{DMF})]$

Brown shard ($0.10 \times 0.30 \times 0.30 \text{ mm}$). $\text{C}_{34}\text{H}_{33}\text{Cu}_2\text{N}_3\text{O}_8$, fw = 738.71 amu, $a = 9.014(5) \text{ \AA}$, $b = 14.696(5) \text{ \AA}$, $c = 28.716(5) \text{ \AA}$, $\alpha = 90^\circ$, $\beta = 92.625(5)^\circ$, $\gamma = 90^\circ$, $V = 3800(3) \text{ \AA}^3$. Monoclinic, $P 2_1/n$, $Z = 4$, $D_c = 1.291 \text{ g cm}^{-3}$, $\mu = 1.167 \text{ mm}^{-1}$, $T = 100(2) \text{ K}$, $R_1 (wR_2) = 0.0505 (0.1408)$ for 5761 unique data with $I > 2\sigma(I)$, $R_1 (wR_2) = 0.0701 (0.1513)$ for all 8506 data ($R_{\text{int}} = 0.0000$).

The asymmetric unit of $[\text{Cu}_2(\text{L}^1)(\text{OAc})(\text{DMF})]$ contained a single molecule with $Z = 4$. The final value of R_1 was 0.0505 and wR_2 was 0.1408. The maximum and minimum electron densities on the final difference Fourier map were 0.768 and $-0.567 \text{ e \AA}^{-3}$, respectively. The residual peak lay closest to the Cu2 atom. All data relating to the X-ray structures (atomic coordinates, structure refinement details and the IUCR CheckCIF^[83] report) are available in **Appendix D**.

5.5.2 X-ray Structure of [Cu₃(L²)₂Cl₂(DMF)₂]

Red planar crystal (0.10 × 0.20 × 0.30 mm). C_{20.67}H_{18.67}Cl_{0.67}CuN_{1.33}O_{2.67}, fw = 415.54 amu, $a = 10.7378(4)$ Å, $b = 15.8005(6)$ Å, $c = 22.1628(10)$ Å, $\alpha = 87.018(3)^\circ$, $\beta = 79.714(4)^\circ$, $\gamma = 81.185(3)^\circ$, $V = 3654.9(3)$ Å³. Triclinic, $P-1$, $Z = 4$, $D_c = 1.133$ g cm⁻³, $\mu = 0.984$ mm⁻¹, $T = 110(2)$ K, $R_1 (wR_2) = 0.0493 (0.1119)$ for 7809 unique data with $I > 2\sigma(I)$, $R_1 (wR_2) = 0.0821 (0.1181)$ for all 14347 data ($R_{\text{int}} = 0.0000$).

The asymmetric unit of [Cu₃(L²)₂Cl₂(DMF)₂] contained two half molecules with $Z = 4$. The final value of R_1 was 0.0493 and wR_2 was 0.1119. A semi-empirical multi-scan^[82] absorption correction was applied to the data. The maximum and minimum electron densities on the final difference Fourier map were 1.864 and -0.801 e Å⁻³, respectively. The residual peak lay closest to H4AA. All data relating to the X-ray structures (atomic coordinates, structure refinement details and the IUCR CheckCIF^[83] report) are available in **Appendix D**.

5.5.3 X-ray Structure of [Ni(L²)]

Red plate crystal (0.03 × 0.20 × 0.60 mm). C₃₁H₂₈N₂NiO₄, fw = 551.26 amu, $a = 25.0542(13)$ Å, $b = 9.6539(5)$ Å, $c = 27.3083(13)$ Å, $\alpha = 90^\circ$, $\beta = 98.568(5)^\circ$, $\gamma = 90^\circ$, $V = 6531.4(6)$ Å³. Monoclinic, $P 2_1/c$, $Z = 8$, $D_c = 1.121$ g cm⁻³, $\mu = 0.626$ mm⁻¹, $T = 296(2)$ K, $R_1 (wR_2) = 0.0603 (0.1237)$ for 5416 unique data with $I > 2\sigma(I)$, $R_1 (wR_2) = 0.1403 (0.1395)$ for all 12840 data ($R_{\text{int}} = 0.1225$).

The asymmetric unit of [Ni(L²)] contained two independent molecules, giving $Z = 8$ for the unit cell contents. The final value of R_1 was 0.0603 and wR_2 was 0.1237. A semi-empirical multi-scan^[82] absorption correction was applied to the data. The maximum and minimum electron densities on the final difference Fourier map were 0.396 and -0.386 e Å⁻³, respectively. The residual peak lies closest to O1A. All data relating to the X-ray structures (atomic coordinates, structure refinement details and the IUCR CheckCIF^[83] report) are available in **Appendix D**.

5.5.4 X-ray Structure of $[\text{Cu}_3(\text{L}^3)_2(\text{H}_2\text{O})_2]\text{Cl}_2$

Brown flat crystal ($0.20 \times 0.07 \times 0.01$ mm). $\text{C}_{29}\text{H}_{26}\text{ClCu}_{1.5}\text{N}_2\text{O}_5$, fw = 613.28 amu, $a = 9.1151(4)$ Å, $b = 25.6003(11)$ Å, $c = 11.5667(6)$ Å, $\alpha = 90^\circ$, $\beta = 100.219(3)^\circ$, $\gamma = 90^\circ$, $V = 2656.3(2)$ Å³. Monoclinic, $P 2_1/c$, $Z = 4$, $D_c = 1.534$ g cm⁻³, $\mu = 1.355$ mm⁻¹, $T = 100(2)$ K, R_1 (wR_2) = 0.0437 (0.0963) for 4299 unique data with $I > 2\sigma(I)$, R_1 (wR_2) = 0.0495 (0.0986) for all 4761 data ($R_{\text{int}} = 0.0206$).

The asymmetric unit of $[\text{Cu}_3(\text{L}^3)_2(\text{H}_2\text{O})_2]\text{Cl}_2$ contained a half molecule and a chloride ion with $Z = 4$. The final value of R_1 was 0.0437 and wR_2 was 0.0963. A semi-empirical multi-scan^[82] absorption correction was applied to the data. The maximum and minimum electron densities on the final difference Fourier map were 1.155 and -0.418 e Å⁻³, respectively. The residual peak lay closest to H4A. All data relating to the X-ray structures (atomic coordinates, structure refinement details and the IUCR CheckCIF^[83] report) are available in **Appendix D**.

5.5.5 X-ray Structure of $[\text{Ni}(\text{L}^3)]$

Green plate-like crystal ($0.06 \times 0.16 \times 0.20$ mm). $\text{C}_{29}\text{H}_{26}\text{N}_2\text{NiO}_6$, fw = 557.208 amu, $a = 24.261(2)$ Å, $b = 9.0885(8)$ Å, $c = 26.956(2)$ Å, $\alpha = 90^\circ$, $\beta = 111.1090(10)^\circ$, $\gamma = 90^\circ$, $V = 5546(3)$ Å³. Monoclinic, $C 2/c$, $Z = 8$, $D_c = 1.335$ g cm⁻³, $\mu = 0.743$ mm⁻¹, $T = 100(2)$ K, R_1 (wR_2) = 0.0412 (0.1221) for 5202 unique data with $I > 2\sigma(I)$, R_1 (wR_2) = 0.0525 (0.1326) for all data ($R_{\text{int}} = 0.0340$).

The asymmetric unit of $[\text{Ni}(\text{L}^3)]$ contained a single molecule with two water molecules, giving $Z = 8$ for the unit cell contents. The final value of R_1 was 0.0412 and wR_2 was 0.1221. A numerical absorption correction multi-scan^[82] was applied to the data. The maximum and minimum electron densities on the final difference Fourier map were 0.625 and -0.303 e Å⁻³, respectively. The residual peak lies closest to H27. All data relating to the X-ray structures (atomic coordinates, structure refinement details and the IUCR CheckCIF^[83] report) are available in **Appendix D**.

5.5.6 X-ray Structure of $[\text{Zn}_2(\text{L}^3)_2]$

Colourless block crystal ($0.15 \times 0.21 \times 0.27$ mm). $\text{C}_{73}\text{H}_{83}\text{N}_9\text{O}_{13}\text{Zn}_2$, fw = 1425.27 amu, $a = 23.1017(3)$ Å, $b = 18.1096(3)$ Å, $c = 16.6460(3)$ Å, $\alpha = 90^\circ$, $\beta = 90^\circ$, $\gamma = 90^\circ$, $V = 6964.06(4)$ Å³. Orthorhombic, $Pna2_1$, $Z = 12$, $D_c = 1.359$ g cm⁻³, $\mu = 1.100$ mm⁻¹, $T = 100(2)$ K, R_1 (wR_2) = 0.0561 (0.1459) for 10839 unique data with $I > 2\sigma(I)$, R_1 (wR_2) = 0.0765 (0.1607) for all 13623 data ($R_{\text{int}} = 0.0503$).

The asymmetric unit of $[\text{Zn}_2(\text{L}^3)_2]$ contained a single molecule with $Z = 12$. The final value of R_1 was 0.0561 and wR_2 was 0.1459. A numerical absorption correction multi-scan^[82] was applied to the data. The maximum and minimum electron densities on the final difference Fourier map were 0.844 and -0.676 e Å⁻³, respectively. The residual peak lies closest to Zn2. All data relating to the X-ray structures (atomic coordinates, structure refinement details and the IUCR CheckCIF^[83] report) are available in **Appendix D**.

5.6 Results and Discussion

5.6.1 Analysis of the X-ray Structure of H_3L^1

H_3L^1 crystallised in the monoclinic space group $P 2_1/n$. Each asymmetric unit consists of an H_3L^1 molecule and a DMF molecule with $Z = 4$. Shown in **Figure 5.6.1** is the thermal ellipsoid plot of H_3L^1 . H_3L^1 has two configurations possible for the central hydroxyl group. The hydroxyl group can either be in an up position or in a down position which gives rise to the disorder seen in the crystal structure. Due to this only the major configuration (62%) of the CHOH group is shown. H_3L^1 has crystallised as a zwitterion, meaning that it has both a positive and a negative charge within the molecule, but has no overall charge. This has occurred by the hydroxyl proton migrating to the nitrogen of the imine bond, thus creating a negatively charged oxygen atom and a positively charged imine nitrogen atom. This suggests that the imine nitrogen atom is more basic than the hydroxyl group.

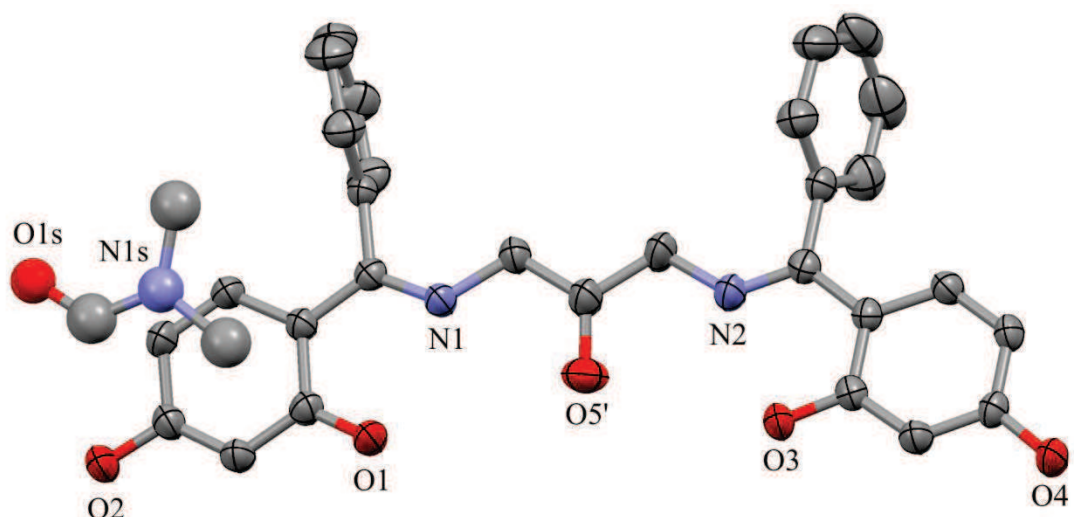


Figure 5.6.1: Partially labelled thermal ellipsoid plot of H_3L^1 . Thermal ellipsoids are drawn at 50% probability, only the major component of the disordered CHOH group is shown for clarity, hydrogen atoms have been omitted for clarity and the DMF solvent molecule was drawn with isotropic thermal parameters.

The structure exhibits intramolecular hydrogen bonding between the zwitterion N-H and the *ortho* phenolic oxygen atoms. This is illustrated by **Figure 5.6.2**.

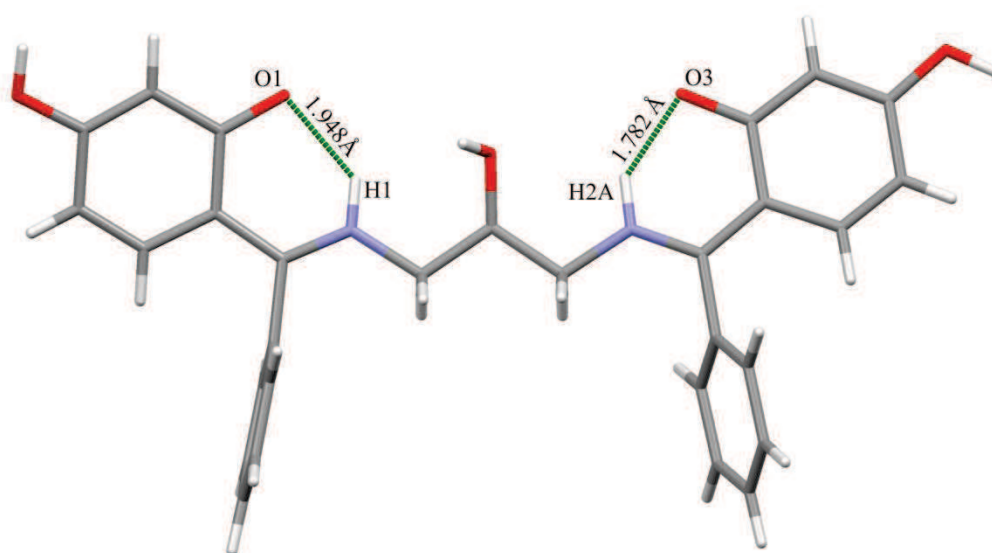


Figure 5.6.2: Intramolecular hydrogen bonding in H_3L^1 .

Table 5.6.1 shows the bond lengths and angles of the intramolecular hydrogen bonds found in the crystal structure. The lengths are reasonably short (between 1.5 - 2.2 Å)^[84] and so can be classified as moderate hydrogen bonds, although as pointed out by Steiner^[84], the H-bond distance is often only an approximate measure of hydrogen bond strength.

Table 5.6.1: Intramolecular hydrogen bond and short contact lengths (Å) and angles (°) for H₃L¹.

| D-H...A | D-H | H...A | D...A | D-H...A |
|-------------|----------|----------|----------|-----------|
| N1-H1...O1 | 0.879(1) | 1.948(9) | 2.629(2) | 133.17(8) |
| N2-H2A...O3 | 0.901(1) | 1.782(8) | 2.532(2) | 139.04(8) |

There are three additional hydrogen bonds that occur between the hydroxyl hydrogens of one ligand and the zwitterion oxygen of an adjacent molecule; and between the hydrogen on the bridging hydroxyl group and the oxygen on the hydroxyl group of an adjacent ligand molecule. The hydrogen bonding in the lattice means that each ligand molecule is connected to five other H₃L¹ molecules. The hydrogen bonding is shown below in **Figure 5.6.3**.

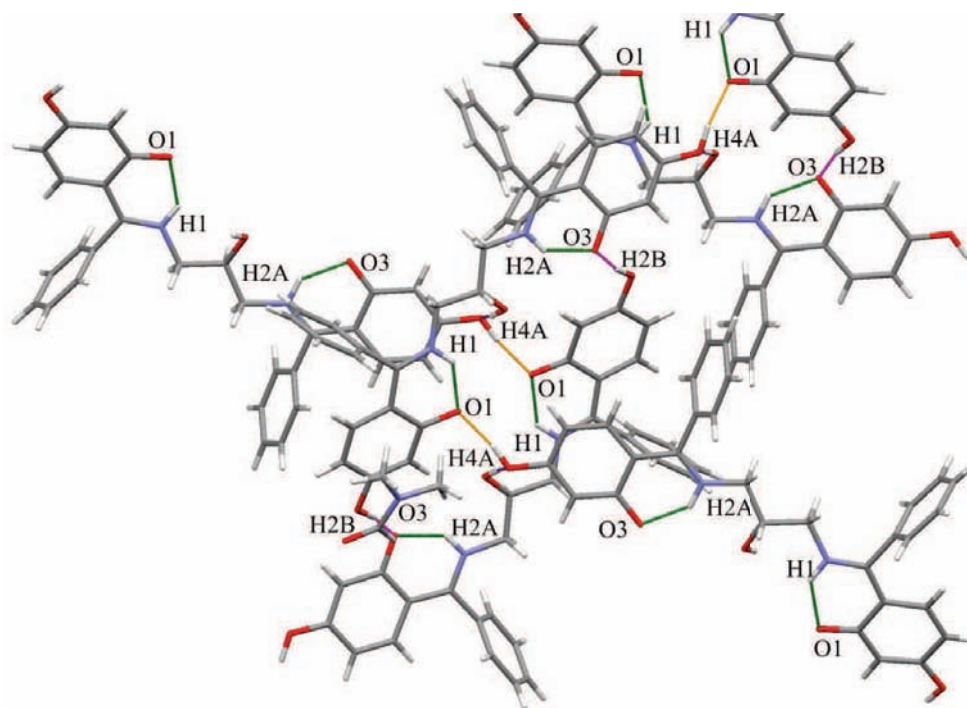


Figure 5.6.3: Hydrogen bonding in the lattice of H₃L¹.

This hydrogen bonding leads to a two-dimensional stacking in layers in the lattice as shown in **Figure 5.6.4**.

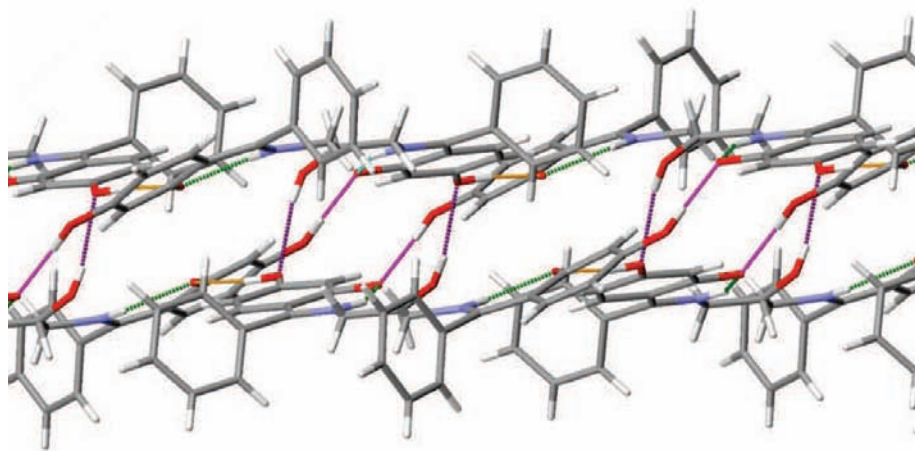


Figure 5.6.4: Stacking of H₃L¹ molecules in the crystal lattice.

There are also short contacts that occur in the crystal lattice of H₃L¹. There are short contacts between a hydrogen on the ligand bridge, H14B, and a hydroxyl group oxygen, O2, on an adjacent ligand molecule; and between a hydrogen on a bridging carbon, H16B, and the oxygen on a DMF molecule, O1s, and between a hydrogen on the free ring, H12, and the hydroxyl oxygen of another ligand, O4. These contacts also help in the stacking, extending the connection between the layers formed by hydrogen bonds. The short contacts are shown in **Figure 5.6.5**.

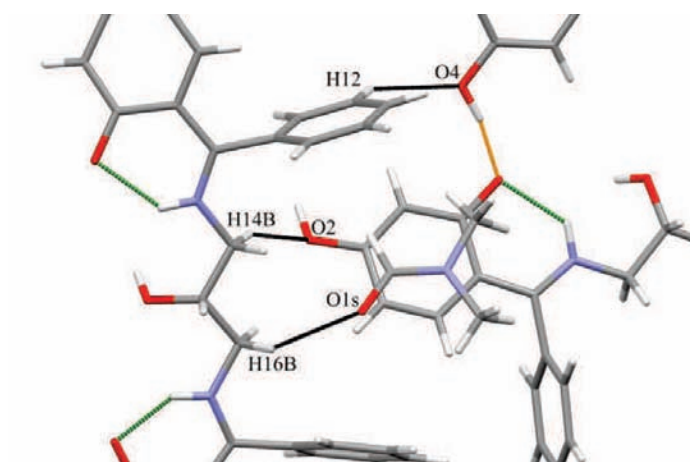


Figure 5.6.5: Short contacts present in the crystal lattice of H₃L¹.

All hydrogen bonds and short contacts described are summarised below in **Table 5.6.2**. The hydrogen bonds in this compound are a mixture of shorter, stronger bonds (1.2 – 1.5 Å)^[84] and longer, weaker bonds (>2.2 Å)^[84].

Table 5.6.2: Intermolecular hydrogen bond and short contact lengths (Å) and angles (°) for H₃L¹.

| D-H...A | D-H | H...A | D...A | D-H...A |
|----------------|----------|----------|----------|-----------|
| O2-H2B...O3 | 0.878(2) | 1.688(2) | 2.552(2) | 167.48(2) |
| O4-H4A...O1 | 0.915(2) | 1.660(2) | 2.563(2) | 168.37(2) |
| O5'-H5'...O4 | 0.820(5) | 1.997(2) | 2.766(5) | 155.89(4) |
| C12-H12...O4 | 0.930(2) | 2.565(2) | 3.352(3) | 142.65(1) |
| C14-H14B...O2 | 0.970(2) | 2.537(2) | 3.457(3) | 158.34(1) |
| C16-H16B...O1s | 0.971(2) | 2.603(2) | 3.474(3) | 149.41(1) |

5.6.2 Analysis of the X-ray Structure of H₂L²

H₂L² crystallised in the monoclinic space group $P 2_1/c$. There are four asymmetric units in the unit cell with a single molecule in the asymmetric unit, thus $Z = 4$. **Figure 5.6.6** shows the thermal ellipsoid plot of the asymmetric unit of H₂L². H₂L² has crystallised as a zwitterion, the same as H₃L¹. Again suggesting the imine nitrogen atom is more basic than the hydroxyl group. This means the oxygen atom will carry a negative charge and the imine nitrogen atom will be positively charged.

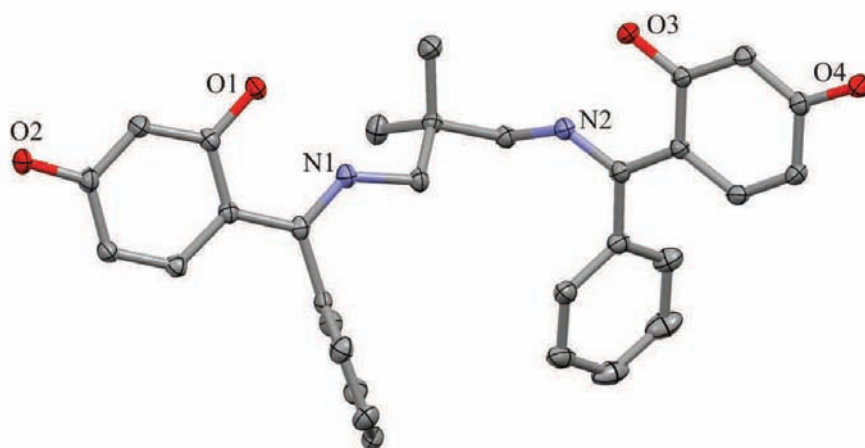


Figure 5.6.6: Partially labelled thermal ellipsoid plot of H_2L^2 . Thermal ellipsoids are drawn at 50% probability, hydrogen atoms have been omitted for clarity.

The structure exhibits intramolecular hydrogen bonding between the imine hydrogen atoms and the *ortho* hydroxyl oxygen atoms. This is shown in **Figure 5.6.7**. These form a six-membered hydrogen-bonded ring structure.

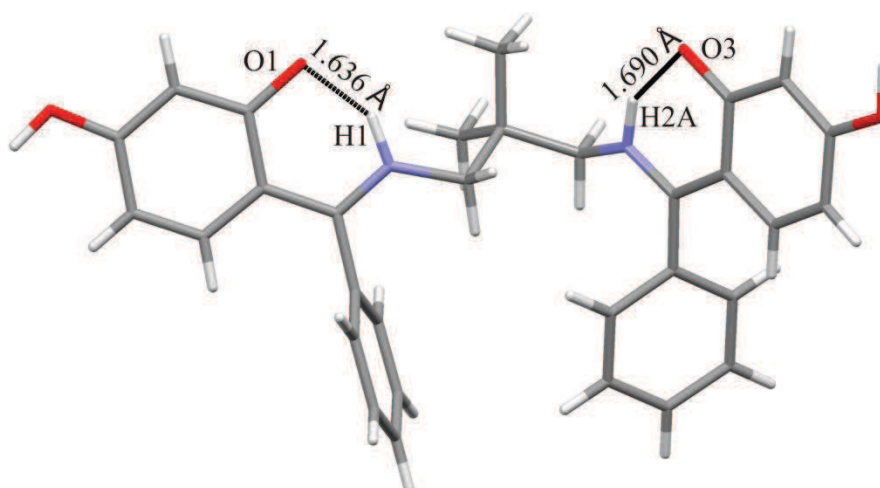


Figure 5.6.7: Intramolecular hydrogen bonding of H_2L^2 .

Table 5.6.3 summarises the bond lengths and angles of the intramolecular hydrogen bonds found in the crystal structure. The lengths are reasonably short, between 1.5 – 2.2 Å^[84] and so can be classified as moderate hydrogen bonds.

Table 5.6.3: Intramolecular hydrogen bond lengths (Å) and angles (°) for H₂L².

| D-H...A | D-H | H...A | D...A | D-H...A |
|-------------|----------|----------|----------|-----------|
| N1-H1...O1 | 0.957(2) | 1.636(2) | 2.496(1) | 147.40(2) |
| N3-H2A...O3 | 0.942(1) | 1.690(2) | 2.530(2) | 146.66(2) |

There are two additional intermolecular hydrogen bonds with each ligand molecule hydrogen-bonded *via* the hydroxyl groups on the phenyl rings. One ligand molecule is hydrogen-bonded to three other ligand molecules as shown in **Figure 5.6.8**.

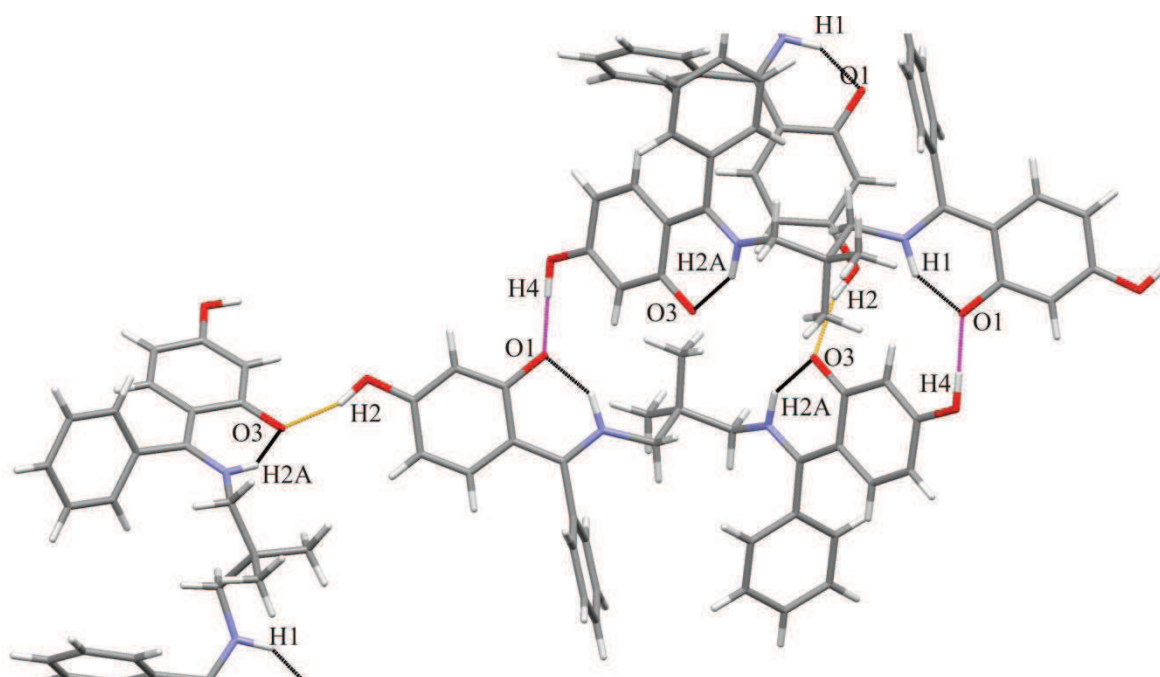


Figure 5.6.8: Hydrogen bonding between H₂L² molecules.

This hydrogen bonding leads to a two-dimensional network, parallel to the *ab* plane, with stacking of the ligand molecules in two directions which creates the lattice as shown in **Figure 5.6.9**. The packing is supported by hydrogen bonding of different ligand hydroxyl groups. There is an interplanar distance of 8.395 Å between two adjacent C20-C25 rings. The two-dimensional network is supported by hydrogen bonds between the *ortho* and *para* hydroxyl groups of two adjacent molecules. The hydrogen bond between O1 and H4 is particularly short with an A...H distance of 1.618(2) Å. Although hydrogen bond length does

not necessarily correlate linearly with bond strength^[84], due to packing constraints in the lattice, it is likely that these short bonds are moderate to strong. It is likely that there are $\pi\cdots\pi$ interactions between the planar aromatic rings that further stabilises the structure.

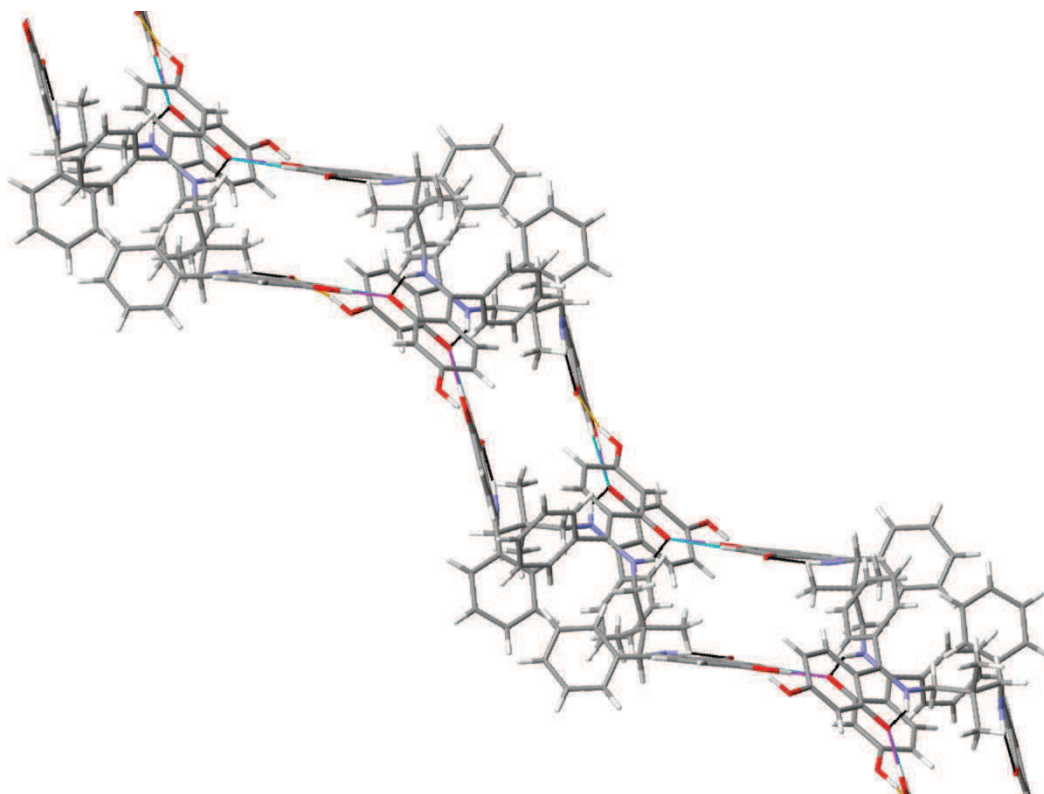


Figure 5.6.9: Stacking of H_2L^2 molecules in the lattice due to hydrogen bonding.

Table 5.6.4 shows the bond lengths and angles of the intermolecular hydrogen bonds found in the crystal structure. The first two lengths are reasonably short (between 1.5 – 2.2 Å)^[84] and so can be classified as moderate hydrogen bonds. However, the last two bond lengths exceeds 2.2 Å^[84] and so would be weak bonds.

Table 5.6.4: Intermolecular short contacts and hydrogen bond lengths (Å) and angles (°) for H₂L².

| D-H...A | D-H | H...A | D...A | D-H...A |
|--------------|----------|----------|----------|-----------|
| O4-H4...O1 | 0.927(2) | 1.618(2) | 2.545(1) | 178.61(2) |
| O2-H2...O3 | 0.934(2) | 1.705(2) | 2.605(2) | 160.60(2) |
| C22-H22...O1 | 0.950(1) | 2.554(1) | 3.211(2) | 126.46(9) |
| C12-H12...O4 | 0.950(2) | 2.566(1) | 3.438(2) | 152.68(1) |

5.6.3 Analysis of the X-ray Structure of [Cu₂(L¹)(OAc)(DMF)].DMF

[Cu₂(L¹)(OAc)(DMF)] crystallised in the monoclinic space group $P 2_1/n$. Each asymmetric unit comprises one [Cu₂(L¹)(OAc)(DMF)] molecule, with $Z = 4$. Shown below in **Figure 5.6.10** is the thermal ellipsoid plot of [Cu₂(L¹)(OAc)(DMF)].

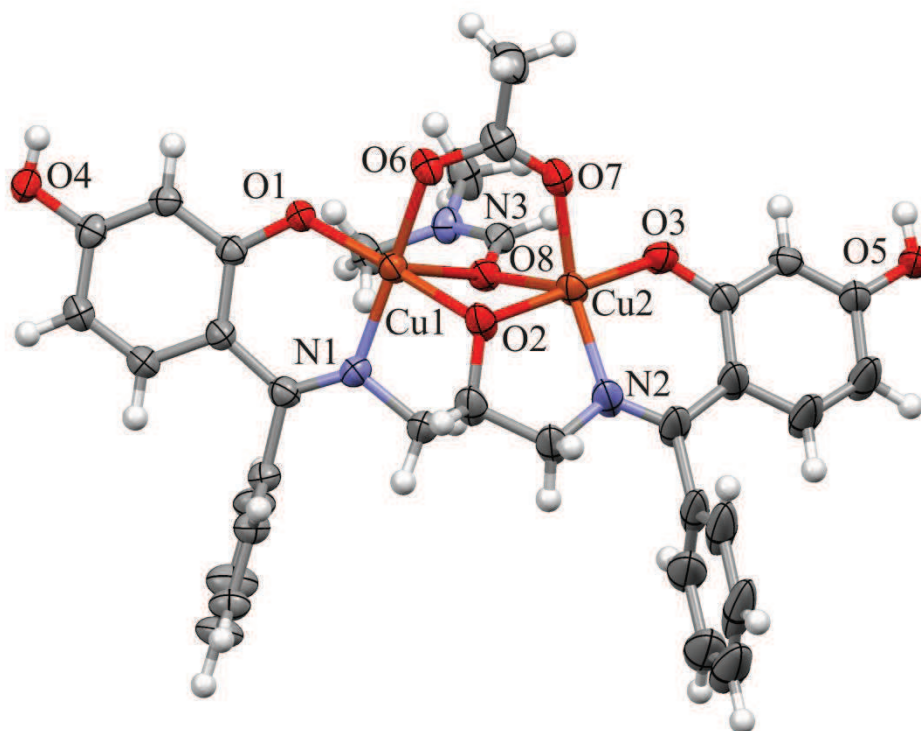


Figure 5.6.10: Partially labelled thermal ellipsoid plot of [Cu₂(L¹)(OAc)(DMF)]. Thermal ellipsoids are drawn at 50% probability, hydrogen atoms have been omitted for clarity. Solvent molecule removed by PLATON's SQUEEZE^[85].

Note that diffuse reflection data associated with disordered solvent was removed using PLATON's SQUEEZE^[85] algorithm. It is estimated that there is one DMF molecule in the asymmetric unit. The ligand has not coordinated the metal in the expected manner, forming a square planar coordination geometry. The hydroxyl group of the di(azomethine) linkage has bridged two copper(II) ions. Each of the two metals centres is coordinated to the ligand *via* the *ortho* phenolic oxygen and an imine nitrogen atom. The bridging hydroxyl group is deprotonated making a pentadentate trianionic ligand. Additionally the metal centres are bridged by an acetate ion. The acetate balances the charge on the complex, which is neutral overall. There is a coordinated DMF molecule bridging the two copper centres. The metal centres thus possess square pyramidal coordination geometry.

The unit cell is illustrated in **Figure 5.6.11** and shows that each of the four $[\text{Cu}_2(\text{L}^1)(\text{OAc})(\text{DMF})]$ molecules is situated on a general position. There are two short contacts within the unit cell. One involving the hydroxyl oxygen atom of one molecule, O4, and a hydrogen on the bridge, H9; and the other between a metal chelated oxygen, O6, and a phenyl ring hydrogen, H20.

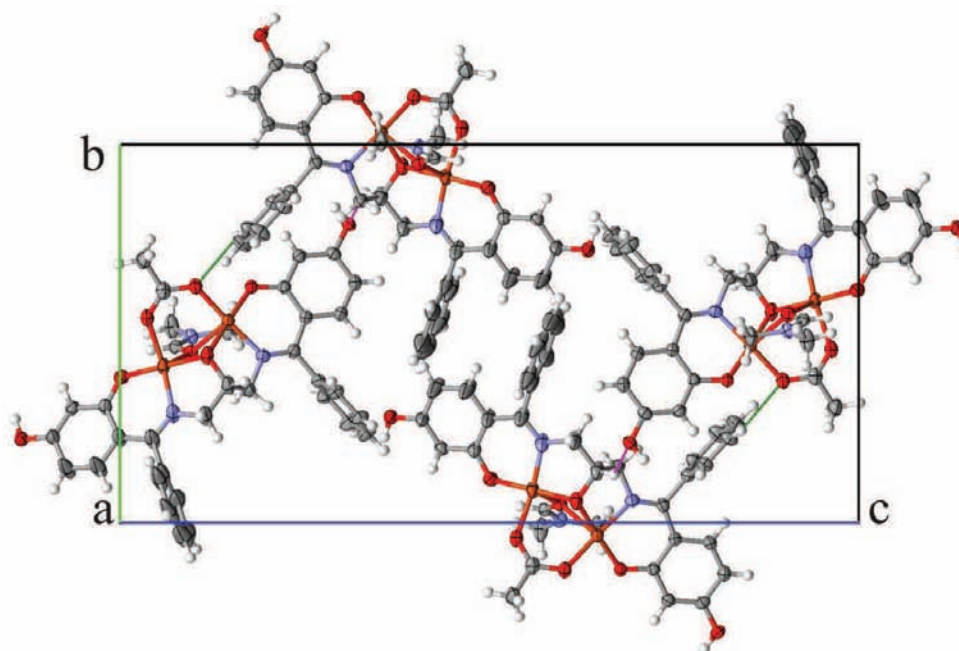


Figure 5.6.11: Packing in the unit cell of $[\text{Cu}_2(\text{L}^1)(\text{OAc})(\text{DMF})]$ as viewed along the *a*-axis.

As would be expected there are hydrogen bonds and short contacts present in the lattice. Each $[\text{Cu}_2(\text{L}^1)(\text{OAc})(\text{DMF})]$ molecule is hydrogen bonded to an adjacent $[\text{Cu}_2(\text{L}^1)(\text{OAc})(\text{DMF})]$ molecule via two hydrogen bonds. The two hydrogen bonds between the $[\text{Cu}_2(\text{L}^1)(\text{OAc})(\text{DMF})]$ molecules are the same, $\text{O5-H5}\cdots\text{O1}$. There are a further three short contacts between adjacent $[\text{Cu}_2(\text{L}^1)(\text{OAc})(\text{DMF})]$ molecules. One is from the oxygen on the same hydroxyl group that forms the hydrogen bond, O5, and a phenyl oxygen, H2. The other two are between an acetate oxygen, O7, and two hydrogens on the DMF molecule, H32 and H33B. This is shown in **Figure 5.6.12**.

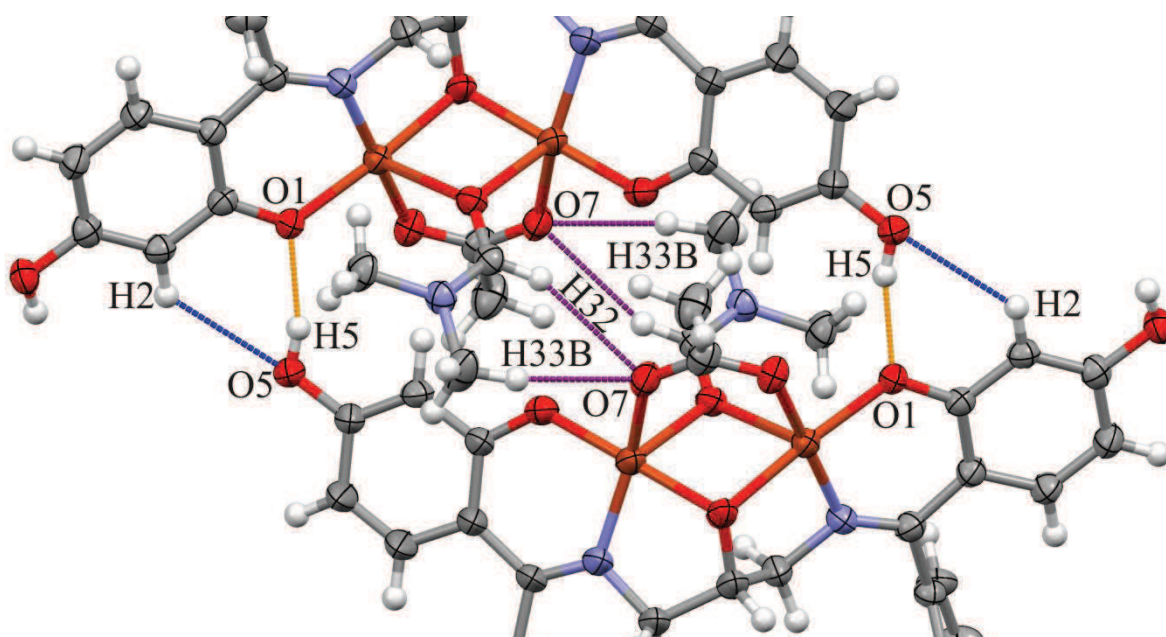


Figure 5.6.12: Hydrogen bonding present between complexes and solvent in $[\text{Cu}_2(\text{L}^1)(\text{OAc})(\text{DMF})]$.

All hydrogen bonds and short contacts are summarised in **Table 5.6.5**.

Table 5.6.5: Hydrogen bond and short contact lengths (Å) and angles (°) for [Cu₂(L¹)(OAc)(DMF)].

| D-H...A | D-H | H...A | D...A | D-H...A |
|---------------|----------|----------|----------|-----------|
| C2-H2...O5 | 0.949(3) | 2.602(2) | 3.312(4) | 131.94(2) |
| O5-H5...O1 | 0.839(3) | 1.906(2) | 2.724(3) | 164.58(2) |
| C33-H33B...O7 | 0.981(4) | 2.369(2) | 3.324(4) | 164.37(2) |
| C32-H32...O7 | 0.949(3) | 2.613(2) | 3.467(4) | 149.91(2) |
| C9-H9...O4 | 1.000(4) | 2.605(3) | 3.405(5) | 136.93(2) |
| C20-H20...O6 | 0.950(4) | 2.549(2) | 3.243(4) | 130.06(2) |
| C33-H33A...O2 | 0.980(4) | 2.378(3) | 3.349(5) | 170.55(2) |

The geometry around each copper(II) ion is square pyramidal. The bond lengths between copper and its coordinated elements are shown in **Table 5.6.6**. The bond angles between copper and its coordinated elements are shown in **Table 5.6.7**. The bond lengths and angles are all within the range of similar structures.^[15]

Table 5.6.6: Table of coordination bond lengths for [Cu₂(L¹)(OAc)(DMF)].

| Bond | Length (Å) | Bond | Length (Å) |
|--------|------------|--------|------------|
| Cu1-N1 | 1.939(3) | Cu2-N2 | 1.948(3) |
| Cu1-O1 | 1.902(2) | Cu2-O3 | 1.875(2) |
| Cu1-O2 | 1.936(3) | Cu2-O2 | 1.939(2) |
| Cu1-O6 | 1.938(2) | Cu2-O7 | 2.000(3) |
| Cu1-O8 | 2.513(3) | Cu2-O8 | 2.295(3) |

The bond lengths are similar, with the exception of the bonds to the acetate and DMF molecules. This is to be expected as the distance between the copper ions sharing these bridging molecules would place restrictions on the bond lengths.

Table 5.6.7: Table of coordination bond angles in [Cu₂(L¹)(OAc)(DMF)].

| Bond Angle | Angle (°) | Bond Angle | Angle (°) |
|------------|-----------|------------|-----------|
| N1-Cu1-O2 | 86.04(1) | N2-Cu2-O2 | 85.41(1) |
| N1-Cu1-O1 | 93.36(1) | N2-Cu2-O3 | 94.20(1) |
| O2-Cu1-O6 | 91.94(1) | O2-Cu2-O7 | 90.44(1) |
| O1-Cu1-O6 | 88.09(1) | O3-Cu2-O7 | 89.84(1) |
| N1-Cu1-O8 | 87.23(1) | N2-Cu2-O8 | 111.83(1) |
| O1-Cu1-O8 | 105.42(9) | O3-Cu2-O8 | 94.81(1) |
| O2-Cu1-O8 | 79.73(9) | O2-Cu2-O8 | 85.49(1) |
| O6-Cu1-O8 | 98.55(9) | O7-Cu2-O8 | 93.18(1) |

The bond angles are slightly distorted from the typical square pyramidal angles of 90°^[86]. This could possibly be attributed to the constraints put on the bonds as each copper(II) ion forms a five membered ring with the bridging oxygen as well as a six membered ring with the other coordinated nitrogen and oxygen from the ligand.

5.6.4 Analysis of the X-ray Structure of [Cu₃(L²)₂Cl₂(DMF)₂].5H₂O.DMF

[Cu₃(L²)₂Cl₂(DMF)₂] crystallised in the triclinic space group of *P*-1. Each asymmetric unit comprises two half [Cu₃(L²)₂Cl₂(DMF)₂] molecules, giving *Z* = 2. Shown below in **Figure 5.6.13** is the thermal ellipsoid plot of [Cu₃(L²)₂Cl₂(DMF)₂]. PLATON's SQUEEZE algorithm was used to remove diffuse reflection data associated with the disordered solvent molecules; one DMF and five water molecules are estimated to be present in the asymmetric unit.

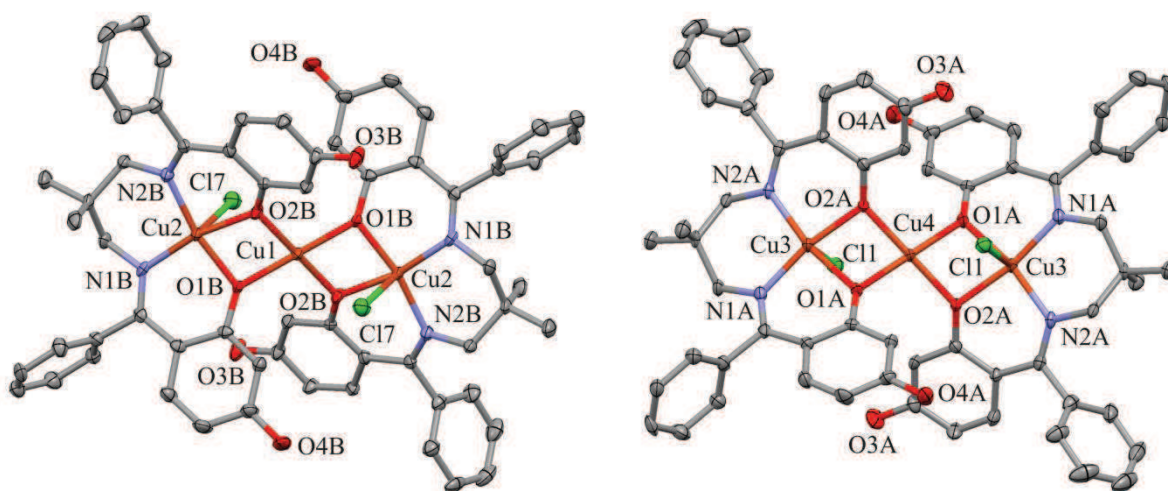


Figure 5.6.13: Partially labelled thermal ellipsoid plot of $[\text{Cu}_3(\text{L}^2)_2\text{Cl}_2(\text{DMF})_2]$. Thermal ellipsoids are drawn at 50% probability, hydrogen atoms and co-crystallised solvent molecules have been omitted for clarity.

Each ligand has coordinated a copper(II) ion. The metal centre is coordinated to the ligand *via* the *ortho* phenolic oxygen atoms and imine nitrogen atoms, thus forming a tetradentate dianionic ligand. However, two of these metal chelates are bridged by a copper(II) ion to form one metal chelate molecule. Each ligand-chelated metal has a chloride ion bound to it thus balancing the charge created by the bridging copper(II) ion and so allowing for an overall neutral molecule. The coordination geometry of the bridging copper(II) ion is square planar as it is chelated *via* the four *ortho* phenolic oxygens of the two ligands. The ligand-chelated copper ions have distorted square pyramidal geometries.

The unit cell is illustrated in **Figure 5.6.14** and shows that each general position is comprised of two half $[\text{Cu}_3(\text{L}^2)_2\text{Cl}_2(\text{DMF})_2]$ molecules which are related by inversion symmetry. There is one short contact present in the unit cell between the *meta* hydroxyl oxygen atom, O3A, and a hydrogen atom on a nearby dihydroxy ring of an adjacent molecule.

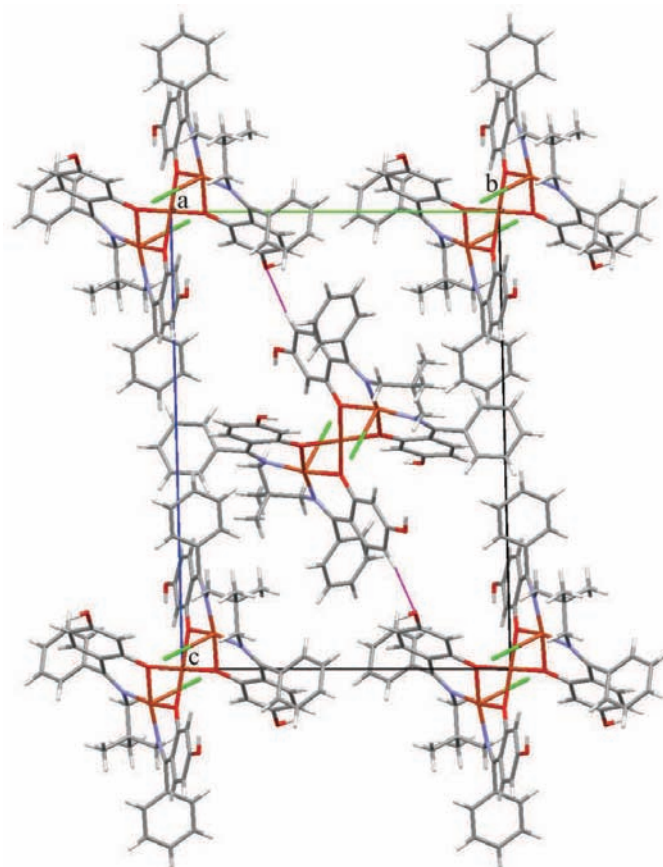


Figure 5.6.14: Packing in the unit cell of $[\text{Cu}_3(\text{L}^2)_2\text{Cl}_2(\text{DMF})_2]$ viewed along the *a*-axis.

There is only one other short contact in the lattice of $[\text{Cu}_3(\text{L}^2)_2\text{Cl}_2(\text{DMF})_2]$ and no hydrogen bonds present. The contact is between the hydroxyl oxygen atom, O3B, and a hydrogen atom on an adjacent molecules benzene ring. **Table 5.6.8** details the data of the short contacts.

Table 5.6.8: Short contact lengths (Å) and angle (°) for $[\text{Cu}_3(\text{L}^2)_2\text{Cl}_2(\text{DMF})_2]$.

| D-H...A | D-H | H...A | D...A | D-H...A |
|-----------------|----------|----------|----------|-----------|
| C4B-H4BA...O3A | 0.948(4) | 2.616(3) | 3.466(6) | 149.33(3) |
| C23B-H23B...O3B | 0.950(5) | 2.685(3) | 3.418(6) | 134.49(3) |

The bond lengths and bond angles of $[\text{Cu}_3(\text{L}^2)_2\text{Cl}_2(\text{DMF})_2]$ A and $[\text{Cu}_3(\text{L}^2)_2\text{Cl}_2(\text{DMF})_2]$ B involving the metal ions and their coordinated elements have been averaged and are shown in **Table 5.6.9** and **Table 5.6.10**, respectively.

Table 5.6.9: Table of average coordination bond lengths in $[\text{Cu}_3(\text{L}^2)_2\text{Cl}_2(\text{DMF})_2]$.

| Bond | Length (Å) |
|--------------------------|------------|
| N-Cu | 1.961(4) |
| O-Cu | 1.944(3) |
| Cl-Cu | 2.910(1) |
| O-Cu _{bridging} | 1.937(3) |

The bond lengths of the coordinated ligand atoms are fairly similar in length and relatively short which indicates a fairly strongly bound metal. The axial chloride ions have longer Cu-Cl bond lengths than bonds to the other donor atoms, which may be due to steric hindrance around the copper consistent with the larger ionic radius of chlorine relative to nitrogen or oxygen. The bond angles are distorted from the typical square pyramidal geometry (90°) which is attributed to the steric constraints within the six-membered ring formed around the ligand coordinated copper ion. The bridging copper ion's bond angles are also distorted from the typical square planar geometry. This phenomenon would be caused by the distortions in the geometries of Cu1 and Cu3. The bond lengths and angles are all within the range of similar structures.^[74, 86]

Table 5.6.10: Table of average coordination bond angles in $[\text{Cu}_3(\text{L}^2)_2\text{Cl}_2(\text{DMF})_2]$.

| Bond Angle | Angle (°) |
|--|-----------|
| N-Cu-N | 100.94(1) |
| N-Cu-O | 90.49(1) |
| O-Cu-O | 78.08(1) |
| O1-Cu _{bridging} -O2 _{int} | 78.43(1) |
| O1-Cu _{bridging} -O2 _{ext} | 101.57(1) |
| Cl-Cu-X* | 88.81(4) |

*X = O1, O2, N1 and N2 in $[\text{Cu}_3(\text{L}^2)_2\text{Cl}_2(\text{DMF})_2]$ A and B.

5.6.5 Analysis of the X-ray Structure of $[\text{Ni}(\text{L}^2)].4\text{H}_2\text{O}.\text{DMF}$

$[\text{Ni}(\text{L}^2)]$ crystallised in the monoclinic space group $P 2_1/c$. Each asymmetric unit comprises two independent $[\text{Ni}(\text{L}^2)]$ molecules, making $Z = 8$. Shown below in **Figure 5.6.15** is the thermal ellipsoid plot of $[\text{Ni}(\text{L}^2)]$.

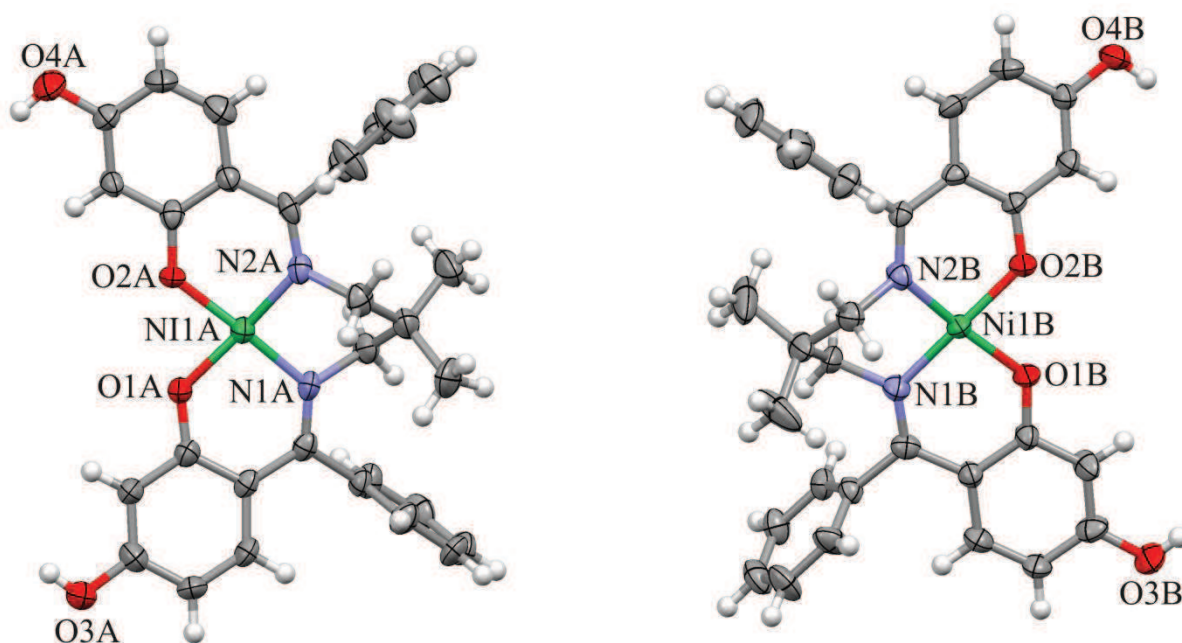


Figure 5.6.15: Partially labelled thermal ellipsoid plot of $[\text{Ni}(\text{L}^2)]$. Thermal ellipsoids are drawn at 50% probability, hydrogen atoms and solvent molecules have been omitted for clarity. Solvent molecules were removed by PLATON's SQUEEZE^[85].

There are two independent molecules in the asymmetric unit labelled A and B. Note that PLATON's SQUEEZE^[85] algorithm was used to remove diffuse reflection data associated with the disordered solvent molecules; one DMF and four H_2O molecules are estimated to be present in the asymmetric unit. The ligand chelates the metal forming a square planar coordination geometry with no axial ligands. The nickel(II) ion is coordinated to the ligand *via* the imine nitrogen atoms and the *ortho* phenolic oxygen atoms. The deprotonation of the *ortho* hydroxyl groups creates a tetradentate dianionic ligand. The molecule is neutral overall when coordinated to the nickel(II) ion.

The unit cell is illustrated in **Figure 5.6.16**. There is one short contact in the unit cell between adjacent $[\text{Ni}(\text{L}^2)]$ molecules. This complex shows no hydrogen bonding present in the crystal lattice in the solvent-free model illustrated above. In the solvated model, even though the solvent molecules were disordered, intermolecular hydrogen-bonds were evident. A water molecule formed a bifurcated hydrogen-bond with the oxygen donor atoms of a $[\text{Ni}(\text{L}^2)]$. In this unsolvated model, the hydroxyl group oxygen, O4A, forms a short contact with a close proximity phenyl hydrogen, H4AA.

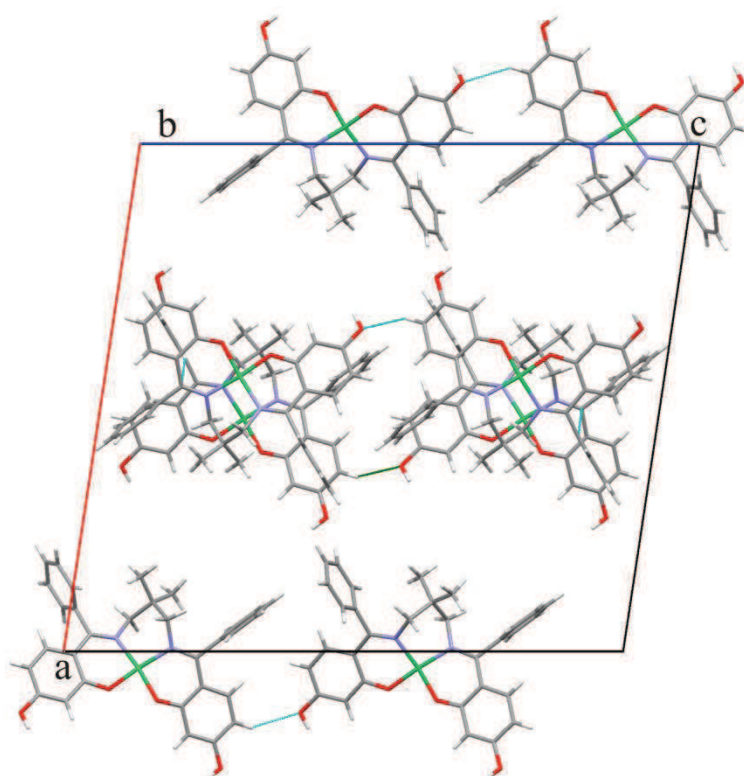


Figure 5.6.16: Packing in the unit cell of $[\text{Ni}(\text{L}^2)]$ as viewed down the b -axis. Disordered solvent molecules have been omitted for clarity in the diagram and in the final structure model.

The crystal lattice is supported by four short contacts between adjacent $[\text{Ni}(\text{L}^2)]$ molecules. Molecule B only has one short contact which links adjacent B molecules together. The other short contacts connect one $[\text{Ni}(\text{L}^2)]$ A to three other $[\text{Ni}(\text{L}^2)]$ A molecules. Shown in **Figure 5.6.17** are all the short contacts present. The contacts mentioned occur between the uncoordinated hydroxyl oxygen, O4A, on one $[\text{Ni}(\text{L}^2)]$ A molecule and nearby $[\text{Ni}(\text{L}^2)]$ A

hydrogen, H4AA, on the dihydroxyl ring; as well as between the uncoordinated hydroxyl oxygen, O3B, on one $[\text{Ni}(\text{L}^2)]$ B molecule and nearby $[\text{Ni}(\text{L}^2)]$ B hydrogen, H28B, on the dihydroxyl ring; as well as between the hydroxyl oxygen of $[\text{Ni}(\text{L}^2)]$ A, O4A, and another benzene ring hydrogen, H21A, and finally between the coordinated oxygen, O2A, on a $[\text{Ni}(\text{L}^2)]$ A molecule and a hydrogen atom, H24A, on a nearby benzene ring of an adjacent $[\text{Ni}(\text{L}^2)]$ molecule.

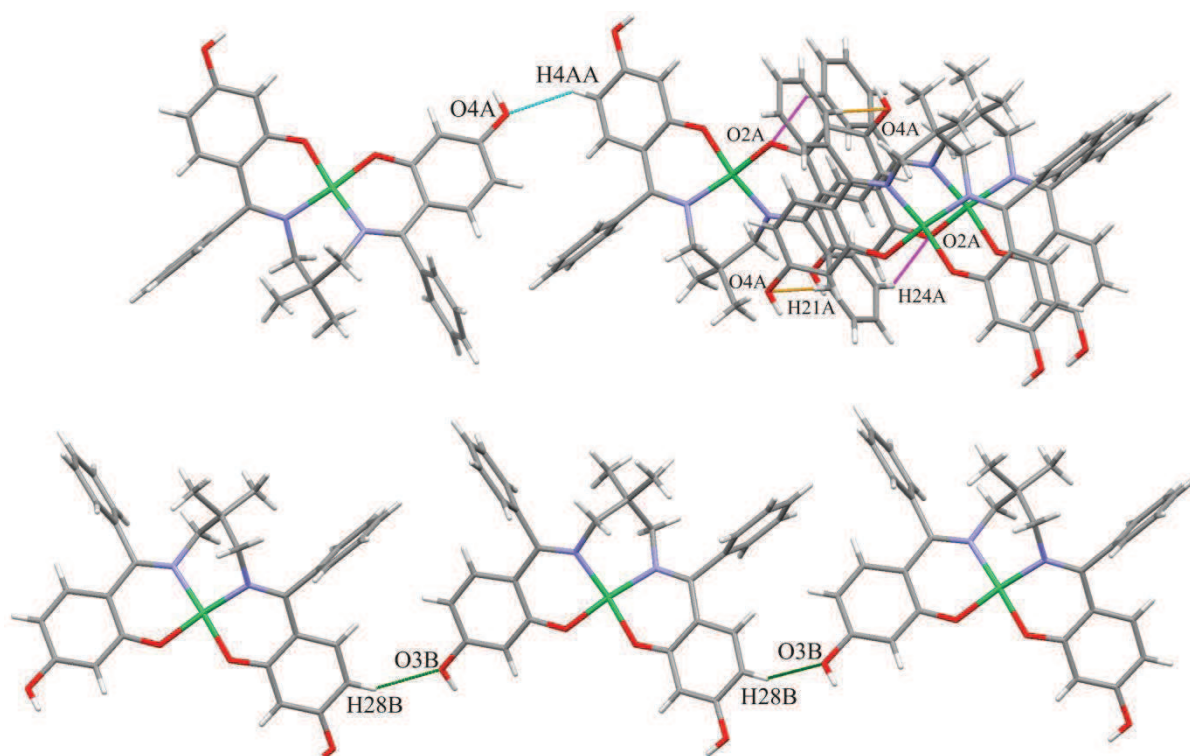


Figure 5.6.17: Short contacts present between $[\text{Ni}(\text{L}^2)]$ molecules.

Table 5.6.11 summarises the bond lengths and angles of all short contacts mentioned above.

Table 5.6.11: Short contact lengths (\AA) and angles ($^\circ$) for $[\text{Ni}(\text{L}^2)]$.

| D-H...A | D-H | H...A | D...A | D-H...A |
|-----------------|----------|----------|----------|-----------|
| C4A-H4AA...O4A | 0.931(5) | 2.512(3) | 3.310(6) | 143.93(3) |
| C24A-H24A...O2A | 0.930(6) | 2.559(3) | 3.342(6) | 142.07(3) |
| C21A-H21A...O4A | 0.930(5) | 2.516(4) | 3.442(6) | 174.21(3) |
| C28B-H28B...O3B | 0.930(5) | 2.486(3) | 3.328(6) | 150.77(3) |

The geometry around the nickel(II) ions is square planar, as would be expected from a tetradentate ligand. The average lengths of each bond between the nickel atom and its coordinated elements are shown in **Table 5.6.12**. The average angles of the separate nickel atoms and their coordinated elements are shown in **Table 5.6.13**.

Table 5.6.12: Table of average coordination bond lengths in $[\text{Ni}(\text{L}^2)]$.

| Bond | Length (Å) |
|-------|------------|
| N1-Ni | 1.906(4) |
| N2-Ni | 1.894(4) |
| O2-Ni | 1.841(3) |
| O3-Ni | 1.844(3) |

Short bond lengths are indicative of a fairly strongly bound metal. The bond angles are slightly distorted from the typical square planar geometry which could be attributed to the six membered chelate rings of the complex. The bond lengths and angles are all within the range reported for similar structures.^[75, 86]

Table 5.6.13: Table of average coordination bond angles for $[\text{Ni}(\text{L}^2)]$.

| Bond Angle | Angle (°) |
|------------|-----------|
| N1-Ni-N2 | 94.75(2) |
| N1-Ni-O1 | 92.03(1) |
| N2-Ni-O2 | 91.87(1) |
| O1-Ni-O2 | 83.09(1) |

5.6.6 Analysis of the X-ray Structure of $[\text{Cu}_3(\text{L}^3)_2(\text{H}_2\text{O})_2]\text{Cl}_2$

$[\text{Cu}_3(\text{L}^3)_2(\text{H}_2\text{O})_2]\text{Cl}_2$ crystallised in the monoclinic space group of $P 2_1/c$. Each asymmetric unit comprises half a $[\text{Cu}_3(\text{L}^3)_2(\text{H}_2\text{O})_2]\text{Cl}_2$ molecule and one chloride ion, giving $Z = 4$. Shown below in **Figure 5.6.18** is the thermal ellipsoid plot of $[\text{Cu}_3(\text{L}^3)_2(\text{H}_2\text{O})_2]\text{Cl}_2$.

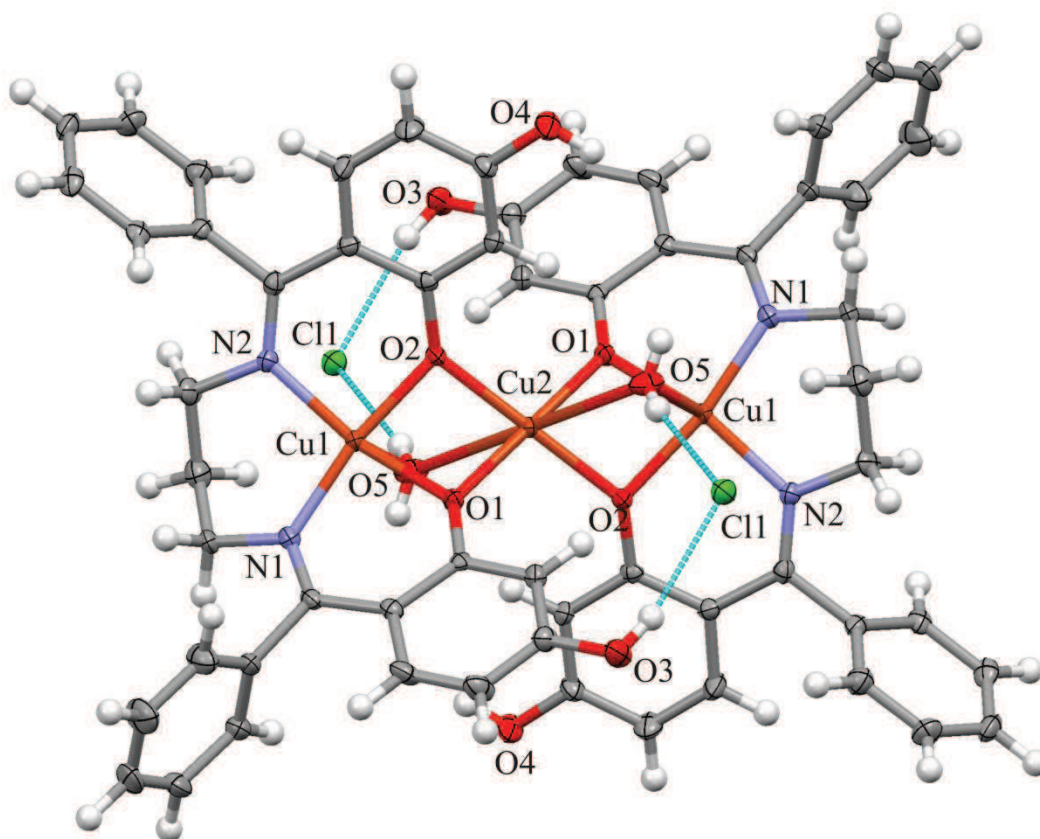


Figure 5.6.18: Partially labelled thermal ellipsoid plot of $[\text{Cu}_3(\text{L}^3)_2(\text{H}_2\text{O})_2]\text{Cl}_2$. Thermal ellipsoids are drawn at 50% probability.

Each ligand has coordinated a copper(II) ion *via* the *ortho* phenolic oxygen atoms and imine nitrogen atoms, thus forming a tetradentate dianionic ligand. Two of these copper(II) chelates are bridged by a copper(II) ion to form a trinuclear $[\text{Cu}_3(\text{L}^3)_2(\text{H}_2\text{O})_2]\text{Cl}_2$ molecule. The ligand-chelated copper(II) ion is further bridged to the bridging copper(II) ion by a water molecule. There is also a chloride ion that is hydrogen-bonded to the hydrogen on the *ortho* phenolic oxygen atom and a hydrogen on one of the bridging water molecules. The coordination geometry of the bridging copper(II) ion is square planar as it is chelated *via* the four *ortho* phenolic oxygens of the two ligands.

The unit cell is illustrated in **Figure 5.6.19**. The only hydrogen bonding in the unit cell is between the chloride ions and the *ortho* phenolic oxygen atom and a hydrogen atom on one of the bridging water molecules.

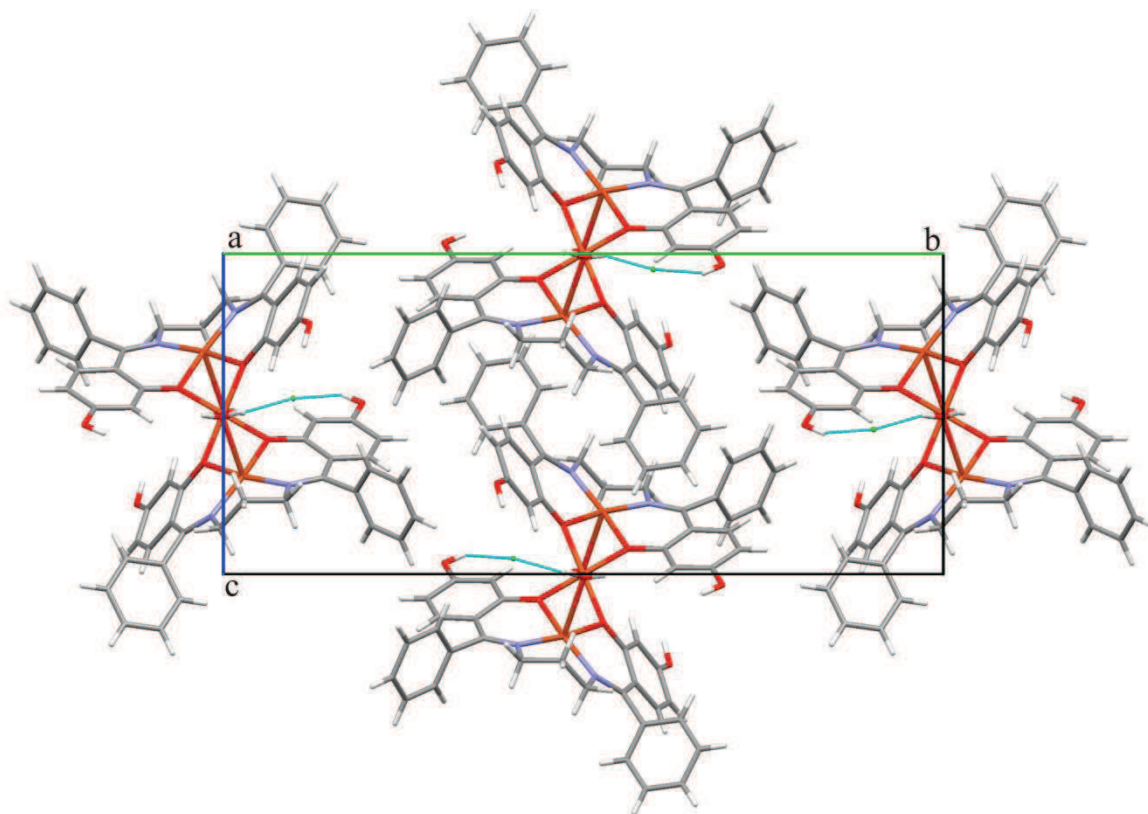


Figure 5.6.19: Packing in the unit cell of $[\text{Cu}_3(\text{L}^3)_2(\text{H}_2\text{O})_2]\text{Cl}_2$ viewed along the a -axis.

As can be seen in **Figure 5.6.20** the only hydrogen bonding in the lattice is by the chloride ions. The hydrogen bonding links adjacent $[\text{Cu}_3(\text{L}^3)_2(\text{H}_2\text{O})_2]\text{Cl}_2$ molecules.

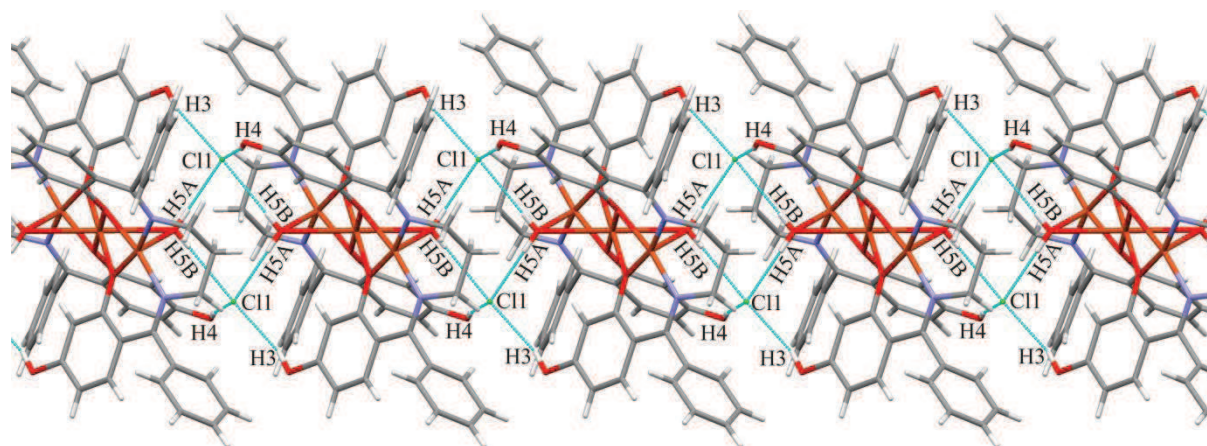


Figure 5.6.20: Hydrogen bonding in the lattice of $[\text{Cu}_3(\text{L}^3)_2(\text{H}_2\text{O})_2]\text{Cl}_2$.

There is one short contact present in the lattice between C11 and H23 on the phenyl ring. This short contact and the hydrogen bonds of $[\text{Cu}_3(\text{L}^3)_2(\text{H}_2\text{O})_2]\text{Cl}_2$ are shown in **Figure 5.6.21**. **Table 5.6.14** is a summary of the bond lengths and angles of the hydrogen bonds and the short contact mentioned.

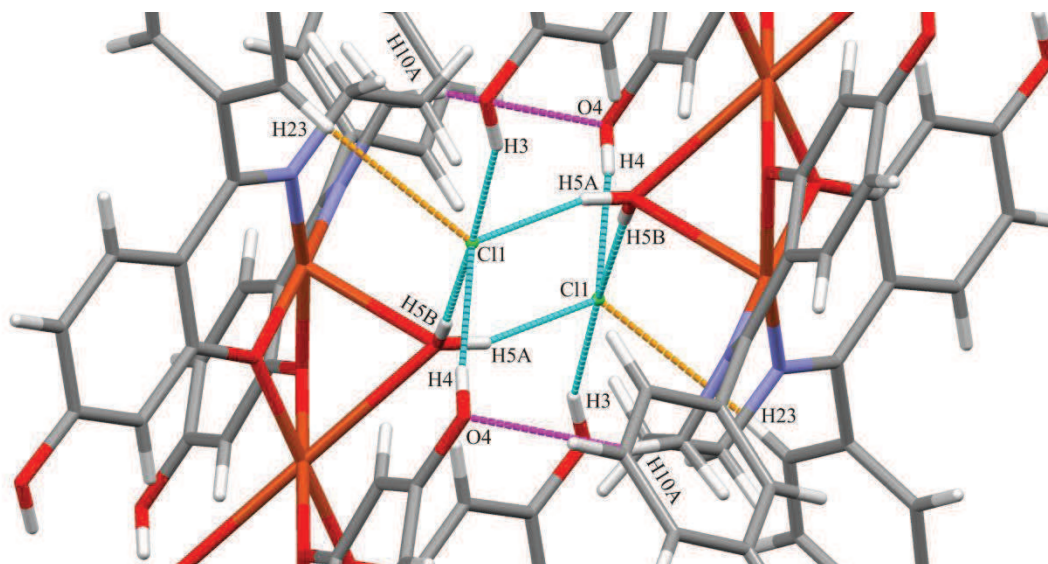


Figure 5.6.21: Short contact and hydrogen bonds in the lattice of $[\text{Cu}_3(\text{L}^3)_2(\text{H}_2\text{O})_2]\text{Cl}_2$.

Table 5.6.14: Hydrogen bonds and short contact lengths (Å) and angles (°) for $[\text{Cu}_3(\text{L}^3)_2(\text{H}_2\text{O})_2]\text{Cl}_2$.

| D-H...A | D-H | H...A | D...A | D-H...A |
|---------------|----------|----------|----------|-----------|
| C10-H10A...O4 | 0.989(4) | 2.652(3) | 3.570(5) | 154.41(2) |
| O4-H4...C11 | 0.840(4) | 2.194(1) | 3.025(4) | 169.84(2) |
| C23-H23...C11 | 0.951(3) | 2.883(8) | 3.727(3) | 148.41(2) |
| O5-H5B...C11 | 0.740(4) | 2.520(4) | 3.258(3) | 176.45(5) |
| O3-H3...C11 | 0.841(3) | 2.403(8) | 3.183(3) | 154.60(2) |
| O5-H5A...C11 | 0.810(4) | 2.280(5) | 3.059(3) | 161.69(4) |

All the copper(II) centres adopted a square planar geometry. The bond lengths of $[\text{Cu}_3(\text{L}^3)_2(\text{H}_2\text{O})_2]\text{Cl}_2$ involving the metal ions and their coordinated elements have been

averaged and are shown in **Table 5.6.15**. The bond angles of $[\text{Cu}_3(\text{L}^3)_2(\text{H}_2\text{O})_2]\text{Cl}_2$ are shown in **Table 5.6.16**.

Table 5.6.15: Table of coordination bond lengths in $[\text{Cu}_3(\text{L}^3)_2(\text{H}_2\text{O})_2]\text{Cl}_2$.

| Bond | Length (Å) | Bond | Length (Å) |
|--------|------------|--------|------------|
| N1-Cu1 | 1.951(3) | O5-Cu1 | 2.410(3) |
| N2-Cu1 | 1.966(3) | O1-Cu2 | 1.936(2) |
| O1-Cu1 | 1.942(3) | O2-Cu2 | 1.960(2) |
| O2-Cu1 | 1.946(3) | O5-Cu2 | 2.695(3) |

The metal-to-ligand bond lengths involving the different ligand donor atoms are fairly similar in length and relatively short, which indicates a fairly strongly-bound metal. The Cu-O bond lengths to the coordinated water molecule are quite long and would suggest it is weakly bound, consistent with its bridging role in the structure. The bond angles are distorted from those typical of a square planar ion, which is attributed to the six membered ring formed around the ligand-bound copper(II) ions. The bridging copper ions bond angles are also distorted from the typical square planar geometry. This phenomenon would be caused by the distortions in the geometries of Cu1. The bond lengths and angles are all within the range of similar structures.^[74, 86]

Table 5.6.16: Table of coordination bond angles in $[\text{Cu}_3(\text{L}^3)_2(\text{H}_2\text{O})_2]\text{Cl}_2$.

| Bond Angle | Angle (°) |
|------------------------|-----------|
| N1-Cu1-N2 | 99.82(1) |
| N2-Cu1-O2 | 90.44(1) |
| O1-Cu1-O2 | 78.57(1) |
| O1-Cu1-N1 | 90.79(1) |
| O1-Cu ₂ -O2 | 78.40(1) |
| Cu1-O5-Cu2 | 69.40(8) |

5.6.7 Analysis of the X-ray Structure of $[\text{Ni}(\text{L}^3)].2\text{H}_2\text{O}$

$[\text{Ni}(\text{L}^3)]$ crystallised in the monoclinic space group of $C 2/c$. Each asymmetric unit comprises one $[\text{Ni}(\text{L}^3)]$ molecule and two water molecules with $Z = 8$. Shown below in **Figure 5.6.22** is the thermal ellipsoid plot of $[\text{Ni}(\text{L}^3)]$.

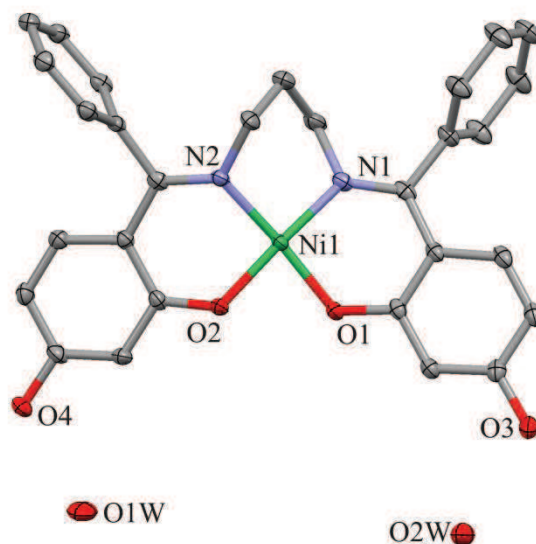


Figure 5.6.22: Partially labelled thermal ellipsoid plot of $[\text{Ni}(\text{L}^3)]$. Thermal ellipsoids are drawn at 50% probability, hydrogen atoms have been omitted for clarity.

The ligand coordinated the metal forming a nominally square planar coordination geometry with no axial ligands present. The nickel(II) ion is coordinated to the ligand *via* the imine nitrogen atoms and the *ortho* phenolic oxygen atoms. The deprotonation of the *ortho* hydroxyl groups creates a tetradentate dianionic ligand.

The unit cell is illustrated in **Figure 5.6.23**. There is hydrogen bonding in the unit cell between the $[\text{Ni}(\text{L}^3)]$ molecules and water; this is also shown in the unit cell diagram.

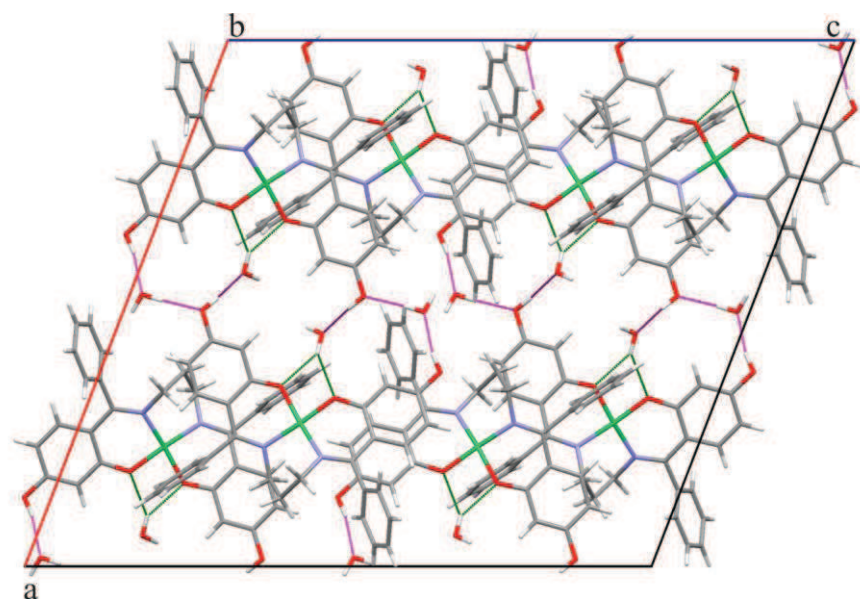


Figure 5.6.23: Packing in the unit cell of $[\text{Ni}(\text{L}^3)]$ viewed along the b -axis.

The structure is solvated by two water molecules for every $[\text{Ni}(\text{L}^3)]$ molecule. The crystal lattice is supported by hydrogen bonds between the $[\text{Ni}(\text{L}^3)]$ molecules and the water molecules and short contacts between the complex molecules themselves. There are four water molecules shared between two $[\text{Ni}(\text{L}^3)]$ molecules. An interesting feature to note is the bifurcated hydrogen bond that forms between the hydrogen on a water molecule, H1WB, and both metal chelated oxygen atoms, O1 and O2. The hydrogen bonding is shown in **Figure 5.6.24**.

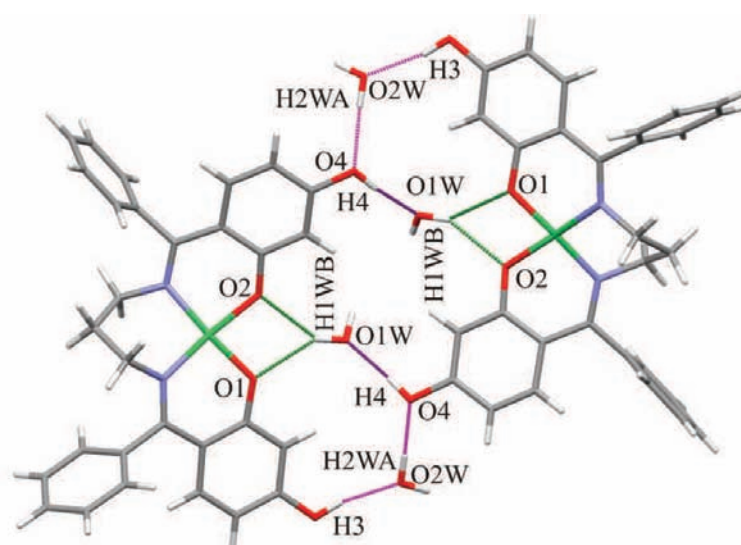


Figure 5.6.24: Hydrogen bonding in the crystal lattice of $[\text{Ni}(\text{L}^3)]$.

There are short contacts present between the O3 free hydroxyl group and the hydrogens in close proximity to it and one short contact between each coordinated oxygen, O1 and O2, and a hydrogen atom of a benzene ring of an adjacent molecule, H26 and H28, respectively. These short contacts are shown below in **Figure 5.6.25**.

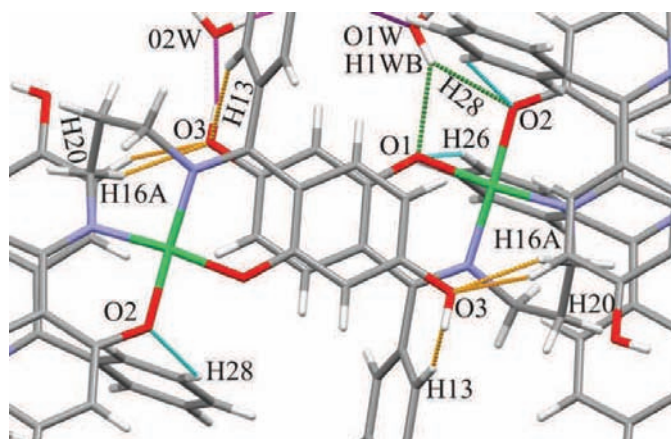


Figure 5.6.25: Short contacts present in the crystal lattice of $[\text{Ni}(\text{L}^3)]$.

The hydrogen bonds and short contacts mentioned have been tabulated with the associated bond lengths and angles in **Table 5.6.17**.

Table 5.6.17: Hydrogen bond and short contact lengths (Å) and angles (°) for $[\text{Ni}(\text{L}^3)]$.

| D-H...A | D-H | H...A | D...A | D-H...A |
|---------------|----------|----------|----------|-----------|
| C26-H26...O1 | 0.950(2) | 2.607(1) | 3.481(2) | 153.01(1) |
| C28-H28...O2 | 0.949(2) | 2.602(1) | 3.238(2) | 124.72(1) |
| C20-H20...O3 | 0.951(2) | 2.483(2) | 3.246(3) | 137.18(1) |
| C16-H16A...O3 | 0.990(2) | 2.582(1) | 3.518(2) | 157.55(1) |
| C13-H13...O3 | 0.950(2) | 2.519(1) | 3.422(2) | 158.79(1) |
| O4-H4...O1W | 0.840(2) | 1.739(2) | 2.575(3) | 174.20(1) |
| O1W-H1WB...O1 | 0.864(2) | 2.176(2) | 2.930(2) | 145.52(3) |
| O1W-H1WB...O2 | 0.864(2) | 2.149(3) | 2.905(2) | 145.86(3) |
| O3-H3...O2W | 0.839(1) | 1.869(2) | 2.692(2) | 166.70(1) |
| O2W-H2WA...O4 | 0.848(2) | 1.911(2) | 2.755(2) | 172.61(3) |

The geometry around the nickel ion is square planar as would be expected from a tetradentate ligand. The bond lengths and bond angles between the nickel ion and its coordinated elements are listed in **Table 5.6.18**.

Table 5.6.18: Table of coordination bond lengths and bond angles in [Ni(L³)].

| Bond | Length (Å) | Bond Angle | Angle (°) |
|-------|------------|------------|-----------|
| N1-Ni | 1.883(1) | N1-Ni-N2 | 92.73(7) |
| N2-Ni | 1.883(2) | N1-Ni-O1 | 93.28(6) |
| O1-Ni | 1.834(2) | N2-Ni-O2 | 92.37(6) |
| O2-Ni | 1.848(1) | O1-Ni-O2 | 82.71(6) |

The bond lengths are very similar in magnitude. They are short, consistent with a strongly bound nickel(II) ion. The bond angles are slightly distorted from the typical square planar geometry which could be attributed to the six membered chelation ring and mixed donor atom set. The bond lengths and angles are all within the range of similar structures.^[75, 86]

5.6.8 Analysis of the X-ray Structure of [Zn₂(L³)₂].5DMF

[Zn₂(L³)₂] crystallised in the orthorhombic space group *Pna*2₁. Each asymmetric unit comprises one [Zn₂(L³)₂] molecule with *Z* = 12. Shown below in **Figure 5.6.26** is the thermal ellipsoid plot of [Zn₂(L³)₂]. PLATON's SQUEEZE^[85] algorithm was used to remove diffuse reflection data associated with the disordered solvent molecules; five DMF molecules are estimated to be present in the asymmetric unit. Disordered solvent molecules have been omitted for clarity.

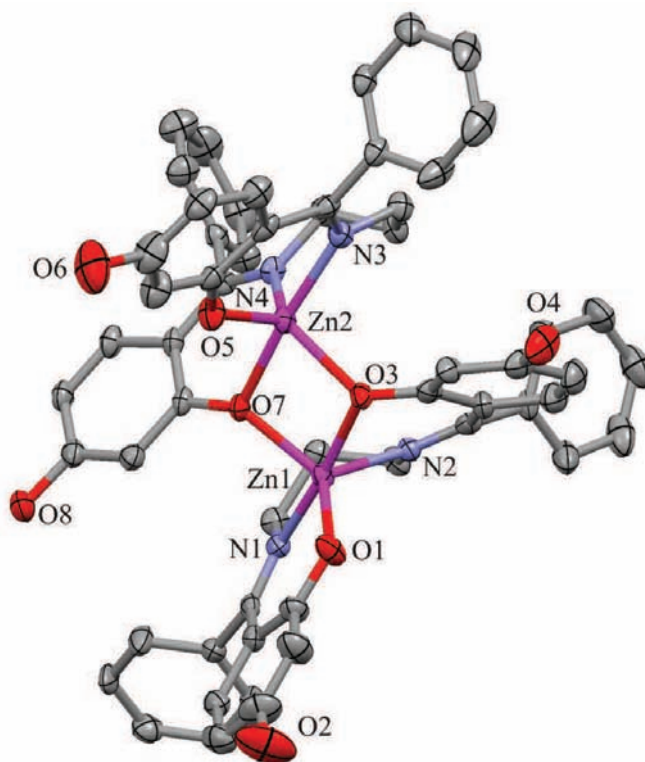


Figure 5.6.26: Partially labelled thermal ellipsoid plot of $[\text{Zn}_2(\text{L}^3)_2]$. Thermal ellipsoids are drawn at 50% probability, hydrogen atoms have been omitted for clarity.

The ligand coordinated the metal in the expected trigonal bipyramidal coordination geometry, however the metal complex then formed a dimer by coordination of the zinc atom to one *ortho* phenolic oxygen of the alternative chelate. The zinc(II) ion is coordinated to the ligand *via* the imine nitrogen atoms and the *ortho* phenolic oxygen atoms. The deprotonation of the *ortho* hydroxyl groups creates a tetradentate dianionic ligand. The molecule is neutral overall, with the zinc(II) ions coordinated balancing the charge of the ligands.

There are no hydrogen bonds present in the lattice of $[\text{Zn}_2(\text{L}^3)_2]$. This is because the final structure model had disordered solvent (DMF) removed using PLATON's SQUEEZE algorithm) and the solvent molecules ordinarily would hydrogen-bond to the phenolic hydrogen bond donors/acceptors in the molecule. There are, however, two short contacts that occur which results in one $[\text{Zn}_2(\text{L}^3)_2]$ molecule being connected to two adjacent $[\text{Zn}_2(\text{L}^3)_2]$

molecules. This is shown in **Figure 5.6.27**. The short contacts mentioned are tabulated with the associated bond lengths and angles in **Table 5.6.19**.

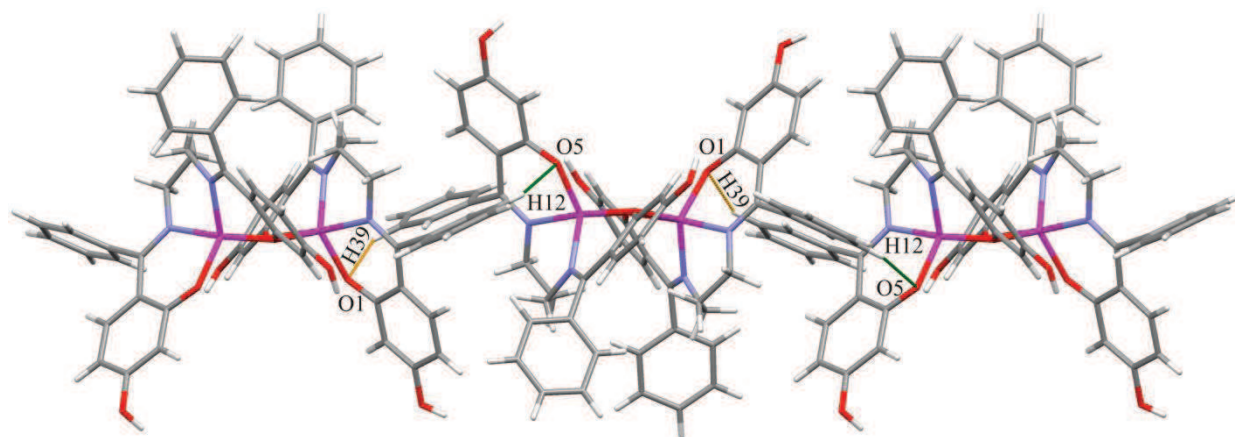


Figure 5.6.27: Short contacts present in the lattice of $[\text{Zn}_2(\text{L}^3)_2]$.

Table 5.6.19: Short contact lengths (Å) and angles (°) for $[\text{Zn}_2(\text{L}^3)_2]$.

| D-H...A | D-H | H...A | D...A | D-H...A |
|--------------|----------|----------|----------|-----------|
| C12-H12...O5 | 0.949(4) | 2.553(3) | 3.341(5) | 140.63(3) |
| C39-H39...O1 | 0.950(5) | 2.547(3) | 3.283(6) | 134.41(3) |

The geometry around the zinc(II) ions in the dinuclear structure is trigonal bipyramidal. The bond lengths of each zinc atom and its coordinated elements are shown in **Table 5.6.20**. The bond angles of the separate zinc atoms and their coordinated elements are given in **Table 5.6.21**.

Table 5.6.20: Table of coordination bond lengths in $[\text{Zn}_2(\text{L}^3)_2]$.

| Bond | Length (Å) | Bond | Length (Å) |
|--------|------------|--------|------------|
| N1-Zn1 | 2.073(3) | N3-Zn2 | 2.096(3) |
| N2-Zn1 | 2.077(3) | N4-Zn2 | 2.054(3) |
| O1-Zn1 | 1.927(3) | O5-Zn2 | 1.921(3) |
| O3-Zn1 | 2.084(3) | O7-Zn2 | 2.081(3) |

The bond distances between Zn1, N1, N2, and O3; and Zn2, N3, N4, O3 and O7 despite the difference in donor atom type and consistent with similar zinc(II) structures in literature.^[87-88] These bond lengths are above 2 Å, which would indicate a fairly weakly bound metal ion. This is implied by the zinc(II) ion being easily removed from the ligand during characterisation such as mass spectrometry. An interesting feature to note is that two of the Zn-O bonds are notably longer; this is due to the hydrogen-bonding that occurs in the solvated model of this compound. The donor oxygen atoms form a hydrogen bond with hydrogen atoms on a nearby DMF molecule. The bond angles are slightly distorted from the typical trigonal bipyramidal geometry which could be attributed to the six membered ring formed by chelation as well as the geometric adjustments required for the formation of a dinuclear complex bearing two sterically bulky tetradentate chelate ligands. The bond lengths and angles are all within the range of similar structures.^[86]

Table 5.6.21: Table of coordination bond angles for [Zn₂(L³)₂].

| Bond | Angle (°) | Bond | Angle (°) |
|------------|-----------|-----------|-----------|
| N1- Zn1-N2 | 95.05(1) | N3-Zn2-N4 | 93.32(2) |
| N1- Zn1-O1 | 91.14(1) | N3-Zn2-O5 | 91.41(1) |
| N2- Zn1-O3 | 84.50(1) | N4-Zn2-O7 | 84.70(2) |
| O1- Zn1-O3 | 94.62(1) | O5-Zn2O7 | 95.26(1) |

The bond lengths and angles around the bonds holding the dinuclear zinc(II) cluster together are tabulated below in **Table 5.6.22**.

Table 5.6.22: Table of coordination bond lengths and bond angles between zinc(II) ions in the dinuclear structure [Zn₂(L³)₂].

| Bond | Length (Å) | Bond | Angle (°) |
|--------|------------|------------|-----------|
| Zn1-O3 | 2.084(3) | O3-Zn1-O7 | 76.78(1) |
| Zn1-O7 | 2.021(3) | Zn1-O3-Zn2 | 102.21(1) |
| Zn2-O7 | 2.081(3) | O3-Zn2-O7 | 76.58(1) |
| Zn2-O3 | 2.034(3) | Zn2-O7-Zn1 | 102.76(1) |

5.7 Concluding Remarks

The two ligand structures reported both had monoclinic space groups. H_3L^1 crystallised with one DMF molecule in the space group of $P 2_1/n$ and H_2L^2 crystallised in the space group $P 2_1/c$. Two of the three copper(II) complexes, $[Cu_2(L^1)(OAc)(DMF)]$ and $[Cu_3(L^3)_2(H_2O)_2]Cl_2$, crystallised in monoclinic space groups of $P 2_1/n$ and $P 2_1/c$, respectively and the third, $[Cu_3(L^2)_2Cl_2(DMF)_2]$, adopted the triclinic space group of $P-1$. All three copper(II) complexes crystallised with solvents and had a proclivity for the formation of multinuclear complexes. The nickel(II) complexes both crystallised in monoclinic space groups. $[Ni(L^2)]$ crystallised with four water molecules and one DMF molecule in the space group of $P 2_1/c$ and $[Ni(L^3)]$ with two water molecules in $C 2/c$. $[Zn_2(L^3)_2]$ was the only complex to adopt an orthorhombic space group of $Pna2_1$. Following the copper(II) complexes, the zinc(II) complex also formed a multinuclear complex and was solvated by five DMF molecules. Also noteworthy is that the extended structures of these complexes are highly complex as a result of extensive intra- and intermolecular hydrogen bonding associated with their crystallisation as water and DMF solvates. Because of the significant level of disorder in all solvent regions of the solvated crystal structures, final crystallographic models were generated by removing reflection data associated the disordered solvent by employing PLATON's SQUEEZE algorithm. While this allows for favourable CIFcheck results and uncomplicated analysis of the structures of the metal complexes, it precludes extensive analysis of the extended structures of the compounds and any hydrogen bonding interactions with solvent molecules.

6. Computational Chemistry

6.1 Introduction

By using mathematics and the laws of physics, computational chemistry calculates structures, reactions, UV-vis spectra, infrared vibrations and NMR spectra. The basis of DFT simulations is due to their popularity in literature to theorise experimental data and then make a comparison. This can also be helpful in the analysis and assignment of data. Some literature examples will be discussed and then an analysis and comparison of the experimental data and calculated data of the compounds of this work will be done. The method used most commonly is that of Density Functional theory (DFT). It provides more realistic results as it takes into account electron correlation and its effects whereas other computational methods only consider the effects as an average, which lowers their accuracy when compared to experimental data.^[89]

In *ab initio* methods a variety of quantum chemical properties are calculated; the main calculation being to determine the wavefunction. These calculations are all done *via* Schrödinger mathematics.^[90] As is the norm for these types of calculations, the Born-Oppenheimer approximation is applied to the nuclei of the molecule being studied. This simply means that the nuclei are seen as fixed which creates an external potential energy where the electrons are moving. This gives the stationary electronic state which can be described by a wavefunction (Ψ) using the Schrödinger equation, as given below.

$$\hat{H}\Psi(r_1, r_2, \dots, r_N) = E \Psi(r_1, r_2, \dots, r_N)$$

where \hat{H} is the Hamiltonian operator and is made up of three terms; kinetic energy, the interaction with external potential energy (the interaction of electrons with the atomic nuclei) and electron-electron interaction:

$$\hat{H} = -\frac{1}{2} \sum_i^N \nabla_i^2 + \hat{V}_{\text{ext}} + \sum_{i<j}^N \frac{1}{|\mathbf{r}_i + \mathbf{r}_j|}$$

Simply put, the wavefunction is a description of where electrons are situated, the electron density distribution. Computational chemistry utilises basis sets in appropriate software to calculate the wavefunction of a molecule. Once the wavefunction is calculated and therefore the electron density distribution, it can be used to determine other properties of the molecule being studied, for instance its molecular wavefunction, orbitals, infrared spectrum and so forth. The basis set employed in this work allows for the inner and outer shell electrons to be treated separately as core electrons and valence electrons are not equivalent. This means the core electron contribution is not calculated as thoroughly as the valence electrons in these calculations and with the application of the double-zeta method (doubly split electron basis set), the valence electrons are calculated twice. DFT focuses on the electron density of the molecule and therefore calculates the wavefunction indirectly which allows for the further calculation of a range of electronic properties.^[89]

In 2009 Salehzadeh *et al.*^[91] did a study on an acyclic pentadentate nickel(II) Schiff base complex and used the X-ray structure acquired to generate fully optimised gas phase structures. The calculations were done by Gaussian 98 using both the Hartree-Fock and DFT levels of theory. The LanL2DZ basis set was used for the metal ion and 6-31G or 3-21G^[92-94] for ligand atoms in the DFT calculations for the complex $[\text{NiL}_{33}(\text{MeOH})]^{2+}$ as shown in **Figure 6.1**. DFT calculations were done on different isomers of $[\text{NiL}_{33}(\text{MeOH})]^{2+}$ to determine whether the complex had indeed adopted the most stable structure in the solid state. The results were positive and confirmed that the gas phase calculation of the most stable isomer (in **Figure 6.1** the most left-hand side structure) matched the solid state X-ray structure of $[\text{NiL}_{33}(\text{MeOH})]^{2+}$. Shown in **Table 6.1** are the X-ray bond lengths for $[\text{NiL}_{33}(\text{MeOH})]^{2+}$ as determined by Salehzadeh *et al.*^[91]

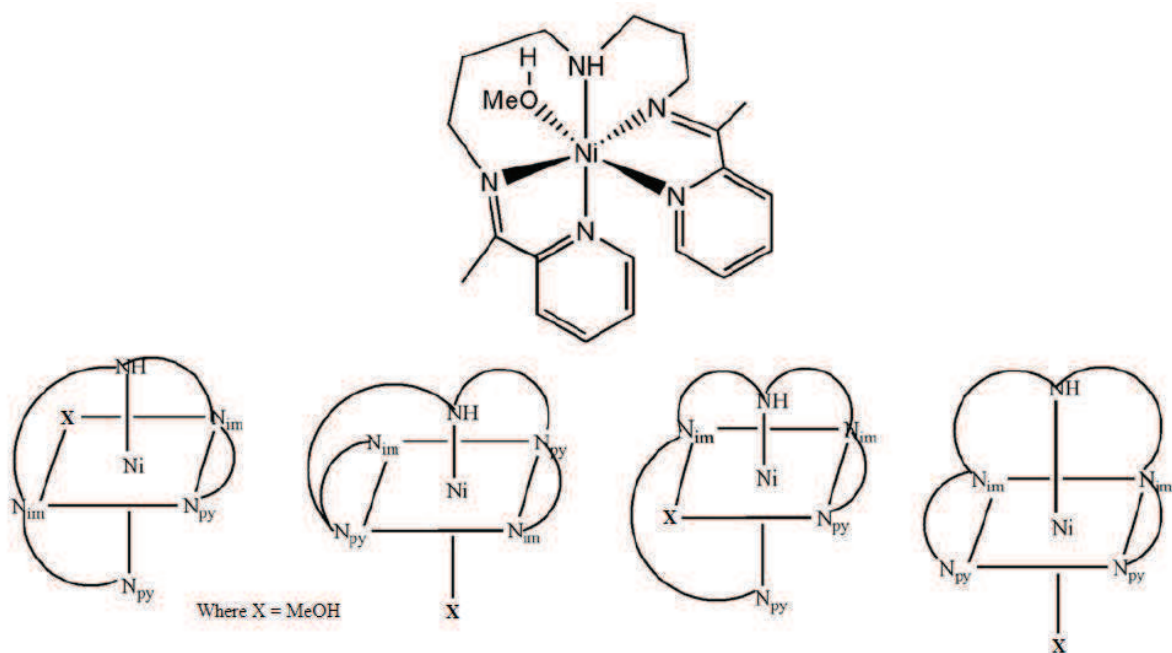


Figure 6.1: Structure and isomers of $[\text{NiL}_{33}(\text{MeOH})]^{2+}$ as determined by Salehzadeh *et al.*^[91] Adapted from Salehzadeh *et al.*^[91]

Table 6.1: Calculated and experimental bond lengths (Å) of $[\text{NiL}_{33}(\text{MeOH})]^{2+}$.

| | X-ray | 6-31G (LanL2DZ for Ni) | 3-21G (LanL2DZ for Ni) |
|--------------|----------|------------------------|------------------------|
| N1-Ni | 2.097(6) | 2.115 | 2.094 |
| N2-Ni | 2.073(7) | 2.116 | 2.094 |
| N3-Ni | 2.108(7) | 2.161 | 2.118 |
| N4-Ni | 2.040(7) | 2.078 | 2.071 |
| N5-Ni | 2.061(6) | 2.140 | 2.117 |
| O1-Ni | 2.192(6) | 2.277 | 2.154 |

In 2010 Trujillo *et al.*^[95] studied unsymmetrical nickel(II) complexes that were substituted with organometallic donor-acceptor compounds. The nickel(II) complexes are shown in **Figure 6.2**. The DFT calculations run by Trujillo *et al.*^[95] were carried out using the Amsterdam Density Functional program.^[96] The basis set used was that of ADF TZP. It was found that the computational results were in good agreement with that obtained experimentally. Shown in **Table 6.2** are the calculated values for the nickel(II) chelates reported by Trujillo *et al.*^[95] The experimental values are given in parentheses when reported.

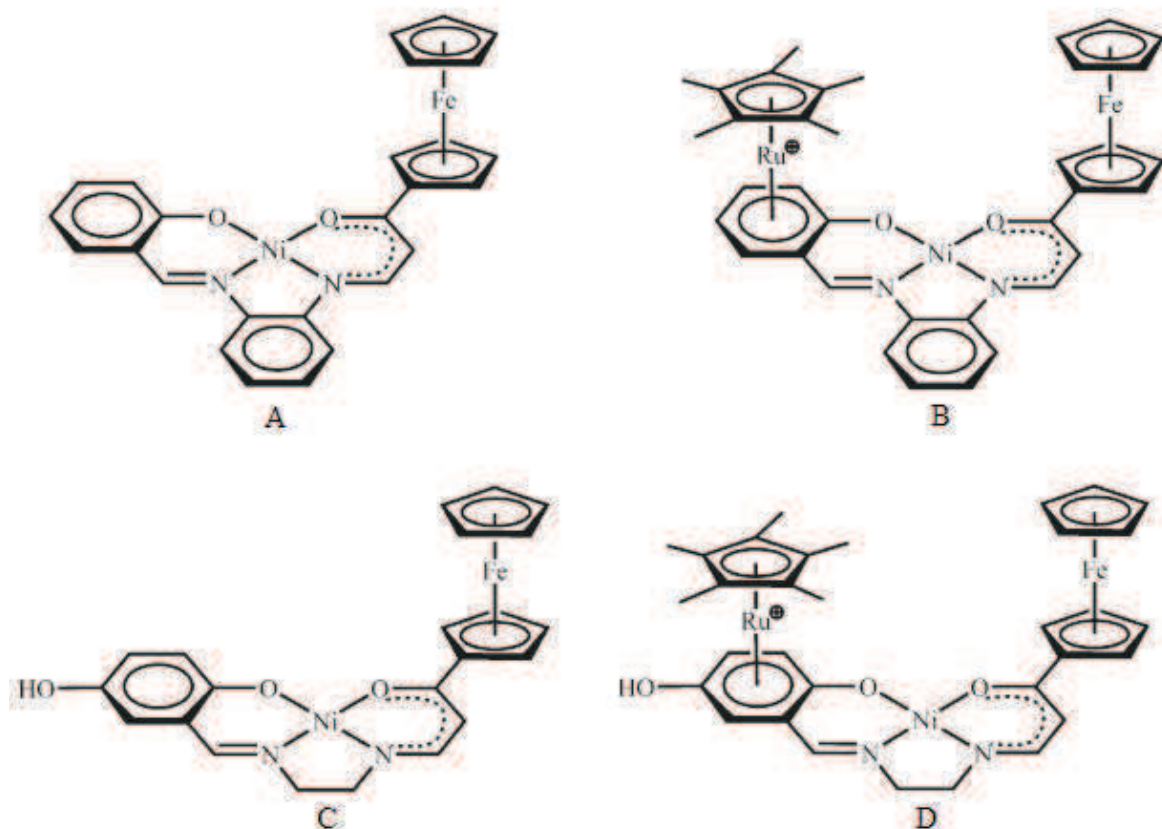


Figure 6.2: Structures of the nickel(II) chelates studied by Trujillo *et al.*^[95] Diagram adapted from Trujillo *et al.*^[95]

Table 6.2: Experimental and calculated bond lengths (Å) in nickel(II) chelates reported by Trujillo *et al.*^[95]

| Bond | A | B | C | D |
|---------|---------------|-------|---------------|---------------|
| Ni-N(1) | 1.887 (1.868) | 1.875 | 1.869 (1.856) | 1.866 (1.834) |
| Ni-O(1) | 1.904 (1.842) | 1.882 | 1.901 (1.846) | 1.873 (1.825) |
| Ni-N(2) | 1.889 (1.848) | 1.892 | 1.862 (1.851) | 1.871 (1.881) |
| Ni-O(2) | 1.886 (1.849) | 1.901 | 1.894 (1.844) | 1.921 (1.852) |

Trujillo *et al.*^[95] did further investigations using TDDFT calculations to determine the theoretical electronic transition energies. It was found that the major features reported in the experimental spectra were reproduced well by the calculated spectra.

In 2011 Chandra *et al.*^[97] synthesised 16-membered mixed-donor macrocyclic Schiff base nickel(II) chelates which were then modelled using MOPAC 2007^[98] in the gas phase with PM6 level of theory. They reported that the root mean square gradient for the molecules were all less than one. The structure of the nickel(II) chelates are shown in **Figure 6.3**.

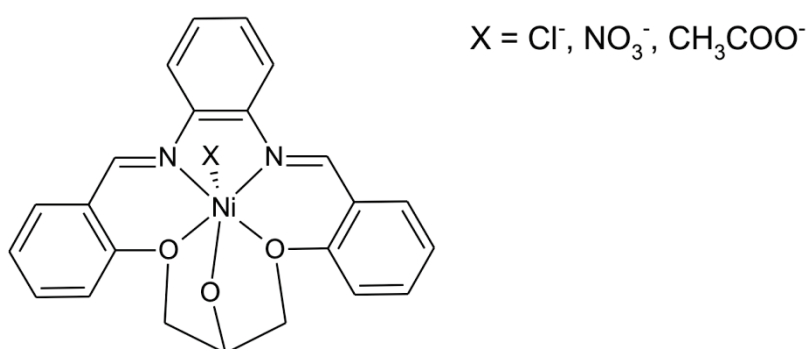


Figure 6.3: 16-membered mixed-donor nickel(II) chelates synthesised by Chandra *et al.*^[97]

Another study done in 2011 by Cao *et al.*^[99] on nickel(II) phosphasalen chelates utilised Gaussian 03^[100] in order to carry out DFT calculations. The study included a comparison of nickel(II) salen experimental and DFT calculated data. The functional applied was that of B3PW91^[101-102] with the associated triple zeta^[103] basis set. The calculations were done in both the singlet and triplet states. The structures of the nickel(II) chelates are shown in **Figure 6.4**. The optimisation proved successful and the calculated parameters for the optimised singlet state were in excellent agreement with the experimental data. The data for the bond angles and bond lengths of these complexes is given in **Table 6.3**.

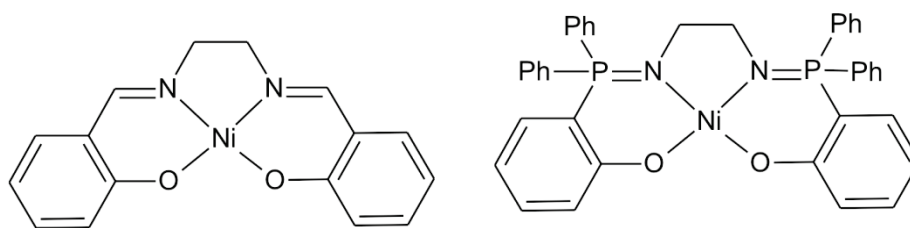


Figure 6.4: Structures of the nickel(II) chelates of salen and phosphasalen ligands.

Table 6.3: Calculated and experimental bond lengths (Å) and bond angles (°) of the nickel(II) chelates of salen and phosphasalen ligands.

| | Ni(salen) | | | Ni(phosphasalen) | | |
|-----------------|-----------|---------|---------|------------------|---------|---------|
| | X-ray | Singlet | Triplet | X-ray | Singlet | Triplet |
| Ni-N2 | 1.851(3) | 1.857 | 1.986 | 1.888(4) | 1.897 | 1.966 |
| Ni-N1 | 1.849(3) | 1.856 | 1.989 | 1.905(4) | 1.894 | 2.011 |
| Ni-O2 | 1.853(3) | 1.847 | 1.900 | 1.863(4) | 1.865 | 1.914 |
| Ni-O1 | 1.851(5) | 1.848 | 1.899 | 1.881(3) | 1.883 | 1.953 |
| O2-Ni-N2 | 94.1(4) | 94.3 | 91.6 | 95.4(2) | 94.7 | 97.5 |
| O1-Ni-N1 | 94.2(4) | 94.0 | 91.5 | 95.4(2) | 95.1 | 96.3 |
| O1-Ni-O2 | 85.5(4) | 85.4 | 105.2 | 83.9(2) | 84.4 | 101.1 |
| N1-Ni-N2 | 86.3(5) | 86.4 | 82.9 | 85.4(2) | 85.8 | 85.8 |

Furthermore, Cao *et al.*^[99] ran electronic transition energy calculations and determined that the singlet state gave the more stable complex rather than the triplet state and was in agreement with the experimental evidence of a low spin state complex.

When all the literature data is compared it shows that theoretical chemistry calculations can be a valuable source of information when considering complexes and their experimental data. There is also evidence that a wide variety of basis sets can be used to optimise data with accurate results. A key advantage of DFT simulations, therefore, is that when an experimental solid state structure is absent, a simulated structure may be sufficiently accurate to allow reliable interpretations of spectroscopic and other data to be made.

6.2 Experimental

DFT geometry optimisation calculations on all metal complexes were performed using Gaussian 09W.^[104] The X-ray coordinates were used where possible as input structures for the optimisation calculations. The calculations used B3LYP as the hybrid functional. The basis set used was LANL2DZ^[92, 105-107] (Los Alamos National Laboratory 2-double-zeta) for the metal complexes and the input structures of the propyl-bridged molecule, [Ni(L³)], was C₂-symmetrised. Infrared spectra were calculated using the same settings as the geometry optimisation calculations for the metal chelates. None of the vibrational frequencies found were imaginary suggesting that the geometry optimised structures were true minima on the potential energy surface. Electronic spectra were calculated using the TD-SCF method solving for 20 states. TD-DFT is one of the computationally most efficient and most recent methods for calculating electronic spectra with moderate to good accuracy. The electronic spectra were also set to include solvation, with a dielectric constant of 38 Debye to represent DMF. The HOMO and LUMO of each were calculated for each molecule. The results of all the DFT calculations were analysed using GaussView version 5.0.9.^[108] All the Gaussian job files are available in **Appendix E**.

6.3 DFT Calculations of Metal Chelates

6.3.1 Geometry Optimisations

These calculations were used to determine the lowest-energy, optimised structure for each of the nickel(II) chelates. The calculated structures were then compared to the experimental X-ray structures. Note that the *in vacuo* calculated structures are not affected by intermolecular forces as would be the case in the X-ray structures. Despite numerous attempts, the optimisations of the polynuclear metal chelates failed to converge and therefore have not been included in this Chapter. The root mean square deviations for the calculated and experimental structures were determined using Discovery Studio Visualiser to measure their similarity. Shown in **Figure 6.5** is the overlay of the X-ray structure (orange) and the calculated structure (blue) with the least-squares fit similarity coefficient.

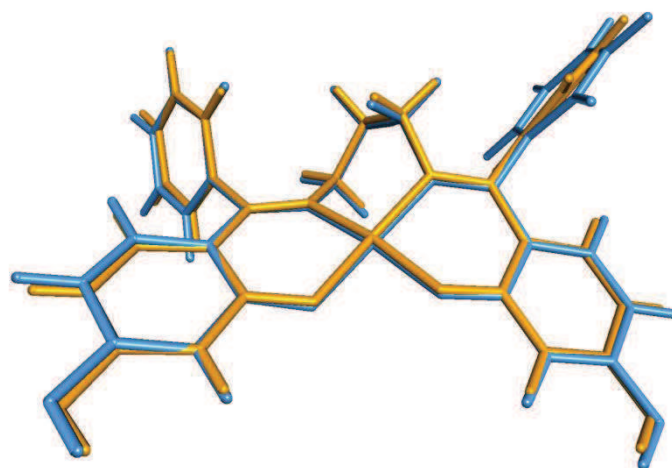


Figure 6.5: Overlay of the X-ray structure (orange) and DFT-optimised structure (blue) of [Ni(L³)], similarity coefficient = 0.990.

The overlay similarity is measured as a fraction between 0 and 1 and so the similarity coefficient for [Ni(L³)] is very favourable consistent with a high similarity between the calculated and X-ray structures. The slight changes seen are attributed to the unchelated phenyl rings. The free phenyl rings have greater rotational freedom and so can be easily distorted from the lowest-energy conformation to allow for more efficient packing of the molecule in the lattice and minimization of unfavourable intermolecular interactions. The bond lengths and bond angles calculated also differ in comparison to the experimentally determined values. The calculated bond lengths are slightly larger than those experimentally determined; however, the percentage differences are still quite low. The bond lengths and bond angles of the DFT calculated and X-ray structures are shown in **Table 6.4**.

Table 6.4: Comparison of selected bond lengths (Å) and angles (°) of the calculated and experimental structure of [Ni(L³)].

| Bond | Expt. (Å) | Calc. (Å) | % Diff | Bond | Expt. (°) | Calc. (°) | % Diff |
|-------|-----------|-----------|--------|----------|-----------|-----------|--------|
| N1-Ni | 1.882(2) | 1.922 | -2.1 | N1-Ni-N2 | 92.76(8) | 93.06 | -0.3 |
| N2-Ni | 1.883(2) | 1.922 | -2.1 | N1-Ni-O1 | 93.21(7) | 91.32 | 2.0 |
| O1-Ni | 1.834(2) | 1.863 | -1.6 | N2-Ni-O3 | 92.37(7) | 91.32 | 1.1 |
| O3-Ni | 1.849(1) | 1.863 | -0.8 | O1-Ni-O3 | 82.75(6) | 85.04 | -2.8 |

*Atom numbers are those of the X-ray structure (**Figure 5.6.24**).

These bond lengths and bond angles show that the coordination sphere of the metal has been well modelled. This is expected as coordination to the metal centre reduces the number of degrees of freedom of the ligand. The present structural data indicate that the DFT calculations at the chosen level of theory suffice to provide an excellent model of the experimental structure against which additional electronic structure information may be reliably determined.

Turning our attention to the structure of $[\text{Ni}(\text{L}^2)]$, as there are two separate $[\text{Ni}(\text{L}^2)]$ molecules in the asymmetric unit, the calculated lowest-energy structure was determined by arbitrarily selecting molecule A from the crystal structure of the complex. This is due to the two molecules being enantiomers of each other and therefore the fit of A will not be optimised to the twist in the di(azomethine) linkage of molecule B. **Figure 6.6** shows an overlay of the DFT calculated and experimental structures of molecule A in $[\text{Ni}(\text{L}^2)]$.

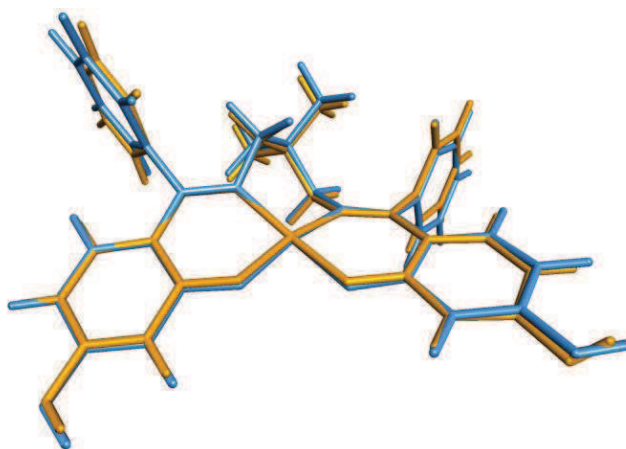


Figure 6.6: Overlay of the X-ray structure of molecule A (orange) and DFT optimised structure (blue) of $[\text{Ni}(\text{L}^2)]$, overlay similarity coefficient = 0.982.

As would be expected, the overlay similarity of molecule B with this optimised structure is 0.789, which is much lower than that for molecule A, 0.982. The phenyl groups adopt only slight variations in their orientations in the gas phase DFT-calculated structures to those seen in the X-ray structures as the latter are affected by nonbonded contacts in the crystal lattice.

Table 6.5 is a comparison of the calculated and observed bond lengths and bond angles for molecule A of $[\text{Ni}(\text{L}^2)]$.

Table 6.5: Comparison of selected bond lengths (Å) and angles (°) of the calculated and experimental structure of $[\text{Ni}(\text{L}^2)]$.

| Bond length (Å) | Expt. | Calc. | % Diff | Bond angle (°) | Expt. | Calc. | % Diff |
|-----------------|----------|-------|--------|----------------|----------|-------|--------|
| N1A-NiA | 1.905(4) | 1.933 | -1.5 | N1A-NiA-N2A | 95.14(2) | 94.75 | 0.4 |
| N2A-NiA | 1.895(3) | 1.933 | -2.0 | N1A-NiA-O2A | 91.75(1) | 91.91 | -0.2 |
| O2A-NiA | 1.846(3) | 1.860 | -0.8 | N2A-NiA-O3A | 92.16(1) | 91.77 | 0.4 |
| O3A-NiA | 1.835(3) | 1.860 | -1.4 | O2A-NiA-O3A | 82.89(1) | 83.46 | -0.7 |

*Atom numbers are those of the X-ray structure (**Figure 5.6.16**).

The bond lengths are slightly longer in the calculated structures than in the X-ray structures, whereas the bond angles of the chelated atoms compare quite favourably. Again, the similarity in the bond lengths and bond angles at the chosen level of theory has sufficed to provide excellent modelling of the coordination sphere of the metal as would be expected against which additional structure information may be reliably determined.

6.3.2 Electronic Transition Calculations

The results of the TD-DFT electronic transition energy calculations were compared with the experimental UV-visible spectra of each metal chelate. Overall, the calculated and experimental data for the nickel chelates are in reasonably close agreement. Overlays of the calculated and experimental UV-visible spectra of $[\text{Ni}(\text{L}^3)]$ and $[\text{Ni}(\text{L}^2)]$ are shown in **Figures 6.7** and **6.9**, respectively. The energy calculations also provide further information regarding which orbitals are likely involved in the transitions that give rise to the spectra.

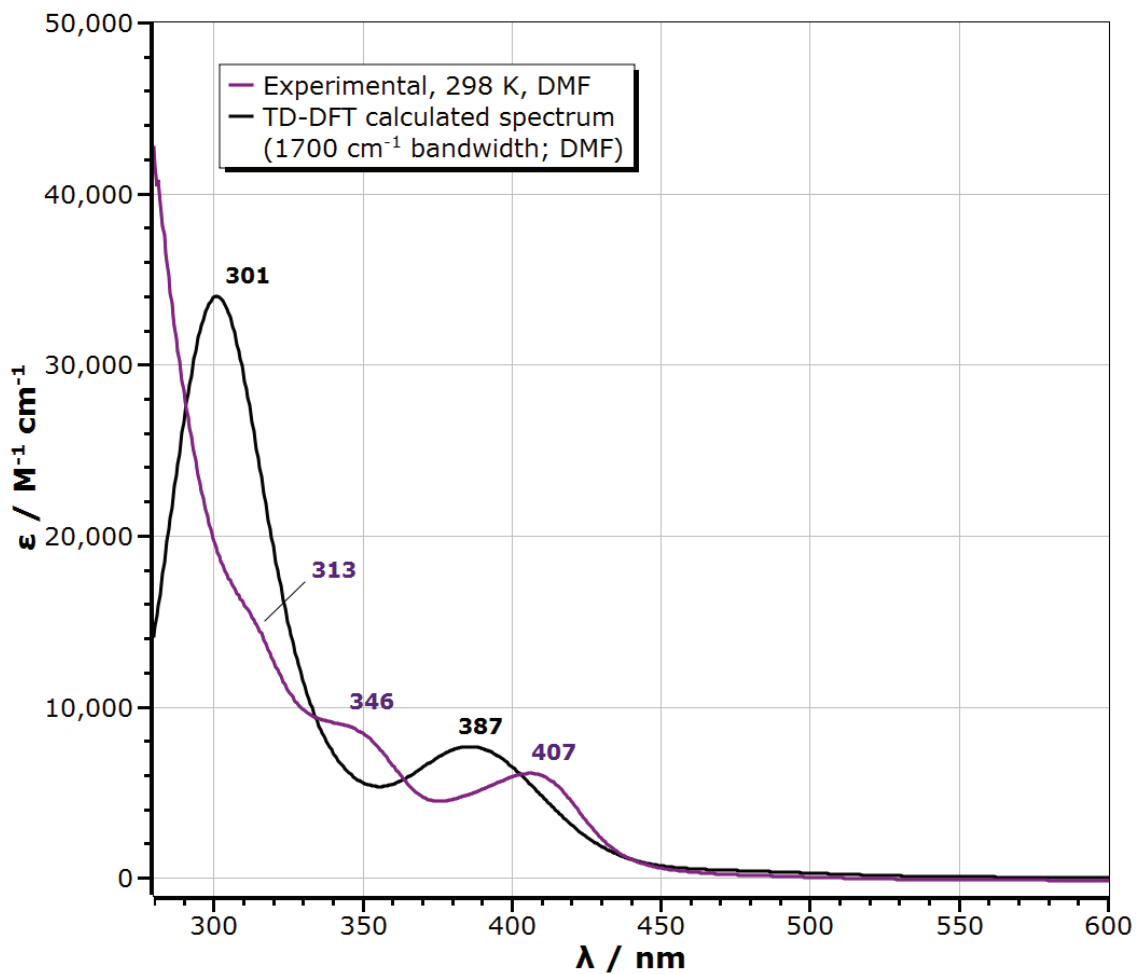


Figure 6.7: Overlay of the calculated and experimental UV-visible spectra of $[\text{Ni}(\text{L}^3)]$.

Figure 6.7 shows that the calculated spectrum is not a perfect reflection of the experimentally obtained spectrum. The calculated spectrum shown in **Figure 6.7** is a result of a mixture of electronic transitions, and not solely a HOMO→LUMO transition. The transitions responsible for the peaks in the spectra have been listed and assigned below in **Table 6.6**.

Table 6.6: Experimental and calculated electronic transitions for [Ni(L³)].

| Expt. (nm) | Calc. (nm) | Molecular Orbitals | Assignment | Oscillator strength |
|---|------------|----------------------------|-------------------------|---------------------|
| 313 (Intraligand $\pi \rightarrow \pi^*$) | 303.0 | HOMO-10 \rightarrow LUMO | $\pi \rightarrow \pi^*$ | 0.3894 |
| | | HOMO-2 \rightarrow LUMO | $\pi \rightarrow \pi^*$ | |
| | | HOMO-1 \rightarrow LUMO | $\pi \rightarrow \pi^*$ | |
| 348 (Intraligand $\pi \rightarrow \pi^*$) | 341.1 | HOMO-2 \rightarrow LUMO | $\pi \rightarrow \pi^*$ | 0.0274 |
| | | HOMO-1 \rightarrow LUMO | | |
| 407 (MLCT) | 390.4 | HOMO \rightarrow LUMO | $\pi \rightarrow \pi^*$ | 0.0863 |

Figure 6.8 is a reference for the Cartesian axes used to assign the molecular orbitals of [Ni(L³)] and **Figure 6.9** illustrates the orbitals that are involved in the transitions responsible for the UV-vis spectrum of [Ni(L³)]. The HOMO is an admixture of a ligand π -symmetry molecular orbital (MO) with the $3d_{xy}$ atomic orbital of the metal ion. The substituent phenyl groups of the ligands are not part of the MO and the bonding electron pair is therefore localised in the xy plane over the framework of the metal and chelating Schiff base ligand. The unoccupied $3d_{yz}$ atomic orbital is mixed with a ligand π^* MO (LUMO+1 and LUMO+2) and some wavefunction amplitude is observed on the peripheral or substituent phenyl rings. Note that because the z - and y - vectors of the Cartesian axis system do not lie along the Ni-N bonds, the atomic orbital labelled $3d_{yz}$ has its lobes pointing along the Ni-N bond vectors and is thus akin to the $3d_{x^2-y^2}$ orbital in a conventional coordination complex with the x - and y -axes colinear with the relevant metal-ligand bond vectors. The remaining orbitals with π -symmetry are admixtures of ligand π MOs and the $3d_{xz}$ MO. Interestingly, the LUMO is an almost pure ligand π^* MO with a negligible contribution from the metal.

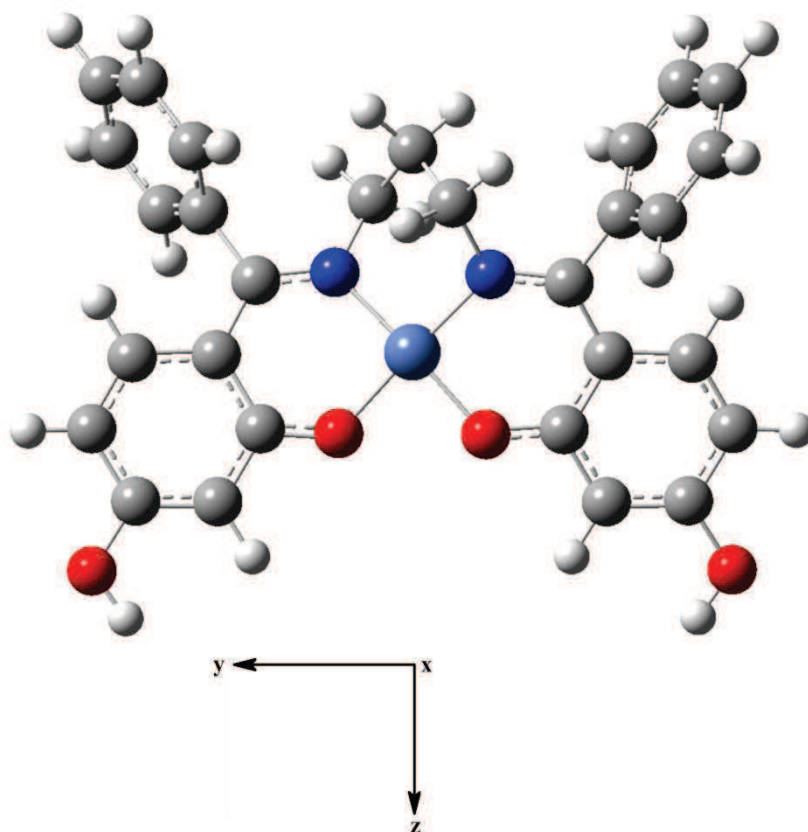


Figure 6.8: Cartesian axes of $[\text{Ni}(\text{L}^3)]$.

Based on the qualitative descriptions of the orbitals involved in the electronic transitions of the complex, the assignment of the MLCT band at ca. 407 nm in the experimental spectrum (390.4 nm in the calculated spectrum) of $[\text{Ni}(\text{L}^3)]$ is correct as this transition is between the HOMO and LUMO. Since the former MO has appreciable metal character ($3d_{xy}$) and the latter virtually pure ligand π^* character, the transition is correctly assigned as a charge (electron) transfer from a metal-based MO to a ligand-based MO.

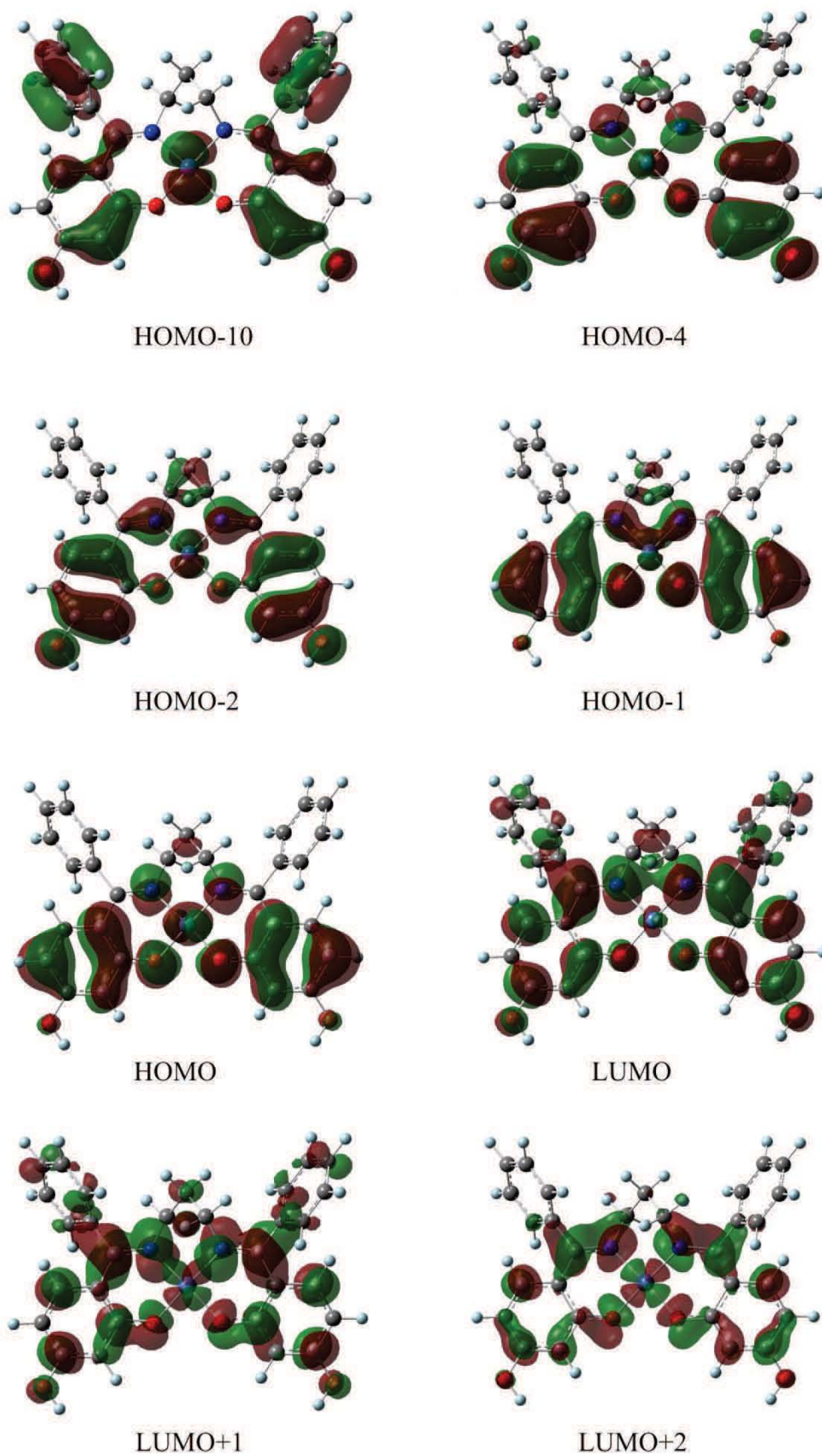


Figure 6.9: Frontier molecular orbitals of $[\text{Ni}(\text{L}^3)]$ involved in the UV-visible electronic transitions of the metal complex.

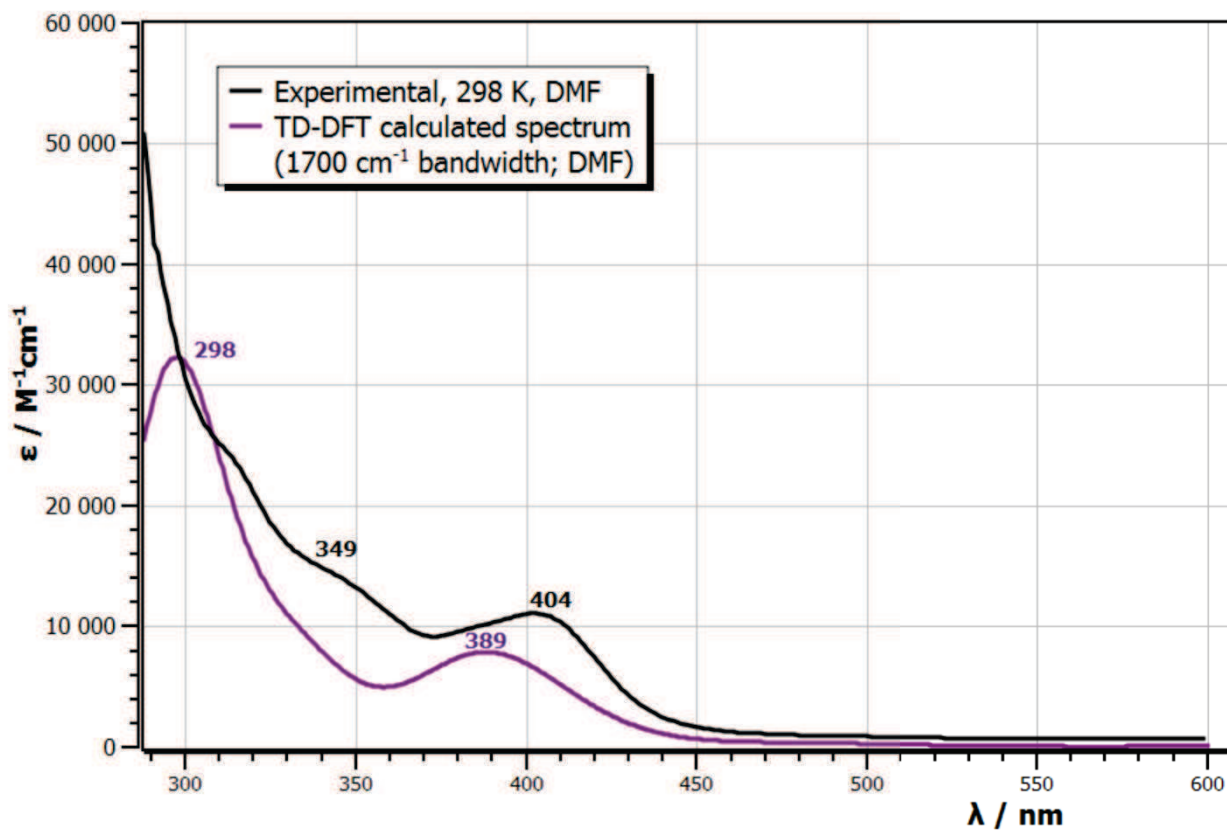


Figure 6.10: Overlay of the calculated and experimental UV-visible spectra for [Ni(L²)].

In **Figure 6.10** the similarity of the two spectra is clearly visible. The calculated spectrum shown in **Figure 6.10** is not the result of HOMO and LUMO transitions only. It involves transitions between various molecular orbitals which have been listed and assigned below in **Table 6.7**.

Table 6.7: Experimental and calculated electronic transitions for [Ni(L²)].

| Expt. (nm) | Calc. (nm) | Molecular Orbitals | Assignment | Oscillator strength |
|------------|------------|--------------------|-------------------------|---------------------|
| - | 299.8 | HOMO-11→LUMO | $\pi \rightarrow \pi^*$ | 0.3480 |
| | | HOMO-2→LUMO | $\pi \rightarrow \pi^*$ | |
| | | HOMO-1→LUMO | | |
| 349 | 338.0 | HOMO-2→LUMO | $\pi \rightarrow \pi^*$ | 0.0352 |
| | | HOMO-1→LUMO | $\pi \rightarrow \pi^*$ | |
| | | HOMO→LUMO+2 | $\pi \rightarrow \pi^*$ | |
| 404 | 391.0 | HOMO→LUMO | $\pi \rightarrow \pi^*$ | 0.0850 |
| | | | | |

The Cartesian axes of [Ni(L²)] are shown in **Figure 6.11**. The orbitals responsible for the transitions in the UV-vis spectrum of [Ni(L²)] are shown in **Figure 6.12**. The HOMO in [Ni(L²)] is an admixture of the $3dxz$ metal ion atomic orbital with a ligand π -symmetry MO. As was the case in [Ni(L³)], the substituent phenyl groups of the ligands are not part of the MO. This implies the bonding electron pair is therefore localised in the xz plane over the framework of the metal and chelating Schiff base ligand. The ligand π^* MO is mixed with a unoccupied $3dxy$ atomic orbital on the metal ion (LUMO+2) and very little wavefunction amplitude is observed on the peripheral or substituent phenyl rings. Note that because the x - and y - vectors of the Cartesian axis system do not lie along the Ni-N bonds, the atomic orbital labelled $3dxy$ has its lobes pointing along the Ni-N bond vectors. The remaining orbitals with π -symmetry are admixtures of ligand π MOs and the $3dyz$ MO on the metal ion. As was noted for [Ni(L³)], the LUMO is an almost pure ligand π^* MO with a negligible contribution from the metal.

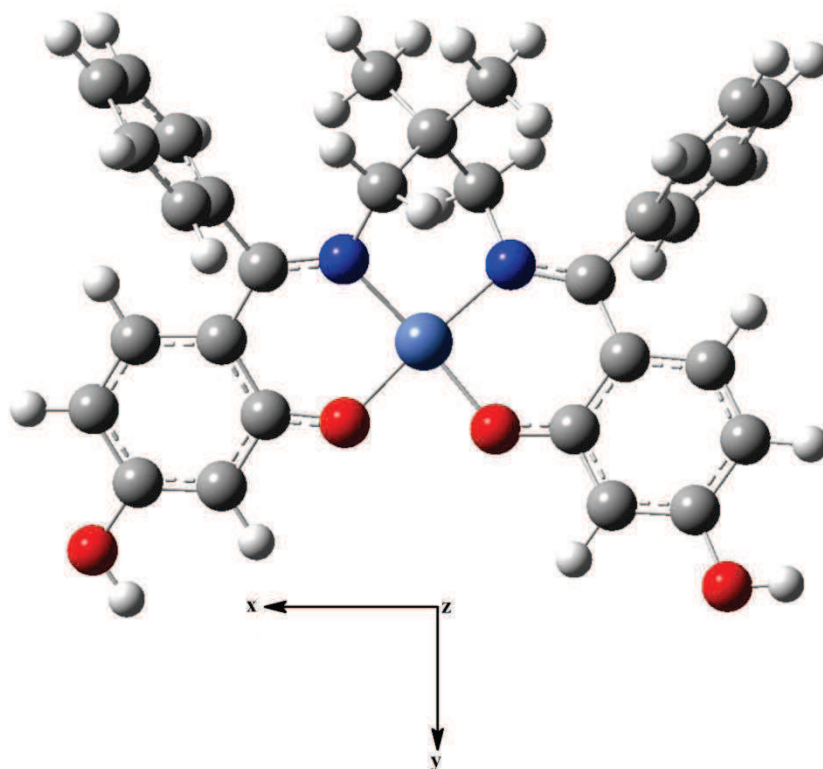


Figure 6.11: Cartesian axes of $[\text{Ni}(\text{L}^2)]$.

The assignment of the MLCT band at ca. 404 nm in the experimental spectrum (391.0 nm in the calculated spectrum) of $[\text{Ni}(\text{L}^2)]$ is confirmed as this transition is between the HOMO and LUMO. Since HOMO has appreciable metal character ($3dxz$) and the LUMO virtually pure ligand π^* character, the transition is correctly assigned as a charge (electron) transfer from a metal-based MO to a ligand-based MO.

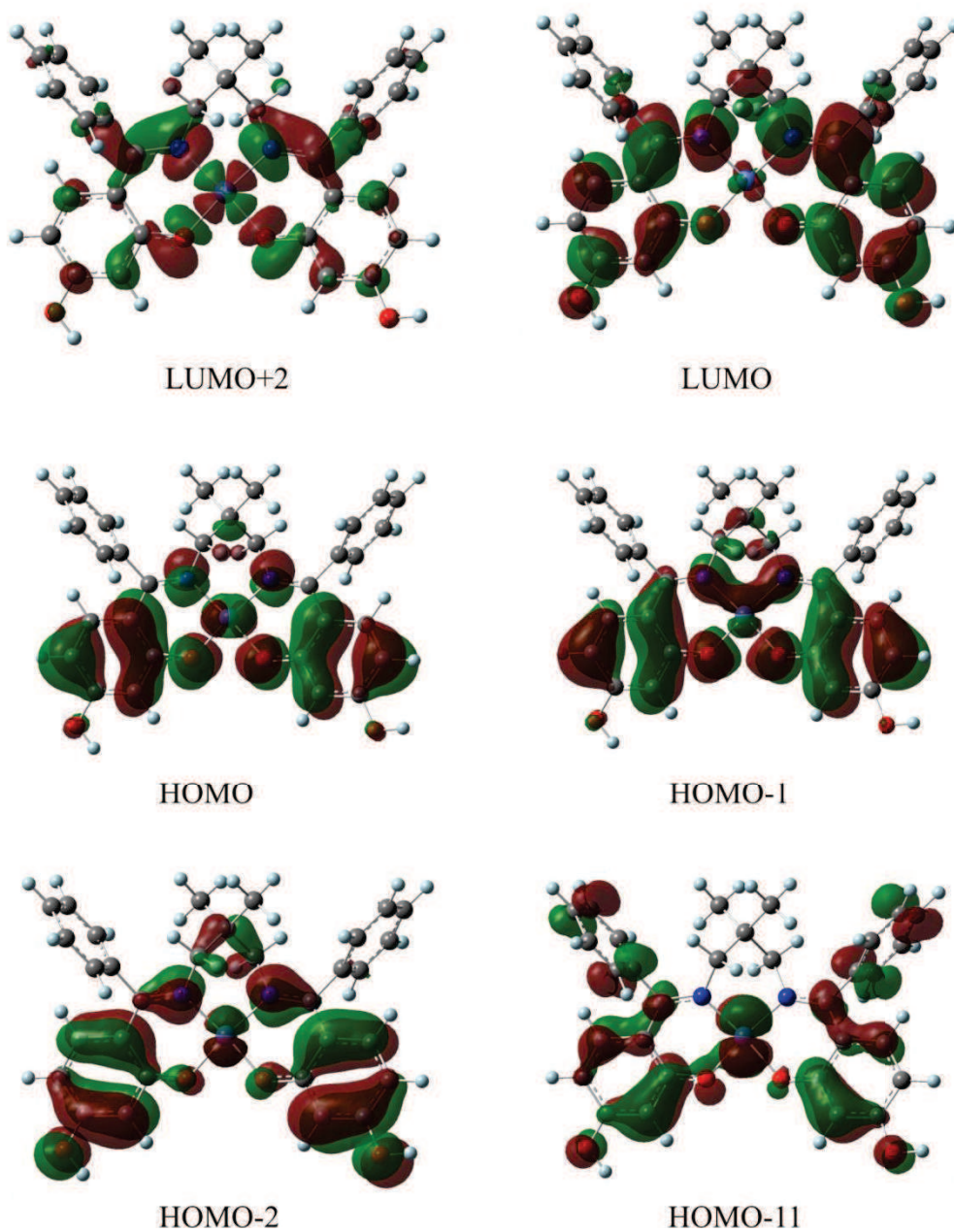


Figure 6.12: Frontier molecular orbitals of $[\text{Ni}(\text{L}^2)]$ involved in the UV-visible electronic transitions of the metal complex.

The NBO 3d atomic orbital energies for the two nickel(II) chelates and their electron populations are given below in **Table 6.8**.

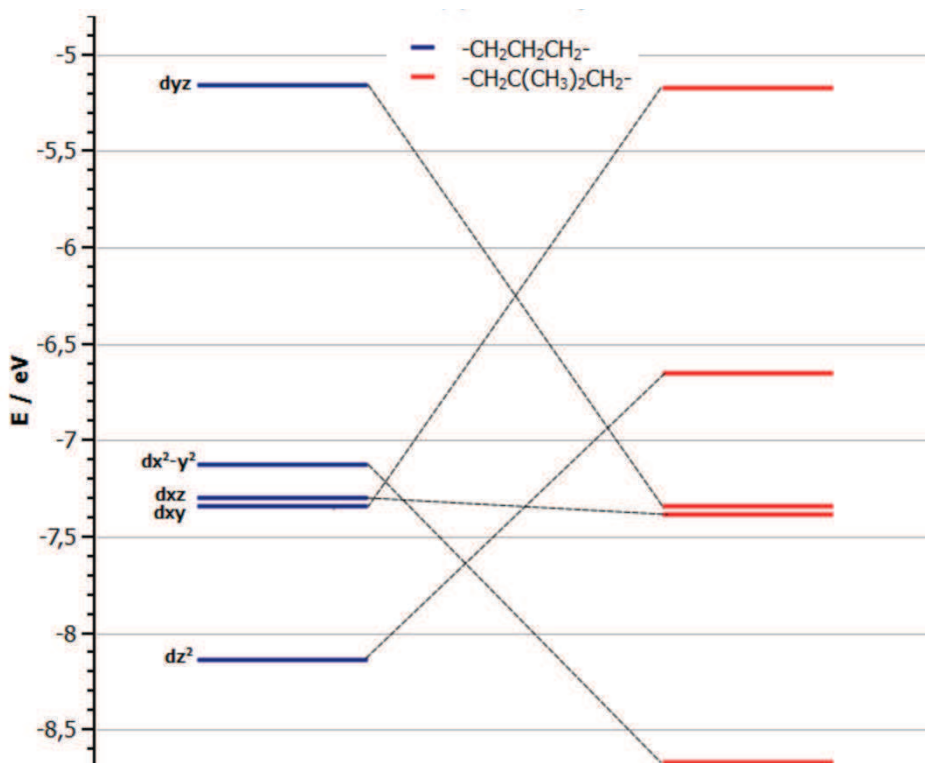


Figure 6.13: Comparative Ni(II) 3d orbital energy level diagram.

Figure 6.13 reflects the changes in the Cartesian axes between the molecules plus the perturbations on the d-orbital energies from the different ligand conformations and structures. It shows clearly that the addition of two methyl groups onto the bridge of the ligand has a significant influence over the ligand conformation. The dyz , dx^2-y^2 and dxz orbitals have all been lowered in energy by the methyl group addition, whereas the dxy and dz^2 orbitals have increased in energy.

Table 6.8: NBO 3d atomic orbital energies and electron populations of [Ni(L²)] and [Ni(L³)].

| | [Ni(L ²)] | | [Ni(L ³)] | |
|-------------------------------------|-----------------------|-------------|-----------------------|-------------|
| | Population | Energy (eV) | Population | Energy (eV) |
| <i>dyz</i> | 1.96 | -7.34 | 0.804 | -5.16 |
| <i>dx²-y²</i> | 1.99 | -8.67 | 1.96 | -7.13 |
| <i>dxz</i> | 1.99 | -7.39 | 1.95 | -7.30 |
| <i>dxy</i> | 0.790 | -5.17 | 1.99 | -7.34 |
| <i>dz²</i> | 1.95 | -6.65 | 1.97 | -8.14 |

In the study done by Trujillo *et al.*^[95] a theoretical investigation of the electronic spectra was done through TDDFT calculations for complexes C and D. They found a good agreement between the experimental and theoretical data, however, the long wavelength bands were found to be red-shifted and the corresponding short wavelength bands were found to be blue-shifted. The study assigned the red-shift of the complexes to the TDDFT calculations underestimating the low-lying excitation energies associated with charge transfer. The blue-shift was said to be due to the overestimation of the energy of the excited states as TDDFT does not account for electronic relaxation effects. Despite these shortcomings, TDDFT is nevertheless useful for identification of low-lying charge transfer and higher-lying π - π^* states for such transition metal complexes.

6.3.3 Infrared Calculations

The vibrational frequencies are calculated not only for comparison with actual infrared spectra, but also to determine if the optimised structure is a minimum energy structure on the potential energy surface. The calculated and experimental spectra were compared visually on the same axis system. **Figure 6.14** shows the overlaid spectra of [Ni(L³)].

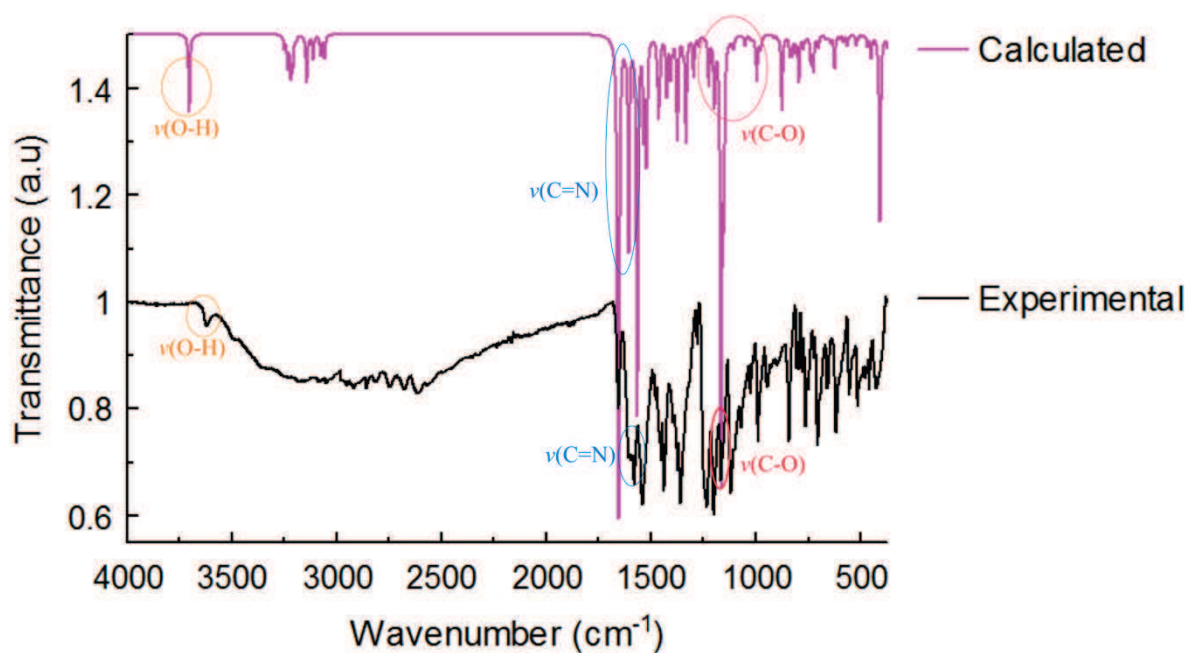


Figure 6.14: Overlay of the calculated and experimental frequency data for $[\text{Ni}(\text{L}^3)]$.

The spectra of $[\text{Ni}(\text{L}^3)]$ show some similarities, however, the relative intensities of the peaks in the calculated spectrum do not correlate well with the experimental spectrum. The $\nu(\text{O-H})$ peak is a good estimation, although the region is broadened by the presence of water molecules in the crystals used. A comparison of the experimental and calculated data for $[\text{Ni}(\text{L}^3)]$ and $[\text{Ni}(\text{L}^2)]$ are shown in **Table 6.9**.

The overlay of the experimentally determined infrared spectrum of $[\text{Ni}(\text{L}^2)]$ and the DFT calculated spectrum is shown in **Figure 6.15**.

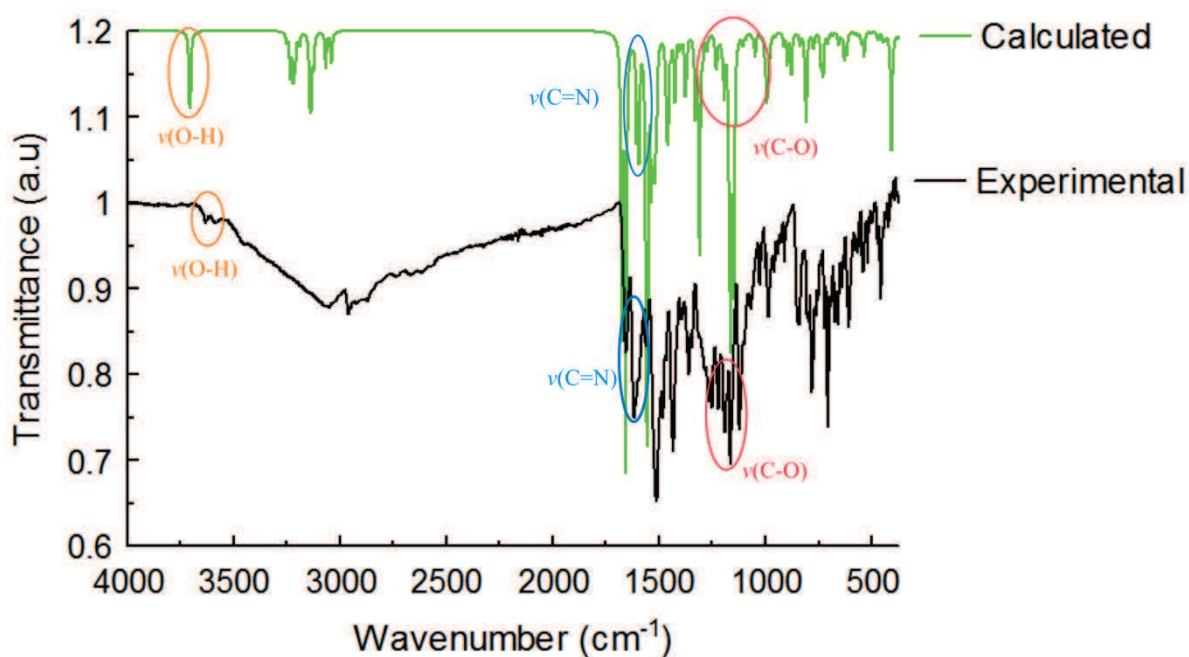


Figure 6.15: Overlay of the calculated and experimental frequency data for [Ni(L²)].

The spectra do show a similarity with an improvement in the correlation of the intensities of the peaks. This may be due to the two conformers present in the solid-state structure. The $\nu(\text{O-H})$ peak is much smaller than the estimated one and this region is broadened by the presence of water molecules in the crystals.

A plot of the experimental frequencies versus the calculated frequencies was done for the O-H, C=N and C-O stretches. If the error between the experimental and calculated frequencies was systematic the slope of this graph could be used to correct for these errors. This proved true for only the imine stretches and the plot is given below in **Figure 6.16**. An interesting feature to note is that there are two imine stretches in the DFT calculated data and this is due to the left hand imine giving a different peak to the right hand imine.

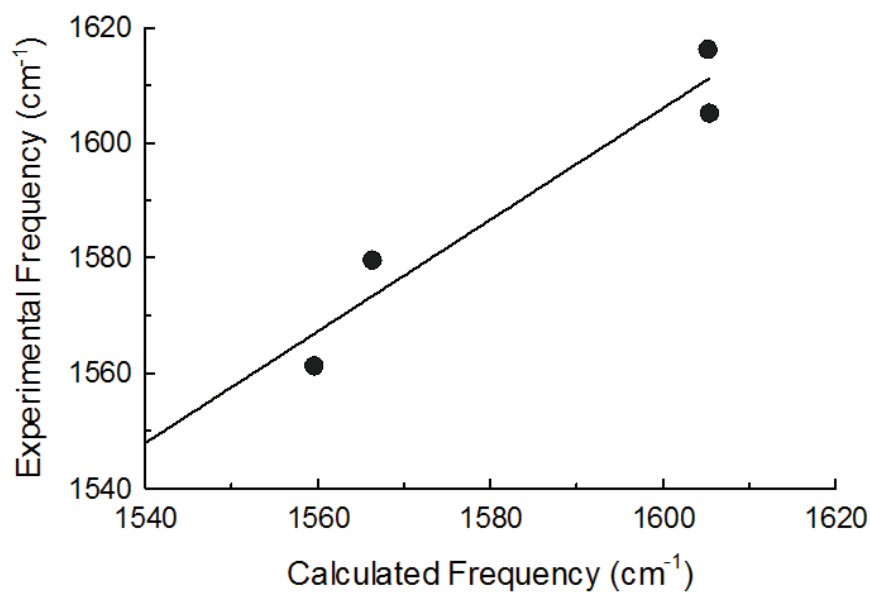


Figure 6.16: Plot of experimental frequency versus calculated frequency for the imine C=N stretching vibrations of both nickel(II) chelates.

By using the calculated slope and y-intercept the function of the plotted graph can be used to determine the experimental frequency using the calculated, or *vice versa*.

$$\text{Experimental frequency} = 0.973 \times \text{calculated frequency} + 50.0 \text{ cm}^{-1}$$

Table 6.9 is a comparison of the regions of interest in the compounds. Although the experimental and calculated frequencies were not exact the percentage differences were reasonably low allowing for a satisfactory comparison.

Table 6.9: Experimental and calculated vibrational frequencies of the nickel(II) chelates.

| Vibration | <u>[Ni(L³)]</u> | | | <u>[Ni(L²)]</u> | | |
|-----------|----------------------------|---------|--------|----------------------------|---------|--------|
| | Expt. | Calc. | % Diff | Expt. | Calc. | % Diff |
| v(O-H) | 3620.83 | 3701.40 | -2.2 | 3631.41 | 3705.81 | -2.0 |
| | 3620.83 | 3701.22 | -2.2 | 3574.60 | 3701.22 | -3.5 |
| v(C=N) | | 1608.05 | | 1616.25 | 1605.19 | 0.7 |
| | 1605.19 | 1605.34 | -0.0 | | 1592.88 | |
| | 1579.69 | 1566.29 | 0.8 | 1561.24 | 1559.55 | 0.1 |
| v(C-O) | | 1563.99 | | | 1553.92 | |
| | | 1333.05 | | | 1237.48 | |
| | | 1330.14 | | | 1232.83 | |
| | 1233.95 | 1225.10 | 0.7 | 1220.47 | 1227.92 | -0.6 |
| | | 1223.99 | | 1190.33 | 1171.98 | 1.5 |
| | 1177.12 | 1165.17 | 1.0 | 1164.02 | 1163.78 | 0.0 |
| | 1166.62 | 1163.41 | 0.3 | | 1147.47 | |

The frequency data were not reported in any of the literature compounds discussed in section 4.1.

6.4 Conclusions

As the correlations between the calculated and experimental data were reasonably good it is clear from this study that the use of the B3LYP/LAND2DZ level of theory was adequate for calculating molecular structures, IR frequencies, and electronic excitation energies for [Ni(L³)] and [Ni(L²)]. A particularly interesting result is that a small change in the substitution pattern of the alkyl chain linking the imine groups of the ligands was capable of substantially affecting the conformation and symmetry of the metal chelates. This had a significant impact on the d-orbital energy level sequence for each complex and also lead to notable differences in the electronic spectra of the two complexes.

7. Biological Studies

7.1 Introduction

Biological studies are a key objective of most drug discovery research programs. In most cases, biological studies involve an initial screening of the synthesised ligands and chelates against their intended targets to determine their half maximal inhibitory concentration (IC₅₀). In this particular instance the focus was on bleomycin type anti-cancer agents and therefore one of the synthesised ligands and five metal complexes were sent to AuTek Biomed's Advanced Material Division at Mintek for cancer screening in the final stages of the project.

It is in a scientist's best interest to design a compound with specific structural features and pharmacological effects.^[109] Humans have been practicing biological screening as far back as can be documented by treating disease with a variety of natural products. This was a trial and error method of discovery. These plant materials could possibly have one or more active components. Over the years scientists have researched these compounds to determine the relationship between these naturally occurring materials and the diseases they are used to treat. Biological screening could date back as far as Shen Nong (2737 B.C. to 2697 B.C.), who tested hundreds of plants for use as medicines.^[109] Biological and chemical methods can be combined to elucidate structure and mechanisms that lead to single compounds being synthesised for therapeutics. Modern drug screening techniques include animal testing, electronic and optical instruments, behaviour observation, mathematical modelling and cell cultures.^[109] These screening methods allow for further modifications to be made on the drugs screened in order for improvements to be made to optimise a drug's toxicity and to reveal major side-effects to allow for them to be reduced.^[109]

Due to copper being a biologically active metal, it is naturally found in all living organisms and is vital to their functioning, for example in redox chemistry and growth.^[110] Our specific interest in copper complexes is due to their potential uses in medicines, for example as anticancer agents.^[111] There are many examples of copper complexes with good anti-tumour activities.^[110-111] Many of these compounds contain Schiff base type ligands.^[110-111]

Gokhale *et al.*^[112] synthesised two Schiff base ligands and chelated them to copper(II) for anti-cancer testing; [Cu(N¹-(2-acetylpyridine)pyridine-2-carboxamidrazone)Cl₂] (**1**) and [Cu(N¹-(2-acetylthiophene)pyridine-2-carboxamidrazone) (**2**).^[112] Only one cell line was tested, mouse melanomal cell line B16F10. Compound (**1**) is shown in **Figure 7.1**.

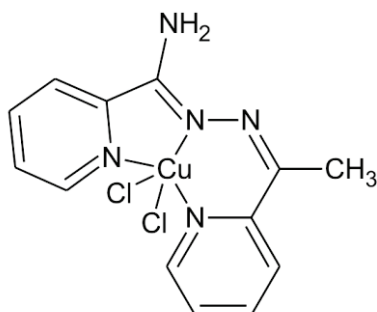


Figure 7.1: Structure of [Cu(N¹-(2-acetylpyridine)pyridine-2-carboxamidrazone)Cl₂].

These compounds were studied by Gokhale *et al.*^[112] and it was found that the ligands would slow cell proliferation whereas the copper compounds would halt cell proliferation altogether. Gokhale *et al.*^[112] suggested that result indicated that chelation of the copper(II) ion was facilitating intracellular transportation which resulted in the estrogen receptor blocking which was suggested by Predki and Sarkar^[113]. The copper(II) chelate shown in **Figure 7.1** was the more potent of the two compounds having an IC₅₀ of 6.8 μM whereas (**2**) was found to be >10 μM.

Hindo *et al.*^[114] synthesised three copper(II) complexes, two of which had a 1:1 stoichiometry of copper(II) to ligand respectively and the third had a 1:2 stoichiometry. These complexes are illustrated in **Figure 7.2**.

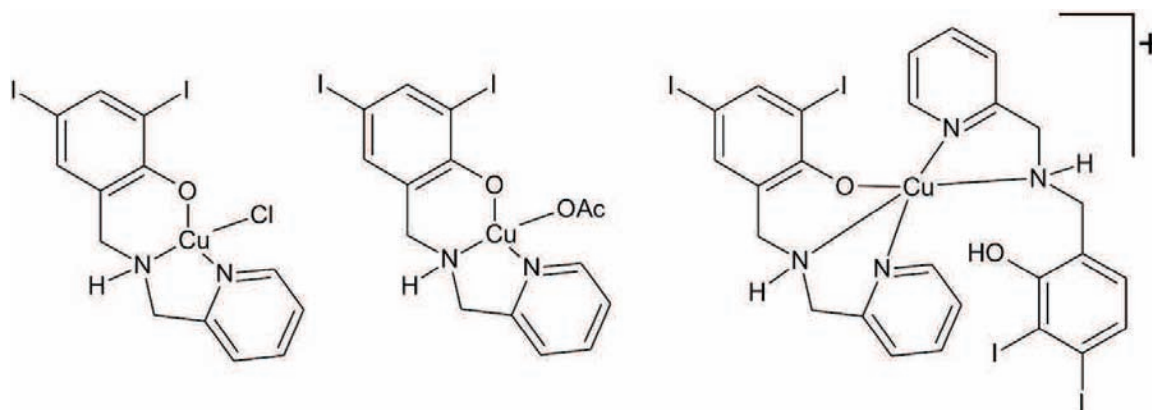


Figure 7.2: Structures of copper(II) complexes of 2,4-diiodo-6-((pyridine-2-ylmethyl)amino)methylphenol redrawn from Hindo *et al.*^[114]

Hindo *et al.*^[114] found that $[\text{Cu}(\text{L}^1)\text{Cl}]$ and $[\text{Cu}(\text{L}^1)\text{OAc}]$ showed effective proteasome-inhibitory activity. The following explanation was put forward as viable. The active species of these compounds could be either $[\text{Cu}(\text{L}^1)]^+$ or solvated versions of this, $[\text{Cu}(\text{L}^1)(\text{H}_2\text{O})]^+$ or $[\text{Cu}(\text{L}^1)(\text{H}_2\text{O})_2]^+$. This active form could then bind a threonine amino-terminal residue of the chymotryptic active centre in 20S proteasome. They based this theory on known lactacystin, ester, epoxyketone, peptide derivative and boronate mechanisms. The IC_{50} values of these compounds against human leukemia Jurkat T cells were found to be low with $[\text{Cu}(\text{L}^1)\text{Cl}]$ as $3.82 \pm 0.01 \mu\text{M}$, $[\text{Cu}(\text{L}^1)\text{OAc}]$ as $4.46 \pm 0.01 \mu\text{M}$ and $[\text{Cu}(\text{HL}^1)(\text{L}^1)\text{OAc}]$ as $3.98 \pm 0.01 \mu\text{M}$. Therefore, this could become a potential novel route to anti-cancer therapy via metal-based proteasome inhibition.

Primik *et al.*^[115] synthesised six indolo[3,2-*c*]quinolines modified at the lactam unit and chelated these ligands to copper(II) (**Figure 7.3**). These compounds were then tested against three human cancer cell lines; non-small lung (**A549**), ovarian cancer (**CH1**), and human colon adenocarcinoma (**SW480**). The results of these tests are given in **Table 7.1**.

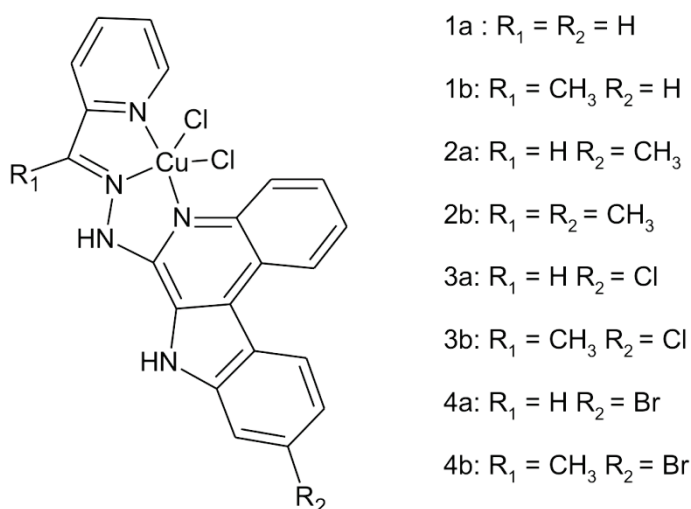


Figure 7.3: Modified indolo[3,2-*c*]quinolines redrawn from Primik *et al.*^[115]

A549 is a more chemoresistant cell line and this is reflected in the tenfold difference between the IC_{50} values of this cell line and the other two tested. Primik *et al.*^[115] found the tested compounds showed almost no change when substitution occurs at R_2 . However, substitution of a methyl group on R_1 resulted in the decrease of the IC_{50} values across the cell lines. The mechanism of action; DNA-intercalation and DNA-cleavage potency for these compounds are being investigated further.

Table 7.1: IC₅₀ values of the modified indolo[3,2-*c*]quinolines copper(II) chelates.^[115]

| | IC ₅₀ (μM) | | | |
|-----------|-----------------------|---------------|---------------|---------------|
| | A549 | CH1 | SW480 | Average |
| 1a | 1.72 ± 0.03 | 0.40 ± 0.07 | 1.3 ± 0.1 | 1.1 ± 0.07 |
| 1b | 0.18 ± 0.04 | 0.030 ± 0.005 | 0.024 ± 0.001 | 0.078 ± 0.015 |
| 2a | 1.7 ± 0.1 | 0.33 ± 0.07 | 0.75 ± 0.04 | 0.93 ± 0.07 |
| 2b | 0.14 ± 0.01 | 0.026 ± 0.006 | 0.024 ± 0.002 | 0.063 ± 0.006 |
| 3a | 1.4 ± 0.3 | 0.41 ± 0.05 | 0.64 ± 0.11 | 0.82 ± 0.15 |
| 3b | 0.23 ± 0.01 | 0.065 ± 0.012 | 0.049 ± 0.003 | 0.11 ± 0.008 |
| 4a | 1.6 ± 0.1 | 0.36 ± 0.03 | 0.47 ± 0.03 | 0.81 ± 0.05 |
| 4b | 0.20 ± 0.03 | 0.052 ± 0.008 | 0.032 ± 0.004 | 0.28 ± 0.01 |

The aims of this chapter are to test the compounds synthesised in this work against four cancer cell lines in order to determine their efficacy as anti-cancer agents. A comparison of ligands and metal compounds will be made, as well as a comparison of the copper(II) chelates and the nickel(II) chelates. Finally, a further comparison of the IC₅₀ values will be done against known commercial anti-cancer drugs and other copper(II) compounds found in the literature.

7.2 Experimental

The procedure followed by Mintek was as follows:

Day one: Cells were trypsinised and distributed in a flat-bottomed 96 well plate to have a final concentration of 2×10^5 cells/mL and left to adhere overnight.

Day two: The compounds were administered at a final starting concentration of 100 μM per well with subsequent serial dilutions (eight in total).

Day four: (72 hours after compound administration), Celltiter One Solution (MTS, Promega, USA) was added and a reading taken after a good colour change was observed. Concentrations were duplicated per plate and experiments were repeated three times.

Finally, sigmoidal curves were fitted to the results using Origin 6.1^[116] to calculate the IC₅₀ value.

The tumour cell lines that the compounds were screened against were non-small lung (A549), human prostate (Du145), human colon adenocarcinoma (HT-29) and a central nervous system (CNS) cell line (U251).

7.3 Results and Discussion

The screening showed that several of the compounds successfully inhibited tumour cell growth to varying extents. The results are shown in Table 7.2. The IC₅₀ values (inoculation concentration) give a measure of the cytotoxicity of the compounds. It is the concentration of the compound required to terminate 50% of the tumour cell population, or the compound concentration that leads to a 0% overall growth rate.

Table 7.2: Tabulation of the half maximal inhibitory concentrations.

| Compound | IC ₅₀ (μM) | | | | Mean IC ₅₀ |
|--|-----------------------|-------------|-------------|-------------|-----------------------|
| | A549 | Du145 | HT-29 | U251 | |
| H ₂ L ² | >50 | >50 | >50 | >50 | >50 |
| [Cu ₃ (L ²) ₂ Cl ₂ (DMF) ₂] | 3.7 (± 0.8) | 12 (± 4) | 6.0 (± 1.4) | 2.8 (± 0.3) | 6.1 (± 1.6) |
| [Ni(L ²)] | >50 | >50 | >50 | >50 | >50 |
| [Cu ₃ (L ³) ₂ (H ₂ O) ₂]Cl ₂ | 5.6 (± 0.8) | 5.2 (± 0.6) | 8.9 (± 1.0) | 8.0 (± 1.0) | 6.9 (± 0.85) |
| [Ni(L ³)] | 29 (± 4) | 21 (± 6) | 50 (± 3) | 39 (± 3) | 35 (± 16) |
| [Cu ₂ (L ¹)(OAc)(DMF)] | 20 (± 2) | 31 (± 6) | >50 | >50 | 38 (± 2) |
| Cisplatin* | 4.0 | 5.0 | 10 | 2.5 | 5.4 |
| 5-Fluorouracil* | 0.20 | 0.40 | 0.16 | 1.0 | 0.44 |
| Etoposide* | 4.0 | 1.3 | 40 | 4.0 | 12 |
| Bleomycin sulphate* | 0.63 | 4.0 | 16 | 0.63 | 5.3 |

*Note that no error data was supplied by the <http://dtp.nci.nih.gov/> for these compounds.

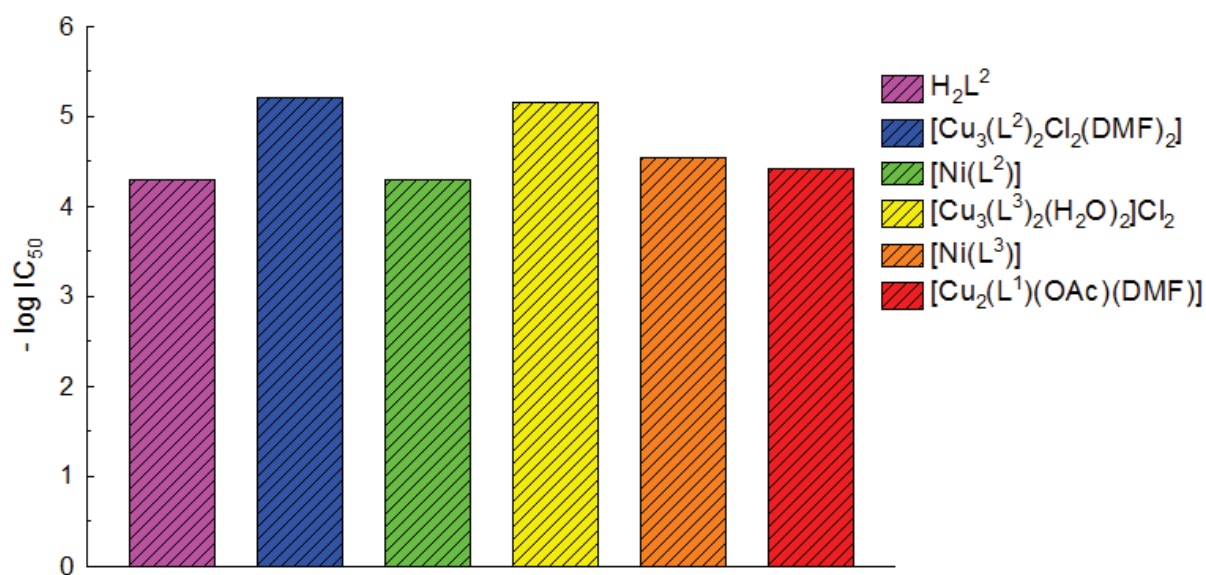


Figure 7.4: Comparison of the $-\log IC_{50}$ values for all compounds averaged across the cell lines.

Table 7.2 and **Figure 7.4** clearly show only two compounds, $[Cu_3(L^2)_2Cl_2(DMF)_2]$ and $[Cu_3(L^3)_2(H_2O)_2]Cl_2$, induce significant inhibitory effects ($< 10 \mu M$). However, another significant feature is that the copper compounds show a better activity than the free ligand and nickel(II) analogues. The exception is $[Cu_2(L^1)(OAc)(DMF)]$ against the human colon adenocarcinoma (HT-29) and central nervous system cancer (U251) cell lines. Since the nickel(II) ion does not produce hydroxyl radicals in solution, the enhanced activity of the copper(II) chelates suggests that hydroxyl radical generation may contribute to the mechanism of action of the compounds. This can be further confirmed by looking at the literature.^[117] For instance, a transition metal ion such as Fe(III) and oxygen are two essential components for bleomycin's action.^[117] The metal forms the active complex and oxygen is essential for hydroxyl radical formation. One of the most important *in vitro* copper redox reactions is that of the Haber Weiss reaction type.^[118] It has also been determined that copper(I) salts will produce hydroxyl radicals with a greater rate constant than that of iron(II) salts.^[119] This is pertinent as copper(II) is reduced in the bleomycin type reactions to copper(I) as per the Haber-Weiss reaction^[44] in order to become active and bleomycin is naturally found to use iron(II) as its metal of chelation^[32]. Hydroxyl radicals are highly reactive and will thus react with almost every type of molecule found in a living system, for

example DNA bases, phospholipids and amino acids.^[119] This type of reactivity would follow the mode of action of bleomycin suggested by Chen and Stubbe^[32].

These results also show that for a compound that generates hydroxyl radicals, having two or three copper(II) ions is evidently advantageous and favours more efficient generation of the cytotoxic agent. It would appear that the trinuclear copper(II) complexes are rather efficient hydroxyl radical generators and it could be expected that at least two of the three copper centres generate hydroxyl radicals simultaneously. This theory could prove highly significant and could possibly be proven by the synthesis of a methoxy derivative of the ligand and chelating it to copper(II) to possibly force a mononuclear complex for comparison in cytotoxicity. This is discussed further in the future work section of this work.

A few commercially available chemotherapeutic agents have been chosen to compare with the compounds synthesised and tested in this work. These compounds are cisplatin, 5-fluorouracil, vinblastine sulfate, etoposide and bleomycin. The IC_{50} values of each compound have been tabulated in **Table 7.2** for simplicity; however, each compound's average $-\log IC_{50}$ value has been graphically compared to the most active compound synthesised in this work, $[Cu_3(L^2)_2Cl_2(DMF)_2]$, for ease of comparison in the discussion. **Figure 7.5** shows the structure of cisplatin, 5-fluorouracil, etoposide and bleomycin.

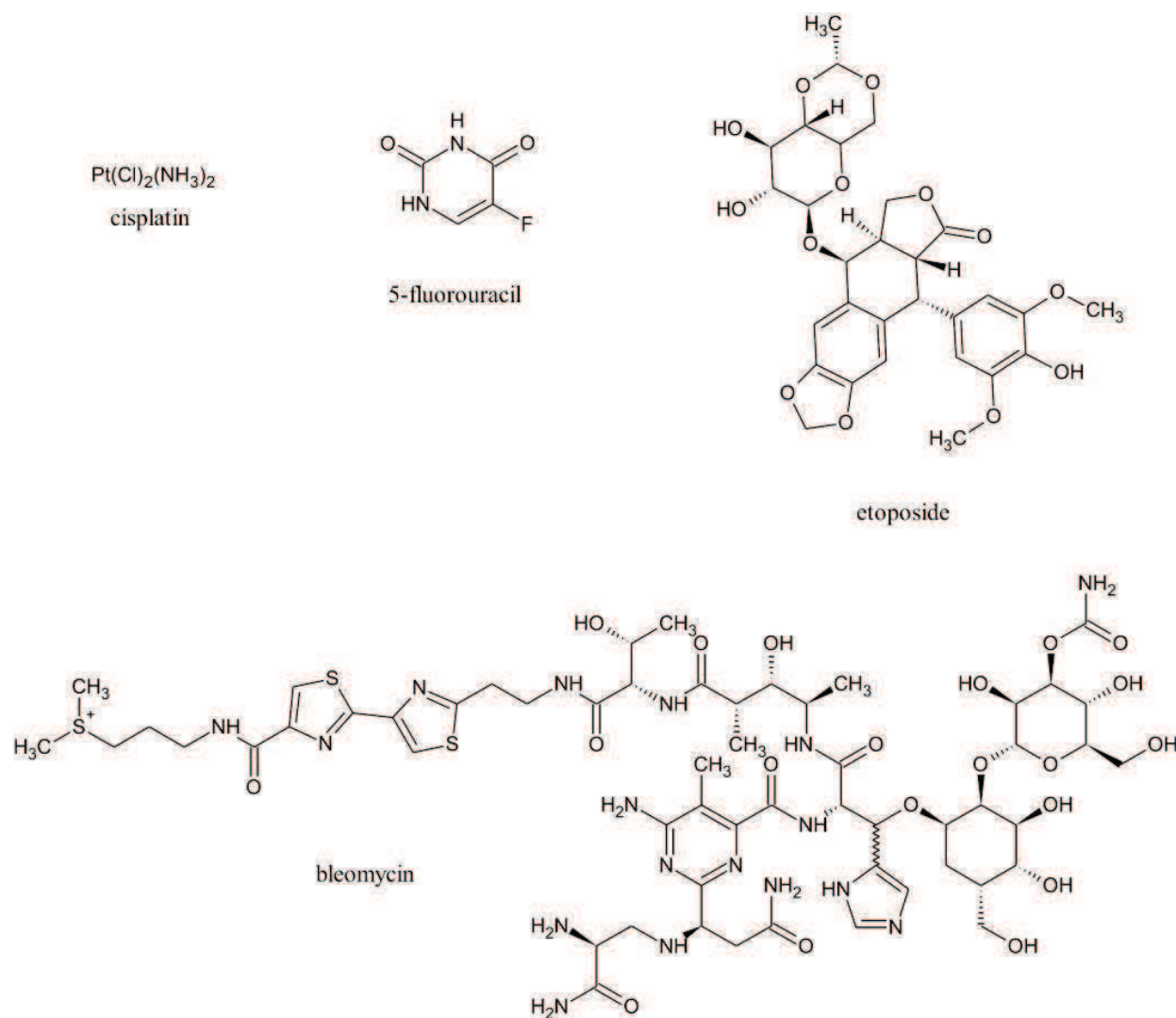


Figure 7.5: Structures of some commercially available chemotherapeutic agents.

A natural starting point is cisplatin, the most commonly known anti-cancer treatment. Cisplatin has been in use clinically since 1971^[120] and has been used for treating a wide range of cancers, the most important of these being testicular and ovarian cancer.^[120] Cisplatin is an alkylating agent and is available only as an infusion intravenously and not as a tablet.^[121] Unfortunately, it has become less useful due to its toxicity and the formation of resistance to its action.

5-Fluorouracil is used in a variety of cancer treatments, a few being breast cancer, ovarian cancer, colon and rectal cancer.^[121] 5-Fluorouracil is an anti-metabolite and is available as an

injection, infusion and topical ointment. 5-Fluorouracil has severe side effects in people with heart problems.

Etoposide is a made from the mandrake plant and is used in chemotherapy for a variety of cancers, a few being Hodgkin's and non-Hodgkin's lymphoma, testicular, prostate, lung and uterine cancer. Etoposide can be given as an infusion or in tablet form. If the compound escapes from the vein during treatment, tissue damage and blistering occurs.^[121] Etoposide also increases the chances of other secondary cancers developing as it can cause severe DNA damage.^[122] This is a good example of the fact that ultra high cytotoxicity is not always desirable. In many instances these high activity compounds have more side effects and damage non-cancerous tissue and in extreme cases can cause secondary tumours. This is one of the reasons cisplatin has remained in clinical use for so long, even though it is not as effective as a drug such as etoposide, since it offers a good balance between toxicity towards tumour cells and relatively unlethal side-effects for the patient. Thus having a lower toxicity than these commercial compounds (e.g. the present trinuclear copper complexes) is not necessarily problematic. Moderately cytotoxic compounds have a chemotherapeutic role in the longer term provided that non-specific cytotoxicity due to their mode of action as radical generators is not generally problematic.

Bleomycin is an anti-tumour antibiotic which is used in chemotherapy against squamous cell cancers, melanoma, sarcoma, Hodgkin's and non-Hodgkin's lymphoma, pleural effusion and most successfully, testicular cancer.^[121] Its comparison is of importance as the compounds screened in this project are bleomycin analogues. It can be given as an injection, infusion or as an interpleural injection. There is no tablet form of bleomycin. Most patients will suffer from hair loss and skin reactions. Bleomycin can cause vascular effects such as heart attack or stroke.^[121]

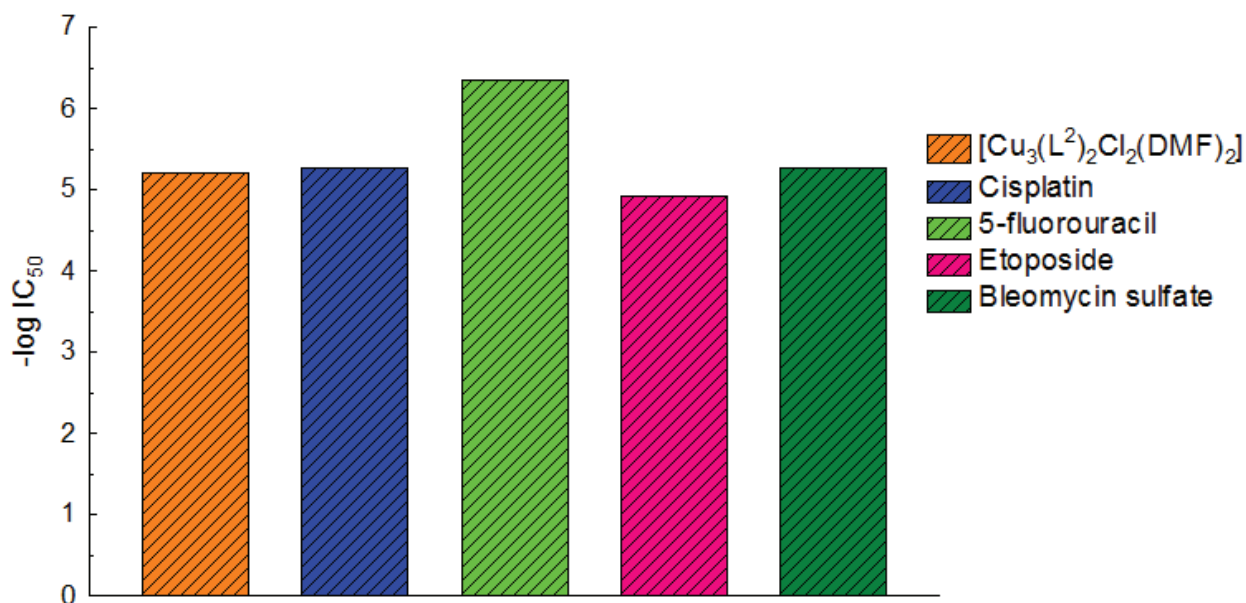


Figure 7.6: Comparison of $-\log IC_{50}$ values of $[Cu_3(L^2)_2Cl_2(DMF)_2]$, cisplatin, 5-fluorouracil, etoposide and bleomycin.

Figure 7.6 illustrates the averages of these compounds across the same four cell lines. The data illustrates that $[Cu_3(L^2)_2Cl_2(DMF)_2]$ compares well with the literature compounds. Note that no standard error data was supplied for the literature compounds by the National Cancer Institute (<http://dtp.nci.nih.gov/>). It has a similar potency to that of 5-fluorouracil and bleomycin sulphate with these compounds only having one-fold increased cytotoxicity. $[Cu_3(L^2)_2Cl_2(DMF)_2]$ shows a slightly higher averaged potency than that of etoposide, 6.1 μM versus 12 μM . These results show promise that the trinuclear copper(II) complexes may be useful as anti-cancer agents and should possibly be sent for further testing.

Shown in **Figure 7.7** is a graph of the literature copper(II) complexes (**Figure 7.3**) discussed in section 7.1 versus the most active copper(II) complex synthesised in this work, $[Cu_3(L^2)_2Cl_2(DMF)_2]$. The data compared are not completely equivalent as the cell lines used in each compound varies, however, for a basic comparison the data provided was utilised. **Figure 7.7** illustrates the average of $[Cu_3(L^2)_2Cl_2(DMF)_2]$ across four cell lines (**A549, Du145, HT-29, U251**); (1) was tested against mouse melanomal cell line B16F10; $[Cu(L^1)Cl]$, $[Cu(L^1)OAc]$ and $[Cu(HL^1)(L^1)OAc]$ against human leukemia Jurkat T and

compounds 1a-4b were averaged against the three human cancer cell lines; non-small lung (A549), ovarian cancer (CH1), and human colon adenocarcinoma (SW480) as calculated in Table 7.1.

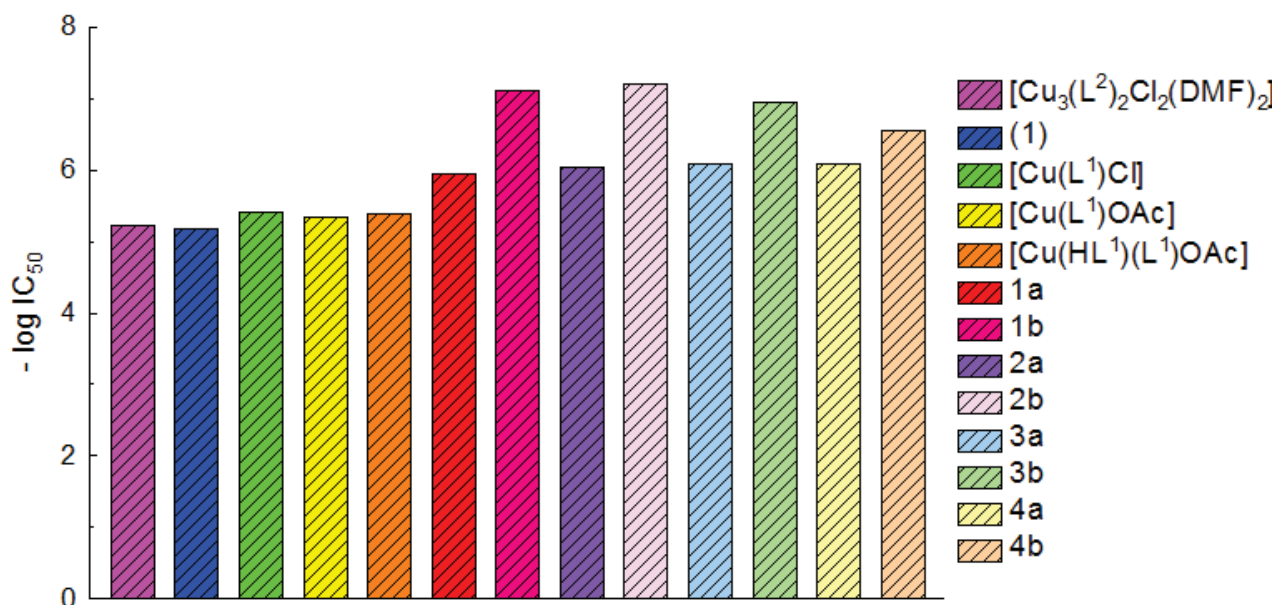


Figure 7.7: Comparison of [Cu₃(L²)₂Cl₂(DMF)₂] and literature copper(II) chelates.

The cytotoxicity of the copper(II) chelate synthesised in this work compares favourably with the copper(II) chelates synthesised by Gokhale *et al.*^[112] and Hindo *et al.*^[114]. The IC₅₀ values are very similar for these compounds however, all the compounds synthesised by Primik *et al.*^[115] are much more cytotoxic than [Cu₃(L²)₂Cl₂(DMF)₂]. Compounds 1a, 2a, 3a and 4a showed on average a seven-fold increase in cytotoxicity, whereas compounds 1b, 2b, 3b and 4b had an average of 63 times higher cytotoxicity. This does not take away from the fact that the copper(II) compounds of this work may be good candidates for further research as was mentioned before as lower cytotoxicity may mean fewer side effects as non-specific cytotoxicity due to their mode of action as radical generators may not be generally problematic.

7.4 Conclusions

As was expected the ligand showed no efficacy with an average IC_{50} value of $>50 \mu\text{M}$ across all four cell lines. The nickel(II) compounds synthesised in this work were not successful in producing significant IC_{50} values to be considered for further testing or development for anti-cancer treatment. This reflects the fact that they are redox inactive and unlikely to generate hydroxyl radicals. $[\text{Ni}(\text{L}^2)]$ had an average IC_{50} value of $>50 \mu\text{M}$ and $[\text{Ni}(\text{L}^3)]$ had an average IC_{50} value of $35(\pm 4) \mu\text{M}$ across all four cell lines. The copper(II) complexes show a low enough IC_{50} value to be considered for further development and testing in anti-cancer treatment. $[\text{Cu}_3(\text{L}^2)_2\text{Cl}_2(\text{DMF})_2]$ has the lowest average IC_{50} value of the copper(II) chelates, $6.1(\pm 1.6) \mu\text{M}$, followed by $[\text{Cu}_3(\text{L}^3)_2(\text{H}_2\text{O})_2]\text{Cl}_2$ with $6.9(\pm 0.85) \mu\text{M}$. A favourable comparison was made between the most active trinuclear copper(II) chelate and the literature compounds which further reinforces the need for development and further testing of these copper(II) chelates.

8. Future Work

8.1 Future Compounds

In a study done by Routier *et al.* ^[123] on metal salen complexes, a hydroxyl group was added at various positions on the ligands to study the effect on DNA cleavage. It was found that the cleavage activities of the compounds were dependent on the position of the hydroxyl group. The most effective of the three was the *para* isomer and then the *ortho* isomer; the *meta* isomer was found to be inactive (*ortho*, *meta* and *para* refer to the relative positions of the two hydroxyl groups of the ligands). If this logic is to be followed, the hydroxyl group on the ligand structures studied here could be rotated and the effect studied both structurally by X-ray diffraction and biologically through tumour cell cytotoxicity screening. The structures synthesised in this project have the hydroxyl positioned in the *meta* position which, according to the study done by Routier *et al.* ^[123], would be a deactivating position. Proposed structures are shown in **Figure 8.1**.

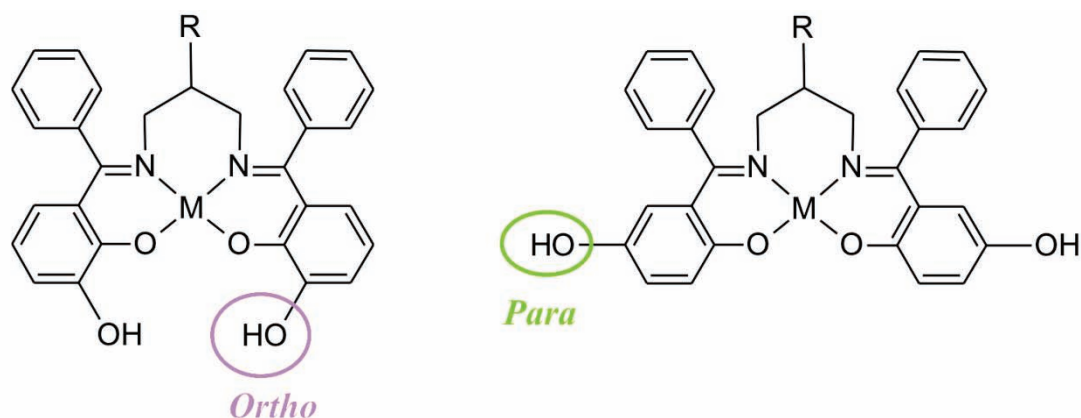


Figure 8.1: Proposed structure for hydroxyl group position rotations to the *ortho* and *para* positions.

A proposed synthesis for the starting material for use in the ligand synthesis is shown below in **Figure 8.2**. The synthesis is a three step reaction. ^[124] A Grignard reaction allows for the addition of the benzene ring to the benzaldehyde for the backbone of the ligands. An alcohol oxidation or Jones oxidation ^[125] to reform the carbonyl group; and finally, a methoxy

deprotection to form the dihydroxybenzophenone ligand system. Both 2,3-dimethoxy benzaldehyde^[126] (*ortho*) and 2,5-dimethoxybenzaldehyde^[127] (*para*) starting materials are readily available from Sigma-Aldrich. Once these products are formed the condensation reaction as discussed in **Chapter 3 (Figure 3.5)** can be followed to synthesise the ligand system desired.

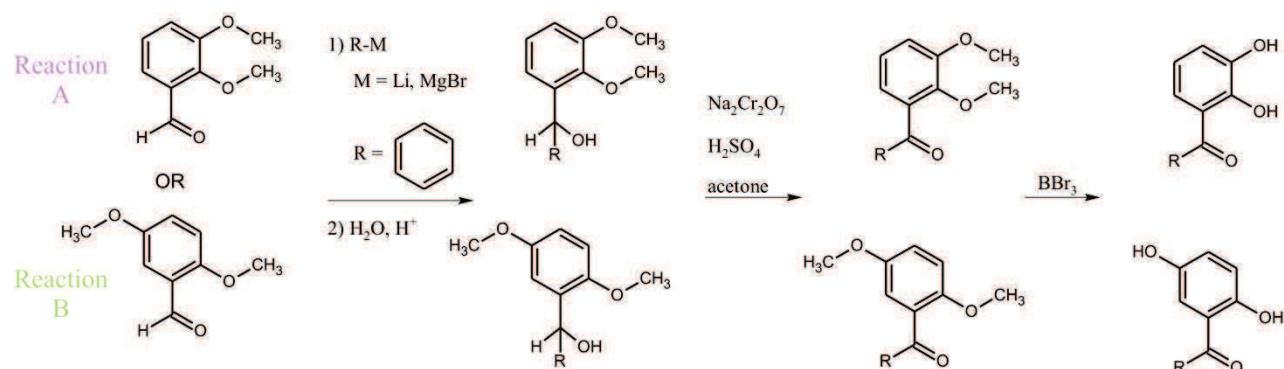


Figure 8.2: Proposed synthesis of the *ortho* and *para* dimethoxybenzophenones.

As these compounds are bleomycin analogues, their interaction with DNA must be studied. Due to solubility issues, titrations to determine the interaction of the compounds with DNA were not possible in the present thesis and so future work could be focused on increasing solubility of these compounds in solvents such as water. This will allow DNA binding studies to be conducted using UV-vis spectroscopy to follow the interaction. One such way would be to add an imidazole group, which would not only increase solubility but also permit an enhanced electrostatic interaction with DNA. The positive charge given by the imidazolium group would be attracted to the negative charge of the phosphate backbone in DNA; this allows for optimal positioning of the phenyl groups for intercalation. This concept was shown in a study on a non-Schiff base Cu(II) complex done by Pamatong *et al.*^[1] where the ligand structure was designed specifically with a positively charged ammonium group to interact with the DNA backbone. The efficiency of the compounds was attributed to both the aromatic regions and the cationic ammonium group on the molecule. Shown in **Figure 8.3** is a proposed structure for the inclusion of an imidazole functional group in the ligand.

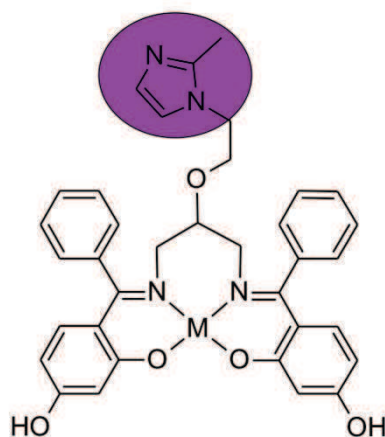


Figure 8.3: Proposed structure highlighting the inclusion of an imidazole functional group to the compounds synthesised in this project.

A proposed synthetic route for addition of imidazole is shown in **Figure 8.5**. To synthesise the ligand for the proposed structure, the 1,3-diamino-2-hydroxypropane must be di-*tert*-butyl dicarbonate protected. This is easily synthesised by the addition of di-*tert*-butyl dicarbonate to the diamine as shown in **Figure 8.4**. A biphasic mixture of potassium hydroxide and dichloromethane (DCM) is used to deprotonate the hydroxyl group in the presence of the imidazole and thus the SN2 reaction will occur allowing for the formation of the stable ether derivative. The amine groups can then be deprotected and reacted as normal with the benzophenone. At pH 7 the imidazole group will be present predominantly as its imidazolium form and give the cationic derivative necessary for DNA interaction.

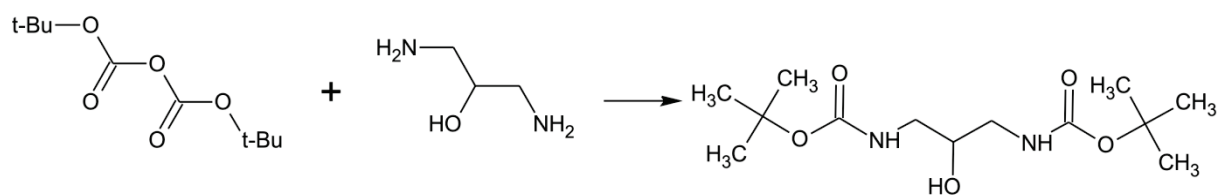


Figure 8.4: Protection of amine groups with t-Boc.

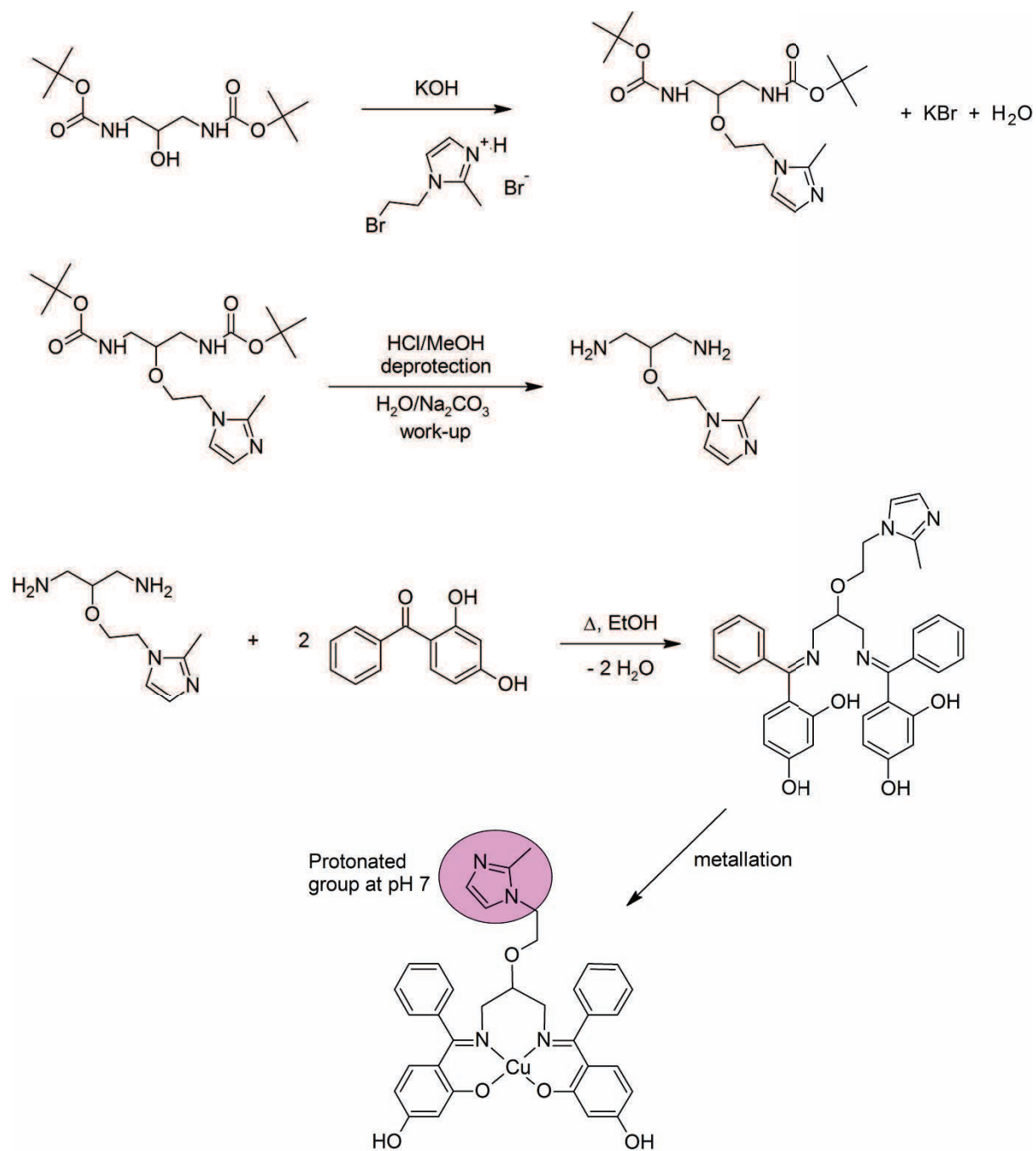


Figure 8.5: Synthetic route for addition of an imidazole group.

Biotin tagging of compounds is becoming popular in targeted drug design research as it is believed to be a way to target cancer cells.^[128-129] Cancer cells are rapidly proliferating and so therefore require more of certain vitamins. Biotin is one of those vitamins as it is used in growth and development of cells.^[128-129] The biotin tag can be synthetically attached using the

same synthetic route followed in **Figure 8.4** and **Figure 8.5** using a commercially available biotinylation agent. The biotinylation agent and product are shown in **Figure 8.6**.

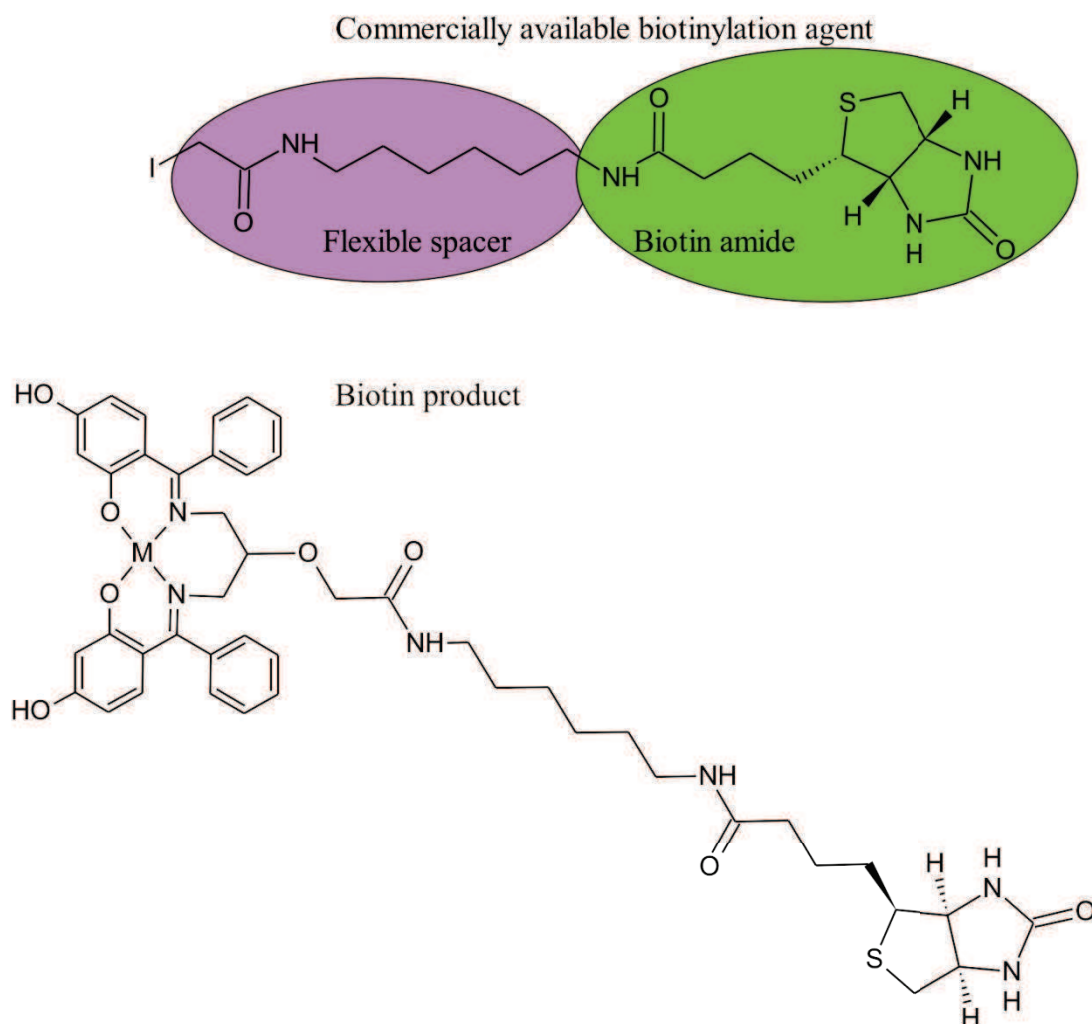


Figure 8.6: Biotinylation agent and product for biotin tagging.

However, it has been suggested that this method of cell targeting has its limitations. Two examples of such limitations^[129] would be minimal drug delivery and one drug molecule per biotin molecule. And the latter is problematic as these biotin-drug molecules are small enough to be excreted by the kidney and reabsorbed in proximal tubules which could lead to accumulation in the kidney which could be toxic. Therefore research has widened to include biotin polymeric carrier systems. One such system is that of dendrimers. Dendrimers are three dimensional macromolecules that can enclose hydrophobic molecules in a cavity

while the exterior can be altered to enhance solubility.^[128] Yang *et al.*^[128] and Yellepeddi *et al.*^[129] studied polyamidoamine (PAMAM) dendrimers. Yellepeddi *et al.*^[129] found that by biotin tagging the PAMAM dendrimer, it increased the intake of the dendrimer by human ovarian cancer cells by 12% with respect to human embryonic kidney cells. Yang *et al.*^[128] also found that by biotin tagging the dendrimer, it increased its uptake. This would be a preferable method to use for the compounds synthesised in this project as they have been found to be hydrophobic. **Figure 8.7** is an illustration of the conjugation of a PAMAM dendrimer to biotin as suggested by Yellepeddi *et al.*^[129].

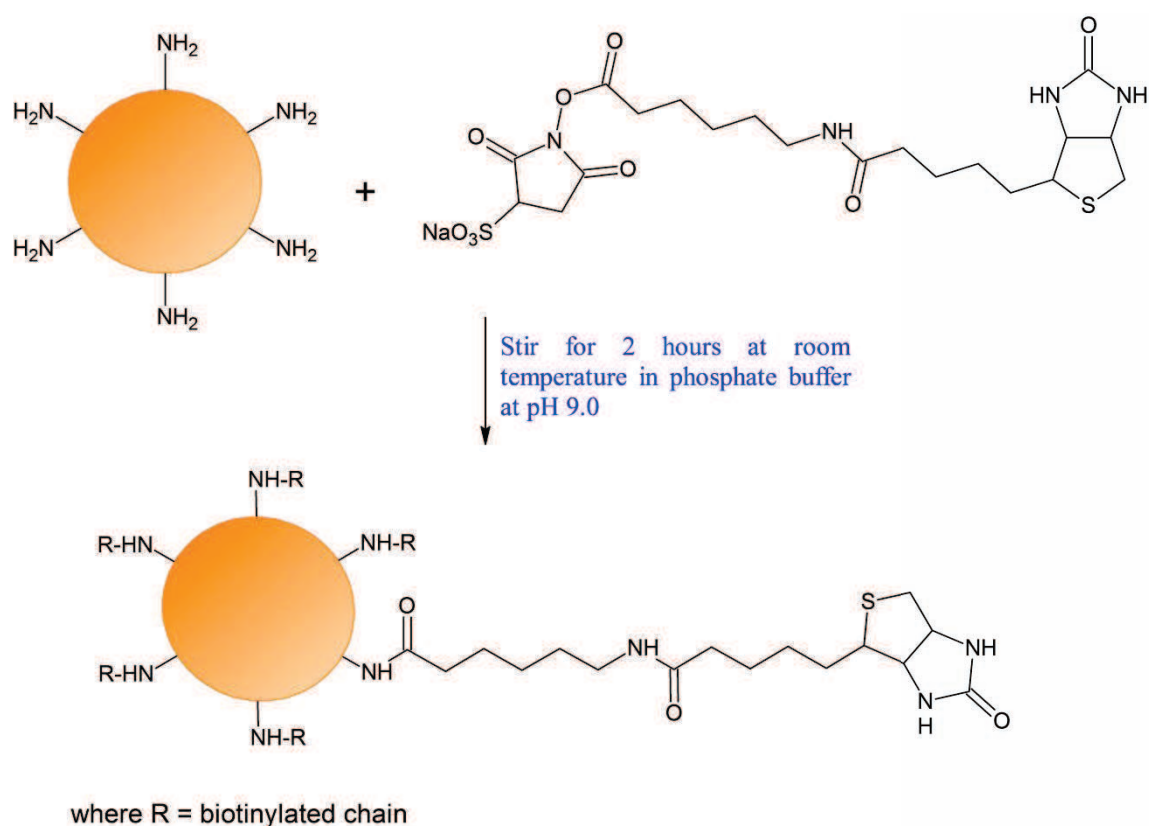


Figure 8.7: Conjugation of biotin to a PAMAM dendrimer.

These examples show a few of the possible directions this research could take. Some of these changes could potentially transform the metal chelates from moderately cytotoxic compounds to more powerful ones.

An alternative ligand prepared from 2,4-dimethoxybenzaldehyde (commercially available from Sigma-Aldrich^[130]) may prevent the formation of a trinuclear copper(II) complex and allow the synthesis of the mononuclear complex shown in **Figure 8.8**. This chelate could be evaluated in a manner similar to that of the analogous trinuclear complex and a comparison of the cytotoxicity profiles can be made on the basis of the number of metal ions in the complex.

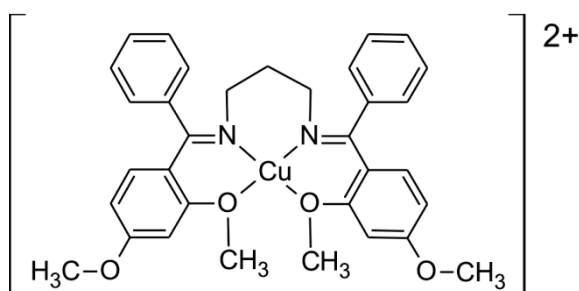


Figure 8.8: Methylated mononuclear copper(II) compound.

A key advantage of the structure shown in **Figure 8.8** is that not only would formation of trinuclear species be thwarted by the methoxy groups, but the complex carries a +2 charge and would thus be a highly soluble complex capable of electrostatically targeting the anionic poly(phosphate) backbone of dsDNA.

9 Conclusions

The aim of the project was to synthesise a range of novel complexes that were bleomycin analogues with the intention of evaluating them as anti-cancer agents. The intention was to mimic the mode of action of bleomycin in order to cleave double-stranded DNA. Three novel ligands were synthesised and characterised, two of these were studied by X-ray diffraction. Using these three ligands, six metal complexes were synthesised and characterised - by NMR, IR, EPR/ESR and UV/visible spectroscopy as well as single crystal X-ray crystallography. Six of these complexes were studied by X-ray diffraction.

Both ligands crystallised as zwitterions in monoclinic space groups. This was indicative of the imine nitrogen atom being more basic than the hydroxyl group which results in the hydroxyl proton migrating to the nitrogen of the imine bond, thus creating a negatively charged oxygen atom and a positively charged imine nitrogen atom. The nickel(II) complexes adopted the expected square planar coordination geometry (N_2O_2 donor set) with Ni-N and Ni-O average distances of 1.892(3) Å and 1.845(2) Å, respectively. The copper(II) and zinc(II) complexes, however, favoured formation of multinuclear complexes *via* bridging of ionised oxygen donor atoms. The mean Cu-N and Cu-O distances were 1.953(3) Å and 2.082(3) Å, respectively. The averages for the Zn-N and Zn-O distances were 2.074(3) Å and 2.042(3) Å, respectively.

The ESR data for $[Cu_3(L^2)_2Cl_2(DMF)_2]$ and $[Cu_3(L^3)_2(H_2O)_2]Cl_2$, showed two antiferromagnetically coupled copper(II) ions which left the third copper(II) as an $S = \frac{1}{2}$ centre with hyperfine coupling constant to the $I = \frac{3}{2}$ Cu nucleus of *ca.* 76 G. In DMF solution, super-hyperfine coupling (*ca.* 12 G) was found to occur to two nitrogen atoms which is consistent with the donor atom set of the terminal copper(II) centres being the site of the unpaired spin density.

Density functional theory was used to calculate the lowest-energy, optimised structure as well as the electronic transition and infrared spectra of the mononuclear nickel(II) complexes. The

simulations produced structures for $[\text{Ni}(\text{L}^2)]$ and $[\text{Ni}(\text{L}^3)]$ with similarity coefficients of 0.982 and 0.990, respectively. Both the calculated electronic spectra and the infrared spectra compared favourably with the experimental data.

One ligand and the copper(II) and nickel(II) complexes were sent to MINTEK (Project AuTEK) for anti-cancer screening. The biological studies of each compound showed a lower activity than was expected, however this leaves room for further structure-based design modifications. The trinuclear copper(II) complexes, $[\text{Cu}_3(\text{L}^2)_2\text{Cl}_2(\text{DMF})_2]$ and $[\text{Cu}_3(\text{L}^3)_2(\text{H}_2\text{O})_2]\text{Cl}_2$, the bleomycin analogues that are capable of generating hydroxyl radicals, had IC_{50} values of 6(2) and 7(1) μM , respectively. The complexes $[\text{Ni}(\text{L}^2)]$ and $[\text{Ni}(\text{L}^3)]$ were comparatively inactive with mean IC_{50} values of >50 and 35(16) μM , respectively. This is consistent with the fact that they do not readily generate reactive oxygen species in a cellular environment.

10. References

- [1] F. V. Pamatong, C. A. Detmer and J. R. Bocarsly, *Journal of the American Chemical Society* **1996**, *118*, 5339-5345.
- [2] J. Zander, in *Native_Copper_Macro_Digon3.jpg*, (2012, July 06), Wikipedia, Wikimedia Foundation, inc, **2009**, <http://en.wikipedia.org/wiki/File:NatCopper.jpg>.
- [3] E. Hutchinson, *Chemistry: the Elements and Their Reactions*, W. B. Saunders Company, **1959**, p. 717.
- [4] F. A. Cotton, G. Wilkinson and P. L. Gaus, *Basic Inorganic Chemistry*, John Wilkinson & Sons, INC., **1995**, p. 838.
- [5] E. de Barry Barnett and C. L. Wilson, *Inorganic Chemistry: A Textbook for Advanced Students*, Longmans, Green and Co LTD, **1959**, p. 599.
- [6] D. F. Shriver and P. W. Atkins, *Inorganic Chemistry*, Oxford University Press, **1999**, p. 763.
- [7] Materialschemist, in *Nickel_chunk.jpg*, (2012, July 06), Wikipedia, Wikimedia Foundation, inc, **2009**, http://en.wikipedia.org/wiki/File:Nickel_chunk.jpg.
- [8] R. K. Thauer, G. Diekert and P. Schönheit, *Trends in Biochemical Science* **1980**, *5*, 304-306.
- [9] C. Holliger, A. J. Pierik, E. J. Reijerse and W. R. Hagen, *Journal of the American Chemical Society* **1993**, *115*, 5651-5656.
- [10] M. Anke, L. Angelow, M. Gleis, M. Müller and H. Illing, *Fresenius' Journal of Analytical Chemistry* **1995**, *352*, 92-96.
- [11] M. Cempel and G. Nickel, *Polish Journal of Environ. Stud.* **2006**, *15*, 375-382.
- [12] L. Mao, K. Yamamoto, W. Zhou and L. Jin, *Electroanalysis* **2000**, *12*, 72-77.
- [13] S. Kumar, D. Nath Dhar and P. N. Sexana, *Journal of Scientific and Industrial Research* **2009**, *68*, 181-187.
- [14] M. Kabak, A. Elmali, Y. Elerman and I. Svoboda, *Zeitschrift für Naturforschung* **2003**, *58b*, 1141-1146.
- [15] H.-H. Yao, W.-T. Huang, J.-M. Lo, F.-L. Liao and P. Chattopadhyay, *Journal of Coordination Chemistry* **2005**, *58*, 975-984.
- [16] P. Roy and M. Manassero, *Dalton Transactions* **2010**, *39*, 1539-1545.
- [17] H. H. A. Dollwett and J. R. J. Sorenson, *Trace Elements in Medicine* **1985**, *2*, 80-87.

- [18] P. Y. Bruice, *Organic Chemistry*, Pearson Education, Inc., **2007**, p. 1319.
- [19] T. L. Brown, J. LeMay, H. Eugene, B. E. Bursten and C. J. Murphy, *Chemistry The Central Science*, Pearson Prentice Hall, **2006**, p. 1127.
- [20] J. Clayden, N. Greeves, S. Warren and P. Wothers, *Organic Chemistry*, Oxford University Press, **2007**, p. 1512.
- [21] S. Trzaska, *C&EN News* **2002**, 83.
- [22] J. Reedijk, *Pure and Applied Chemistry* **1987**, 59, 181-192.
- [23] S. Striegler and M. G. Gichinga, *Chemical Communications* **2008**, 5930-5932.
- [24] A. Arola-Arnal, J. Benet-Buchholz, S. Neidle and R. Vilar, *Inorganic Chemistry* **2008**, 47, 11910-11919.
- [25] D. Cairns, R. J. Anderson, P. J. Perry and T. C. Jenkins, *Current Pharmaceutical Design* **2002**, 8, 2491-2504.
- [26] J. Cuesta, M. A. Read and S. Neidle, *Mini Reviews in Medicinal Chemistry* **2003**, 3, 11-21.
- [27] A. De Cian, L. Lacroix, C. Douarre, N. Temime-Smaali, C. Trentesaux, J.-F. Riou and J.-L. Mergny, *Biochimie* **2008**, 90, 131-155.
- [28] L. R. Kellend, *European Journal of Cancer* **2005**, 41, 971-979.
- [29] J.-L. Mergny and C. Hélène, *Nature Medicine* **1998**, 4, 1366-1367.
- [30] E. M. Rezler, D. J. Bearss and L. H. Hurley, *Current Opinion in Pharmacology* **2002**, 2, 415-423.
- [31] E. M. Rezler, D. J. Bearss and L. H. Hurley, *Annual Review of Pharmacology and Toxicology* **2003**, 43, 359-379.
- [32] J. Chen and J. Stubbe, *Nature Reviews Cancer* **2005**, 5, 102-112.
- [33] R. T. Dorr, *Seminars in Oncology* **1992**.
- [34] S. M. Hecht, *Journal of Natural Products* **2000**, 63, 158-168.
- [35] Y. Hashimoto, H. Iijima, Y. Nozaki and K. Shudo, *Biochemistry* **1986**, 25, 5103-5110.
- [36] A. T. Abraham, X. Zhou and S. M. Hecht, *Journal of the American Chemical Society* **2001**, 123, 5167-5175.
- [37] J. Chen, X. Wang, Y. Shao, J. Zhu, Y. Zhu, Y. Li, Q. Xu and Z. Guo, *Inorganic Chemistry* **2007**, 46, 3306-3312.
- [38] F. Mancin, P. Scrimin, P. Tecilla and U. Tonellato, *Journal of the Chemical Society, Chemical Communications* **2005**, 2540-2548.
- [39] S. Hashimoto, B. Wang and S. M. Hecht, *Journal of the American Chemical Society* **2001**, 123, 7437-7438.

- [40] J. C. Wu, J. W. Kozarich and J. Stubbe, *Biochemistry* **1985**, *24*, 7562-7568.
- [41] L. F. Povirk, M. Hogan and N. Dattagupta, *Biochemistry* **1979**, *18*, 96-101.
- [42] I. Detmer, Charles A., F. V. Pamatong and J. R. Bocarsly, *Inorganic Chemistry* **1996**, *35*, 6292-6298.
- [43] G. Buonocore, S. Perrone and M. L. Tataranno, *Seminars in Fetal & Neonatal Medicine* **2010**, *15*, 186-190.
- [44] J. P. Kehrer, *Toxicology* **2000**, *149*, 43-50.
- [45] J. Stieglitz and P. N. Leech, *Journal of the American Chemical Society* **1914**, *36*, 272-301.
- [46] M. B. Smith and J. March, *March's Advanced Organic Chemistry: Reactions, Mechanisms, and Structure*, John Wiley & Sons, Inc, **2001**, p. 2101.
- [47] C. J. Cooper, M. D. Jones, S. K. Brayshaw, B. Sonnex, M. L. Russell, M. F. Mahon and D. R. Allan, *Journal of the Chemical Society, Dalton Transactions* **2011**, *40*, 3677-3682.
- [48] A. A. Osowole, *E-Journal of Chemistry* **2008**, *5*, 130-135.
- [49] B. Dede, F. Karipcin and M. Cengiz, *Journal of Hazardous Materials* **2009**, *163*, 1148-1156.
- [50] D. L. Pavia, G. M. Lampman and G. S. Kriz, *Introduction to Spectroscopy: A Guide for Students of Organic Chemistry*, Brookes/Cole Thomson Learning, United States of America, **2001**, p. 579.
- [51] P. Atkins and J. de Paula, *Atkins' Physical Chemistry*, Oxford University Press, New York, **2006**, p. 1064.
- [52] R. S. Downing and F. L. Urbach, *Journal of the American Chemical Society* **1969**, *91*, 5977-5983.
- [53] C. J. Hipp and J. W. A. Baker, *Journal of the American Chemical Society* **1970**, *92*, 792-798.
- [54] S. Chandra, D. Jain, A. K. Sharma and P. Sharma, *Molecules* **2009**, *14*, 174-190.
- [55] J. F. Michalec, S. A. Bejune, D. C. Cuttell, G. C. Summerton, J. A. Gertenbach, J. S. Field, R. J. Haines and D. R. McMillin, *Inorganic Chemistry* **2001**, *40*, 2193.
- [56] R. Klement, F. Stock, H. Elias, H. Paulus, P. Pelikán, M. Valko and M. Mazúr, *Polyhedron* **1999**, *18*, 3617-3628.
- [57] D. K. Crites Tears and D. R. McMillin, *Coordination Chemistry Reviews* **2001**, *211*, 195.
- [58] K. A. Jamshid, M. Asadi and A. H. Kianfar, *Journal of Coordination Chemistry* **2009**, *62*, 1187-1198.

- [59] B. S. Garg and D. N. Kumar, *Spectrochimica Acta Part A* **2003**, *59*, 229-234.
- [60] R. Pagadala, P. Ali and J. S. Meshram, *Journal of Coordination Chemistry* **2009**, *62*, 4009-4017.
- [61] S.-L. Zheng and X.-M. Chen, *Australian Journal of Chemistry* **2004**, *57*, 703-712.
- [62] H. Günzler and H.-U. Gremlich, *IR Spectroscopy An Introduction*, Wiley-VCH, **2002**, p. 361.
- [63] A. Lund, M. Shiotani and S. Shimada, *Principles and Applications of ESR Spectroscopy*, Springer, New York, **2011**, p. 461.
- [64] C. Bovet and A. R. Barron, in *EPR Spectroscopy: An Overview*, (2012, June 14), Connexions, Houston, Texas, **2009**, <http://cnx.org/content/m22370/1.3/>.
- [65] J. Losada, I. del Peso and L. Beyer, *Inorganica Chimica Acta* **2001**, *321*, 107-115.
- [66] L. Dyers Jr., S. Y. Que, D. VanDerveer and X. R. Bu, *Inorganica Chimica Acta* **2006**, *359*, 197-203.
- [67] V. B. Arion, P. Rapta, J. Telser, S. S. Shova, M. Breza, K. Lušpai and J. Kožišek, *Inorganic Chemistry* **2011**, *50*, 2918-2931.
- [68] J. Peisach and W. E. Blumberg, *Archives of Biochemistry and Biophysics* **1974**, *165*, 691-708.
- [69] J. Balla, P. V. Bernhardt, P. Buglyo, P. Comba, T. W. Hambley, R. Schmidlin, S. Stebler and K. Várnagy, *Journal of the Chemical Society, Dalton Transactions* **1993**, 1143-1149.
- [70] E. K. Efthimiadou, H. Thomadaki, Y. Sanakis, C. P. Raptopoulou, N. Katsaros, A. Scorilas, A. Karaliota and G. Psomas, *Journal of Inorganic Biochemistry* **2007**, *101*, 64-73.
- [71] T. Yu, W. Su, W. Li, Z. Hong, R. Hua, M. Li, B. Chu, B. Li, Z. Zhang and Z. Z. Hu, *Inorganica Chimica Acta* **2006**, *359*, 2246-2251.
- [72] Cambridge Crystallographic Data Centre, CSDS
- [73] R. S. Black, D. G. Billing, A. Bartyzel and E. Cukrowska, *Acta Crystallographica, Section E: Structure Reports Online* **2010**, *66*, o1002.
- [74] A. Datta, C. R. Choudhury, P. Talukder, S. Mitra, L. Dahlenburg and T. Matsushita, *Journal of Chemical Research* **2003**, 642.
- [75] A. Ray, S. Banerjee, G. M. Rosair, V. Gramlich and S. Mitra, *Structural Chemistry* **2008**, *19*, 459-465.
- [76] Oxford Diffraction Ltd., 170, CrysAis CCD and CrysAlis RED, 2002.
- [77] R. H. Blessing, *Acta Cryst* **1995**, *A51*, 33-38.
- [78] L. J. Farrugia, *J. Appl. Crystallogr.* **1999**, 32.

- [79] G. M. Sheldrick, *SHELXS-97, Program for solution of crystal structures*, University of Gottingen, Germany, **1997**, p.
- [80] G. M. Sheldrick, *SHELXS-97, Program for refinement of crystal structures*, University of Gottingen, Germany, **1997**, p.
- [81] Bruker, Bruker AXS Inc., SAINT, 2007.
- [82] R. H. Blessing, *Acta Crystallographica Section A: Foundations of Crystallography* **1995**, *A51*, 33-38.
- [83] in *International Union of Crystallographic, CheckCIF*, <http://www.iucr.org/>.
- [84] T. Steiner, *Angewandte Chemie International Edition* **2002**, *41*, 48-76.
- [85] A. L. Speck, PLATON, A Multipurpose Crystallographic Tool, 2005.
- [86] D. Venkataraman, Y. Du, S. R. Wilson, K. A. Hirsch, P. Zhang and J. S. Moore, *Journal of Chemical Education* **1997**, *74*, 915-918.
- [87] J. Reglinski, S. Morris and D. E. Stevenson, *Polyhedron* **2002**, *21*, 2175-2182.
- [88] B. Dutta, P. Bag, U. Flörke and K. Nag, *Inorganic Chemistry* **2005**, *44*, 147-157.
- [89] C. J. Cramer, *Essentials of Computational Chemistry: Theories and Models*, John Wiley & Sons, Inc., West Sussex, **2004**, p. 596.
- [90] D. C. Young, *Computational Chemistry: A Practical Guide for Applying Techniques to Real World Problems*, John Wiley & Sons, Inc., New York, **2001**, p. 370.
- [91] S. Salehzadeh, R. Golbedaghi and H. R. Khavasi, *Journal of Coordination Chemistry* **2009**, *62*, 2532-2539.
- [92] P. J. Hay and W. R. Wadt, *Journal of Chemical Physics* **1985**, *82*, 270-283.
- [93] K. D. Dobbs and W. J. Hehre, *Journal of Computational Chemistry* **1987**, *8*, 880-893.
- [94] P. C. Hariharan and J. A. Pople, *Theoretica Chimica Acta* **1973**, *28*, 213-222.
- [95] A. Trujillo, M. Fuentealba, D. Carrillo, C. Manzur, I. Ledoux-Rak, J.-R. Håmon and J.-Y. Saillard, *Inorganic Chemistry* **2010**, *49*, 2750-2764.
- [96] Vrijie Universiteit, Amsterdam Density Functional (ADF) program, 2005.
- [97] S. Chandra, Ruchi, K. Qanungo and S. K. Sharma, *Spectrochimica Acta Part A* **2011**, *79*, 1326-1330.
- [98] J. J. P. Stewart, Stewart Computational, Chemistry, 7.334W, MOPAC, 2007.
- [99] T.-P.-A. Cao, S. Labouille, A. Auffrant, Y. Jean, X. F. Le Goff and P. Le Floch, *Dalton Transactions* **2011**, *40*, 10029-10037.
- [100] M. J. Frisch, G. W. Trucks, H. B. Schlegel, G. E. Scuseria, M. A. Robb, J. R. Cheeseman, J. Montgomery, J. A. , T. Vreven, K. N. Kudin, J. C. Burant, J. M. Millam, S. S. Iyengar, J. Tomasi, V. Barone, B. Mennucci, M. Cossi, G. Scalmani, N. Rega, G. A.

Petersson, H. Nakatsuji, M. Hada, M. Ehara, K. Toyota, R. Fukuda, J. Hasegawa, M. Ishida, T. Nakajima, Y. Honda, O. Kitao, H. Nakai, M. Klene, X. Li, J. E. Knox, H. P. Hratchian, J. B. Cross, V. Bakken, C. Adamo, J. Jaramillo, R. Gomperts, R. E. Stratmann, O. Yazyev, A. J. Austin, R. Cammi, C. Pomelli, J. W. Ochterski, P. Y. Ayala, K. Morokuma, G. A. Voth, P. Salvador, J. J. Dannenberg, V. G. Zakrzewski, S. Dapprich, A. D. Daniels, M. C. Strain, O. Farkas, D. K. Malick, A. D. Rabuck, K. Raghavachari, J. B. Foresman, J. V. Ortiz, Q. Cui, A. G. Baboul, S. Clifford, J. Cioslowski, B. B. Stefanov, G. Liu, A. Liashenko, P. Piskorz, I. Komaromi, R. L. Martin, D. J. Fox, T. Keith, M. A. Al-Laham, C. Y. Peng, A. Nanayakkara, M. Challacombe, P. M. W. Gill, B. Johnson, W. Chen, M. W. Wong, C. Gonzalez and J. A. Pople, Gaussian, Inc., Revision C.02, Gaussian 03, 2004.

[101] A. D. Becke, *Journal of Chemical Physics* **1993**, *98*, 5648-5662.

[102] J. P. Perdew and Y. Wang, *Physical Review. B: Condensed Matter* **1992**, *45*, 13244-13249.

[103] L. E. Roy, P. J. Hay and R. L. Martin, *Journal of Chemical Theory and Computation* **2008**, *4*.

[104] M. J. Frisch, G. W. Trucks, H. B. Schlegel, G. E. Scuseria, M. A. Robb, J. R. Cheeseman, G. Scalmani, V. Barone, B. Mennucci, G. A. Petersson, H. Nakatsuji, M. Caricato, X. Li, H. P. Hratchian, A. F. Izmaylov, J. Bloino, G. Zheng, J. L. Sonnenberg, M. Hada, M. Ehara, K. Toyota, R. Fukuda, J. Hasegawa, M. Ishida, T. Nakajima, Y. Honda, O. Kitao, H. Nakai, T. Vreven, J. J. A. Montgomery, J. E. Peralta, F. Ogliaro, M. Bearpark, J. J. Heyd, E. Brothers, K. N. Kudin, V. N. Staroverov, R. Kobayashi, J. Normand, K. Raghavachari, A. Rendell, J. C. Burant, S. S. Iyengar, J. Tomasi, M. Cossi, N. Rega, J. M. Millam, M. Klene, J. E. Knox, J. B. Cross, V. Bakken, C. Adamo, J. Jaramillo, R. Gomperts, R. E. Stratmann, O. Yazyev, A. J. Austin, R. Cammi, C. Pomelli, J. W. Ochterski, R. L. Martin, K. Morokuma, V. G. Zakrzewski, G. A. Voth, P. Salvador, J. J. Dannenberg, S. Dapprich, A. D. Daniels, O. Farkas, J. B. Foresman, J. V. Ortiz, J. Cioslowski and D. J. Fox, Gaussian, Inc., Revision A.1, Gaussian 09, 2009.

[105] T. H. Dunning Jr. and P. J. Hay, in *Modern Theoretical Chemistry, Ed. H. F. Schaefer III* **1976**, *3*, 1-28.

[106] P. J. Hay and W. R. Wadt, *Journal of Chemical Physics* **1985**, *82*, 299-310.

[107] W. R. Wadt and P. J. Hay, *Journal of Chemical Physics* **1985**, *82*, 284-298.

[108] R. Dennington, T. Keith and J. Millam, Semichem Inc., 5.0.9, GaussView 5.0.9, 2009.

[109] M.-W. Wang, X. Hao and K. Chen, *Philosophical Transactions of The Royal Society B* **2007**, *362*, 1093-1105.

- [110] C. Marzano, M. Pellei, F. Tisato and C. Santini, *Anti-Cancer Agents in Medicinal Chemistry* **2009**, *9*, 185-211.
- [111] I. Iakovidis, I. Delimaris and S. M. Piperakis, *Molecular Biology International* **2011**, 1-13.
- [112] N. H. Gokhale, S. S. Padhye, S. B. Padhye, C. E. Anson and A. K. Powell, *Inorganica Chimica Acta* **2001**, *319*, 90-94.
- [113] P. F. Predki and B. Sarkar, *The Journal of Biological Chemistry* **1992**, *267*, 5842-5846.
- [114] S. S. Hindo, M. Frezza, D. Tomco, M. J. Heeg, L. Hryhorczuk, B. R. McGarvey, Q. Ping Dou and C. N. Verani, *European Journal of Medicinal Chemistry* **2009**, *44*, 4353-4361.
- [115] M. F. Primik, S. Göschl, M. A. Jakupec, A. Roller, B. K. Keppler and V. B. Arion, *Inorganic Chemistry* **2010**, *49*, 11084-11095.
- [116] OriginLab Corporation, in *OriginLab Data Analysis and Graphing Software*, (2012, June 07), OriginLab Corporation,, Northhampton, **2012**, <http://www.originlab.com/>.
- [117] D. S. Sigman, D. R. Graham, V. D'Aurora and A. M. Stern, *The Journal of Biological Chemistry* **1979**, *254*, 12269-12272.
- [118] Sigma-Aldrich, in *Sigma-Aldrich*, (2012, April 18), Sigma-Aldrich,, South Africa, **2012**, <http://www.sigmaaldrich.com/life-science/cell-culture/learning-center/media-expert/copper.html>.
- [119] B. Halliwell and J. M. C. Gutteridge, *Biochemical Journal* **1984**, *219*, 1-14.
- [120] O. Rixe, W. Ortuzar, M. Alvarez, R. Parker, E. Reed, K. Paull and T. Fojo, *Biochemical Pharmacology* **1996**, *52*, 1855-1865.
- [121] The Cleveland Clinic Foundation, in *Chemocare.com, Care During Chemotherapy and Beyond* (2012, April 18), Scott Hamilton CARES initiative,, Cleveland, Ohio, **2005**, <http://www.chemocare.com/>.
- [122] National Institutes of Health, in *MedlinePlus Trusted Health Information for You*, (2012, April 18), National Institutes of Health,, Bethesda, Maryland, **2012**, <http://www.nlm.nih.gov/medlineplus/medlineplus.html>.
- [123] S. Routier, H. Vezin, E. Lamour, J.-L. Bernier, J.-P. Catteau and C. Bailly, *Nucleic Acids Research* **1999**, *27*, 4160-4166.
- [124] M. Albrecht, S. Mirtschin, M. de Groot, I. Janser, J. Runsink, G. Raabe, M. Kogej, C. A. Schalley and R. Fröhlich, *Journal of the American Chemical Society* **2005**, *127*, 10371-10387.
- [125] I. Heilbron, E. R. H. Jones and F. Sondheimer, *Journal of the Chemical Society* **1949**, 604-607.

- [126] Sigma-Aldrich, **(2012)**, *2,3-dimethoxybenzaldehyde*, D130206.
- [127] Sigma-Aldrich, **(2012)**, *2,5-dimethoxybenzaldehyde*, D130605.
- [128] W. Yang, Y. Cheng, T. Xu, X. Wang and L.-P. Wen, *European Journal of Medicinal Chemistry* **2009**, *44*, 862-868.
- [129] V. K. Yellepeddi, A. Kumar and S. Palakurthi, *Anticancer Research* **2009**, *29*, 2933-2944.
- [130] Sigma-Aldrich, **(2012)**, *2,4-dimethoxybenzaldehyde*, D130400.

Appendix A: NMR Spectra

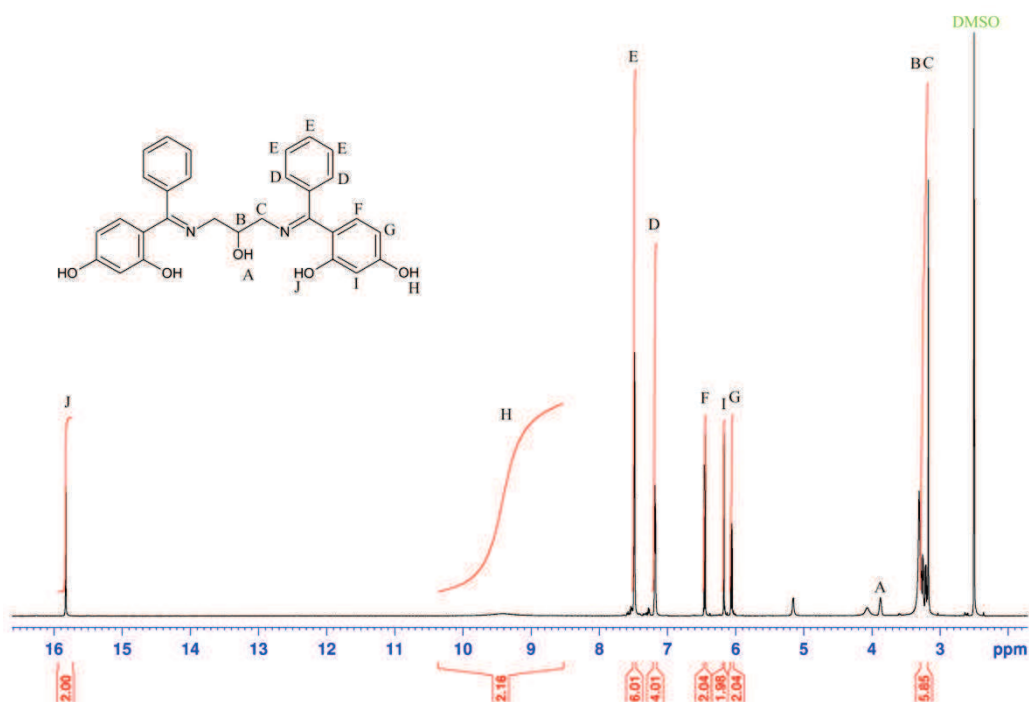


Figure A.1: ^1H NMR spectrum of H_3L^1 in $\text{DMSO-}d_6$.

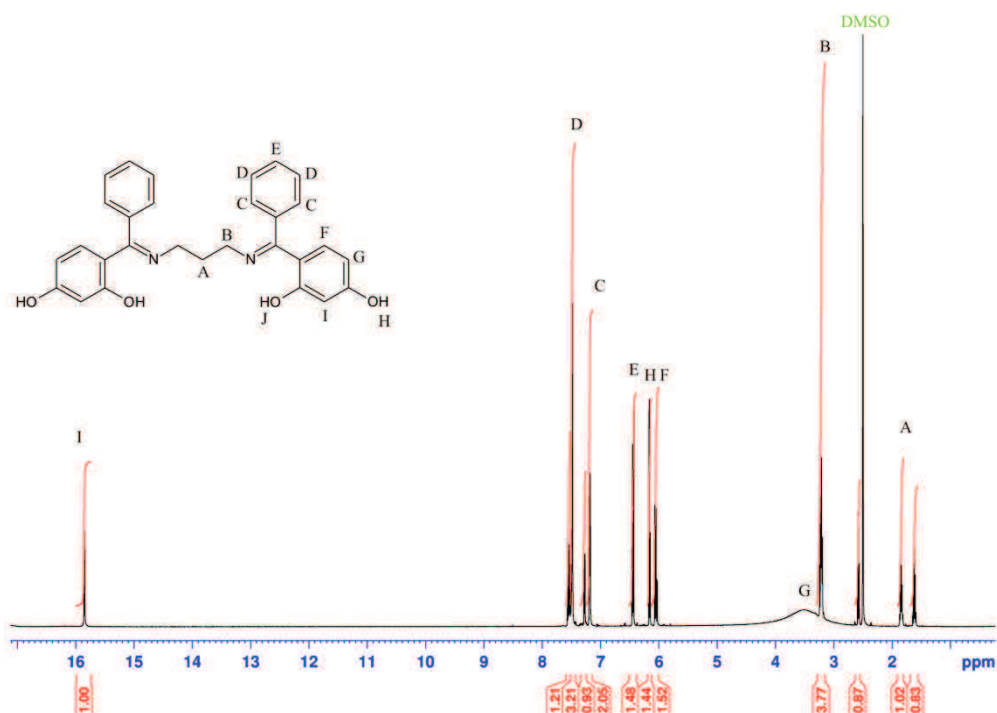


Figure A.2: ^1H NMR spectrum of H_2L^3 in $\text{DMSO-}d_6$.

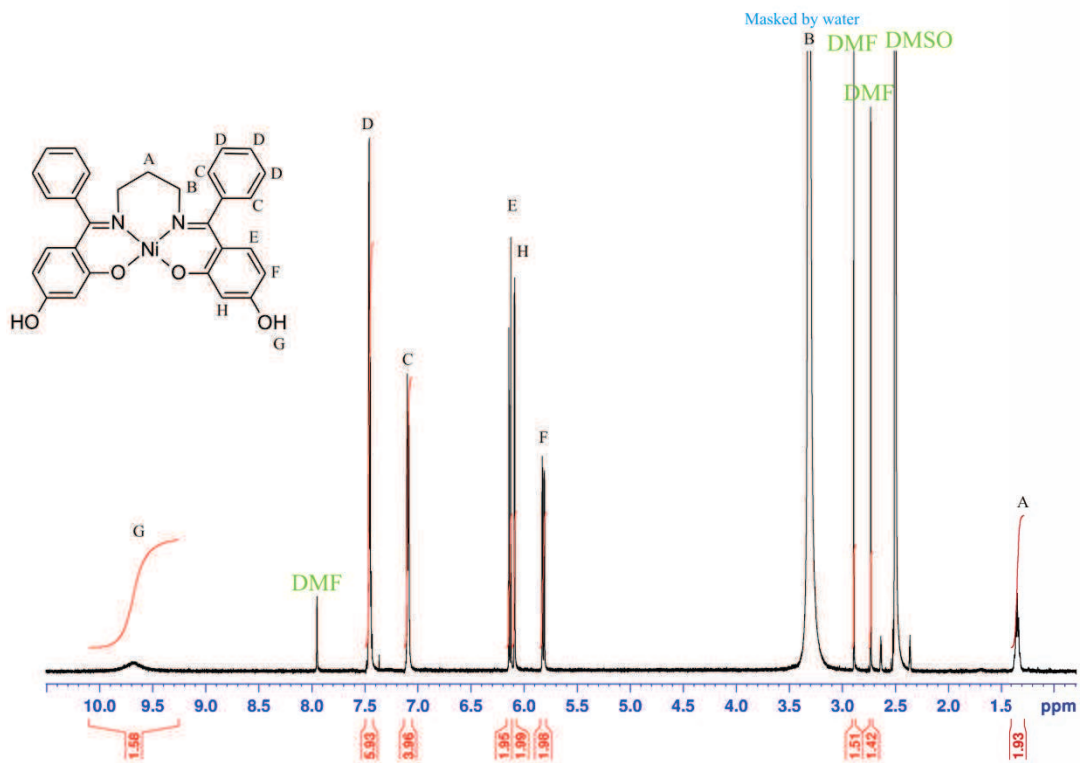


Figure A.3: ^1H NMR spectrum of $[\text{Ni}(\text{L}^3)]$ in $\text{DMSO-}d_6$.

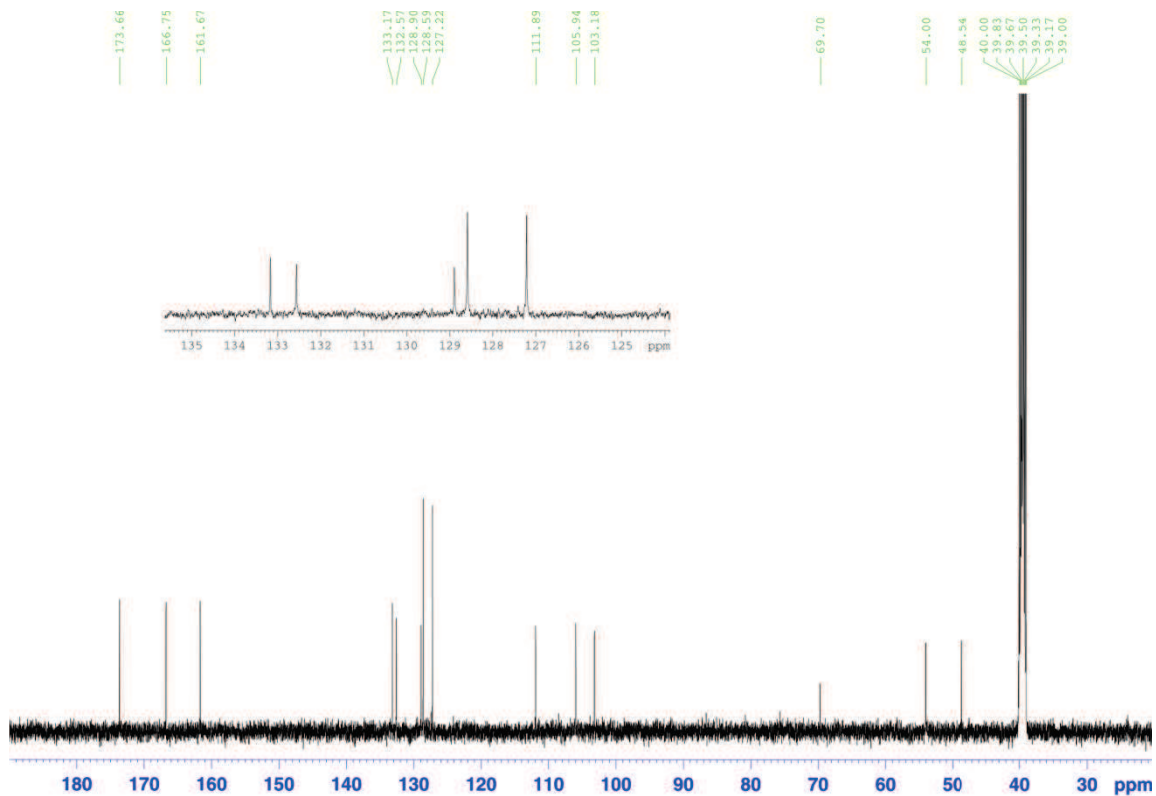


Figure A.4: ^{13}C NMR spectrum of H_3L^1 in $\text{DMSO-}d_6$.

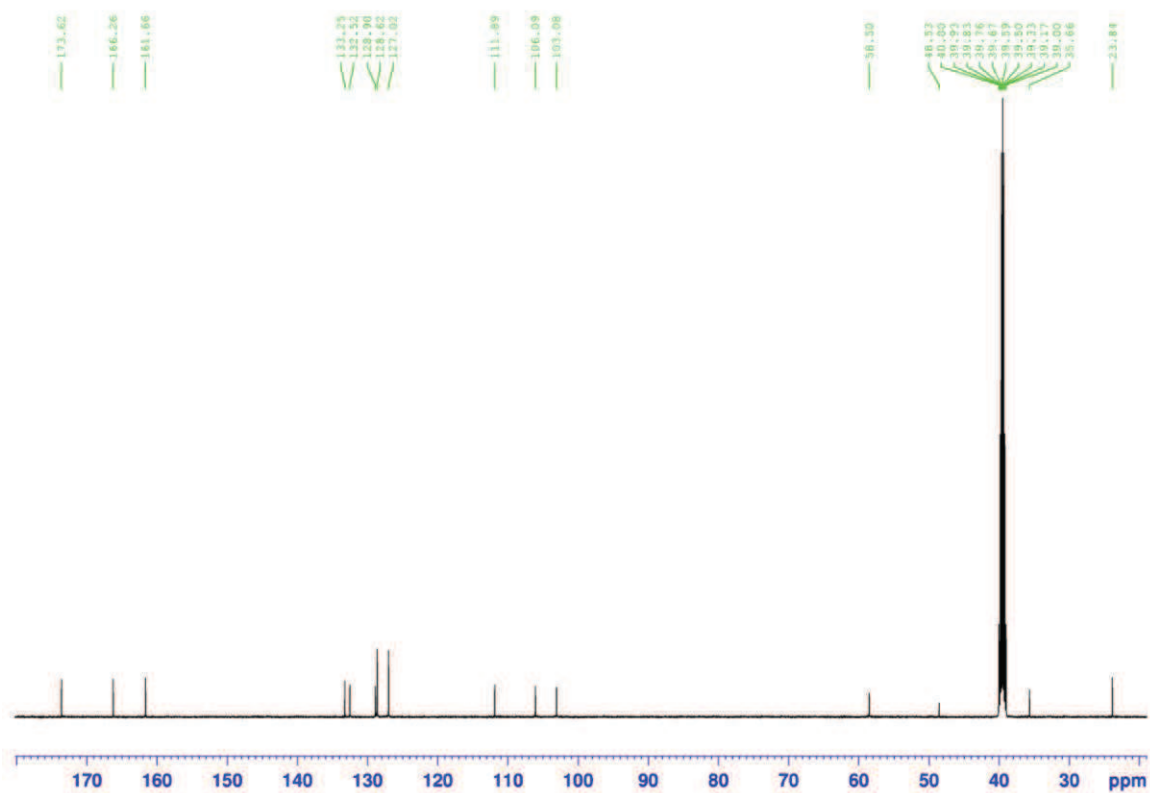


Figure A.5: ^{13}C NMR spectrum of H_2L^2 in $\text{DMSO-}d_6$.

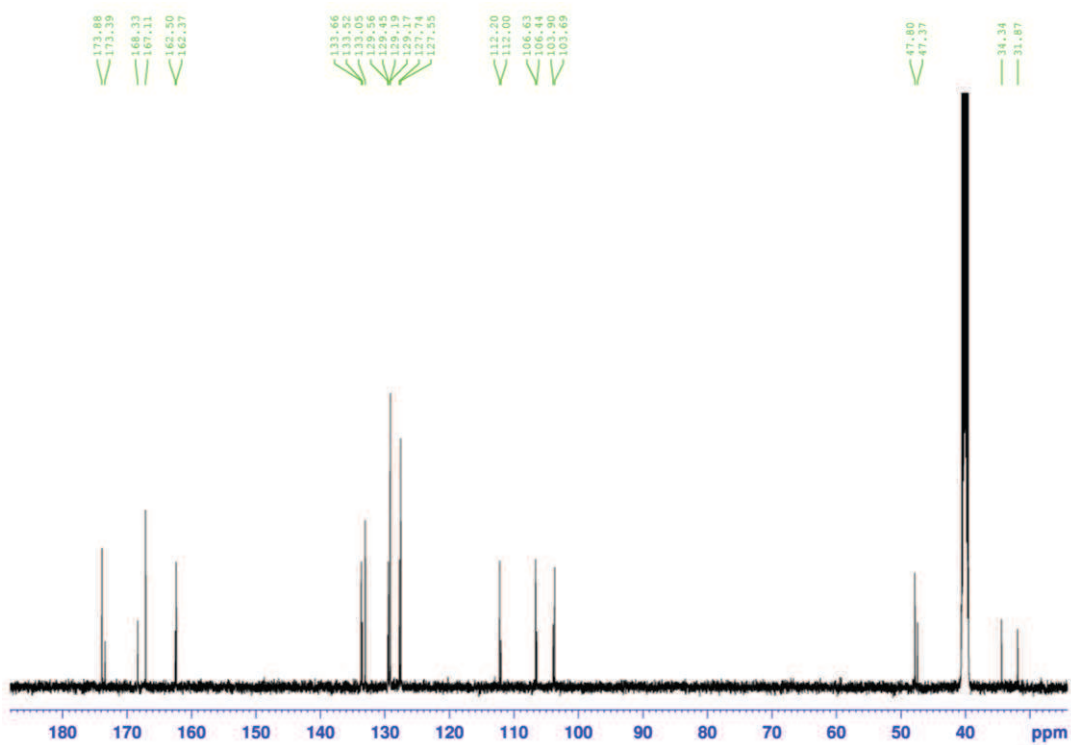


Figure A.6: ^{13}C NMR spectrum of H_2L^3 in $\text{DMSO-}d_6$.

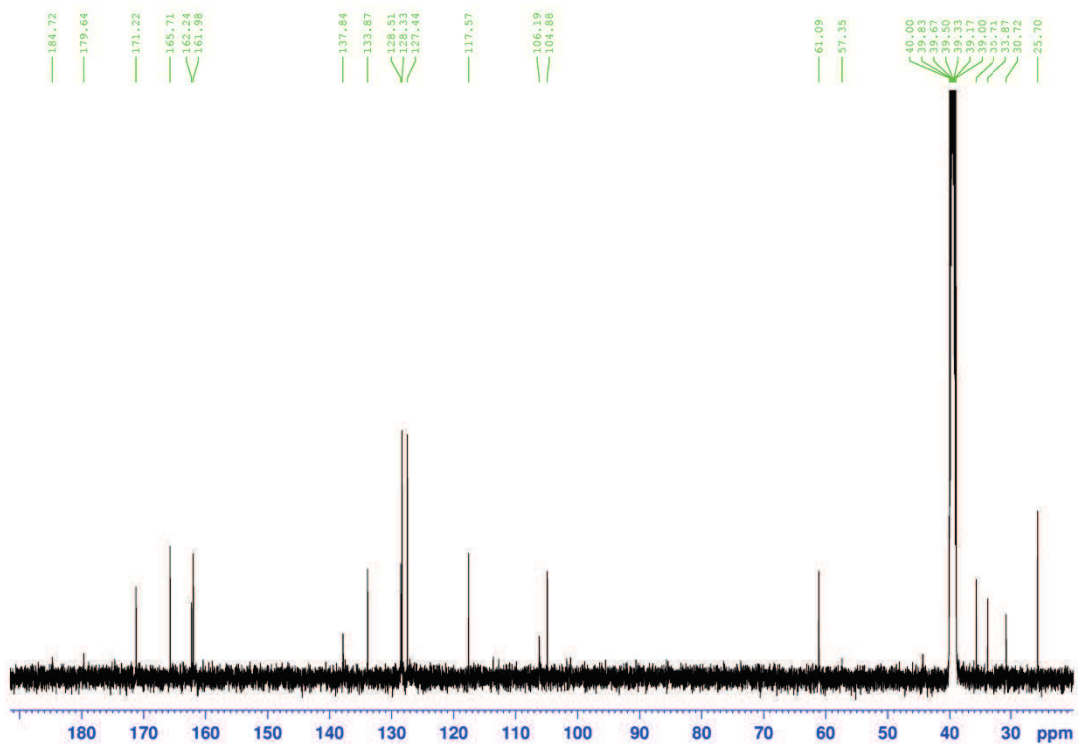


Figure A.7: ^{13}C NMR spectrum of $[\text{Ni}(\text{L}^2)]$ in $\text{DMSO-}d_6$.

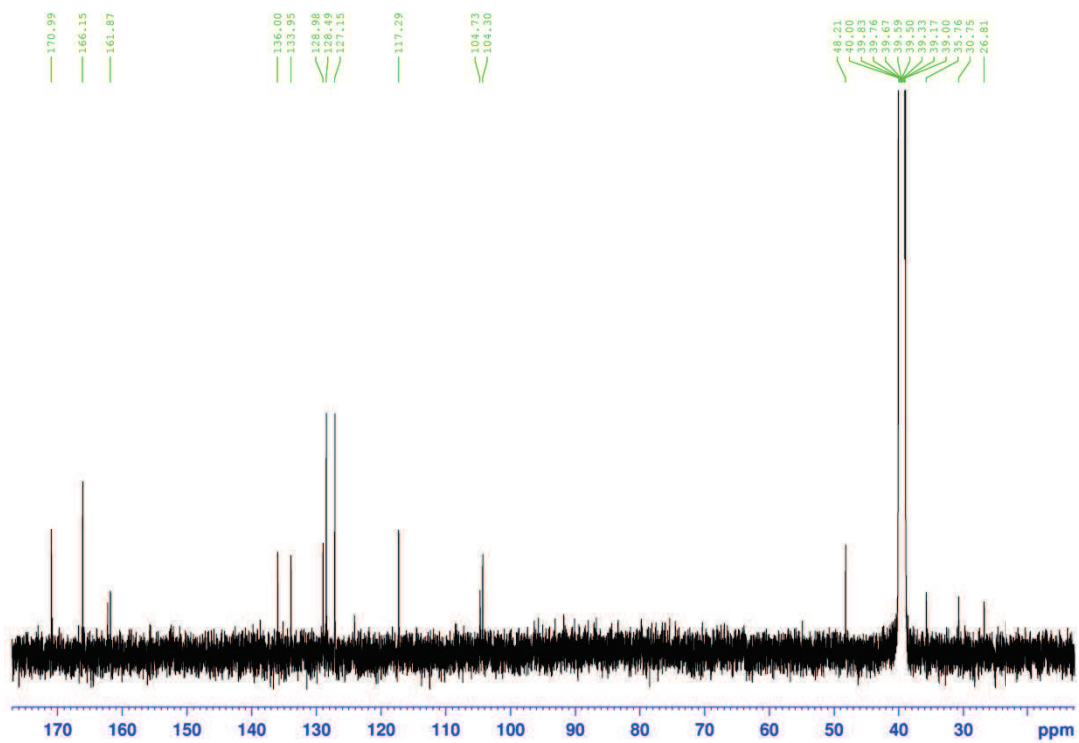


Figure A.8: ^{13}C NMR spectrum of $[\text{Ni}(\text{L}^3)]$ in $\text{DMSO-}d_6$.

Appendix B: UV-vis Spectra

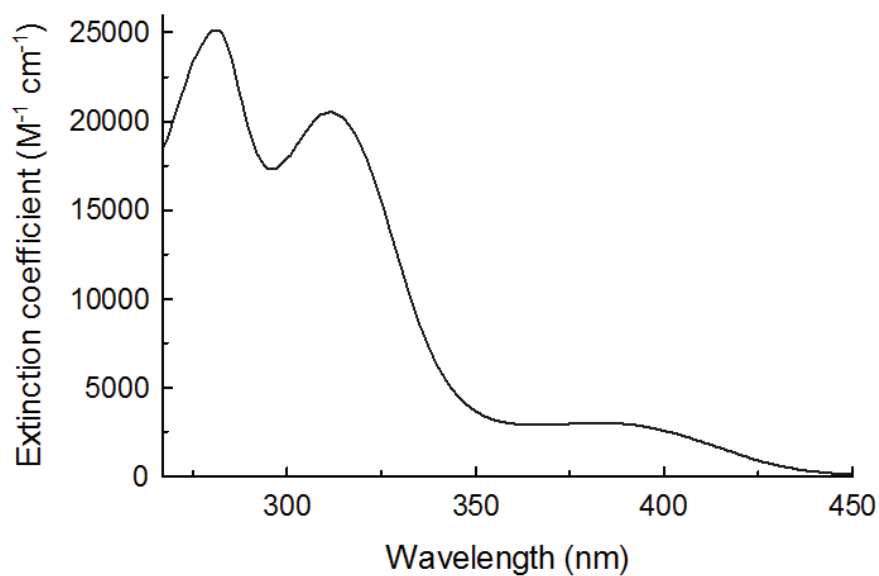


Figure B.1: UV-vis spectrum of H_3L_1 in DMF at 298 K.

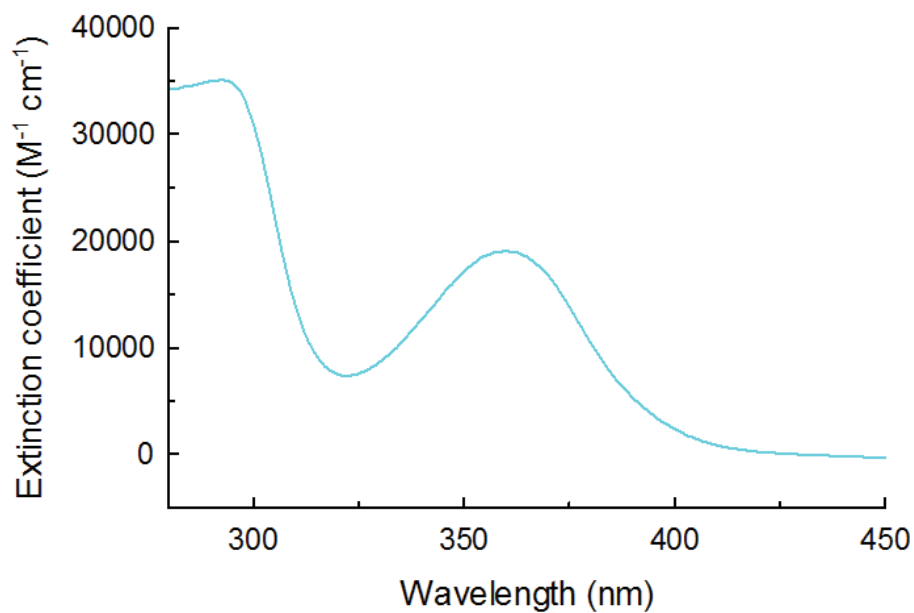


Figure B.2: UV-vis spectrum of $[Cu_2(L^1)(OAc)(DMF)]$ in DMF at 298 K.

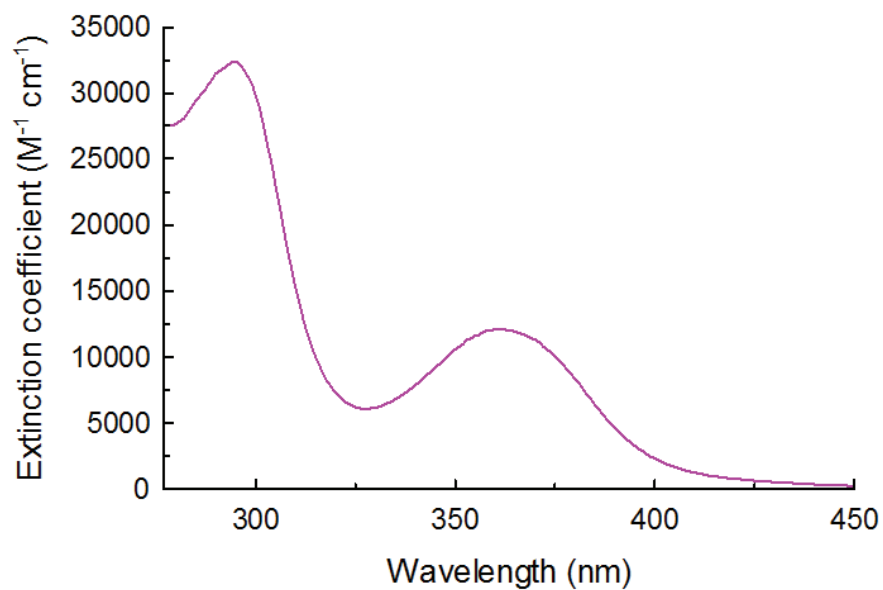


Figure B.3: UV-vis spectrum of $[\text{Cu}_3(\text{L}^2)_2\text{Cl}_2(\text{DMF})_2]$ in DMF at 298 K.

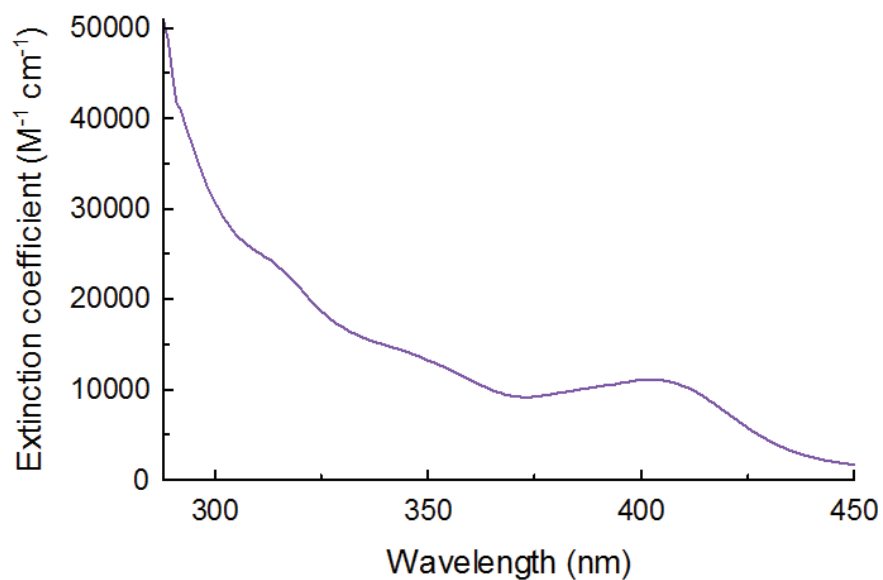


Figure B.4: UV-vis spectrum of $[\text{Ni}(\text{L}^2)]$ in DMF at 298 K.

Appendix C: Infrared Spectra

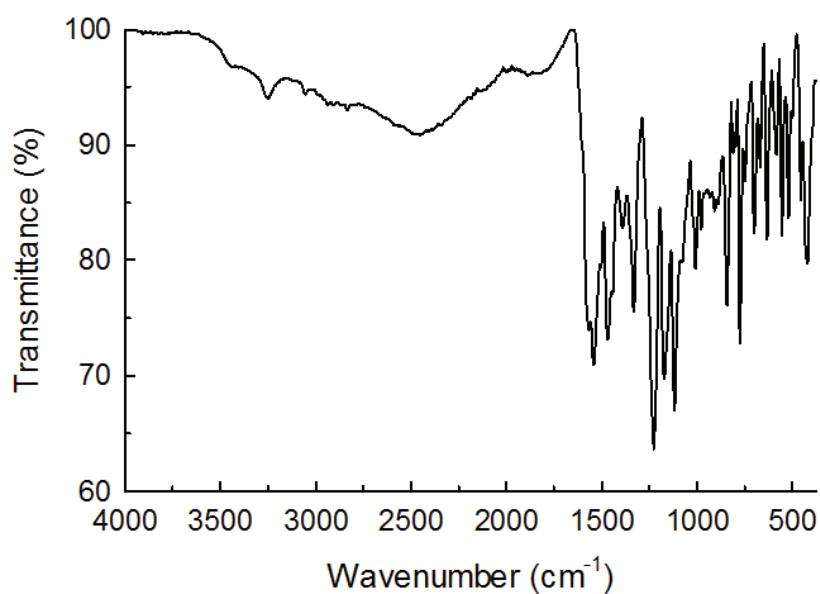


Figure C.1: Infrared spectrum of H_3L^1 .

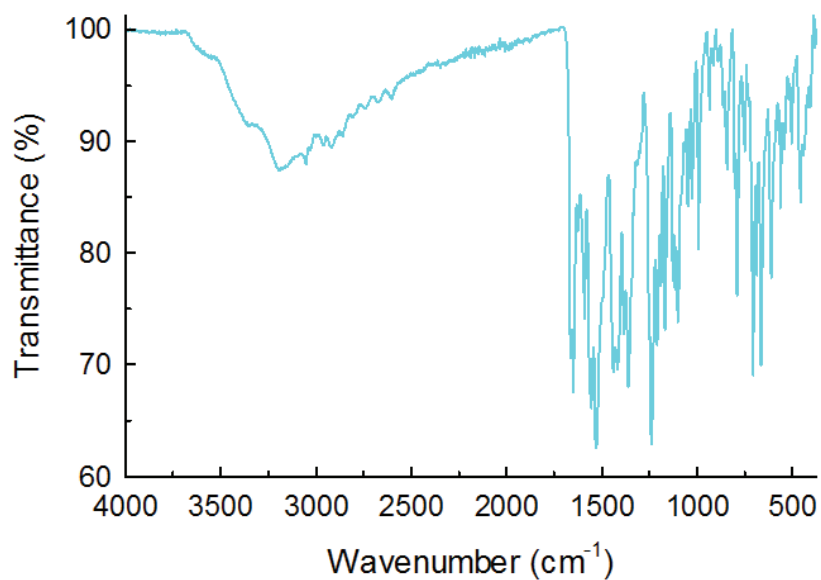


Figure C.2: Infrared spectrum of $[Cu_2(L^1)(OAc)(DMF)]$.

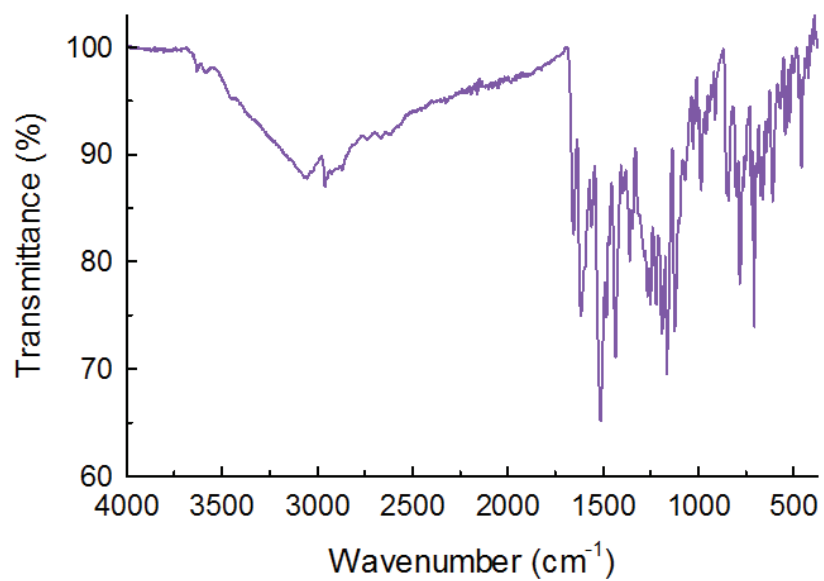


Figure C.3: Infrared spectrum of [Ni(L²)].

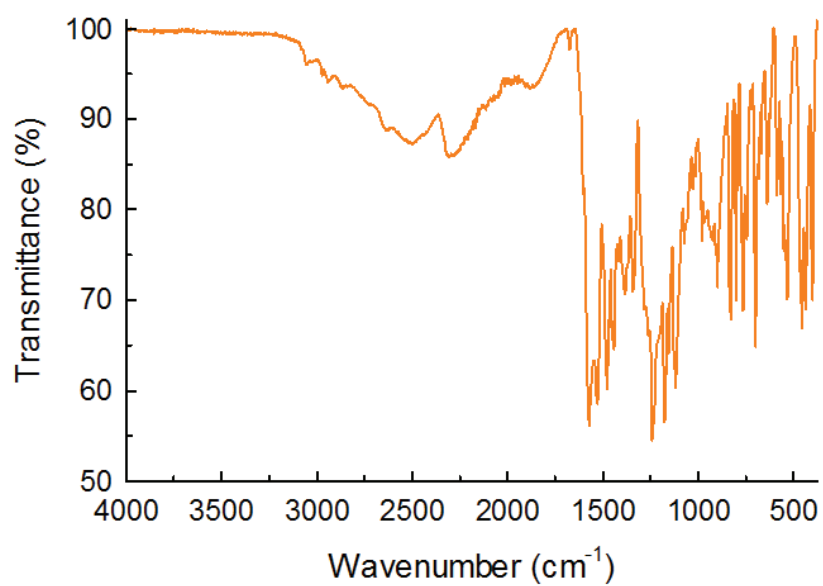


Figure C.4: Infrared spectrum of H₂L³.

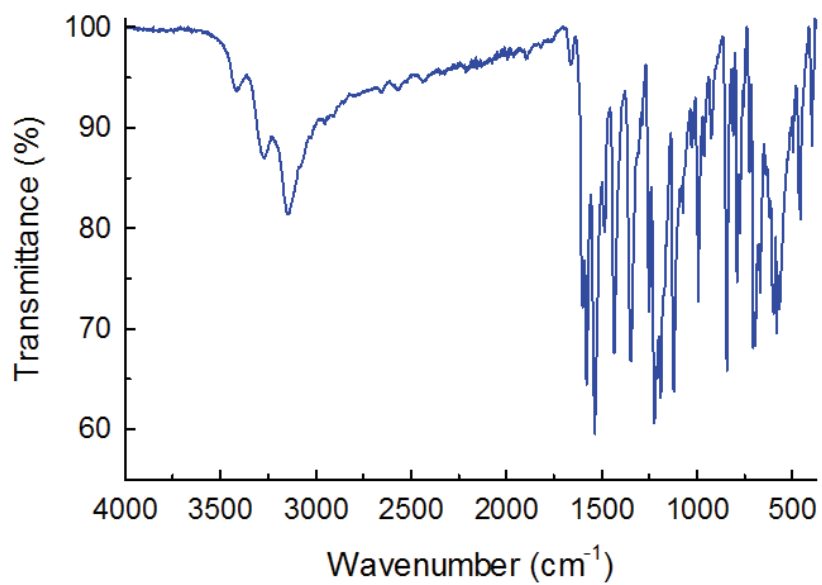


Figure C.5: Infrared spectrum of $[\text{Cu}_3(\text{L}^3)_2(\text{H}_2\text{O})_2]\text{Cl}_2$.

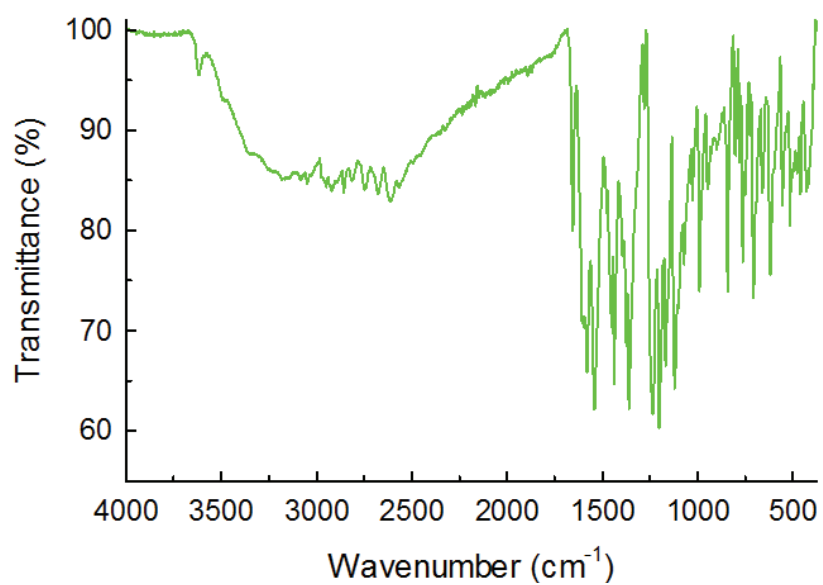


Figure C.6: Infrared spectrum of $[\text{Ni}(\text{L}^3)]$.

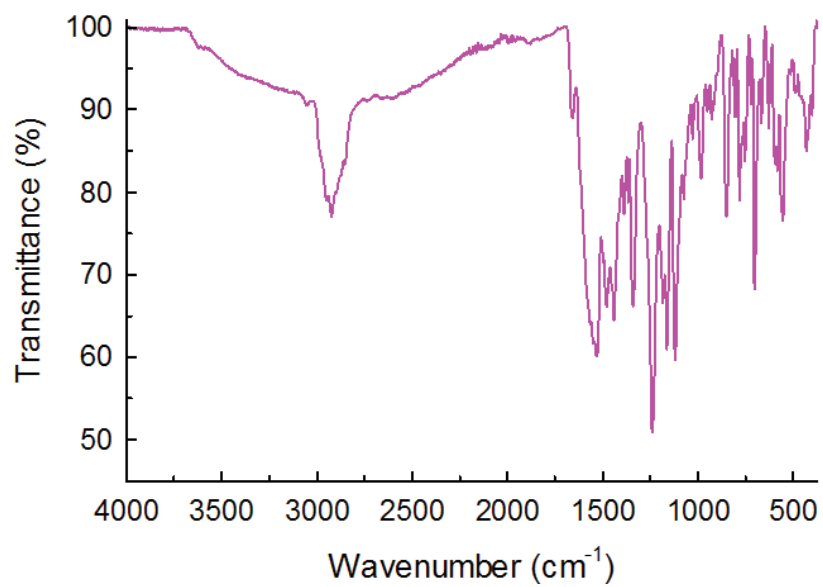


Figure C.7: Infrared spectrum of $[\text{Zn}_2(\text{L}^3)_2]$.

Appendix D: Crystallographic data

Table D.1: Crystal data and structure refinement for H₃L¹.

| | | |
|-----------------------------------|---|----------------|
| Identification code | jdp_oh_bzph | |
| Empirical formula | C ₃₂ H ₃₃ N ₃ O ₆ | |
| Formula weight | 555.61 | |
| Temperature | 296(2) K | |
| Wavelength | 0.71073 Å | |
| Crystal system | Monoclinic | |
| Space group | P 21/n | |
| Unit cell dimensions | a = 12.631(5) Å | α = 90° |
| | b = 15.619(5) Å | β = 92.792(5)° |
| | c = 14.201(5) Å | γ = 90° |
| Volume | 2798.3(17) Å ³ | |
| Z | 4 | |
| Density (calculated) | 1.319 Mg/m ³ | |
| Absorption coefficient | 0.092 mm ⁻¹ | |
| F(000) | 1176 | |
| Crystal size | 0.40 × 0.40 × 0.30 mm ³ | |
| Theta range for data collection | 2.87 to 28.79° | |
| Index ranges | -16 ≤ h ≤ 16, -19 ≤ k ≤ 18, -18 ≤ l ≤ 18 | |
| Reflections collected | 11679 | |
| Independent reflections | 6293 [R(int) = 0.0487] | |
| Absorption correction | Semi-empirical from equivalents | |
| Max. and min. Transmission | 0.9730 and 0.9642 | |
| Refinement method | Full-matrix least-squares on F ² | |
| Data/ restraints/ parameters | 6293 / 4 / 397 | |
| Goodness-of-fit on F ² | 0.879 | |
| Final R indices [I > 2σ(I)] | R1 = 0.0532, wR2 = 0.1233 | |
| R indices (all data) | R1 = 0.1053, wR2 = 0.1404 | |
| Largest diff. Peak and hole | 0.262 and -0.199 e.Å ⁻³ | |

Table D.2: Crystal data and structure refinement for H₂L².

| | | |
|-----------------------------------|---|-------------------|
| Identification code | jdp_0408ni | |
| Empirical formula | C ₃₁ H ₃₀ N ₂ O ₄ | |
| Formula weight | 494.57 | |
| Temperature | 100(2) K | |
| Wavelength | 0.71073 Å | |
| Crystal system | Monoclinic | |
| Space group | P 21/c | |
| Unit cell dimensions | a = 9.0140(2) Å | α = 90° |
| | b = 21.4340(4) Å | β = 103.2280(10)° |
| | c = 13.6800(2) Å | γ = 90° |
| Volume | 2572.93(8) Å ³ | |
| Z | 4 | |
| Density (calculated) | 1.277 Mg/m ³ | |
| Absorption coefficient | 0.085 mm ⁻¹ | |
| F(000) | 1048 | |
| Crystal size | 0.21 × 0.09 × 0.08 mm ³ | |
| Theta range for data collection | 1.90 to 28.28° | |
| Index ranges | -11 ≤ h ≤ 12, -28 ≤ k ≤ 27, -17 ≤ l ≤ 18 | |
| Reflections collected | 24513 | |
| Independent reflections | 6342 [R(int) = 0.0483] | |
| Absorption correction | Semi-empirical from equivalents | |
| Max. and min. Transmission | 0.9933 and 0.9824 | |
| Refinement method | Full-matrix least-squares on F ² | |
| Data/ restraints/ parameters | 6342 / 0 / 352 | |
| Goodness-of-fit on F ² | 1.044 | |
| Final R indices [I > 2σ(I)] | R1 = 0.0466, wR2 = 0.1091 | |
| R indices (all data) | R1 = 0.0637, wR2 = 0.1160 | |
| Largest diff. Peak and hole | 0.277 and -0.237 e.Å ⁻³ | |

Table D.3: Crystal data and structure refinement for [Cu₂(L¹)(OAc)(DMF)].

| | |
|-----------------------------------|---|
| Identification code | Benz_cu_crystal2_100k |
| Empirical formula | C ₃₄ H ₃₃ Cu ₂ N ₃ O ₈ |
| Formula weight | 738.71 |
| Temperature | 100(2) |
| Wavelength | 0.71073 Å |
| Crystal system | Monoclinic |
| Space group | P21/n |
| Unit cell dimensions | a = 9.014(5) Å α = 90° b = 14.696(5) Å β = 92.625(5) ° c = 28.716(5) Å γ = 90° |
| Volume | 3800(3) Å ³ |
| Z | 4 |
| Density (calculated) | 1.291 Mg/m ³ |
| Absorption coefficient | 1.167 mm ⁻¹ |
| F(000) | 1520 |
| Crystal size | 0.40 × 0.35 × 0.30 mm ³ |
| Theta range for data collection | 2.84 to 28.71° |
| Index ranges | -12 ≤ h ≤ 10, 0 ≤ k ≤ 18, -9 ≤ l ≤ 38 |
| Reflections collected | 8506 |
| Independent reflections | 8506 [R(int) = 0.0000] |
| Absorption correction | Semi-empirical from equivalents |
| Max. and min. Transmission | 0.7209 and 0.6524 |
| Refinement method | Full-matrix least-squares on F ² |
| Data/ restraints/ parameters | 8506 / 81 / 429 |
| Goodness-of-fit on F ² | 0.926 |
| Final R indices [I > 2σ(I)] | R1 = 0.0505, wR2 = 0.1408 |
| R indices (all data) | R1 = 0.0701, wR2 = 0.1513 |
| Largest diff. Peak and hole | 0.768 and -0.567 e.Å ⁻³ |

Table D.4: Crystal data and structure refinement for [Cu₃(L²)₂Cl₂(DMF)₂].

| | |
|-----------------------------------|---|
| Identification code | 0408cu_t52_sqz |
| Empirical formula | C _{20.67} H _{18.67} Cl _{0.67} Cu N _{1.33} O _{2.67} |
| Formula weight | 415.54 |
| Temperature | 110(2) K |
| Wavelength | 0.71073 Å |
| Crystal system | Triclinic |
| Space group | P-1 |
| Unit cell dimensions | a = 10.7378(4) Å α = 87.018(3)° b = 15.8005(6) Å β = 79.714(4)° c = 22.1628(10) Å γ = 81.185(3)° |
| Volume | 3654.9(3) Å ³ |
| Z | 6 |
| Density (calculated) | 1.133 Mg/m ³ |
| Absorption coefficient | 0.984 mm ⁻¹ |
| F(000) | 1282 |
| Crystal size | 0.30 × 0.20 × 0.10 mm ³ |
| Theta range for data collection | 2.79 to 26.06° |
| Index ranges | -12 ≤ h ≤ 13, -19 ≤ k ≤ 19, 0 ≤ l ≤ 27 |
| Reflections collected | 14347 |
| Independent reflections | 14347 [R(int) = 0.0000] |
| Absorption correction | Semi-empirical from equivalents |
| Max. and min. Transmission | 0.9080 and 0.7567 |
| Refinement method | Full-matrix least-squares on F ² |
| Data/ restraints/ parameters | 14347 / 0 / 724 |
| Goodness-of-fit on F ² | 0.822 |
| Final R indices [I > 2σ(I)] | R1 = 0.0493, wR2 = 0.1119 |
| R indices (all data) | R1 = 0.0821, wR2 = 0.1181 |
| Largest diff. Peak and hole | 1.864 and -0.801 e.Å ⁻³ |

Table D.5: Crystal data and structure refinement for [Ni(L²)].

| | |
|-----------------------------------|---|
| Identification code | 0408ni |
| Empirical formula | C ₃₁ H ₂₈ N ₂ Ni O ₄ |
| Formula weight | 551.26 |
| Temperature | 296 |
| Wavelength | 0.71073 Å |
| Crystal system | Monoclinic |
| Space group | P21/c |
| Unit cell dimensions | a = 25.0542(13) Å α = 90° b = 9.6539(5) Å β = 98.568(5)° c = 27.3083(13) Å γ = 90° |
| Volume | 6531.4(6) Å ³ |
| Z | 8 |
| Density (calculated) | 1.121 Mg/m ³ |
| Absorption coefficient | 0.626 mm ⁻¹ |
| F(000) | 2304 |
| Crystal size | 0.60 × 0.20 × 0.03 mm ³ |
| Theta range for data collection | 2.95 to 26.06° |
| Index ranges | -30 ≤ h ≤ 29, -11 ≤ k ≤ 10, -33 ≤ l ≤ 33 |
| Reflections collected | 46899 |
| Independent reflections | 12840 [R(int) = 0.053] |
| Absorption correction | Semi-empirical from equivalents |
| Max. and min. Transmission | 0.9815 and 0.7050 |
| Refinement method | Full-matrix least-squares on F ² |
| Data/ restraints/ parameters | 12840 / 0 / 693 |
| Goodness-of-fit on F ² | 0.794 |
| Final R indices [I > 2σ(I)] | R1 = 0.0603, wR2 = 0.1237 |
| R indices (all data) | R1 = 0.1403, wR2 = 0.1395 |
| Largest diff. Peak and hole | 0.396 and -0.386 e.Å ⁻³ |

Table D.6: Crystal data and structure refinement for [Cu₃(L³)₂(H₂O)₂]Cl₂.

| | |
|-----------------------------------|---|
| Identification code | mo_om_jdp_cu_propyl_data3_0m |
| Empirical formula | C ₂₉ H ₂₆ Cl Cu _{1.50} N ₂ O ₅ |
| Formula weight | 613.28 |
| Temperature | 100(2) K |
| Wavelength | 0.71073 Å |
| Crystal system | Monoclinic |
| Space group | P21/c |
| Unit cell dimensions | a = 9.1151(4) Å α = 90° b = 25.6003(11) Å β = 100.219(3)° c = 11.5667(6) Å γ = 90° |
| Volume | 2656.3(2) Å ³ |
| Z | 4 |
| Density (calculated) | 1.534 Mg/m ³ |
| Absorption coefficient | 1.355 mm ⁻¹ |
| F(000) | 1258 |
| Crystal size | 0.20 × 0.07 × 0.01 mm ³ |
| Theta range for data collection | 1.59 to 26.37° |
| Index ranges | -11 ≤ h ≤ 11, -32 ≤ k ≤ 31, -6 ≤ l ≤ 14 |
| Reflections collected | 16963 |
| Independent reflections | 4761 [R(int) = 0.0206] |
| Absorption correction | Semi-empirical from equivalents |
| Max. and min. Transmission | 0.9866 and 0.7733 |
| Refinement method | Full-matrix least-squares on F ² |
| Data/ restraints/ parameters | 4761 / 234 / 357 |
| Goodness-of-fit on F ² | 1.174 |
| Final R indices [I > 2σ(I)] | R1 = 0.0437, wR2 = 0.0963 |
| R indices (all data) | R1 = 0.0495, wR2 = 0.0986 |
| Largest diff. Peak and hole | 1.155 and -0.418 e.Å ⁻³ |

Table D.7: Crystal data and structure refinement for [Ni(L³)].

| | | |
|-----------------------------------|--|-------------------|
| Identification code | jdp_2610ni | |
| Empirical formula | C ₂₉ H ₂₈ N ₂ Ni O ₆ | |
| Formula weight | 559.24 | |
| Temperature | 100(2) K | |
| Wavelength | 0.71073 Å | |
| Crystal system | Monoclinic | |
| Space group | C2/c | |
| Unit cell dimensions | a = 24.261(2) Å | α = 90° |
| | b = 9.0890(8) Å | β = 111.1090(10)° |
| | c = 26.956(2) Å | γ = 90° |
| Volume | 5545.2(8) Å ³ | |
| Z | 8 | |
| Density (calculated) | 1.340 Mg/m ³ | |
| Absorption coefficient | 0.744 mm ⁻¹ | |
| F(000) | 2336 | |
| Crystal size | 0.19 × 0.16 × 0.06 mm ³ | |
| Theta range for data collection | 1.94 to 28.27° | |
| Index ranges | -31 ≤ h ≤ 29, 0 ≤ k ≤ 12, 0 ≤ l ≤ 35 | |
| Reflections collected | 6502 | |
| Independent reflections | 6502 [R(int) = 0.0000] | |
| Absorption correction | Semi-empirical from equivalents | |
| Max. and min. Transmission | 0.9568 and 0.8656 | |
| Refinement method | Full-matrix least-squares on F ² | |
| Data/ restraints/ parameters | 6502 / 4 / 361 | |
| Goodness-of-fit on F ² | 1.056 | |
| Final R indices [I > 2σ(I)] | R1 = 0.0377, wR2 = 0.0938 | |
| R indices (all data) | R1 = 0.0484, wR2 = 0.0981 | |
| Largest diff. Peak and hole | 0.360 and -0.269 e.Å ⁻³ | |

Table D.8: Crystal data and structure refinement for [Zn₂(L³)₂].

| | |
|-----------------------------------|---|
| Identification code | jdp_zn2610 |
| Empirical formula | C ₅₈ H ₄₈ N ₄ O ₈ Zn ₂ |
| Formula weight | 1059.74 |
| Temperature | 100(2) K |
| Wavelength | 0.71073 Å |
| Crystal system | Orthorhombic |
| Space group | P n a 21 |
| Unit cell dimensions | a = 23.1020(3) Å α = 90° b = 18.1100(3) Å β = 90° c = 16.6460(3) Å γ = 90° |
| Volume | 6964.31(19) Å ³ |
| Z | 4 |
| Density (calculated) | 1.011 Mg/m ³ |
| Absorption coefficient | 0.733 mm ⁻¹ |
| F(000) | 2192 |
| Crystal size | 0.25 × 0.15 × 0.15 mm ³ |
| Theta range for data collection | 1.88 to 28.27° |
| Index ranges | -30 ≤ h ≤ 28, -19 ≤ k ≤ 24, -15 ≤ l ≤ 22 |
| Reflections collected | 35623 |
| Independent reflections | 13618 [R(int) = 0.0533] |
| Absorption correction | Semi-empirical from equivalents |
| Max. and min. Transmission | 0.8981 and 0.8380 |
| Refinement method | Full-matrix least-squares on F ² |
| Data/ restraints/ parameters | 13618 / 1 / 654 |
| Goodness-of-fit on F ² | 0.838 |
| Final R indices [I > 2σ(I)] | R1 = 0.0484, wR2 = 0.1089 |
| R indices (all data) | R1 = 0.0630, wR2 = 0.1156 |
| Largest diff. Peak and hole | 0.406 and -0.361 e.Å ⁻³ |

checkCIF/PLATON report (basic structural check)

No syntax errors found.

Please wait while processing

[CIF dictionary](#)

[Interpreting this report](#)

Datablock: benz_cu_crystal2_100k

Bond precision: C-C = 0.0067 Å Wavelength=0.71073

Cell: a=9.014(5) b=14.696(5) c=28.716(5)

alpha=90 beta=92.625(5) gamma=90

Temperature: 100 K

| | Calculated | Reported |
|----------------|-------------------|-------------------|
| Volume | 3800(3) | 3800(3) |
| Space group | P 21/n | P 1 21/n 1 |
| Hall group | -P 2yn | -P 2yn |
| Moiety formula | C34 H33 Cu2 N3 O8 | C34 H33 Cu2 N3 O8 |
| Sum formula | C34 H33 Cu2 N3 O8 | C34 H33 Cu2 N3 O8 |
| Mr | 738.73 | 738.71 |
| Dx, g cm-3 | 1.291 | 1.291 |
| Z | 4 | 4 |
| Mu (mm-1) | 1.167 | 1.167 |
| F000 | 1520.0 | 1520.0 |
| F000' | 1523.15 | |
| h, k, lmax | 12, 19, 38 | 12, 18, 38 |
| Nref | 9830 | 8506 |
| Tmin, Tmax | 0.633, 0.705 | 0.652, 0.721 |
| Tmin' | 0.621 | |

Correction method= MULTI-SCAN

Data completeness= 0.865 Theta(max)= 28.710

R(reflections)= 0.0505(5761) wR2(reflections)= 0.1513(8506)

S = 0.926 Npar= 429

The following ALERTS were generated. Each ALERT has the format

test-name_ALERT_alert-type_alert-level.

Click on the hyperlinks for more details of the test.

Alert level B

[PLAT220_ALERT_2_B](#) Large Non-Solvent C Ueq(max)/Ueq(min)

... 4.9 Ratio

[PLAT241_ALERT_2_B](#) Check High Ueq as Compared to Neighbors

for C13

[PLAT420_ALERT_2_B](#) D-H Without Acceptor O4 - H4 ...

?

Despite isotropic restraints for one phenyl and one phenoxide group of the ligand, thermal motion was high for one half of the molecule consistent with positional disorder. The data were not of high enough quality to refine the data with two contributing conformations to the electron density. Further, one DMF and at least one water molecule were disordered in a solvent-filled void in the ASU. The electron density for the disordered solvent was removed using PLATON's SQUEEZE algorithm. This is why O4-H4 has no H-bond partner. We have done the best we can with a fundamentally bad crystal.

Alert level C

[PLAT213_ALERT_2_C](#) Atom C13 has ADP max/min Ratio
 3.7 prola
[PLAT213_ALERT_2_C](#) Atom C14 has ADP max/min Ratio
 3.4 prola
[PLAT213_ALERT_2_C](#) Atom C24 has ADP max/min Ratio
 3.1 prola
[PLAT213_ALERT_2_C](#) Atom C25 has ADP max/min Ratio
 3.2 prola
[PLAT213_ALERT_2_C](#) Atom C26 has ADP max/min Ratio
 3.4 prola
[PLAT213_ALERT_2_C](#) Atom C27 has ADP max/min Ratio
 3.6 prola
[PLAT222_ALERT_3_C](#) Large Non-Solvent H Uiso(max)/Uiso(min)
 .. 4.6 Ratio
[PLAT241_ALERT_2_C](#) Check High Ueq as Compared to Neighbors
 for C14
[PLAT241_ALERT_2_C](#) Check High Ueq as Compared to Neighbors
 for C27
[PLAT250_ALERT_2_C](#) Large U3/U1 Ratio for Average U(i,j) Tensor
 2.9
[PLAT341_ALERT_3_C](#) Low Bond Precision on C-C Bonds
 0.0067 Ang

Alert level G

[PLAT003_ALERT_2_G](#) Number of Uiso or Uij Restrained Atom Sites
 10
[PLAT005_ALERT_5_G](#) No _iucr_refine_instructions_details in the CIF
 ?
[PLAT007_ALERT_5_G](#) Note: Number of Unrefined D-H Atoms
 2
[PLAT128_ALERT_4_G](#) Alternate Setting of Space-group P21/c
 P21/n
[PLAT153_ALERT_1_G](#) The su's on the Cell Axes are Equal
 0.00500 Ang.
[PLAT232_ALERT_2_G](#) Hirshfeld Test Diff (M-X) Cu1 -- O8 ..
 5.6 su
[PLAT605_ALERT_4_G](#) Structure Contains Solvent Accessible VOIDS of
 . 414 A**3
[PLAT793_ALERT_4_G](#) The Model has Chirality at C9 (Verify)
 R
[PLAT860_ALERT_3_G](#) Note: Number of Least-Squares Restraints
 81
[PLAT869_ALERT_4_G](#) ALERTS Related to the use of SQUEEZE
 Suppressed !

0 **ALERT level A** = Most likely a serious problem - resolve or explain
 3 **ALERT level B** = A potentially serious problem, consider carefully
 11 **ALERT level C** = Check. Ensure it is not caused by an omission or oversight
 10 **ALERT level G** = General information/check it is not something unexpected

1 ALERT type 1 CIF construction/syntax error, inconsistent or missing data
 14 ALERT type 2 Indicator that the structure model may be wrong or deficient
 3 ALERT type 3 Indicator that the structure quality may be low
 4 ALERT type 4 Improvement, methodology, query or suggestion
 2 ALERT type 5 Informative message, check

It is advisable to attempt to resolve as many as possible of the alerts in all categories. Often the minor alerts point to easily fixed oversights, errors and omissions in your CIF or refinement strategy, so attention to these fine details can be worthwhile. In order to resolve some of the more serious problems it may be necessary to carry out additional measurements or structure refinements. However, the purpose of your study may justify the reported deviations and the more serious of these should normally be commented upon in the discussion or experimental section of a paper or in the "special_details" fields of the CIF. checkCIF was carefully designed to identify outliers and unusual parameters, but every test has its limitations

and alerts that are not important in a particular case may appear. Conversely, the absence of alerts does not guarantee there are no aspects of the results needing attention. It is up to the individual to critically assess their own results and, if necessary, seek expert advice.

Publication of your CIF in IUCr journals

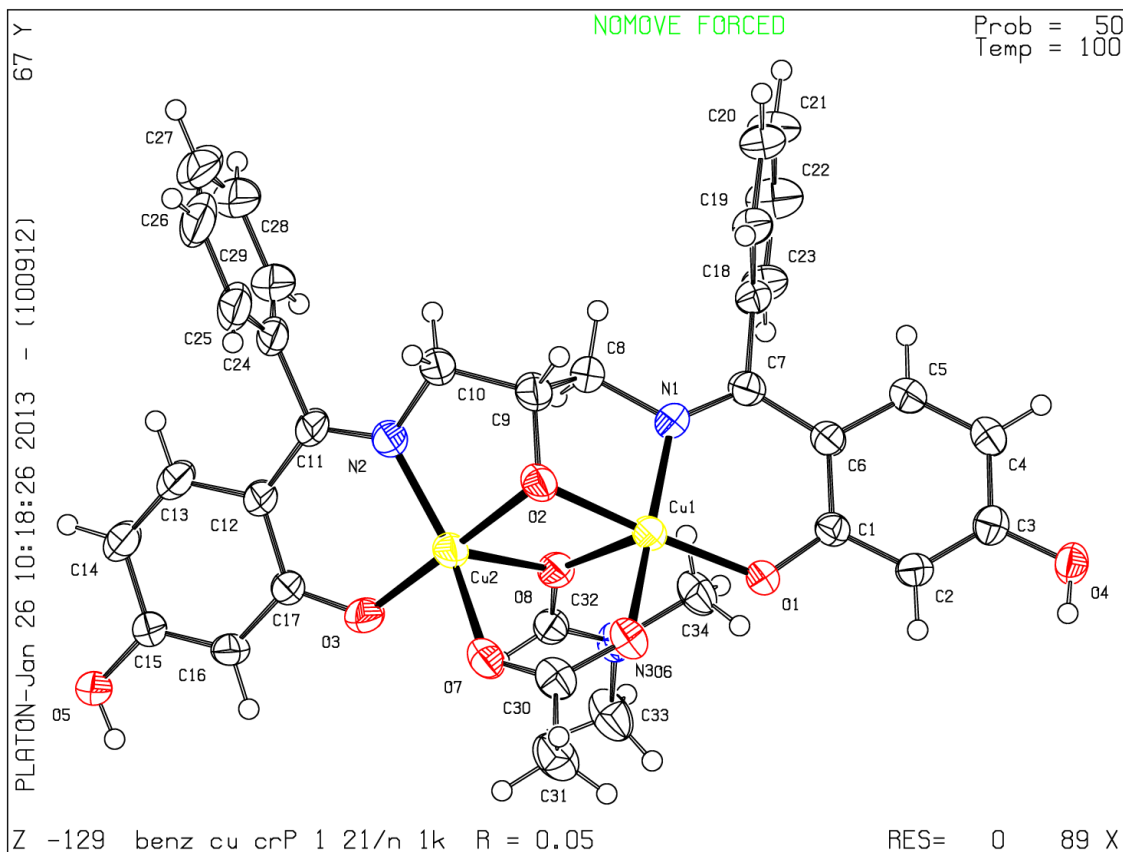
A basic structural check has been run on your CIF. These basic checks will be run on all CIFs submitted for publication in IUCr journals (*Acta Crystallographica*, *Journal of Applied Crystallography*, *Journal of Synchrotron Radiation*); however, if you intend to submit to *Acta Crystallographica Section C* or *E*, you should make sure that [full publication checks](#) are run on the final version of your CIF prior to submission.

Publication of your CIF in other journals

Please refer to the *Notes for Authors* of the relevant journal for any special instructions relating to CIF submission.

PLATON version of 05/11/2012; check.def file version of 05/11/2012

Datablock benz_cu_crystal2_100k - ellipsoid plot



[Download CIF editor \(pubCIF\) from the IUCr](#)
[Download CIF editor \(enCIFer\) from the CCDC](#)
[Test a new CIF entry](#)

checkCIF/PLATON report (basic structural check)

No syntax errors found.
Please wait while processing

[CIF dictionary](#)
[Interpreting this report](#)

Datablock: 0408cu_t52_sqz

Bond precision: C-C = 0.0061 Å Wavelength=0.71073
Cell: a=10.7378 (4) b=15.8005 (6) c=22.1628 (10)
alpha=87.018 (3) beta=79.714 (4) gamma=81.185 (3)
Temperature: 110 K

| | Calculated | Reported |
|----------------|-----------------------|--|
| Volume | 3654.9(3) | 3654.9(3) |
| Space group | P -1 | P-1 |
| Hall group | -P 1 | ? |
| Moiety formula | C62 H56 Cl2 Cu3 N4 O8 | ? |
| Sum formula | C62 H56 Cl2 Cu3 N4 O8 | C20.67 H18.67 Cl0.67 Cu N1.33 O2.67 |
| Mr | 1246.66 | 415.54 |
| Dx, g cm-3 | 1.133 | 1.133 |
| Z | 2 | 6 |
| Mu (mm-1) | 0.984 | 0.984 |
| F000 | 1282.0 | 1282.0 |
| F000' | 1284.93 | |
| h, k, lmax | 13, 19, 27 | 13, 19, 27 |
| Nref | 14463 | 14347 |
| Tmin, Tmax | 0.790, 0.906 | 0.757, 0.908 |
| Tmin' | 0.744 | |

Correction method= MULTI-SCAN
Data completeness= 0.992 Theta(max)= 26.060
R(reflections)= 0.0493(7809) wR2(reflections)= 0.1181(14347)
S = 0.822 Npar= 724

The following ALERTS were generated. Each ALERT has the format
test-name_ALERT_alert-type_alert-level.
Click on the hyperlinks for more details of the test.

Alert level B

[PLAT420_ALERT_2_B](#) D-H Without Acceptor O3A - H3A ... ?
[PLAT420_ALERT_2_B](#) D-H Without Acceptor O3B - H3B ... ?
[PLAT420_ALERT_2_B](#) D-H Without Acceptor O4A - H4A ... ?
[PLAT420_ALERT_2_B](#) D-H Without Acceptor O4B - H4B ... ?

This alert results from our implementation of PLATON's SQUEEZE algorithm to remove difficult to model solvent from the model. From the "disordered" electron density three DMF molecules and 4 or 5 water molecules exist in the ASU. The alert may be ignored.

Alert level C

[PLAT094_ALERT_2_C](#) Ratio of Maximum / Minimum Residual Density
2.33
[PLAT220_ALERT_2_C](#) Large Non-Solvent C Ueq(max)/Ueq(min) ... 3.1
Ratio
[PLAT341_ALERT_3_C](#) Low Bond Precision on C-C Bonds 0.0061
Ang

Alert level G

[CELLZ01_ALERT_1_G](#) Difference between formula and atom_site contents detected.
[CELLZ01_ALERT_1_G](#) ALERT: check formula stoichiometry or atom site occupancies.
From the CIF: _cell_formula_units_Z 6
From the CIF: _chemical_formula_sum C20.67 H18.67 Cl0.67 Cu N1.33
O2
TEST: Compare cell contents of formula and atom_site data

| atom | Z*formula | cif sites | diff |
|------|-----------|-----------|-------|
| C | 124.02 | 124.00 | 0.02 |
| H | 112.02 | 112.00 | 0.02 |
| Cl | 4.02 | 4.00 | 0.02 |
| Cu | 6.00 | 6.00 | 0.00 |
| N | 7.98 | 8.00 | -0.02 |
| O | 16.02 | 16.00 | 0.02 |

[PLAT005 ALERT 5 G](#) No `_iucr_refine_instructions_details` in the CIF ?
[PLAT007 ALERT 5 G](#) Note: Number of Unrefined D-H Atoms 4
[PLAT045 ALERT 1 G](#) Calculated and Reported Z Differ by 0.33
 Ratio
[PLAT093 ALERT 1 G](#) No su's on H-positions, refinement reported as . mixed
[PLAT232 ALERT 2 G](#) Hirshfeld Test Diff (M-X) Cu2 -- N1B .. 5.4 su
[PLAT606 ALERT 4 G](#) VERY LARGE Solvent Accessible VOID(S) in Structure
 !
[PLAT710 ALERT 4 G](#) Delete 1-2-3 or 2-3-4 Linear Torsion Angle ... # 21
 CU2 -CU1 -CU2 -O2B -30.00 39.00 2.766 1.555 1.555 1.555
[PLAT710 ALERT 4 G](#) Delete 1-2-3 or 2-3-4 Linear Torsion Angle ... # 25
 CU2 -CU1 -CU2 -O1B 121.00 39.00 2.766 1.555 1.555 1.555
[PLAT710 ALERT 4 G](#) Delete 1-2-3 or 2-3-4 Linear Torsion Angle ... # 30
 CU2 -CU1 -CU2 -N2B -57.00 39.00 2.766 1.555 1.555 1.555
[PLAT710 ALERT 4 G](#) Delete 1-2-3 or 2-3-4 Linear Torsion Angle ... # 35
 CU2 -CU1 -CU2 -N1B 145.00 39.00 2.766 1.555 1.555 1.555
[PLAT710 ALERT 4 G](#) Delete 1-2-3 or 2-3-4 Linear Torsion Angle ... # 38
 O1B -CU1 -O1B -C1B 7.00 0.00 2.766 1.555 1.555 1.555
[PLAT710 ALERT 4 G](#) Delete 1-2-3 or 2-3-4 Linear Torsion Angle ... # 43
 O1B -CU1 -O1B -CU2 9.00 0.00 2.766 1.555 1.555 1.555
[PLAT710 ALERT 4 G](#) Delete 1-2-3 or 2-3-4 Linear Torsion Angle ... # 52
 O2B -CU1 -O2B -C31B 29.00 23.00 2.766 1.555 1.555 1.555
[PLAT710 ALERT 4 G](#) Delete 1-2-3 or 2-3-4 Linear Torsion Angle ... # 57
 O2B -CU1 -O2B -CU2 -167.00 23.00 2.766 1.555 1.555 1.555
[PLAT710 ALERT 4 G](#) Delete 1-2-3 or 2-3-4 Linear Torsion Angle ... # 172
 C31A-O2A -CU4 -O2A 120.00 30.00 1.555 1.555 1.555 2.575
[PLAT710 ALERT 4 G](#) Delete 1-2-3 or 2-3-4 Linear Torsion Angle ... # 173
 CU3 -O2A -CU4 -O2A -25.00 30.00 1.555 1.555 1.555 2.575
[PLAT710 ALERT 4 G](#) Delete 1-2-3 or 2-3-4 Linear Torsion Angle ... # 187
 CU3 -CU4 -CU3 -O1A -143.00 11.00 2.575 1.555 1.555 1.555
[PLAT710 ALERT 4 G](#) Delete 1-2-3 or 2-3-4 Linear Torsion Angle ... # 191
 CU3 -CU4 -CU3 -O2A 9.00 11.00 2.575 1.555 1.555 1.555
[PLAT710 ALERT 4 G](#) Delete 1-2-3 or 2-3-4 Linear Torsion Angle ... # 196
 CU3 -CU4 -CU3 -N1A -169.00 11.00 2.575 1.555 1.555 1.555
[PLAT710 ALERT 4 G](#) Delete 1-2-3 or 2-3-4 Linear Torsion Angle ... # 201
 CU3 -CU4 -CU3 -N2A 32.00 11.00 2.575 1.555 1.555 1.555
[PLAT710 ALERT 4 G](#) Delete 1-2-3 or 2-3-4 Linear Torsion Angle ... # 202
 O1A -CU4 -O1A -C1A -53.90 1.40 2.575 1.555 1.555 1.555
[PLAT710 ALERT 4 G](#) Delete 1-2-3 or 2-3-4 Linear Torsion Angle ... # 207
 O1A -CU4 -O1A -CU3 102.10 1.30 2.575 1.555 1.555 1.555
[PLAT720 ALERT 4 G](#) Number of Unusual/Non-Standard Labels 2
[PLAT869 ALERT 4 G](#) ALERTS Related to the use of SQUEEZE Suppressed
 !

0 **ALERT level A** = Most likely a serious problem - resolve or explain
 4 **ALERT level B** = A potentially serious problem, consider carefully
 3 **ALERT level C** = Check. Ensure it is not caused by an omission or oversight
 26 **ALERT level G** = General information/check it is not something unexpected

4 ALERT type 1 CIF construction/syntax error, inconsistent or missing data
 7 ALERT type 2 Indicator that the structure model may be wrong or deficient
 1 ALERT type 3 Indicator that the structure quality may be low
 19 ALERT type 4 Improvement, methodology, query or suggestion
 2 ALERT type 5 Informative message, check

It is advisable to attempt to resolve as many as possible of the alerts in all categories. Often the minor alerts point to easily fixed oversights, errors and omissions in your CIF or refinement strategy, so attention to these fine details can be worthwhile. In order to resolve some of the more serious problems it may be necessary to carry out additional measurements or structure refinements. However, the purpose of your study may justify the reported deviations and the more serious of these should normally be commented upon in the discussion or experimental section of a paper or in the "special_details" fields of the CIF. `checkCIF` was carefully designed to identify outliers and unusual parameters, but every test has its limitations and alerts that are not important in a particular case may appear. Conversely, the absence of alerts does not guarantee there are no aspects of the results needing attention. It is up to the individual to critically assess their own results and, if necessary, seek expert advice.

Publication of your CIF in IUCr journals

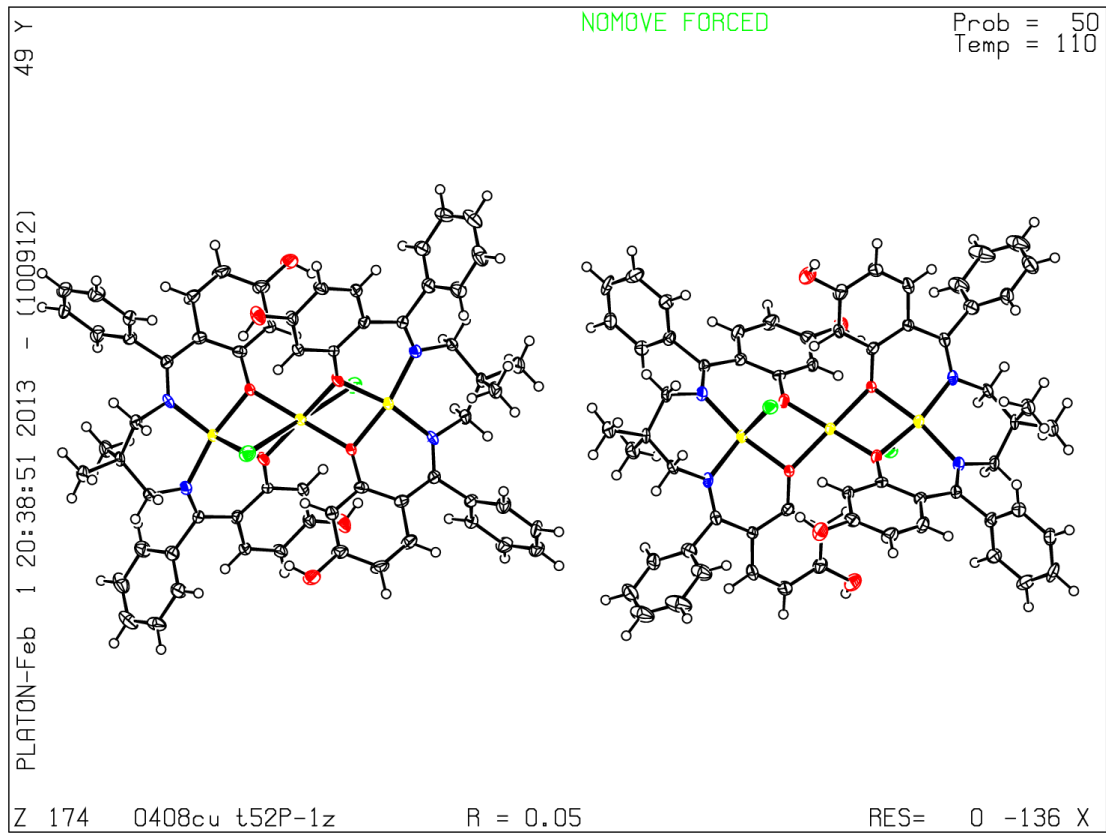
A basic structural check has been run on your CIF. These basic checks will be run on all CIFs submitted for publication in IUCr journals (*Acta Crystallographica*, *Journal of Applied Crystallography*, *Journal of Synchrotron Radiation*); however, if you intend to submit to *Acta Crystallographica Section C or E*, you should make sure that [full publication checks](#) are run on the final version of your CIF prior to submission.

Publication of your CIF in other journals

Please refer to the *Notes for Authors* of the relevant journal for any special instructions relating to CIF submission.

PLATON version of 05/11/2012; check.def file version of 05/11/2012

Datablock 0408cu_t52_sqz - ellipsoid plot



[Download CIF editor \(pubCIF\) from the IUCr](#)
[Download CIF editor \(enCIFer\) from the CCDC](#)
[Test a new CIF entry](#)

checkCIF/PLATON report (basic structural check)

No syntax errors found.

Please wait while processing

[CIF dictionary](#)

[Interpreting this report](#)

Datablock: mo_om_jdp_cu_propyl_data3_0m

Bond precision: C-C = 0.0053 A Wavelength=0.71073

Cell: a=9.1151(4) b=25.6003(11) c=11.5667(6)

alpha=90 beta=100.219(3) gamma=90

Temperature: 100 K

| | Calculated | Reported |
|----------------|---------------------------|-------------------------|
| Volume | 2656.3(2) | 2656.3(2) |
| Space group | P 21/c | P21/c |
| Hall group | -P 2ybc | ? |
| Moiety formula | C58 H52 Cu3 N4 O10, 2(C1) | C29 H26 Cl Cu1.50 N2 O5 |
| Sum formula | C58 H52 Cl2 Cu3 N4 O10 | C29 H26 Cl Cu1.50 N2 O5 |
| Mr | 1226.59 | 613.28 |
| Dx, g cm-3 | 1.534 | 1.534 |
| Z | 2 | 4 |
| Mu (mm-1) | 1.355 | 1.355 |
| F000 | 1258.0 | 1258.0 |
| F000' | 1260.95 | |
| h, k, lmax | 11, 31, 14 | 11, 32, 14 |
| Nref | 5440 | 4761 |
| Tmin, Tmax | 0.892, 0.987 | 0.773, 0.987 |
| Tmin' | 0.763 | |

Correction method= MULTI-SCAN

Data completeness= 0.875 Theta(max)= 26.370

R(reflections)= 0.0437(4299) wR2(reflections)= 0.0986(4761)

S = 1.174 Npar= 357

The following ALERTS were generated. Each ALERT has the format

test-name_ALERT_alert-type_alert-level.

Click on the hyperlinks for more details of the test.

● Alert level C

[PLAT094_ALERT_2_C](#) Ratio of Maximum / Minimum Residual Density

.... 2.76

[PLAT220_ALERT_2_C](#) Large Non-Solvent C Ueq(max)/Ueq(min)

... 3.2 Ratio

● Alert level G

[PLAT003_ALERT_2_G](#) Number of Uiso or Uij Restrained Atom Sites

.... 39

[PLAT005_ALERT_5_G](#) No _iucr_refine_instructions_details in the CIF

?

[PLAT007_ALERT_5_G](#) Note: Number of Unrefined D-H Atoms

..... 2

[PLAT042_ALERT_1_G](#) Calc. and Reported MoietyFormula Strings

Differ ?

[PLAT045_ALERT_1_G](#) Calculated and Reported Z Differ by

0.50 Ratio

[PLAT083_ALERT_2_G](#) SHELXL Second Parameter in WGHT Unusually

Large. 8.56

[PLAT232_ALERT_2_G](#) Hirshfeld Test Diff (M-X) Cu1 -- O5 ..

7.3 su

[PLAT710_ALERT_4_G](#) Delete 1-2-3 or 2-3-4 Linear Torsion Angle ...
 # 19
 O1 -CU1 -CU2 -CU1 -142.00 17.00 1.555 1.555 1.555
 3.667
[PLAT710_ALERT_4_G](#) Delete 1-2-3 or 2-3-4 Linear Torsion Angle ...
 # 20
 O2 -CU1 -CU2 -CU1 72.00 17.00 1.555 1.555 1.555
 3.667
[PLAT710_ALERT_4_G](#) Delete 1-2-3 or 2-3-4 Linear Torsion Angle ...
 # 21
 N1 -CU1 -CU2 -CU1 -116.00 17.00 1.555 1.555 1.555
 3.667
[PLAT710_ALERT_4_G](#) Delete 1-2-3 or 2-3-4 Linear Torsion Angle ...
 # 22
 N2 -CU1 -CU2 -CU1 51.00 17.00 1.555 1.555 1.555
 3.667
[PLAT710_ALERT_4_G](#) Delete 1-2-3 or 2-3-4 Linear Torsion Angle ...
 # 23
 O5 -CU1 -CU2 -CU1 -38.00 17.00 1.555 1.555 1.555
 3.667
[PLAT710_ALERT_4_G](#) Delete 1-2-3 or 2-3-4 Linear Torsion Angle ...
 # 24
 O1 -CU2 -O1 -C1 -162.00 15.00 3.667 1.555 1.555
 1.555
[PLAT710_ALERT_4_G](#) Delete 1-2-3 or 2-3-4 Linear Torsion Angle ...
 # 29
 O1 -CU2 -O1 -CU1 32.00 15.00 3.667 1.555 1.555
 1.555
[PLAT710_ALERT_4_G](#) Delete 1-2-3 or 2-3-4 Linear Torsion Angle ...
 # 53
 O2 -CU2 -O2 -C17 85.00 4.00 3.667 1.555 1.555
 1.555
[PLAT710_ALERT_4_G](#) Delete 1-2-3 or 2-3-4 Linear Torsion Angle ...
 # 58
 O2 -CU2 -O2 -CU1 -124.00 4.00 3.667 1.555 1.555
 1.555
[PLAT860_ALERT_3_G](#) Note: Number of Least-Squares Restraints
 234

0 **ALERT level A** = Most likely a serious problem - resolve or explain
 0 **ALERT level B** = A potentially serious problem, consider carefully
 2 **ALERT level C** = Check. Ensure it is not caused by an omission or oversight
 17 **ALERT level G** = General information/check it is not something unexpected

2 ALERT type 1 CIF construction/syntax error, inconsistent or missing data
 5 ALERT type 2 Indicator that the structure model may be wrong or deficient
 1 ALERT type 3 Indicator that the structure quality may be low
 9 ALERT type 4 Improvement, methodology, query or suggestion
 2 ALERT type 5 Informative message, check

It is advisable to attempt to resolve as many as possible of the alerts in all categories. Often the minor alerts point to easily fixed oversights, errors and omissions in your CIF or refinement strategy, so attention to these fine details can be worthwhile. In order to resolve some of the more serious problems it may be necessary to carry out additional measurements or structure refinements. However, the purpose of your study may justify the reported deviations and the more serious of these should normally be commented upon in the discussion or experimental section of a paper or in the "special_details" fields of the CIF. checkCIF was carefully designed to identify outliers and unusual parameters, but every test has its limitations and alerts that are not important in a particular case may appear. Conversely, the absence of alerts does not guarantee there are no aspects of the results needing attention. It is up to the individual to critically assess their own results and, if necessary, seek expert advice.

Publication of your CIF in IUCr journals

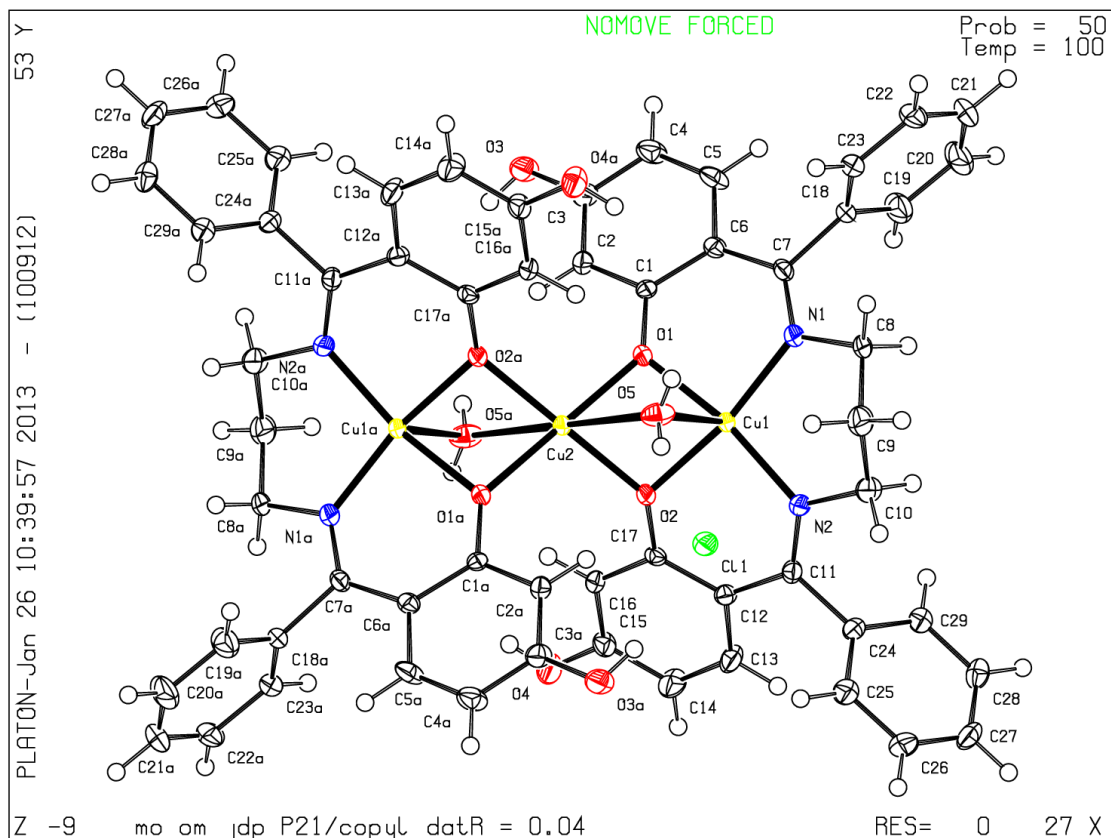
A basic structural check has been run on your CIF. These basic checks will be run on all CIFs submitted for publication in IUCr journals (*Acta Crystallographica*, *Journal of Applied Crystallography*, *Journal of Synchrotron Radiation*); however, if you intend to submit to *Acta Crystallographica Section C* or *E*, you should make sure that [full publication checks](#) are run on the final version of your CIF prior to submission.

Publication of your CIF in other journals

Please refer to the *Notes for Authors* of the relevant journal for any special instructions relating to CIF submission.

PLATON version of 05/11/2012; check.def file version of 05/11/2012

Datablock mo_om_jdp_cu_propyl_data3_0m - ellipsoid plot



[Download CIF editor \(pubCIF\) from the IUCr](#)
[Download CIF editor \(enCIFer\) from the CCDC](#)
[Test a new CIF entry](#)

checkCIF/PLATON report (basic structural check)

No syntax errors found.

Please wait while processing

[CIF dictionary](#)

[Interpreting this report](#)

Datablock: jdp_0408ni

Bond precision: C-C = 0.0021 Å Wavelength=0.71073

Cell: a=9.0140(2) b=21.4340(4) c=13.6800(2)

alpha=90 beta=103.228(1) gamma=90

Temperature: 100 K

| | Calculated | Reported |
|------------------------|---------------|---------------|
| Volume | 2572.93(8) | 2572.93(8) |
| Space group | P 21/c | P21/c |
| Hall group | -P 2ybc | -P 2ybc |
| Moiety formula | C31 H30 N2 O4 | C31 H30 N2 O4 |
| Sum formula | C31 H30 N2 O4 | C31 H30 N2 O4 |
| Mr | 494.57 | 494.57 |
| Dx, g cm ⁻³ | 1.277 | 1.277 |
| Z | 4 | 4 |
| Mu (mm ⁻¹) | 0.085 | 0.085 |
| F000 | 1048.0 | 1048.0 |
| F000' | 1048.47 | |
| h, k, lmax | 12, 28, 18 | 12, 28, 18 |
| Nref | 6372 | 6342 |
| Tmin, Tmax | 0.991, 0.993 | 0.982, 0.993 |
| Tmin' | 0.982 | |

Correction method= MULTI-SCAN

Data completeness= 0.995 Theta(max)= 28.280

R(reflections)= 0.0466(4875) wR2(reflections)= 0.1160(6342)

S = 1.044 Npar= 352

The following ALERTS were generated. Each ALERT has the format

test-name_ALERT_alert-type_alert-level.

Click on the hyperlinks for more details of the test.

● Alert level C

[PLAT309_ALERT_2_C](#) Single Bonded Oxygen (C-O .GT. 1.3 Ang)

O1

[PLAT309_ALERT_2_C](#) Single Bonded Oxygen (C-O .GT. 1.3 Ang)

O3

● Alert level G

[PLAT005_ALERT_5_G](#) No _iucr_refine_instructions_details in the CIF

?

[PLAT180_ALERT_4_G](#) Check Cell Rounding: # of Values Ending with 0 =

3

[PLAT605 ALERT 4 G](#) Structure Contains Solvent Accessible VOIDS of .
55 A**3

[PLAT869 ALERT 4 G](#) ALERTS Related to the use of SQUEEZE Suppressed
!

0 **ALERT level A** = Most likely a serious problem - resolve or explain
0 **ALERT level B** = A potentially serious problem, consider carefully
2 **ALERT level C** = Check. Ensure it is not caused by an omission or oversight
4 **ALERT level G** = General information/check it is not something unexpected

0 ALERT type 1 CIF construction/syntax error, inconsistent or missing data

2 ALERT type 2 Indicator that the structure model may be wrong or deficient

0 ALERT type 3 Indicator that the structure quality may be low

3 ALERT type 4 Improvement, methodology, query or suggestion

1 ALERT type 5 Informative message, check

It is advisable to attempt to resolve as many as possible of the alerts in all categories. Often the minor alerts point to easily fixed oversights, errors and omissions in your CIF or refinement strategy, so attention to these fine details can be worthwhile. In order to resolve some of the more serious problems it may be necessary to carry out additional measurements or structure refinements. However, the purpose of your study may justify the reported deviations and the more serious of these should normally be commented upon in the discussion or experimental section of a paper or in the "special_details" fields of the CIF. checkCIF was carefully designed to identify outliers and unusual parameters, but every test has its limitations and alerts that are not important in a particular case may appear. Conversely, the absence of alerts does not guarantee there are no aspects of the results needing attention. It is up to the individual to critically assess their own results and, if necessary, seek expert advice.

Publication of your CIF in IUCr journals

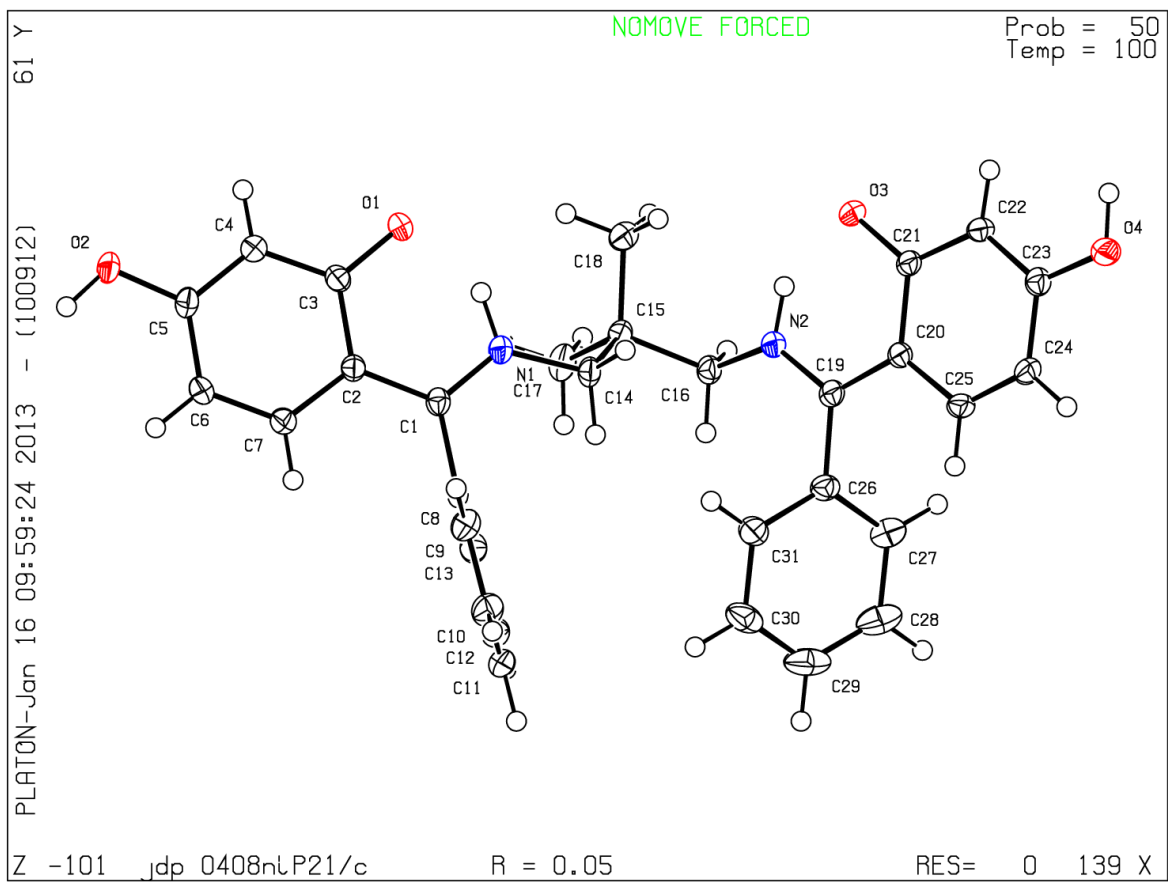
A basic structural check has been run on your CIF. These basic checks will be run on all CIFs submitted for publication in IUCr journals (*Acta Crystallographica*, *Journal of Applied Crystallography*, *Journal of Synchrotron Radiation*); however, if you intend to submit to *Acta Crystallographica Section C* or *E*, you should make sure that [full publication checks](#) are run on the final version of your CIF prior to submission.

Publication of your CIF in other journals

Please refer to the *Notes for Authors* of the relevant journal for any special instructions relating to CIF submission.

PLATON version of 05/11/2012; check.def file version of 05/11/2012

Datablock jdp_0408ni - ellipsoid plot



[Download CIF editor \(pubCIF\) from the IUCr](#)
[Download CIF editor \(enCIFer\) from the CCDC](#)
[Test a new CIF entry](#)

checkCIF/PLATON report (basic structural check)

No syntax errors found.

Please wait while processing

[CIF dictionary](#)

[Interpreting this report](#)

Datablock: jdp_oh_bzph

Bond precision: C-C = 0.0031 A Wavelength=0.71073

Cell: a=12.631(5) b=15.619(5) c=14.201(5)

alpha=90 beta=92.792(5) gamma=90

Temperature: 296 K

| | Calculated | Reported |
|----------------|--------------------------|--------------------------|
| Volume | 2798.3(17) | 2798.3(17) |
| Space group | P 21/n | P21/n |
| Hall group | -P 2yn | -P 2yn |
| Moiety formula | C29 H26 N2 O5, C3 H7 N O | C29 H26 N2 O5, C3 H7 N O |
| Sum formula | C32 H33 N3 O6 | C32 H33 N3 O6 |
| Mr | 555.61 | 555.61 |
| Dx, g cm-3 | 1.319 | 1.319 |
| Z | 4 | 4 |
| Mu (mm-1) | 0.092 | 0.092 |
| F000 | 1176.0 | 1176.0 |
| F000' | 1176.56 | |
| h, k, lmax | 17, 21, 19 | 16, 19, 18 |
| Nref | 7289 | 6293 |
| Tmin, Tmax | 0.964, 0.973 | 0.964, 0.973 |
| Tmin' | 0.964 | |

Correction method= MULTI-SCAN

Data completeness= 0.863 Theta(max)= 28.790

R(reflections)= 0.0532(3336) wR2(reflections)= 0.1404(6293)

S = 0.879 Npar= 397

The following ALERTS were generated. Each ALERT has the format

test-name_ALERT_alert-type_alert-level.

Click on the hyperlinks for more details of the test.

Alert level B

[PLAT415](#) [ALERT 2](#) [B](#) Short Inter D-H..H-X H3SA .. H5A .. 1.98 Ang.

NB: this may be ignored as atom H5A belongs to the minor component of the disordered hydroxyl group (involving atom O5) on the central carbon of the propyl bridge. The model is correct.

Alert level C

[PLAT244](#) [ALERT 4](#) [C](#) Low 'Solvent' Ueq as Compared to Neighbors of N1S
[PLAT309](#) [ALERT 2](#) [C](#) Single Bonded Oxygen (C-O .GT. 1.3 Ang) O3

Alert level G

[REFLT03](#) [ALERT 1](#) [G](#) ALERT: Expected hkl max differ from CIF values

From the CIF: _diffrn_reflns_theta_max 28.79
From the CIF: _reflns_number_total 6293
From the CIF: _diffrn_reflns_limit_max hkl 16. 18. 18.
From the CIF: _diffrn_reflns_limit_min hkl -16. -19. -18.
TEST1: Expected hkl limits for theta max
Calculated maximum hkl 17. 21. 19.
Calculated minimum hkl -17. -21. -19.

| | | |
|-----------------------------------|--|---------|
| PLAT002_ALERT_2_G | Number of Distance or Angle Restraints on AtSite | 8 |
| PLAT005_ALERT_5_G | No <code>_iucr_refine_instructions_details</code> in the CIF | ? |
| PLAT007_ALERT_5_G | Note: Number of Unrefined D-H Atoms | 2 |
| PLAT128_ALERT_4_G | Alternate Setting of Space-group P21/c | P21/n |
| PLAT301_ALERT_3_G | Note: Main Residue Disorder | 3 Perc. |
| PLAT720_ALERT_4_G | Number of Unusual/Non-Standard Labels | 6 |
| PLAT779_ALERT_4_G | Suspect or Irrelevant (Bond) Angle in CIF # | 125 |
| | O5 -C15 -H15 1.555 1.555 1.555 42.20 Deg. | |
| PLAT860_ALERT_3_G | Note: Number of Least-Squares Restraints | 4 |
| PLAT951_ALERT_5_G | Reported and Calculated Kmax Values Differ by .. | 2 |

- 0 **ALERT level A** = Most likely a serious problem - resolve or explain
- 1 **ALERT level B** = A potentially serious problem, consider carefully
- 2 **ALERT level C** = Check. Ensure it is not caused by an omission or oversight
- 10 **ALERT level G** = General information/check it is not something unexpected

- 1 ALERT type 1 CIF construction/syntax error, inconsistent or missing data
- 3 ALERT type 2 Indicator that the structure model may be wrong or deficient
- 2 ALERT type 3 Indicator that the structure quality may be low
- 4 ALERT type 4 Improvement, methodology, query or suggestion
- 3 ALERT type 5 Informative message, check

It is advisable to attempt to resolve as many as possible of the alerts in all categories. Often the minor alerts point to easily fixed oversights, errors and omissions in your CIF or refinement strategy, so attention to these fine details can be worthwhile. In order to resolve some of the more serious problems it may be necessary to carry out additional measurements or structure refinements. However, the purpose of your study may justify the reported deviations and the more serious of these should normally be commented upon in the discussion or experimental section of a paper or in the "special_details" fields of the CIF. `checkCIF` was carefully designed to identify outliers and unusual parameters, but every test has its limitations and alerts that are not important in a particular case may appear. Conversely, the absence of alerts does not guarantee there are no aspects of the results needing attention. It is up to the individual to critically assess their own results and, if necessary, seek expert advice.

Publication of your CIF in IUCr journals

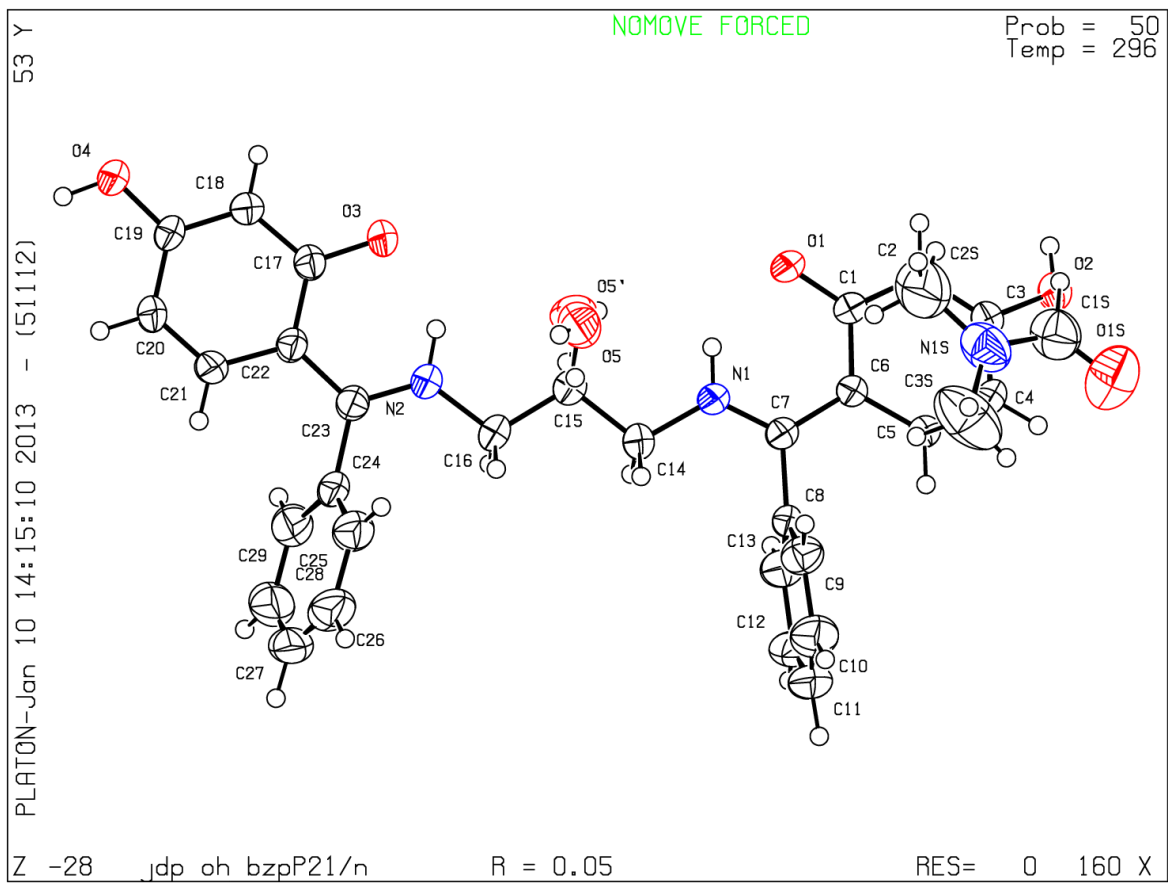
A basic structural check has been run on your CIF. These basic checks will be run on all CIFs submitted for publication in IUCr journals (*Acta Crystallographica*, *Journal of Applied Crystallography*, *Journal of Synchrotron Radiation*); however, if you intend to submit to *Acta Crystallographica Section C* or *E*, you should make sure that [full publication checks](#) are run on the final version of your CIF prior to submission.

Publication of your CIF in other journals

Please refer to the *Notes for Authors* of the relevant journal for any special instructions relating to CIF submission.

PLATON version of 05/11/2012; check.def file version of 05/11/2012

Datablock `jdp_oh_bzph` - ellipsoid plot



[Download CIF editor \(pubCIF\) from the IUCr](#)
[Download CIF editor \(enCIFer\) from the CCDC](#)
[Test a new CIF entry](#)

checkCIF/PLATON report (basic structural check)

No syntax errors found.

Please wait while processing

[CIF dictionary](#)

[Interpreting this report](#)

Datablock: jdp_oh_bzph

Bond precision: C-C = 0.0031 A Wavelength=0.71073

Cell: a=12.631(5) b=15.619(5) c=14.201(5)

alpha=90 beta=92.792(5) gamma=90

Temperature: 296 K

| | Calculated | Reported |
|----------------|--------------------------|--------------------------|
| Volume | 2798.3(17) | 2798.3(17) |
| Space group | P 21/n | P21/n |
| Hall group | -P 2yn | -P 2yn |
| Moiety formula | C29 H26 N2 O5, C3 H7 N O | C29 H26 N2 O5, C3 H7 N O |
| Sum formula | C32 H33 N3 O6 | C32 H33 N3 O6 |
| Mr | 555.61 | 555.61 |
| Dx, g cm-3 | 1.319 | 1.319 |
| Z | 4 | 4 |
| Mu (mm-1) | 0.092 | 0.092 |
| F000 | 1176.0 | 1176.0 |
| F000' | 1176.56 | |
| h, k, lmax | 17, 21, 19 | 16, 19, 18 |
| Nref | 7289 | 6293 |
| Tmin, Tmax | 0.964, 0.973 | 0.964, 0.973 |
| Tmin' | 0.964 | |

Correction method= MULTI-SCAN

Data completeness= 0.863 Theta(max)= 28.790

R(reflections)= 0.0532(3336) wR2(reflections)= 0.1404(6293)

S = 0.879 Npar= 397

The following ALERTS were generated. Each ALERT has the format

test-name_ALERT_alert-type_alert-level.

Click on the hyperlinks for more details of the test.

Alert level B

[PLAT415](#) [ALERT 2](#) [B](#) Short Inter D-H..H-X H3SA .. H5A .. 1.98 Ang.

NB: this may be ignored as atom H5A belongs to the minor component of the disordered hydroxyl group (involving atom O5) on the central carbon of the propyl bridge. The model is correct.

Alert level C

[PLAT244](#) [ALERT 4](#) [C](#) Low 'Solvent' Ueq as Compared to Neighbors of N1S
[PLAT309](#) [ALERT 2](#) [C](#) Single Bonded Oxygen (C-O .GT. 1.3 Ang) O3

Alert level G

[REFLT03](#) [ALERT 1](#) [G](#) ALERT: Expected hkl max differ from CIF values

From the CIF: _diffn_reflns_theta_max 28.79
From the CIF: _reflns_number_total 6293

From the CIF: _diffn_reflns_limit_max hkl 16. 18. 18.
From the CIF: _diffn_reflns_limit_min hkl -16. -19. -18.

TEST1: Expected hkl limits for theta max

Calculated maximum hkl 17. 21. 19.

Calculated minimum hkl -17. -21. -19.

| | | |
|-----------------------------------|--|---------|
| PLAT002_ALERT_2_G | Number of Distance or Angle Restraints on AtSite | 8 |
| PLAT005_ALERT_5_G | No <code>_iucr_refine_instructions_details</code> in the CIF | ? |
| PLAT007_ALERT_5_G | Note: Number of Unrefined D-H Atoms | 2 |
| PLAT128_ALERT_4_G | Alternate Setting of Space-group P21/c | P21/n |
| PLAT301_ALERT_3_G | Note: Main Residue Disorder | 3 Perc. |
| PLAT720_ALERT_4_G | Number of Unusual/Non-Standard Labels | 6 |
| PLAT779_ALERT_4_G | Suspect or Irrelevant (Bond) Angle in CIF # | 125 |
| | O5 -C15 -H15 1.555 1.555 1.555 42.20 Deg. | |
| PLAT860_ALERT_3_G | Note: Number of Least-Squares Restraints | 4 |
| PLAT951_ALERT_5_G | Reported and Calculated Kmax Values Differ by .. | 2 |

- 0 **ALERT level A** = Most likely a serious problem - resolve or explain
- 1 **ALERT level B** = A potentially serious problem, consider carefully
- 2 **ALERT level C** = Check. Ensure it is not caused by an omission or oversight
- 10 **ALERT level G** = General information/check it is not something unexpected

- 1 ALERT type 1 CIF construction/syntax error, inconsistent or missing data
- 3 ALERT type 2 Indicator that the structure model may be wrong or deficient
- 2 ALERT type 3 Indicator that the structure quality may be low
- 4 ALERT type 4 Improvement, methodology, query or suggestion
- 3 ALERT type 5 Informative message, check

It is advisable to attempt to resolve as many as possible of the alerts in all categories. Often the minor alerts point to easily fixed oversights, errors and omissions in your CIF or refinement strategy, so attention to these fine details can be worthwhile. In order to resolve some of the more serious problems it may be necessary to carry out additional measurements or structure refinements. However, the purpose of your study may justify the reported deviations and the more serious of these should normally be commented upon in the discussion or experimental section of a paper or in the "special_details" fields of the CIF. `checkCIF` was carefully designed to identify outliers and unusual parameters, but every test has its limitations and alerts that are not important in a particular case may appear. Conversely, the absence of alerts does not guarantee there are no aspects of the results needing attention. It is up to the individual to critically assess their own results and, if necessary, seek expert advice.

Publication of your CIF in IUCr journals

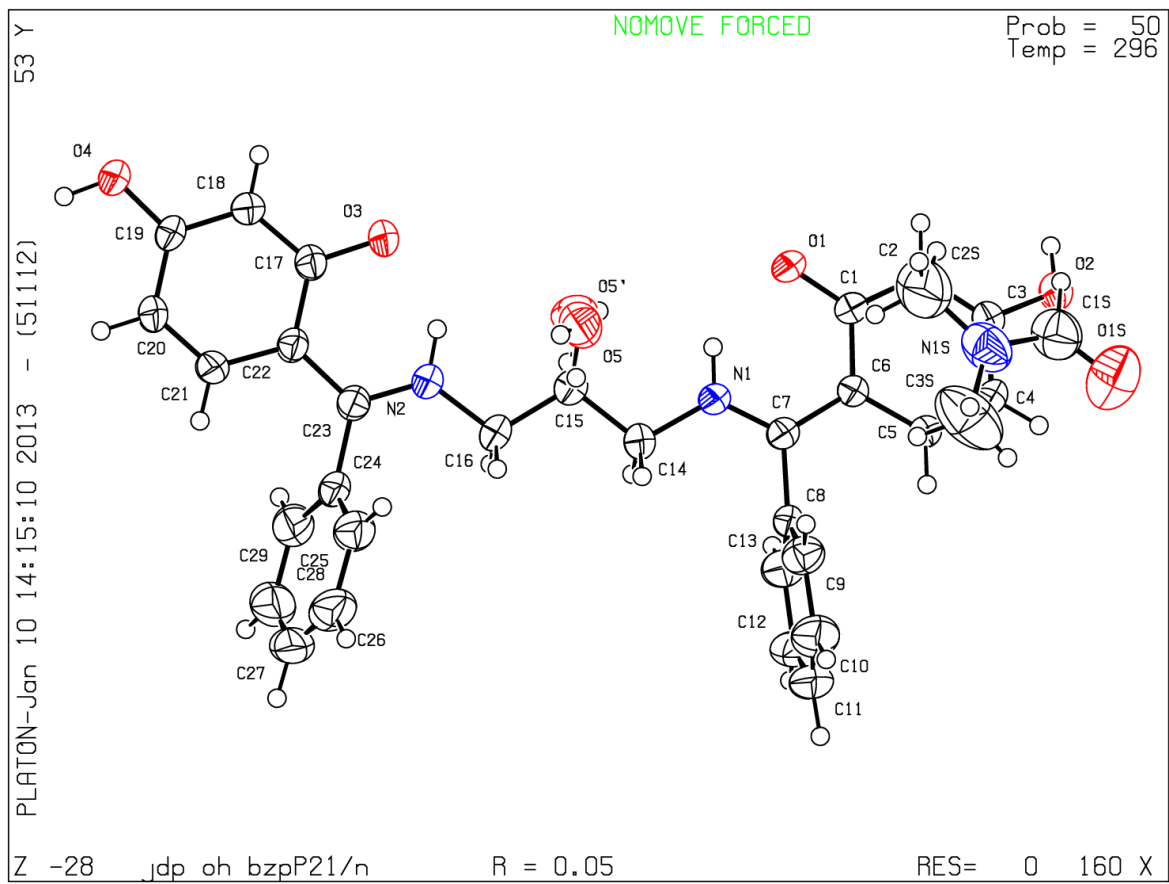
A basic structural check has been run on your CIF. These basic checks will be run on all CIFs submitted for publication in IUCr journals (*Acta Crystallographica*, *Journal of Applied Crystallography*, *Journal of Synchrotron Radiation*); however, if you intend to submit to *Acta Crystallographica Section C* or *E*, you should make sure that [full publication checks](#) are run on the final version of your CIF prior to submission.

Publication of your CIF in other journals

Please refer to the *Notes for Authors* of the relevant journal for any special instructions relating to CIF submission.

PLATON version of 05/11/2012; check.def file version of 05/11/2012

Datablock `jdp_oh_bzph` - ellipsoid plot



[Download CIF editor \(pubCIF\) from the IUCr](#)
[Download CIF editor \(enCIFer\) from the CCDC](#)
[Test a new CIF entry](#)

checkCIF/PLATON report (basic structural check)

No syntax errors found.

Please wait while processing

[CIF dictionary](#)

[Interpreting this report](#)

Datablock: 0408ni

Bond precision: C-C = 0.0068 Å Wavelength=0.71073

Cell: a=25.0542 (13) b=9.6539 (5) c=27.3083 (13)

alpha=90 beta=98.568 (5) gamma=90

Temperature: 296 K

| | Calculated | Reported |
|------------------------|------------------|------------------|
| Volume | 6531.4 (6) | 6531.4 (6) |
| Space group | P 21/c | P 1 21/c 1 |
| Hall group | -P 2ybc | -P 2ybc |
| Moiety formula | C31 H28 N2 Ni O4 | ? |
| Sum formula | C31 H28 N2 Ni O4 | C31 H28 N2 Ni O4 |
| Mr | 551.24 | 551.26 |
| Dx, g cm ⁻³ | 1.121 | 1.121 |
| Z | 8 | 8 |
| Mu (mm ⁻¹) | 0.626 | 0.626 |
| F000 | 2304.0 | 2304.0 |
| F000' | 2307.57 | |
| h, k, lmax | 30, 11, 33 | 30, 11, 33 |
| Nref | 12895 | 12840 |
| Tmin, Tmax | 0.861, 0.981 | 0.705, 0.982 |
| Tmin' | 0.687 | |

Correction method= MULTI-SCAN

Data completeness= 0.996 Theta(max)= 26.060

R(reflections)= 0.0603(5416) wR2(reflections)= 0.1395(12840)

S = 0.794 Npar= 693

The following ALERTS were generated. Each ALERT has the format

test-name_ALERT_alert-type_alert-level.

Click on the hyperlinks for more details of the test.

Alert level B

Crystal system given = monoclinic

[PLAT420_ALERT_2_B](#) D-H Without Acceptor O3A - H3A ...

?

[PLAT420_ALERT_2_B](#) D-H Without Acceptor O3B - H3B ...

?

[PLAT420_ALERT_2_B](#) D-H Without Acceptor O4A - H4A ...

?

[PLAT420_ALERT_2_B](#) D-H Without Acceptor O4B - H4B ...

?

These may be ignored as the disordered solvent (8 water molecules and half a DMF molecule) was removed with PLATON's SQUEEZE algorithm.

Alert level C

[GOODF01_ALERT_2_C](#) The least squares goodness of fit parameter lies

outside the range 0.80 <> 2.00

Goodness of fit given = 0.794

[RINTA01_ALERT_3_C](#) The value of Rint is greater than 0.12

Rint given 0.123

[PLAT026_ALERT_3_C](#) Ratio Observed / Unique Reflections too Low
.... 42 Perc.
[PLAT220_ALERT_2_C](#) Large Non-Solvent C Ueq(max)/Ueq(min)
... 3.5 Ratio
[PLAT234_ALERT_4_C](#) Large Hirshfeld Difference C15B -- C16B ..
0.17 Ang.
[PLAT241_ALERT_2_C](#) Check High Ueq as Compared to Neighbors
for O1B
[PLAT242_ALERT_2_C](#) Check Low Ueq as Compared to Neighbors
for C15B
[PLAT331_ALERT_2_C](#) Small Average Phenyl C-C Dist. C20A -C25A
1.37 Ang.
[PLAT331_ALERT_2_C](#) Small Average Phenyl C-C Dist. C20B -C25B
1.37 Ang.
[PLAT341_ALERT_3_C](#) Low Bond Precision on C-C Bonds
0.0068 Ang

Alert level G

[PLAT005_ALERT_5_G](#) No _iucr_refine_instructions_details in the CIF
?
[PLAT007_ALERT_5_G](#) Note: Number of Unrefined D-H Atoms
..... 4
[PLAT093_ALERT_1_G](#) No su's on H-positions, refinement reported as
. mixed
[PLAT606_ALERT_4_G](#) VERY LARGE Solvent Accessible VOID(S) in
Structure !
[PLAT720_ALERT_4_G](#) Number of Unusual/Non-Standard Labels
..... 2
[PLAT869_ALERT_4_G](#) ALERTS Related to the use of SQUEEZE
Suppressed !

0 **ALERT level A** = Most likely a serious problem - resolve or explain
4 **ALERT level B** = A potentially serious problem, consider carefully
10 **ALERT level C** = Check. Ensure it is not caused by an omission or oversight
6 **ALERT level G** = General information/check it is not something unexpected

1 ALERT type 1 CIF construction/syntax error, inconsistent or missing data
10 ALERT type 2 Indicator that the structure model may be wrong or deficient
3 ALERT type 3 Indicator that the structure quality may be low
4 ALERT type 4 Improvement, methodology, query or suggestion
2 ALERT type 5 Informative message, check

It is advisable to attempt to resolve as many as possible of the alerts in all categories. Often the minor alerts point to easily fixed oversights, errors and omissions in your CIF or refinement strategy, so attention to these fine details can be worthwhile. In order to resolve some of the more serious problems it may be necessary to carry out additional measurements or structure refinements. However, the purpose of your study may justify the reported deviations and the more serious of these should normally be commented upon in the discussion or experimental section of a paper or in the "special_details" fields of the CIF. checkCIF was carefully designed to identify outliers and unusual parameters, but every test has its limitations and alerts that are not important in a particular case may appear. Conversely, the absence of alerts does not guarantee there are no aspects of the results needing attention. It is up to the individual to critically assess their own results and, if necessary, seek expert advice.

Publication of your CIF in IUCr journals

A basic structural check has been run on your CIF. These basic checks will be run on all CIFs submitted for publication in IUCr journals (*Acta Crystallographica*, *Journal of Applied Crystallography*, *Journal of Synchrotron Radiation*); however, if you intend to submit to *Acta Crystallographica Section C* or *E*, you should make sure that [full publication checks](#) are run on

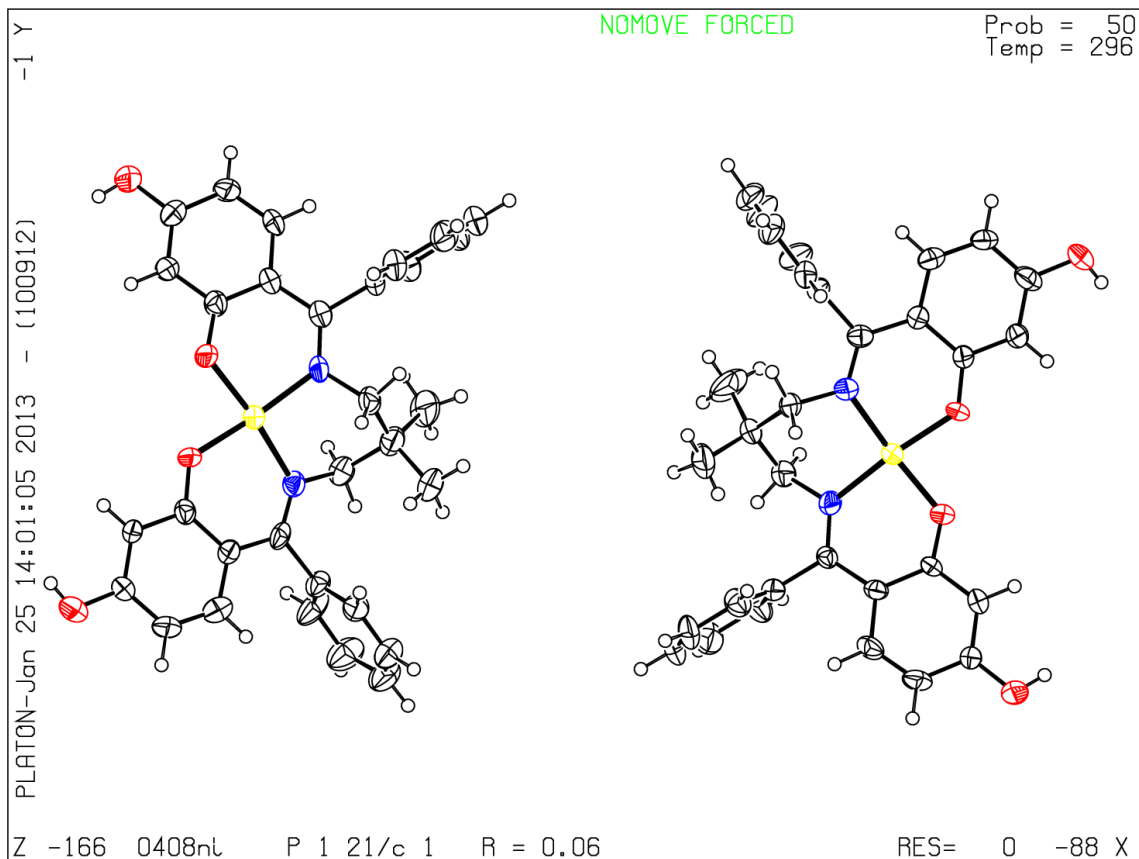
the final version of your CIF prior to submission.

Publication of your CIF in other journals

Please refer to the *Notes for Authors* of the relevant journal for any special instructions relating to CIF submission.

PLATON version of 05/11/2012; check.def file version of 05/11/2012

Datablock 0408ni - ellipsoid plot



[Download CIF editor \(pubCIF\) from the IUCr](#)

[Download CIF editor \(enCIFer\) from the CCDC](#)

[Test a new CIF entry](#)

checkCIF/PLATON report (basic structural check)

No syntax errors found.

Please wait while processing

[CIF dictionary](#)

[Interpreting this report](#)

Datablock: jdp_2610ni

Bond precision: C-C = 0.0029 Å Wavelength=0.71073

Cell: a=24.261(2) b=9.0890(8) c=26.956(2)

alpha=90 beta=111.109(1) gamma=90

Temperature: 100 K

| | Calculated | Reported |
|----------------|---------------------------|------------------|
| Volume | 5545.2(8) | 5545.2(8) |
| Space group | C 2/c | C2/c |
| Hall group | -C 2yc | -C 2yc |
| Moiety formula | C29 H24 N2 Ni O4, 2(H2 O) | ? |
| Sum formula | C29 H28 N2 Ni O6 | C29 H28 N2 Ni O6 |
| Mr | 559.22 | 559.24 |
| Dx, g cm-3 | 1.340 | 1.340 |
| Z | 8 | 8 |
| Mu (mm-1) | 0.744 | 0.744 |
| F000 | 2336.0 | 2336.0 |
| F000' | 2339.69 | |
| h, k, lmax | 32, 12, 35 | 31, 12, 35 |
| Nref | 6879 | 6502 |
| Tmin, Tmax | 0.868, 0.956 | 0.866, 0.957 |
| Tmin' | 0.868 | |

Correction method= MULTI-SCAN

Data completeness= 0.945 Theta(max)= 28.270

R(reflections)= 0.0377(5155) wR2(reflections)= 0.0981(6502)

S = 1.056 Npar= 361

The following ALERTS were generated. Each ALERT has the format

test-name_ALERT_alert-type_alert-level.

Click on the hyperlinks for more details of the test.

Alert level B

[PLAT420_ALERT_2_B](#) D-H Without Acceptor O1W - H1WA ... ?
[PLAT420_ALERT_2_B](#) D-H Without Acceptor O2W - H2WB ... ?

This arises because disordered solvent H-bonded to the ordered solvent water molecules could not be modeled and had to be removed with PLATON's SQUEEZE algorithm. The alerts may be ignored.

Alert level G

[PLAT002_ALERT_2_G](#) Number of Distance or Angle Restraints on AtSite 6
[PLAT005_ALERT_5_G](#) No _iucr_refine_instructions_details in the CIF ?
[PLAT007_ALERT_5_G](#) Note: Number of Unrefined D-H Atoms 2
[PLAT605_ALERT_4_G](#) Structure Contains Solvent Accessible VOIDS of . 156
A**3
[PLAT710_ALERT_4_G](#) Delete 1-2-3 or 2-3-4 Linear Torsion Angle ... # 3
N2 -NI1 -O1 -C1 -109.40 0.40 1.555 1.555 1.555 1.555
[PLAT710_ALERT_4_G](#) Delete 1-2-3 or 2-3-4 Linear Torsion Angle ... # 4
O1 -NI1 -N2 -C17 -78.80 0.40 1.555 1.555 1.555 1.555
[PLAT710_ALERT_4_G](#) Delete 1-2-3 or 2-3-4 Linear Torsion Angle ... # 7
O1 -NI1 -N2 -C16 100.10 0.40 1.555 1.555 1.555 1.555
[PLAT720_ALERT_4_G](#) Number of Unusual/Non-Standard Labels 4

0 **ALERT level A** = Most likely a serious problem - resolve or explain
2 **ALERT level B** = A potentially serious problem, consider carefully
0 **ALERT level C** = Check. Ensure it is not caused by an omission or oversight
10 **ALERT level G** = General information/check it is not something unexpected

0 ALERT type 1 CIF construction/syntax error, inconsistent or missing data
3 ALERT type 2 Indicator that the structure model may be wrong or deficient
1 ALERT type 3 Indicator that the structure quality may be low
6 ALERT type 4 Improvement, methodology, query or suggestion
2 ALERT type 5 Informative message, check

It is advisable to attempt to resolve as many as possible of the alerts in all categories. Often the minor alerts point to easily fixed oversights, errors and omissions in your CIF or refinement strategy, so attention to these fine details can be worthwhile. In order to resolve some of the more serious problems it may be necessary to carry out additional measurements or structure refinements. However, the purpose of your study may justify the reported deviations and the more serious of these should normally be commented upon in the discussion or experimental section of a paper or in the "special_details" fields of the CIF. checkCIF was carefully designed to identify outliers and unusual parameters, but every test has its limitations and alerts that are not important in a particular case may appear. Conversely, the absence of alerts does not guarantee there are no aspects of the results needing attention. It is up to the individual to critically assess their own results and, if necessary, seek expert advice.

Publication of your CIF in IUCr journals

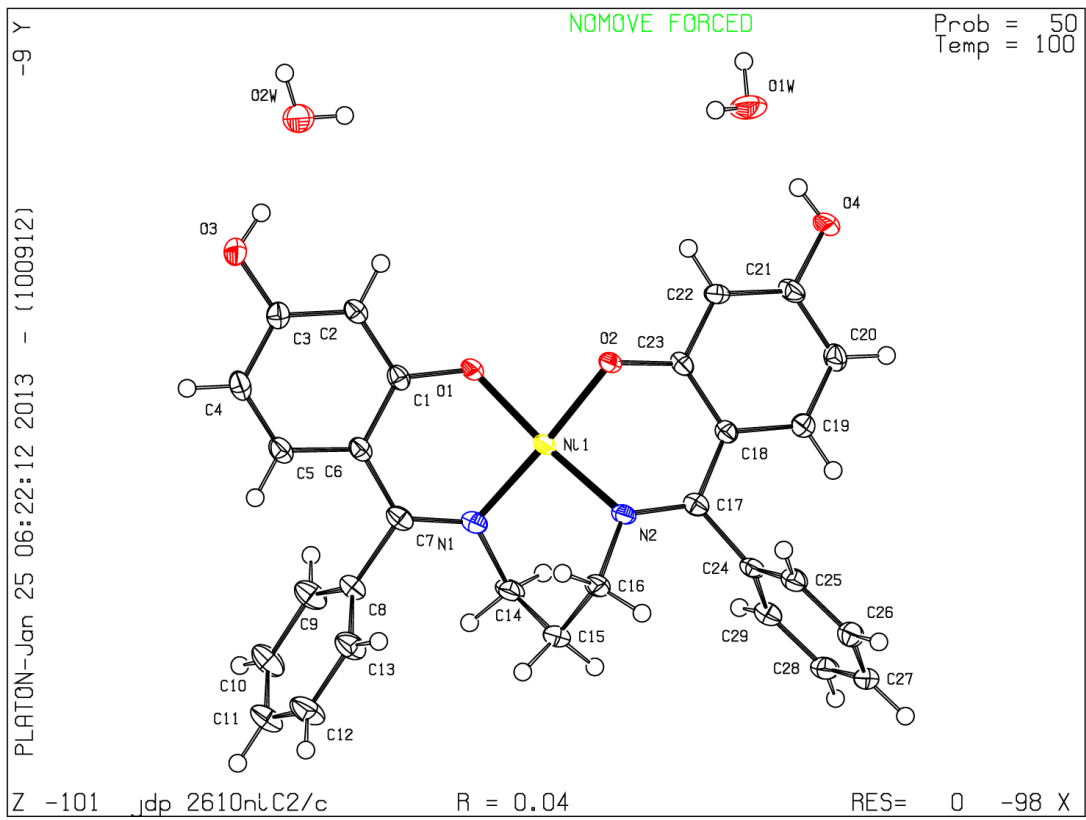
A basic structural check has been run on your CIF. These basic checks will be run on all CIFs submitted for publication in IUCr journals (*Acta Crystallographica*, *Journal of Applied Crystallography*, *Journal of Synchrotron Radiation*); however, if you intend to submit to *Acta Crystallographica Section C* or *E*, you should make sure that [full publication checks](#) are run on the final version of your CIF prior to submission.

Publication of your CIF in other journals

Please refer to the *Notes for Authors* of the relevant journal for any special instructions relating to CIF submission.

PLATON version of 05/11/2012; check.def file version of 05/11/2012

Datablock jdp_2610ni - ellipsoid plot



a

[Download CIF editor \(pubCIF\) from the IUCr](#)
[Download CIF editor \(enCIFer\) from the CCDC](#)
[Test a new CIF entry](#)

checkCIF/PLATON report (basic structural check)

No syntax errors found.

Please wait while processing

[CIF dictionary](#)

[Interpreting this report](#)

Datablock: jdp_zn2610

Bond precision: C-C = 0.0060 A Wavelength=0.71073

Cell: a=23.1020(3) b=18.1100(3) c=16.6460(3)

 alpha=90 beta=90 gamma=90

Temperature: 100 K

| | Calculated | Reported |
|----------------|-------------------|-------------------|
| Volume | 6964.31(19) | 6964.31(19) |
| Space group | P n a 21 | P n a 21 |
| Hall group | P 2c -2n | P 2c -2n |
| Moiety formula | C58 H48 N4 O8 Zn2 | C58 H48 N4 O8 Zn2 |
| Sum formula | C58 H48 N4 O8 Zn2 | C58 H48 N4 O8 Zn2 |
| Mr | 1059.79 | 1059.74 |
| Dx, g cm-3 | 1.011 | 1.011 |
| Z | 4 | 4 |
| Mu (mm-1) | 0.733 | 0.733 |
| F000 | 2192.0 | 2192.0 |
| F000' | 2195.09 | |
| h, k, lmax | 30, 24, 22 | 30, 24, 22 |
| Nref | 8918[17251] | 13618 |
| Tmin, Tmax | 0.876, 0.896 | 0.838, 0.898 |
| Tmin' | 0.833 | |

Correction method= MULTI-SCAN

Data completeness=

1.53/0.79

Theta(max)= 28.270

R(reflections)= 0.0484(wR2(reflections)= 0.1156(
10751) 13618)

S = 0.838

Npar= 654

The following ALERTS were generated. Each ALERT has the format **test-name_ALERT_alert-type_alert-level**. Click on the hyperlinks for more details of the test.

● Alert level B

[PLAT111_ALERT_2_B](#) ADDSYM Detects (Pseudo) Centre of Symmetry
90 PerFi

This can be ignored: the crystal is a racemic twin and the structure has been refined with the appropriate twin law.

[PLAT420_ALERT_2_B](#) D-H Without Acceptor O2 - H2 ...
?
[PLAT420_ALERT_2_B](#) D-H Without Acceptor O4 - H4 ...
?
[PLAT420_ALERT_2_B](#) D-H Without Acceptor O6 - H6 ...
?
[PLAT420_ALERT_2_B](#) D-H Without Acceptor O8 - H8 ...
?

These flags may be ignored: the solvent (5 DMF molecules) was disordered and the electron density due to the disordered solvent region has been removed using PLATON's SQUEEZE algorithm The ligand OH groups were H-bonded to disordered solvent molecules; removal of the solvent molecules thus creates OH groups that are not H-bonded in the structure.

● Alert level C

[STRVA01_ALERT_4_C](#) Flack test results are meaningless.
From the CIF: `_refine_ls_abs_structure_Flack` 0.000
From the CIF: `_refine_ls_abs_structure_Flack_su` 1.700
[PLAT220_ALERT_2_C](#) Large Non-Solvent O Ueq(max)/Ueq(min) ...
3.6 Ratio
[PLAT230_ALERT_2_C](#) Hirshfeld Test Diff for C49 -- C50 .. 5.7
su

● Alert level G

[PLAT005_ALERT_5_G](#) No `_iucr_refine_instructions_details` in the CIF
?
[PLAT007_ALERT_5_G](#) Note: Number of Unrefined D-H Atoms
4
[PLAT032_ALERT_4_G](#) Std. Uncertainty on Flack Parameter Value High .
1.700
[PLAT083_ALERT_2_G](#) SHELXL Second Parameter in WGHT Unusually
Large. 8.91
[PLAT093_ALERT_1_G](#) No su's on H-positions, refinement reported as .
mixed
[PLAT113_ALERT_2_G](#) ADDSYM Suggests Possible Pseudo/New Space-
group. Pbcn
[PLAT180_ALERT_4_G](#) Check Cell Rounding: # of Values Ending with 0 =
3
[PLAT606_ALERT_4_G](#) VERY LARGE Solvent Accessible VOID(S) in
Structure !
[PLAT710_ALERT_4_G](#) Delete 1-2-3 or 2-3-4 Linear Torsion Angle ... #
15
N1 -ZN1 -O3 -C29 -131.50 1.10 1.555 1.555 1.555
1.555
[PLAT710_ALERT_4_G](#) Delete 1-2-3 or 2-3-4 Linear Torsion Angle ... #
19
N1 -ZN1 -O3 -ZN2 25.60 1.20 1.555 1.555 1.555
1.555
[PLAT710_ALERT_4_G](#) Delete 1-2-3 or 2-3-4 Linear Torsion Angle ... #
36

N3 -ZN2 -O7 -C58 -119.40 1.10 1.555 1.555 1.555
 1.555
[PLAT710 ALERT 4 G](#) Delete 1-2-3 or 2-3-4 Linear Torsion Angle ... #
 40
 N3 -ZN2 -O7 -ZN1 36.20 1.10 1.555 1.555 1.555
 1.555
[PLAT710 ALERT 4 G](#) Delete 1-2-3 or 2-3-4 Linear Torsion Angle ... #
 44
 O3 -ZN1 -N1 -C7 -135.60 1.10 1.555 1.555 1.555
 1.555
[PLAT710 ALERT 4 G](#) Delete 1-2-3 or 2-3-4 Linear Torsion Angle ... #
 48
 O3 -ZN1 -N1 -C14 40.40 1.30 1.555 1.555 1.555
 1.555
[PLAT710 ALERT 4 G](#) Delete 1-2-3 or 2-3-4 Linear Torsion Angle ... #
 60
 O7 -ZN2 -N3 -C36 -154.10 0.90 1.555 1.555 1.555
 1.555
[PLAT710 ALERT 4 G](#) Delete 1-2-3 or 2-3-4 Linear Torsion Angle ... #
 64
 O7 -ZN2 -N3 -C43 23.30 1.20 1.555 1.555 1.555
 1.555
[PLAT850 ALERT 4 G](#) Check Flack Parameter Exact Value 0.00 and su ..
 1.70
[PLAT869 ALERT 4 G](#) ALERTS Related to the use of SQUEEZE Suppressed
 !

0 **ALERT level A** = Most likely a serious problem - resolve or explain
 5 **ALERT level B** = A potentially serious problem, consider carefully
 3 **ALERT level C** = Check. Ensure it is not caused by an omission or oversight
 18 **ALERT level G** = General information/check it is not something unexpected

1 ALERT type 1 CIF construction/syntax error, inconsistent or missing data
 9 ALERT type 2 Indicator that the structure model may be wrong or deficient
 0 ALERT type 3 Indicator that the structure quality may be low
 14 ALERT type 4 Improvement, methodology, query or suggestion
 2 ALERT type 5 Informative message, check

It is advisable to attempt to resolve as many as possible of the alerts in all categories. Often the minor alerts point to easily fixed oversights, errors and omissions in your CIF or refinement strategy, so attention to these fine details can be worthwhile. In order to resolve some of the more serious problems it may be necessary to carry out additional measurements or structure refinements. However, the purpose of your study may justify the reported deviations and the more serious of these should normally be commented upon in the discussion or experimental section of a paper or in the "special_details" fields of the CIF. checkCIF was carefully designed to identify outliers and unusual parameters, but every test has its limitations and alerts that are not important in a particular case may appear. Conversely, the absence of alerts does not guarantee there are no aspects of the results needing attention. It is up to the individual to critically assess their own results and, if necessary, seek expert advice.

Publication of your CIF in IUCr journals

A basic structural check has been run on your CIF. These basic checks will be run on all CIFs submitted for publication in IUCr

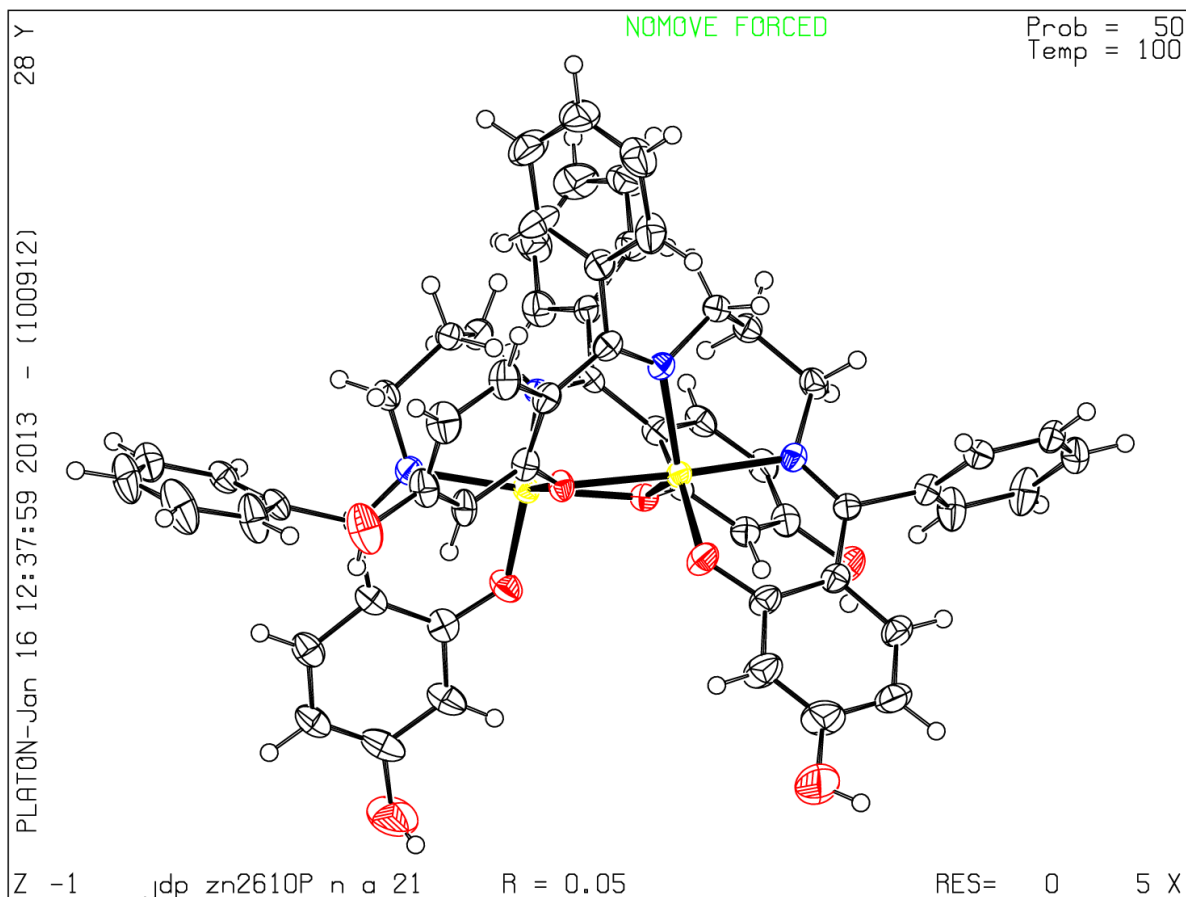
journals (*Acta Crystallographica*, *Journal of Applied Crystallography*, *Journal of Synchrotron Radiation*); however, if you intend to submit to *Acta Crystallographica Section C* or *E*, you should make sure that [full publication checks](#) are run on the final version of your CIF prior to submission.

Publication of your CIF in other journals

Please refer to the *Notes for Authors* of the relevant journal for any special instructions relating to CIF submission.

PLATON version of 05/11/2012; check.def file version of 05/11/2012

Datablock jdp_zn2610 - ellipsoid plot



[Download CIF editor \(pubCIF\) from the IUCr](#)
[Download CIF editor \(enCIFer\) from the CCDC](#)
[Test a new CIF entry](#)